

**BIOTRANSFORMATION OF FURANIC AND PHENOLIC COMPOUNDS  
WITH HYDROGEN PRODUCTION IN  
MICROBIAL ELECTROLYSIS CELLS**

A Dissertation  
Presented to  
The Academic Faculty

by

Xiaofei Zeng

In Partial Fulfillment  
of the Requirements for the Degree  
Doctor of Philosophy in the  
School of Civil and Environmental Engineering

Georgia Institute of Technology  
December 2016

**COPYRIGHT © 2016 BY XIAOFEI ZENG**

**BIOTRANSFORMATION OF FURANIC AND PHENOLIC COMPOUNDS  
WITH HYDROGEN PRODUCTION IN  
MICROBIAL ELECTROLYSIS CELLS**

Approved by:

Dr. Spyros G. Pavlostathis, Advisor  
School of Civil and Environmental  
Engineering  
*Georgia Institute of Technology*

Dr. Ching-Hua Huang  
School of Civil and Environmental  
Engineering  
*Georgia Institute of Technology*

Dr. Jim Spain  
School of Civil and Environmental  
Engineering  
*Georgia Institute of Technology*

Dr. Lawrence Bottomley  
School of Chemistry and Biochemistry  
*Georgia Institute of Technology*

Dr. Abhijeet Borole  
Biosciences Division  
*Oak Ridge National Laboratory*

Date Approved: November 4, 2016

## ACKNOWLEDGEMENTS

I am very grateful to have met and been supported by many people along the way. First and foremost, I would like to express my deepest gratitude to my advisor, Dr. Spyros G. Pavlostathis. I genuinely appreciate the opportunity he gave me to pursue this doctoral research. Dr. Pavlostathis is a wise and kind mentor, who has helped me to develop and grow not only as a student but also as a person. He has always been willing to take time to help me improve, even when I stumbled or made mistakes. He has taught me to be thorough and self-confident, to identify priorities and to communicate well. His sincerity and dedication have always inspired me to strive for excellence in my life and work.

I would like to thank my dissertation committee members, Dr. Abhijeet Borole for the help on the initiation of this research and the continual guidance, Dr. Jim Spain for his strong interest in this work and insightful comments, Dr. Ching-Hua Huang for being an outstanding role model for me, and Dr. Lawrence Bottomley for his precious time, challenging questions, and constructive feedback.

I really appreciate the help I got from my fellow graduate students at Georgia Tech. I would especially like to thank my dear colleague and friend, Christy Dykstra. She has shared her knowledge and skills with me, and been very helpful in developing my English and writing. I will never forget how selfless she has been helping me and all other people working in our laboratory. Every time I was out of town, Christy was always willing to take care of my bioreactors. I would also like to thank former members in Dr. Pavlostathis' research group, Dr. Ulas Tezel, Dr. Teresa Misiti, and Dr. Peizhe Sun. I have benefited significantly from the laboratory procedures, instrumentation methods, and publications developed by them. I would also like to thank Dr. Fei He for training me

on protein analysis, Angela Pena-Gonzalez for helping me with phylogenetic analysis, and Dr. Yuzhong Zhang for helping me with MatLab programming.

I would like to thank staff members in the School of Civil and Environmental Engineering, Robert Simon, Jenny Eaton, and Jessica Brown, for their assistance. I would especially thank Dr. Guangxuan Zhu for his timely assistance with laboratory instruments, and also for his support and advice at my most difficult time.

I want to give a formal thank-you to my husband, Ziyi Jiang, and my parents, grandparents, and parents-in-law, who have given me endless love, unconditional support, and tremendous strength. I would like to thank Mrs. JoAnn Pavlostathis for her continual care and encouragement. I would also like to express my gratitude to all my dear friends and fellow students for cheering me along. My time at Georgia Tech would not have been the same without them.

Finally, I would like to acknowledge the financial support provided by the U.S. Department of Energy, BioEnergy Technologies Office under the Carbon, Hydrogen and Separations Efficiency (CHASE) in Bio-Oil Conversion Pathways program.

# TABLE OF CONTENT

	Page
<b>ACKNOWLEDGEMENTS</b>	<b>III</b>
<b>LIST OF TABLES</b>	<b>V</b>
<b>LIST OF FIGURES</b>	<b>VI</b>
<b>SUMMARY</b>	<b>XI</b>
<b>CHAPTER 1 INTRODUCTION</b>	<b>1</b>
1.1 Preface	1
1.2 Research Objectives	3
1.3 Motivation and Significance	4
<b>CHAPTER 2 BACKGROUND</b>	<b>6</b>
2.1 Furanic and Phenolic Compounds	6
2.1.1 Source	6
2.1.2 Chemical, Physicochemical and Toxicological Properties	7
2.1.3 Biotransformation Potential	10
2.2 Microbial Electrolysis Cell	12
2.2.1 Thermodynamics	13
2.2.2 Exoelectrogenesis	15
2.2.3 MEC Performance and Anode Substrates	19
<b>CHAPTER 3 MATERIALS AND METHODS</b>	<b>22</b>
3.1 Chemicals	22
3.2 Analytical Methods	23
3.2.1 pH	23

3.2.2	Chemical Oxygen Demand (COD)	23
3.2.3	Gas Production and Composition	24
3.2.4	Furanic and Phenolic Compounds	24
3.2.5	Volatile Fatty Acids	25
3.2.6	Biotransformation Products	25
3.2.7	Protein	26
3.2.8	Microbial Community Analysis	26
3.2.9	Electric Current	27
3.2.10	Cyclic Voltammetry	28
3.2.11	Electrochemical Impedance Spectroscopy	30
3.3	Calculations	33
3.3.1	Current Density	33
3.3.2	Coulombic Efficiency	33
3.3.3	Anode Efficiency	33
3.3.4	Cathode Efficiency	34
3.3.5	H <sub>2</sub> Yield	34
3.3.6	Electrical Energy Efficiency	35
3.3.7	Overall Energy Efficiency	36
<b>CHAPTER 4 ENRICHMENT OF ANODE MICROBIAL COMMUNITY</b>		<b>38</b>
4.1	Introduction	38
4.2	Materials and Methods	39
4.2.1	MFC	39
4.2.2	Inoculation and Enrichment Procedures	41
4.2.3	Bioanode Microbial Community Analysis	43
4.3	Results and Discussion	44

4.3.1	MFC Fed with Furanic and Phenolic Compounds Along with Glucose	44
4.3.2	MFC Fed with Furanic and Phenolic Compounds without Glucose	46
4.3.3	Microbial Community Structure	47
4.4	Summary	49
<b>CHAPTER 5 HYDROGEN PRODUCTION IN MEC USING FURANIC AND PHENOLIC COMPOUNDS</b>		<b>50</b>
5.1	Introduction	50
5.2	Materials and Methods	51
5.2.1	MEC	51
5.2.2	MEC Operation	52
5.2.3	Experimental Controls	53
5.2.4	Anode Microbial Community Analysis	53
5.3	Results and Discussion	54
5.3.1	MEC Startup	54
5.3.2	MEC Performance with Increased Substrate Concentration	57
5.3.3	Biotransformation of the Furanic and Phenolic Compounds	65
5.3.4	Exoelectrogenesis in MEC Bioanode	78
5.3.5	Anode Microbial Community	87
5.3.6	MEC Internal Resistance	91
5.4	Summary	97
<b>CHAPTER 6 BIOTRANSFORMATION OF FURANIC AND PHENOLIC COMPOUNDS IN MEC BIOANODE</b>		<b>99</b>
6.1	Introduction	99
6.2	Materials and Methods	101
6.2.1	MEC	101

6.2.2	Fermentative Culture	101
6.2.3	Batch Runs in MEC Bioanode and Fermentative Culture	102
6.2.4	Fermentative Transformation by Different Microbial Communities	103
6.2.5	Microaerophilic Bioanode	104
6.2.6	Identification of Metabolites	105
6.2.7	Fermentative Culture Microbial Community Analysis	108
6.3	Results and Discussion	109
6.3.1	MEC Bioanode Runs with Individual Compounds	109
6.3.2	Metabolic Fate of Parent Compounds in MEC Bioanode	115
6.3.3	Metabolic Fate in Parent Compounds in Fermentative Culture	124
6.3.4	SA, VA and HBA Biotransformation Pathways	129
6.3.5	Microbial Communities	137
6.3.6	Alternative Microbial Communities and Metabolic Conditions	141
6.3.7	Substrate Utilization and Partition of Electron Equivalents	145
6.4	Summary	150
<b>CHAPTER 7 INHIBITORY EFFECT OF FURANIC AND PHENOLIC COMPOUNDS IN MEC BIOANODE</b>		<b>152</b>
7.1	Introduction	152
7.2	Materials and Methods	154
7.2.1	MEC Bioanode	154
7.2.2	Batch Runs with Parent Compounds Mixture	154
7.2.3	Batch Runs with Individual Parent Compounds	155
7.2.4	Batch Runs with Catechol and Phenol	156
7.2.5	Extent of Inhibition and IC <sub>50</sub> Calculations	157
7.2.6	Synergy Assessment	157



7.3 Results and Discussion	160
7.3.1 Inhibitory Effect of the Furanic and Phenolic Mixture	160
7.3.2 Inhibition by Parent Compounds vs. Transformation Products	165
7.3.3 Inhibitory Effect of Individual Parent Compounds	168
7.3.4 Inhibitory Effect of Catechol and Phenol	179
7.3.5 Reversibility of Inhibition	181
7.4 Summary	185
<b>CHAPTER 8 PERFORMANCE EVALUATION OF A CONTINUOUS-FLOW BIOANODE MEC FED WITH FURANIC AND PHENOLIC COMPOUNDS</b>	<b>186</b>
8.1 Introduction	186
8.2 Materials and Methods	187
8.2.1 Continuous-flow Anode MEC	187
8.2.2 Evaluation of the Effect of HRT, OLR and Applied Voltage	189
8.2.3 Inhibition Test of Continuous-flow Bioanode	190
8.2.4 Anode Microbial Community Analysis	190
8.2.5 Biomass Yield Coefficient Calculations	191
8.3 Results and Discussion	192
8.3.1 Phase I – Effect of HRT on MEC performance	194
8.3.2 Phase II – Effect of OLR on MEC performance	201
8.3.3 Phase II – Effect of OLR on COD Balance	205
8.3.4 Phase II – Effect of OLR on Anode Microbial Community	208
8.3.5 Phase III – Effect of Applied Voltage on MEC Performance	213
8.3.6 Inhibition of Continuous-flow Bioanode	216
8.4 Summary	219
<b>CHAPTER 9 CONCLUSIONS AND RECOMMENDATIONS</b>	<b>220</b>

9.1 Conclusions	220
9.2 Recommendations	223
<b>REFERENCES</b>	<b>226</b>

## LIST OF TABLES

	Page
<b>Table 2.1.</b> Chemical and physicochemical properties of the furanic and phenolic compounds used in this study.	8
<b>Table 2.2.</b> Half reduction reactions and standard potentials of the five compounds.	9
<b>Table 2.3.</b> Performance of MECs fed with various types of substrates.	20
<b>Table 4.1.</b> Composition of Trace Metal and Vitamin Stock Solutions.	42
<b>Table 4.2.</b> MFC Operation Schedule during Startup.	43
<b>Table 5.1.</b> Efficiency parameters of the MEC fed with the mixture of the five compounds.	62
<b>Table 5.2.</b> Volumetric transformation rate of the furanic and phenolic compounds tested at various initial concentrations in the MEC bioanode.	71
<b>Table 5.3.</b> Possible fermentation of the identified transformation products to acetate and other products ( $\Delta G^{\circ}$ ; Gibbs free energy at pH 7 and 298 K).	77
<b>Table 5.4.</b> MEC internal resistance ( $R_{total}$ ) associated with the anode ( $R_a$ ), cathode ( $R_c$ ), and the solution plus cation exchange membrane ( $R_{s+m}$ ) at the end of batch runs conducted with various initial concentrations of furanic and phenolic compounds.	96
<b>Table 6.1.</b> Possible metabolites of SA, VA, HBA, FF, and HMF. Parameters listed are based on LC/MS-MS analysis unless otherwise stated.	106
<b>Table 6.2.</b> Electron balance of batch runs conducted with individual furanic and phenolic compounds.	114
<b>Table 6.3.</b> Hypothetical fermentative reactions of the phenolic compounds ( $\Delta G^{\circ}$ ; Gibbs free energy change at pH 7 and 298 K).	136
<b>Table 6.4.</b> Microbial community composition (%) of the MEC bioanode and fermentative culture biofilms at phylum and genus levels.	139
<b>Table 6.5.</b> Substrate utilization and partitioning to biomass and other products with numerical illustration for the two furanic and three phenolic compounds used in the present study.	147
<b>Table 7.1.</b> Inhibitory concentration ( $IC_{50}$ ) and extent of inhibition observed at the highest concentration of each parent compound attained in batch runs <sup>a,b</sup> .	174
<b>Table 8.1.</b> MEC Performance under Various HRT, OLR and Applied Voltage Conditions.	198

## LIST OF FIGURES

	Page
<b>Figure 2.1.</b> Schematic of a MEC resulting in H <sub>2</sub> production.	13
<b>Figure 2.2.</b> Schematic of exoelectrogenesis using direct and indirect extracellular electron transfer mechanisms.	16
<b>Figure 3.1.</b> Cyclic voltammograms of a carbon felt anode electrode (A) and a non-active biofilm-attached anode electrode (B) in anolyte.	29
<b>Figure 3.2.</b> Non-active and active bioanode voltammograms conducted with different scan directions. Left column: E <sub>oc</sub> → + 0.3 V → - 0.7 V; middle column: - 0.7 V → + 0.3 V → - 0.7 V; right column: E <sub>oc</sub> → - 0.7 V → + 0.3 V.	30
<b>Figure 3.3.</b> Equivalent circuit used in EIS representative of anode or cathode half-cell (A), and the MEC whole-cell (B).	32
<b>Figure 4.1.</b> MFC Setup.	40
<b>Figure 4.2.</b> MFC current production in batch runs conducted with 200 mg/L furanic and phenolic mixture in the presence or absence of glucose at different external resistance.	44
<b>Figure 4.3.</b> Time course of five parent compounds during MFC startup. Abbreviations: HMF, 5-hydroxymethylfurfural; FF, furfural; SA, syringic acid; VA, vanillic acid; HBA, 4-hydroxybenzoic acid.	45
<b>Figure 4.4.</b> Catechol and phenol measured at the end of feeding cycles conducted with glucose (Glu) and furanic and phenolic compounds as the sole carbon and energy source (1-9).	47
<b>Figure 4.5.</b> MFC anode microbial community structures at the phylum (A) and genus (B) level.	48
<b>Figure 5.1.</b> MEC Setup. 1, anode chamber; 2, cathode chamber; 3, cation exchange membrane; 4, potentiostat; 5, displacement reservoir; 6, glass burette. 7, Ag/AgCl reference electrode.	52
<b>Figure 5.2.</b> Current and cumulative H <sub>2</sub> production during the MEC startup.	56
<b>Figure 5.3.</b> Current production in an un-inoculated, abiotic MEC at increasing applied voltage.	56
<b>Figure 5.4.</b> Current and cumulative H <sub>2</sub> production during four batch runs conducted at increased initial substrate concentrations in the MEC anode (A, 200 mg/L; B, 400 mg/L; C, 800 mg/L; D, 1200 mg/L). Error bars represent mean ± standard deviation, <i>n</i> = 3.	59
<b>Figure 5.5.</b> Current and H <sub>2</sub> production at 200 mg/L initial substrate concentration after the observed inhibition during the 1200 mg/L batch run.	60
<b>Figure 5.6.</b> H <sub>2</sub> diffusion from the cathode to the anode headspace in a biomass-free MEC with an open circuit.	65
<b>Figure 5.7.</b> Normalized concentration profiles of the five compounds fed to the MEC anode at various initial concentrations (200 to 1200 mg/L total concentration).	66

- Figure 5.8.** Cyclic voltammograms of a non-active bioanode in the absence and presence of a mixture of the five compounds, as well as an active bioanode after 1 d of incubation with the compounds mixture. 68
- Figure 5.9.** Cyclic voltammograms of a non-active bioanode in the presence of individual furanic and phenolic compounds. 69
- Figure 5.10.** Transformation products detected during the four batch assays at increased initial substrate concentrations in the MEC anode (200-1200 mg/L). 73
- Figure 5.11.** LC/MS chromatograms at the end of four batch assays revealing unidentified metabolites. (A) MS scan in negative mode; (B) MS scan in positive mode; (C) UV absorbance at 254 nm. 74
- Figure 5.12.** NaAc concentration and pH (A), current and H<sub>2</sub> production (B), as well as electrode potential (C) measured during the batch run conducted with 200 mg/L NaAc. 79
- Figure 5.13.** NaAc concentration and pH (A), current and H<sub>2</sub> production (B), as well as electrode potential (C) measured during the batch run conducted with 400 mg/L NaAc. 80
- Figure 5.14.** NaAc concentration and pH (A), current and H<sub>2</sub> production (B), as well as electrode potential (C) measured during the batch run conducted with 800 mg/L NaAc. Arrows indicate pH adjustment. 81
- Figure 5.15.** Cyclic voltammograms of the bioanode fed with 200 mg/L NaAc at the beginning of a batch run (non-active), after 1 day of incubation (active) and after the anode was rinsed with fresh anolyte. 84
- Figure 5.16.** Current production of MEC fed with furanic and phenolic substrates and amended with RF (A) and AQDS (B) at 1 and 10 μM. 86
- Figure 5.17.** Composition of the MEC anode microbial community at phylum level. 87
- Figure 5.18.** Phylogenetic tree of the dominant bacteria identified in the MEC anode. Fraction of bacterial population and GenBank accession numbers shown in parentheses. *Escherichia coli* K12 was used as the outgroup. 90
- Figure 5.19.** Bode (left column) and Nyquist (right column) plots of electrochemical impedance spectra of MEC whole-cell in batch runs conducted with 200-1200 mg/L initial concentration of furanic and phenolic compounds. Lines represent data fit using the equivalent circuit shown in Figure 3.3B. 92
- Figure 5.20.** Bode (left column) and Nyquist (right column) plots of electrochemical impedance spectra of MEC anode half-cell in batch runs conducted with 200-1200 mg/L initial concentration of furanic and phenolic compounds. Lines represent data fit using the equivalent circuit shown in Figure 3.3A. 93
- Figure 5.21.** Bode (left column) and Nyquist (right column) plots of electrochemical impedance spectra of MEC cathode half-cell in batch runs conducted with 200-1200 mg/L initial concentration of furanic and phenolic compounds. Lines represent data fit using the equivalent circuit shown in Figure 3.3A. 94
- Figure 6.1.** Removal of parent compounds (A), current (B) and cathodic H<sub>2</sub> production (C) during MEC bioanode batch runs conducted with SA, VA, HBA, FF, or HMF. Error bars represent standard deviations ( $n = 2$ ). 111
- Figure 6.2.** Biotransformation products of SA (A), VA (B), HBA (C), FF (D), and HMF (E) in MEC bioanode batch runs. Error bars represent standard deviations ( $n = 2$ ). Abbreviations: SA, syringic acid; DHMBA, 3,4-dihydroxy-5-

- methoxybenzoic acid; GA, gallic acid; VA, vanillic acid; PA, protocatechuic acid; HBA, 4-hydroxybenzoic acid; FA, furoic acid; HMF-OH, 2,5-Bis(hydroxymethyl)furan. 116
- Figure 6.3.** Mass spectra of metabolites identified in LC/MS-MS. Blue diamond symbols indicate m/z of precursor ions. 122
- Figure 6.4.** Phenol GC/MS mass spectra in the NIST Standard Reference Database and in sample resulting from the biotransformation of 4-hydroxybenzoic acid (HBA). 123
- Figure 6.5.** Biotransformation products of SA (A), VA (B), HBA (C), FF (D), and HMF (E) in batch runs conducted with the fermentative culture. Error bars represent standard deviations ( $n = 2$ ). Abbreviations: SA, syringic acid; DHMBA, 3,4-dihydroxy-5-methoxybenzoic acid; GA, gallic acid; VA, vanillic acid; PA, protocatechuic acid; HBA, 4-hydroxybenzoic acid; FA, furoic acid; HMF-OH, 2,5-Bis(hydroxymethyl)furan. 126
- Figure 6.6.** Proposed biotransformation pathways of SA (A), VA (B) and HBA (C) under MEC bioanode conditions based on identified metabolites. Solid arrows denote fermentative steps; hollow arrow denotes exoelectrogenic step. Phloroglucinol in brackets is a hypothetical intermediate. 131
- Figure 6.7.** Transhydroxylation of pyrogallol to phloroglucinol and subsequent ring cleavage reactions (Schink et al., 2000). 133
- Figure 6.8.** Removal of catechol and phenol (A) and current production (B) in a MEC bioanode under microaerophilic conditions. 144
- Figure 6.9.** Substrate utilization and partitioning in a MEC bioanode in two sequential sub-processes: fermentation, followed by exoelectrogenesis. 145
- Figure 6.10.** Electron equivalents partitioning to biomass, current and non-exoelectrogenic end products per unit of each compound utilized. 148
- Figure 7.1.** Current (A), total concentration of the parent compounds (B), and transformation products (C) in consecutive batch runs conducted with increasing initial total concentrations of the parent compounds mixture from 0.8 to 8 g/L. Error bars represent stand deviations ( $n = 2$ ). 161
- Figure 7.2.** Current (B) and pH (C) during a control batch run conducted with sequential additions of sodium acetate (NaAc) at concentrations of 0.1 - 10 g/L (A) in the absence of any furanic or phenolic compounds. 162
- Figure 7.3.** Current (A), total concentration of the parent compounds (B), and transformation products (C) in a single batch run conducted with repetitive additions of 0.8 g/L parent compounds mixture. Error bars represent standard deviations ( $n = 2$ ). 167
- Figure 7.4.** Time course of the concentration of individual compounds (A and B) and current (C and D) in batch runs conducted with sequential additions of individual compounds at increasing levels. Broken lines indicate pre-specified, cumulative concentration in the absence of transformation. Error bars represent standard deviations ( $n = 2$ ). Abbreviations: furfural (FF), 5-hydroxymethylfurfural (HMF), syringic acid (SA), vanillic acid (VA), and 4-hydroxybenzoic acid (HBA). 169
- Figure 7.5.** Inhibitory effect of individual furanic (A) and phenolic compounds (B), as well as transformation products (C) on exoelectrogenesis based on current

- decrease in batch runs conducted with sequential additions of individual compounds at increasing levels. Error bars represent standard deviations ( $n = 6$ ). Abbreviations: furfural (FF), 5-hydroxymethyl furfural (HMF), syringic acid (SA), vanillic acid (VA), and 4-hydroxybenzoic acid (HBA). 171
- Figure 7.6.** Bioanode cyclic voltammetry plots under non-inhibited and maximum inhibition conditions in batch runs conducted with individual compounds. Abbreviations: furfural (FF), 5-hydroxymethylfurfural (HMF), syringic acid (SA), vanillic acid (VA), and 4-hydroxybenzoic acid (HBA). 172
- Figure 7.7.** Effect of individual compounds concentrations on the cathodic  $H_2$  production rate in batch runs conducted with sequential additions of individual compounds at increasing concentrations. Error bars represent standard deviations ( $n = 2$ ). Abbreviations: furfural (FF), 5-hydroxymethylfurfural (HMF), syringic acid (SA), vanillic acid (VA), and 4-hydroxybenzoic acid (HBA). 172
- Figure 7.8.**  $IC_{50}$  and log  $Kow$  values of the five parent compounds. Abbreviations: furfural (FF), 5-hydroxymethyl furfural (HMF), syringic acid (SA), vanillic acid (VA), and 4-hydroxybenzoic acid (HBA). 175
- Figure 7.9.** Effect of buffer strength on the extent of inhibition by three phenolic acids. Error bars represent standard deviations ( $n = 3$ ). Abbreviations: syringic acid (SA), vanillic acid (VA), and 4-hydroxybenzoic acid (HBA). 176
- Figure 7.10.** Comparison of observed inhibition by the five parent compounds mixture to the additive inhibition calculated from the individual components based on effect summation, concentration addition and independent action methods. 178
- Figure 7.11.** Recovery of exoelectrogenesis from inhibition by individual furanic (A) and phenolic (B) compounds, as well as transformation products (C) in batch runs conducted with fresh anolyte and 1 g/L NaAc. Current (I) was normalized to that achieved under non- inhibited, control conditions ( $I_{non-in}$ ). Abbreviations: furfural (FF), 5-hydroxymethyl furfural (HMF), syringic acid (SA), vanillic acid (VA), and 4-hydroxybenzoic acid (HBA). 182
- Figure 8.1.** Continuous-flow bioanode MEC. 1, mixture of furanic and phenolic compounds; 2, anolyte; 3, effluent waste; 4, syringe pump; 5, positive displacement pump; 6, glass burette; 7, acid brine displacement reservoir; 8, anode chamber; 9, cation exchange membrane; 10, cathode chamber; 11, potentiostat. 188
- Figure 8.2.** MEC response to various operating conditions. (A) HRT and OLR; (B) applied voltage; (C) current; (D) influent and effluent sCOD. Error bars represent mean values  $\pm$  one standard deviation,  $n = 3$ . 193
- Figure 8.3.** Current (A),  $H_2$  production rate (B) and acetate concentration (C) during stable MEC operation at various HRT, OLR and applied voltage values. Error bars represent mean values  $\pm$  one standard deviation,  $n \geq 4$ . 196
- Figure 8.4.** Concentration of the five parent compounds (A, anode; B, cathode) and detected metabolites (C, anode; D, cathode) during an open circuit batch assay. Error bars represent mean values  $\pm$  one standard deviation,  $n = 2$ . 197

- Figure 8.5.** MEC anode protein concentration normalized to anode empty bed volume at various OLR values and an HRT of 6 h. Error bars represent mean values  $\pm$  one standard deviation,  $n = 2$ . 200
- Figure 8.6.** Soluble COD removed (A) and its components (B) at various OLR values and an HRT of 6 h. 206
- Figure 8.7.** Anode microbial community composition in duplicate at various OLR values and an HRT of 6 h. 210
- Figure 8.8.** Concentration of the furanic and phenolic compounds in anode (solid lines) and cathode (dashed lines) during the abiotic batch assays conducted at 0.6 V and 1.0 V. Error bars represent mean values  $\pm$  one standard deviation,  $n = 2$ . 214
- Figure 8.9.** Current production in the continuous-flow bioanode MEC at 0.8, 1.2 and 3.6 g/L influent concentration of the furanic and phenolic compounds (A) and comparison of extent of inhibition between the batch and continuous-flow operation (B). Error bars represent mean values  $\pm$  one standard deviation ( $n = 6$ ). 217



## SUMMARY

Lignocellulosic biomass is an abundant, renewable energy source for biofuel production, providing an important alternative to fossil fuels. However, the pretreatment of biomass for biofuel production produces furanic and phenolic compounds, contributing to the corrosiveness, instability, and toxicity of various biomass-derived streams, thus presenting a significant challenge in downstream processes and waste disposal. Microbial electrolysis cell (MEC) is an emerging bioelectrochemical technology, which converts organic wastes in the bioanode and produces H<sub>2</sub> in the abiotic cathode. Integration of MEC in biofuel production not only offers an alternative method for waste handling, but also production of renewable H<sub>2</sub> for the downstream hydrogenation of biomass-derived bio-oil, thus reducing the external H<sub>2</sub> supply currently derived from natural gas (i.e., methane), a non-renewable fossil fuel. Considering that furanic and phenolic compounds are among the most problematic components of biomass-derived waste streams, it is critical to understand the biotransformation of these compounds in MEC for H<sub>2</sub> production.

This study focused on two furanic (furfural, FF; 5-hydroxymethyl furfural, HMF) and three phenolic (syringic acid, SA; vanillic acid, VA; 4-hydroxybenzoic acid, HBA) compounds, commonly produced during biomass pretreatment. FF and HMF are predominant furan derivatives from biomass carbohydrates, while SA, VA, and HBA represent phenolic acids derived from three major lignin units (syringyl, guaiacyl and *p*-hydroxyphenyl). The objectives of this study were to: a) achieve efficient conversion of the selected furanic and phenolic compounds with H<sub>2</sub> production in a MEC; (b) elucidate the metabolic fate of the furanic and phenolic compounds in the MEC bioanode; (c)

assess the inhibitory effect of the furanic and phenolic compounds on MEC bioanode microbial processes; and (d) delineate the specific role of microorganisms in different physiological groups in the MEC bioanode.

The five furanic and phenolic compounds as a mixture were utilized as the sole carbon and energy source in the MEC bioanode, resulting in cathodic H<sub>2</sub> production at promising Coulombic efficiency (44 – 69%) and H<sub>2</sub> yield (26 - 42%). MEC batch runs conducted with individual compounds showed that the two furanic compounds (FF and HMF) were more favorable substrates for use in the bioanode, contributing to the cathodic H<sub>2</sub> production to a higher degree than the three phenolic compounds (SA, VA, and HBA).

The furanic and phenolic compounds were not directly utilized by bioanode exoelectrogens. Instead, fermentation of the parent compounds first took place, resulting in mainly acetate, which was used in the subsequent exoelectrogenesis. The fermentation proceeded independently from the rate and extent of exoelectrogenesis, but the extent of fermentative transformation controlled the exoelectrogenic activity. The analysis of phenolic metabolites revealed different extent of biotransformation of SA, VA and HBA, attributed to the difference in their number and position of hydroxy (–OH) and methoxy (–O–CH<sub>3</sub>) substituents. The aromatic ring of SA was cleaved via the phloroglucinol pathway resulting in acetate production, which was further used by exoelectrogens, whereas the biotransformation of VA and HBA resulted in the production of persistent aromatic metabolites, i.e., catechol and phenol, respectively.

The furanic and phenolic compounds at high concentrations inhibited exoelectrogenesis, but not fermentation, primarily caused by the parent compounds, as

opposed to their transformation products. The IC<sub>50</sub> of individual compounds determined in inhibition batch assays was 2.7 - 3.0 g/L for the furanic compounds and 1.9 - 2.1 g/L for the phenolic compounds, suggesting that the phenolic compounds were more inhibitory than the furanic compounds. An additive, but not synergistic inhibitory effect on exoelectrogenesis was observed with the mixture of the five parent compounds.

The performance of a continuous-flow bioanode MEC was evaluated at various hydraulic retention times (HRTs, 6 – 24 h), organic loading rates (OLRs, 3.1 – 4.9 g COD/L-d), and applied voltage (0.6 and 1.0 V). At a low OLR, all HRTs tested resulted in complete transformation of the parent furanic and phenolic compounds. An increased H<sub>2</sub> production rate was achieved by increasing the OLR or the applied voltage, but was further limited by the rate of exoelectrogenesis. The trade-offs of using high OLR and applied voltage were lower biotransformation extent of the parent compounds, lower MEC effluent quality, and lower overall energy efficiency.

The MEC anode biofilm microbial community consisted of three major phyla: *Proteobacteria* (68 – 85%), *Bacteroidetes* (2-17%), and *Firmicutes* (9-12%).

Phylogenetic analysis identified species closely related to putative exoelectrogens, furanic and phenolic degraders, and other fermentative bacteria, supporting the observed fermentative/exoelectrogenic biotransformation in the MEC bioanode. Hydrogenotrophic methanogens were present when a high OLR was applied, diverting the electron flow from exoelectrogenesis to methanogenesis. Maintaining a balanced growth between exoelectrogenic and non-exoelectrogenic species is critical for achieving high MEC performance.

This research is the first systematic, comprehensive study on the metabolic fate, contribution to cathodic H<sub>2</sub> production, and inhibitory effect of furanic and phenolic compounds in MECs. Results of this study can be used to guide the design and optimization of MECs converting biomass-derived waste streams to renewable H<sub>2</sub>. Reducing the discharge of organic wastes and minimizing external H<sub>2</sub> supply, currently derived from natural gas, will promote carbon-neutral, sustainable biofuel production.

# CHAPTER 1

## INTRODUCTION

### 1.1 Preface

Lignocellulosic biomass is an abundant, renewable energy source for biofuel production, providing an important alternative to fossil fuels. During the pretreatment of lignocellulosic biomass, furanic and phenolic compounds are produced from the decomposition of biomass carbohydrates and lignin, presenting a significant challenge in downstream processes. Furanic and phenolic compounds contribute to the instability and corrosiveness of pyrolysis-derived bio-oil, as well as the inhibitory effect of biomass hydrolysates on microorganisms involved in dark fermentation for H<sub>2</sub> and ethanol production (Jones et al., 2009; Monlau et al., 2014; Piotrowski et al., 2014). Due to the cytotoxic and mutagenic effects of furanic and phenolic compounds (Almeida et al., 2009), the disposal of biomass-derived waste streams bearing these compounds has raised environmental concerns.

Microbial electrolysis cell (MEC) is an emerging bioelectrochemical technology, which converts organic wastes in the bioanode and produces H<sub>2</sub> in the abiotic cathode (Liu et al., 2005). In a MEC, organic compounds are utilized as substrates (i.e., as carbon source and electron donors) by the bioanode microorganisms. During microbial metabolism, electrons are extracted from the organic compounds and then transferred to the anode electrode. With a small voltage supply, the electrons are transferred via an electric circuit to the cathode where reduction of protons takes place (usually abiotically) with the production of H<sub>2</sub>. Integration of MEC in biofuel production offers not only an

alternative method for waste handling, but also renewable H<sub>2</sub> for use in the downstream hydrogenation of biomass-derived bio-oil, thus reducing the external H<sub>2</sub> supply currently derived from natural gas (i.e., methane), a non-renewable fossil fuel. The fact that the MEC technology can achieve simultaneous waste treatment and renewable H<sub>2</sub> production, makes it more advantageous than existing methods used to deal with furanic and phenolic compounds in biomass-derived streams, such as solvent extraction and use of genetically engineered, tolerant microorganisms in dark fermentation (Piotrowski et al., 2014).

Several studies have demonstrated the use of lignocellulosic effluent, refinery wastewater and switchgrass-derived bio-oil aqueous phase in MECs for H<sub>2</sub> production (Lalaurette et al., 2009; Lewis et al., 2015; Ren et al., 2013b). Such feedstocks contain readily biodegradable carbohydrates (e.g., sugars and acetic acid) in addition to furanic and phenolic compounds. However, the fate and effect of furanic and phenolic compounds in MECs, which are among the most problematic components in the biomass-derived streams, have been poorly understood. It remains unclear whether furanic and phenolic compounds can effectively contribute to MEC H<sub>2</sub> production. Very limited information is available on the biotransformation of furanic and phenolic compounds in bioanodes, e.g., pathways, extent, and responsible microbial species/processes. Potential inhibitory effect of furanic and phenolic compounds on vital microbial processes (e.g., fermentation, exoelectrogenesis) in MEC bioanodes also needs to be assessed.

This study investigated two furanic (furfural, FF; 5-hydroxymethyl furfural, HMF) and three phenolic (syringic acid, SA; vanillic acid, VA; 4-hydroxybenzoic acid, HBA) compounds commonly found in biomass-derived streams (Borole et al., 2013;

Klinke et al., 2004b; Ren et al., 2016). FF and HMF are predominant furan derivatives from biomass carbohydrates, while SA, VA, and HBA represent phenolic acids derived from three major lignin units (syringyl, guaiacyl and *p*-hydroxyphenyl) (Klinke et al., 2004b; Monlau et al., 2014). The fate and effect of the selected furanic and phenolic compounds delineated in this study provide currently lacking information that can be used to understand and improve MEC applications for converting biomass-derived waste streams to renewable H<sub>2</sub>.

## 1.2 Research Objectives

The overall goal of this study was to produce H<sub>2</sub> through the biotransformation of the two furanic (FF and HMF) and three phenolic (SA, VA, and HBA) compounds using MEC technology. The specific research objectives were to:

1. Achieve efficient conversion of the selected furanic and phenolic compounds with H<sub>2</sub> production in a MEC.
2. Elucidate the metabolic fate of the furanic and phenolic compounds in the MEC bioanode.
3. Assess the inhibitory effect of the furanic and phenolic compounds on MEC bioanode microbial processes.
4. Delineate the specific role of microorganisms in different physiological groups in the MEC bioanode.

### 1.3 Motivation and Significance

The use of lignocellulosic biomass for energy production has significant environmental advantages over fossil fuels, given the increasing concerns of CO<sub>2</sub> emissions, climate change, and depletion of fossil fuel reserves. Pyrolysis is a high-temperature (300-600 °C) process widely utilized to produce hydrocarbon fuels from lignocellulosic biomass (Jones et al., 2009). Due to the high oxygen content of biomass, downstream hydrogenation is required to deoxygenate the pyrolysis-derived bio-oil, producing hydrocarbon fuels with high heating values, as well as reducing the bio-oil corrosiveness, while enhancing its stability (Jones et al., 2009). The hydrogenation process uses large quantities of H<sub>2</sub>, currently generated by reforming natural gas (i.e., methane), a non-renewable fossil fuel (Jones et al., 2009). Another challenge in pyrolysis of lignocellulosic biomass is that the pyrolysis bio-oil is a mixture of aqueous and organic phases, due to the high water content of biomass (Imam and Capareda, 2012; Park et al., 2016). After separation, only the organic phase is used for fuel production, whereas the aqueous phase accounting for up to 70% of the bio-oil, is a low-value product, commonly regarded as waste needing to be further managed and then disposed of (Imam and Capareda, 2012). Using MEC technology to convert the bio-oil aqueous phase to H<sub>2</sub> addresses both issues of waste handling and renewable H<sub>2</sub> supply, improving the economics and sustainability of biofuel production. The bio-oil aqueous phase contains readily biodegradable sugars and volatile fatty acids, but also significant amounts of furanic and phenolic compounds (Lewis et al., 2015; Ren et al., 2016). Thus, it is critical to understand the biotransformation of furanic and phenolic compounds in the MEC bioanode.



MEC is one type of bioelectrochemical systems (BESs), sharing the same anode principles and processes as other BESs, such as microbial fuel cell (MFC)(Wang and Ren, 2013). In early BES studies, acetate was the most commonly used bioanode substrate (Wang and Ren, 2013). As BES applications are expanding, an increasing number, variety, and complexity of compounds are being used in bioanodes, including chlorinated compounds (Pham et al., 2009), proteins (Lu et al., 2010), azo dyes (Fernando et al., 2013), carbohydrates (Montpart et al., 2015), fermentation effluents and domestic, industrial and food-processing wastewaters (Kadier et al., 2014). However, our understanding of biotransformation pathways of fermentable, organic compounds in bioanodes is still limited. Results of this study focusing on furanic and phenolic compounds can shed light on metabolic fate and limiting steps in the biotransformation of complex organic compounds in bioanodes, which are directly related to the overall performance of BESs.

This research is the first systematic, comprehensive study on the metabolic fate, contribution to cathodic H<sub>2</sub> production, and inhibitory effect of furanic and phenolic compounds in MECs. Results of this study can be used to guide the design and optimization of MECs converting biomass-derived waste streams to renewable H<sub>2</sub>. Reducing the discharge of organic wastes and minimizing external H<sub>2</sub> supply, currently derived from natural gas, will promote carbon-neutral, sustainable biofuel production.

## CHAPTER 2

### BACKGROUND

#### 2.1 Furanic and Phenolic Compounds

##### 2.1.1 Source

Lignocellulosic biomass is composed of three major types of polymers: cellulose, hemicellulose, and lignin. During thermal or thermochemical pretreatment of lignocellulosic biomass, which is commonly applied in biofuel production, the biomass carbohydrate polymers (i.e., cellulose, hemicellulose) and lignin degraded, releasing sugar monomers, furanic compounds, phenolic compounds, and weak acids. Furanic compounds are generally formed from sugar degradation during the thermochemical treatment of lignocellulosic biomass (Jönsson et al., 2013; Monlau et al., 2014). The most predominant biomass-derived furanic compounds are furfural (FF) and 5-hydroxymethyl furfural (HMF), derived from pentose and hexose, respectively, via a number of pathways (Rasmussen et al., 2014).

Phenolic compounds, including alcohols, aldehydes and acids, are mainly generated from the degradation of lignin polymers (Jönsson et al., 2013; Klinke et al., 2004b; Monlau et al., 2014). This study focuses on phenolic acids, because they partially result in the corrosiveness of biomass pretreatment effluents. Syringic acid (SA), vanillic acid (VA), and 4-hydroxybenzoic acid (HBA) are generated from the degradation of syringyl (S), guaiacyl (G), and *p*-hydroxyphenyl (H) units of lignin polymers, respectively, and thus have different degrees of methoxylation (Klinke et al., 2004b). The types of phenolic compounds formed during lignocellulosic biomass breakdown are

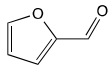
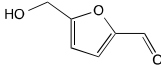
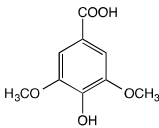
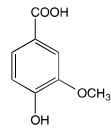
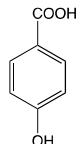
highly dependent on the type of biomass (i.e., the ratio of H/G/S units in lignin) and the pretreatment methods (Klinke et al., 2004b).

FF, HMF, SA, VA, and HBA are among the most commonly found furanic and phenolic compounds in lignocellulosic biomass hydrolysates (Klinke et al., 2004b), pyrolysates (Borole and Mielenz, 2011), and biorefinery wastewater (Borole et al., 2013). Depending upon the type of biomass, pretreatment method and conditions, furanic compounds are present at a total concentration up to 5 g/L, while phenolic compounds are present at a total concentration up to 3 g/L (Mills et al., 2009).

#### 2.1.2 Chemical, Physicochemical and Toxicological Properties

The chemical and physicochemical properties of the selected furanic and phenolic compounds are summarized in Table 2.1. The five compounds are soluble in water (1.5-364 g/L at 25°C), not volatile (Henry's law constant =  $10^{-14}$  -  $10^{-6}$  atm-m<sup>3</sup>/mol), and have a low hydrophobicity (log K<sub>ow</sub> = -0.09 to 1.58). Therefore, the selected furanic and phenolic compounds are widely found in biomass hydrolysates and aqueous phase of pyrolysates. The furanic and phenolic compounds have relatively a high oxygen content, thus contributing to a significant consumption of H<sub>2</sub> in the downstream hydrogenation process used for bio-oil upgrade. The acidity of the phenolic compounds (pK<sub>a</sub> < 4.5) contributes to the corrosiveness of the bio-oil, which makes storage, transport and downstream processing of biomass-derived streams problematic. The standard potential at pH 7.0 (E<sup>0'</sup>) of the five compounds is from -0.388 to -0.303 V compared to the E<sup>0'</sup> value of -0.414 V for proton reduction to H<sub>2</sub>. Thus, an external voltage supply is needed to electrochemically produce H<sub>2</sub> from these compounds.

**Table 2.1.** Chemical and physicochemical properties of the furanic and phenolic compounds used in this study.

Property	Furfural (FF)	5-Hydroxy-methyl furfural (HMF)	Syringic acid (SA)	Vanillic acid (VA)	4-Hydroxy-benzoic acid (HBA)
CAS number	98-01-1	67-47-0	530-57-4	121-34-6	99-96-7
Structure					
Molecular formula	C <sub>5</sub> H <sub>4</sub> O <sub>2</sub>	C <sub>6</sub> H <sub>6</sub> O <sub>3</sub>	C <sub>9</sub> H <sub>10</sub> O <sub>5</sub>	C <sub>8</sub> H <sub>8</sub> O <sub>4</sub>	C <sub>7</sub> H <sub>6</sub> O <sub>3</sub>
Molecular Weight	96.08	126.11	198.17	168.15	138.12
logK <sub>ow</sub>	0.41 <sup>a</sup>	-0.09 <sup>b</sup>	1.04 <sup>a</sup>	1.43 <sup>a</sup>	1.58 <sup>a</sup>
Henry's constant (atm·m <sup>3</sup> /mol, 25 °C) <sup>b</sup>	3.8×10 <sup>-6</sup>	5.4×10 <sup>-10</sup>	4.0×10 <sup>-14</sup>	4.6×10 <sup>-12</sup>	5.6×10 <sup>-12</sup>
Water solubility (g/L, 25 °C)	74 <sup>c</sup>	7×10 <sup>8</sup> <sup>b</sup>	1.5 <sup>b</sup>	1.5 <sup>d</sup>	5.0 <sup>d</sup>
pK <sub>a</sub>	NA <sup>e</sup>	13.65 <sup>f</sup>	3.93 <sup>f</sup>	4.16 <sup>f</sup>	4.38 <sup>f</sup>
G <sub>f</sub> <sup>0</sup> (kJ/mol)	-102.87 <sup>g</sup>	-260.41 <sup>h</sup>	-583.95 <sup>h</sup>	-494.08 <sup>g</sup>	-416.5 <sup>g</sup>
E <sup>0'</sup> (V) <sup>i</sup>	-0.386	-0.388	-0.367	-0.341	-0.303
ThOD (g O <sub>2</sub> /g) <sup>j</sup>	1.67	1.57	1.45	1.52	1.62
Electron equivalents (e <sup>-</sup> mol/mol)	20	24	36	32	28

<sup>a</sup> Data from Hansch et al. (1995); <sup>b</sup> Predicted by EPISuite (EPA, 2012); <sup>c</sup> Data from Yalkowsky and He (2003); <sup>d</sup> Data from Yalkowsky and Dannenfelser (1992); <sup>e</sup> NA, not available; <sup>f</sup> Predicted by (ChemAxon); <sup>g</sup> Data from Yaws (2003); <sup>h</sup> Values calculated based on the group contribution method (Mavrovouniotis, 1990); <sup>i</sup> Half reactions with HCO<sub>3</sub><sup>-</sup> as the oxidized species at pH 7.0, equations listed in Table 2.2; <sup>j</sup> ThOD, theoretical oxygen demand

**Table 2.2.** Half reduction reactions and standard potentials of the five compounds.

Reduced compound	Reaction	$E^{\circ'}$ , V
Furfural	$5 \text{ HCO}_3^- + 25 \text{ H}^+ + 20 \text{ e}^- \rightarrow \text{C}_5\text{H}_4\text{O}_2 + 13 \text{ H}_2\text{O}$	-0.386
5-Hydroxymethylfurfural	$6 \text{ HCO}_3^- + 30 \text{ H}^+ + 24 \text{ e}^- \rightarrow \text{C}_6\text{H}_6\text{O}_3 + 15 \text{ H}_2\text{O}$	-0.388
Syringic acid	$9 \text{ HCO}_3^- + 45 \text{ H}^+ + 36 \text{ e}^- \rightarrow \text{C}_9\text{H}_{10}\text{O}_5 + 22 \text{ H}_2\text{O}$	-0.367
Vanillic acid	$8 \text{ HCO}_3^- + 40 \text{ H}^+ + 32 \text{ e}^- \rightarrow \text{C}_8\text{H}_8\text{O}_4 + 20 \text{ H}_2\text{O}$	-0.341
4-Hydroxybenzoic acid	$7 \text{ HCO}_3^- + 35 \text{ H}^+ + 28 \text{ e}^- \rightarrow \text{C}_7\text{H}_6\text{O}_3 + 18 \text{ H}_2\text{O}$	-0.303

Furanic and phenolic compounds are among the most toxic components of biomass hydrolysates. Many studies have found furanic and phenolic compounds to be highly inhibitory to bacteria and yeasts involved in dark fermentation for H<sub>2</sub> and ethanol production. Typical concentrations of these compounds found in hydrolysate can result in significant or even complete inhibition of H<sub>2</sub> and ethanol production (Cao et al., 2010; Palmqvist and Hahn-Hägerdal, 2000; Quéméneur et al., 2012). In general, any of these compounds at a concentration higher than 1.5 g/L can significantly inhibit the activity of H<sub>2</sub>- and ethanol- producing microorganisms, depending on the tolerance of the specific microbial culture used in dark fermentation (Klinke et al., 2004b; Monlau et al., 2014).

Modes of inhibition of furanic and phenolic compounds have also been extensively studied in H<sub>2</sub> and ethanol producing microorganisms in dark fermentation. FF and HMF are known to inhibit glycolytic enzymes essential to the central metabolism of H<sub>2</sub> and ethanol fermenters (Almeida et al., 2009). They also lead to significant NADH consumption used in reductive transformations, thus decreasing intracellular levels of NADH (Ask et al., 2013). FF has been reported to damage yeast DNA (Almeida et al., 2009). A combination of these inhibitory effects of furanic compounds results in reduced

growth rates and fermentative activity of H<sub>2</sub>- and ethanol-producing microorganisms (Almeida et al., 2009). In contrast to FF and HMF, which primarily target intracellular sites, phenolic compounds compromise cell membrane integrity and functionality by partitioning into cell membranes, changing membrane permeability and fluidity (Heipieper et al., 1994; Monlau et al., 2014; Palmqvist and Hahn-Hägerdal, 2000). To overcome the toxicity of furanic and phenolic compounds, physical and/or chemical removal, as well as microbial and enzymatic processes have been explored. However, these methods have the trade-offs of lowering biofuel yield and economics, and they do not lessen the challenge of downstream wastewater treatment (Piotrowski et al., 2014).

There is very limited information on the inhibitory effect of furanic and phenolic compounds on the bioanode microbial activity. Catal et al. (2008) reported that syringaldehyde, *trans*-4-hydroxy-3-methoxy and 4-hydroxy cinnamic acids at a concentration above 20 mM, as well as benzyl alcohol and acetophenone at 0.2 mM, severely inhibited electricity generation from glucose using a microbial fuel cell (MFC).

### 2.1.3 Biotransformation Potential

Biodegradation of FF, HMF, SA, VA and HBA was observed in several studies under both aerobic and anaerobic conditions, but their aerobic biotransformation pathways have been better understood than anaerobic pathways. Under aerobic conditions, both FF and HMF were transformed to 2-furoic acid as an important intermediate, which was then activated by CoA thioester addition for ring cleavage, resulting in 2-oxoglutarate entering the tricarboxylic acid cycle (Koopman et al., 2010; Wierckx et al., 2011a). Most furanic compound degrading microorganisms characterized to date are aerobic Gram-negative

bacteria, belonging to a relatively small number of genera. Aerobic biotransformation of SA and VA was initiated with *O*-demethylation, resulting in central intermediates of protocatechuate and 3-*O*-methylgallate, respectively, which were subject to ring cleavage in a further dioxygenase-dependent reaction (Abe et al., 2005; Kasai et al., 2004). HBA was also converted to protocatechuate, but with a monooxygenase, prior to the aromatic ring cleavage (Fuchs et al., 2011).

Because this study focused on oxygen-free, bioanode conditions, anaerobic biotransformation pathways of the furanic and phenolic compounds are more relevant. Reports on anaerobic degradation of FF are scarce. Only two microorganisms, both *Desulfovibrio* strains, are known to convert FF anaerobically to 2-furoic acid and/or furfuryl alcohol, then eventually to acetate (Boopathy and Daniels, 1991; Brune et al., 1983; Folkerts et al., 1989). HMF was anaerobically transformed to 2,5-bis(hydroxymethyl)furan (HMF-OH) by *Clostridium acetobutylicum* and enteric bacteria via a 2e<sup>-</sup> reduction (Boopathy et al., 1993; Zhang et al., 2012). Several studies reported SA degradation in mixed cultures containing nitrate reducers, sulfate reducers, fermentative acetogens, and/or methanogens. SA was sequentially *O*-demethylated by the acetogens; the aromatic ring was mineralized by sulfate and nitrate reducers, or fermented to acetate by the fermenters (Kreikenbohm and Pfennig, 1985; Phelps and Young, 1997; Sembiring and Winter, 1990). VA was reported to be transformed to protocatechuate and/or catechol under fermentative/methanogenic conditions, via a similar *O*-demethylation reaction as in the case of SA transformation (Bache and Pfennig, 1981; Kaiser and Hanselmann, 1982; Taylor, 1983). Subsequent aromatic ring cleavage of VA, with the production of CH<sub>4</sub> and CO<sub>2</sub>, was reported in one study (Healy and

Young, 1979). During the anaerobic biotransformation of HBA, benzoic acid and phenol were usually observed as dehydroxylation and decarboxylation products, respectively (Kuhn et al., 1989; Tschech and Schink, 1986; Zhang and Wiegel, 1990). Further degradation of HBA to CH<sub>4</sub> and CO<sub>2</sub> was also reported (Healy and Young, 1979; Kuhn et al., 1989).

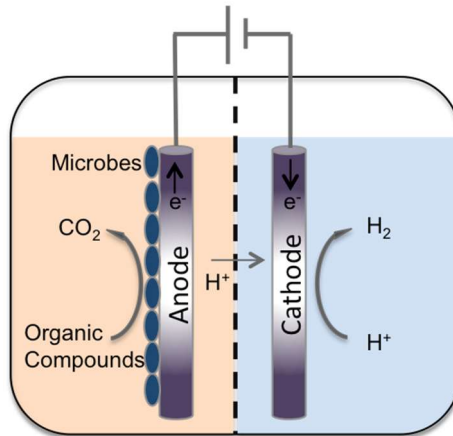
Although several recent studies have used furanic and phenolic compounds in bioanodes of bioelectrochemical systems, the biodegradation extent and biotransformation pathways were not examined (Borole et al., 2009; Catal et al., 2008; Friman et al., 2013; Luo et al., 2009; Song et al., 2014). Thus, our understanding of the biotransformation of these compounds under bioanode conditions is very limited.

## **2.2 Microbial Electrolysis Cell**

The production of H<sub>2</sub> in a MEC is achieved by combining bacterial metabolism with electrochemistry. Essential components of a typical MEC include a bioanode, a platinum-coated carbon cathode, a cation exchange membrane, and an electric circuit with an external voltage supply (Figure 2.1). Two half reactions take place in the anode and cathode, respectively. The half reaction in the anode is the oxidation of the organic substrate through microbial metabolism, in which the organic substrate is the electron donor and electrode is the electron acceptor. In the absence of an external electron acceptor, microbes release the electrons to the anode electrode and perform “anode-respiration”. The cathode half reaction is proton reduction to H<sub>2</sub> with electrons transferred from the anode to the cathode electrode. This half reaction occurs abiotically on the surface of the cathode electrode. For the two half reactions to combine, the protons



and electrons are transported from the anode to the cathode through a cation exchange membrane and an electrical circuit, respectively. A small voltage input ( $> 0.3$  V) is also required for  $H_2$  production in the MEC cathode compartment (Liu et al., 2005; Rozendal et al., 2006).



**Figure 2.1.** Schematic of a MEC resulting in  $H_2$  production.

### 2.2.1 Thermodynamics

The requirement of an external voltage supply distinguishes the MEC from other bioelectrochemical systems, which is attributed to the thermodynamic threshold of  $H_2$  evolution. For a reaction to occur spontaneously, the Gibbs free energy of the reaction ( $\Delta G$ ) must be negative. The Gibbs free energy can be expressed in the form of the reduction potential of a reaction ( $\Delta E$ ), as follows:

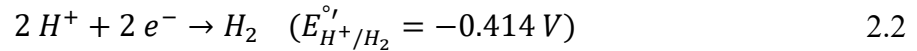
$$\Delta G = -nF\Delta E \quad 2.1$$

where  $n$  is the number of electrons involved in the reaction,  $F$  is Faraday's constant (96485 C/e<sup>-</sup> mol), and  $\Delta E$  is the reduction potential of a reaction determined by the

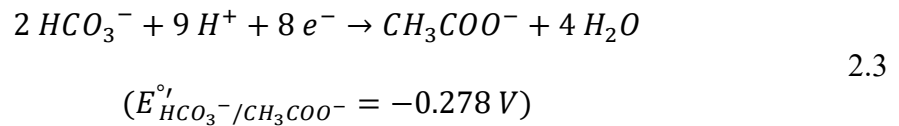
reduction potential of the reduction and oxidation half reactions (i.e.,  $\Delta E = E_{red\ rxn} - E_{ox\ rxn}$ ).

A negative  $\Delta G$  value requires a positive  $\Delta E$  value (i.e.,  $E_{red\ rxn} > E_{ox\ rxn}$ ).

However, the reduction half reaction in the MEC is proton reduction to  $H_2$  (Equation 2.2), which has a low standard reduction potential ( $E^{\circ'} = -0.414\ V$ ,  $25\ ^\circ C$ ,  $1\ bar$ ,  $pH\ 7.0$ ).



Acetate is a common electron donor used in MEC anodes. The half reaction of acetate oxidation, written as the reduction half reaction, is as follows:

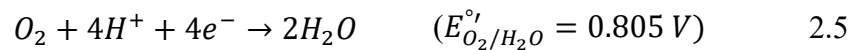


Using acetate as an example, the standard potential of the overall reaction ( $\Delta E^{\circ'}$ ) in a MEC can be calculated as follows:

$$\Delta E^{\circ'} = E_{H^+/H_2}^{\circ'} - E_{HCO_3^-/CH_3COO^-}^{\circ'} = -0.136\ V \quad 2.4$$

Therefore, a minimum voltage input of  $0.136\ V$  is required to result in a positive  $\Delta E^{\circ'}$  (i.e.,  $\Delta G^{\circ'} < 0$ ). In practice, a higher voltage ( $0.3 - 1.0\ V$ ) is usually applied due to energy loss in the system (Logan et al., 2008).

Water electrolysis for  $H_2$  production involves the same reduction half reaction shown in Equation 2.2, but a different oxidation half reaction, as follows:

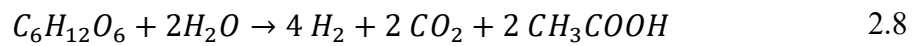
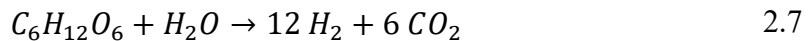


The standard potential of the overall reaction in water electrolysis can be calculated as follows:

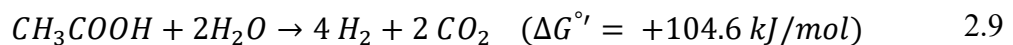
$$\Delta E^{\circ'} = E_{H^+/H_2}^{\circ'} - E_{O_2/H_2O}^{\circ'} = -1.219 V \quad 2.6$$

Thus, the voltage input for water electrolysis is almost an order of magnitude higher than that for microbial electrolysis. In practice, water electrolysis usually need a voltage input greater than 1.7 V (Logan and Rabaey, 2012).

MEC is an electrically driven H<sub>2</sub> evolution process, which is distinct from fermentation. A significant advantage of MEC over fermentation for H<sub>2</sub> production is that thermodynamic limitations in converting organic compounds to H<sub>2</sub> can be overcome by the applied voltage, resulting in higher H<sub>2</sub> yield. For instance, the stoichiometric H<sub>2</sub> potential of glucose is 12 mol H<sub>2</sub>/mol glucose (Equation 2.7), but microbial fermentation of glucose results in only 4 mol H<sub>2</sub>/mol glucose, if acetate is produced (Equation 2.8).



Because further fermentation of acetate to H<sub>2</sub> is not thermodynamically favorable (Equation 2.9), the theoretical maximum H<sub>2</sub> production is 4 mol H<sub>2</sub>/mol glucose, while the remaining 8 mol H<sub>2</sub>/mol glucose potential is not achievable via fermentation.

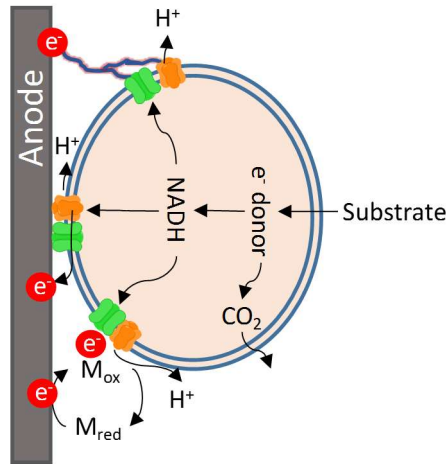


In the case of MEC, because an external voltage is added to overcome such thermodynamic limit for H<sub>2</sub> production, the theoretical upper H<sub>2</sub> yield in a MEC is thus 12 mol H<sub>2</sub>/mol glucose, i.e., 3-fold higher than that of fermentation.

### 2.2.2 Exoelectrogenesis

Exoelectrogenesis is a key microbial process in bioanodes to result in electroactivity (Figure 2.2). The first step in exoelectrogenesis is intracellular utilization of substrate,

during which electrons were transferred from the electron donor(s) (e.g., acetate) to intracellular reducing power (e.g., NADH). The second step is extracellular electron transfer (EET). The NADH or other intracellular electron carriers formed in the first step, pass through cytochromes in the cell membrane and eventually transfer the electrons to outer membrane proteins, which are able to deliver the electrons to the anode electrode via different EET mechanisms (Nealson and Rowe, 2016; Torres et al., 2010).



**Figure 2.2.** Schematic of exoelectrogenesis using direct and indirect extracellular electron transfer mechanisms.

Bacteria are known to use two distinct EET mechanisms (Nealson and Rowe, 2016), as shown in Figure 2.2. The first EET mechanism is direct electron transfer using outer-membrane c-type cytochromes or nanowires. Outer-membrane c-type cytochromes are redox proteins, which can directly interact with a solid electrode surface (Magnuson et al., 2001). Bacteria using outer-membrane c-type cytochromes for EET require direct contact with the electrode, thus their growth is restricted to a short distance from the electrode. In contrast, bacterial nanowires, which are nanometer scale diameter and micrometer scale length proteinaceous filaments extending from the cell membrane to the

electrode surface, enable long-distance electron transfer (Gorby et al., 2006; Reguera et al., 2005). Bacterial nanowires were first characterized as metal-like conductor upon discovery (Gorby et al., 2006; Malvankar et al., 2011), but recent studies claim that nanowires are extensions of the outer membrane and periplasm comprised of multiheme cytochromes, transferring electrons on redox basis, as opposed to having metal-like conductivity (Pirbadian et al., 2014; Snider et al., 2012). The second EET mechanism is indirect electron transfer via redox-active, organic electron shuttles secreted by exoelectrogens, including flavins, phenazines, and quinones (Marsili et al., 2008; Newman and Kolter, 2000; Rabaey et al., 2005). The electron shuttling compounds, carrying electrons from the bacteria, diffuse to the electrode surface where they discharge the electrons and are oxidized. The electron shuttles in the oxidized form then diffuse back to the cells to receive electrons and get reduced again. Thus, the electron shuttling compounds can be repeatedly used without being consumed. Besides the diffusive transport, electron shuttling compounds can also mediate EET by bounding to membrane proteins (Marsili et al., 2008; Okamoto et al., 2014).

Exoelectrogens include phylogenetically diverse microorganisms in *Alpha-*, *Beta-*, *Gamma-*, and *Delta-Proteobacteria*, *Firmicutes*, *Acidobacteria* phyla, and a yeast (Logan, 2009). Most exoelectrogenic bacteria are Gram-negative belonging to the phylum *Proteobacteria*, including the well-studied *Geobacter sulfurreducens* and *Shewanella oneidensis*. Other frequently identified exoelectrogens are *Pseudomonas aeruginosa*, *Rhodospirillum rubrum*, *Escherichia coli*, *Clostridium butyricum* EG3, and *Thermincola* spp. (Logan, 2009; Zhi et al., 2014). Most of these species are known to utilize solid Fe (III) as an electron acceptor, and they are anaerobic, Gram-negative,

oligotrophs (Torres et al., 2010). Some exoelectrogens can use more than one EET mechanisms. However, it is not obvious under which conditions an EET mechanism is more important than the other. For example, *Shewanella oneidensis* is capable of producing electron shuttles (Marsili et al., 2008) and nanowires (Gorby et al., 2006). *Geobacter sulfurreducens* uses nanowires for long-distance electron transfer (Malvankar et al., 2011), but it also secretes and uses bound electron mediators (Okamoto et al., 2014).

Exoelectrogens use a limited number of substrates, acetate being the most common among different strains, although H<sub>2</sub>, lactate, formate, and propionate are also possible (Lovley et al., 1993; Speers and Reguera, 2012). Thus, when bioanode substrates are complex, fermentable organic compounds, which are expected in practical MEC applications, a fermentative process is required to break down the complex compounds to mainly acetate, which can then be used by exoelectrogens (Kiely et al., 2011b; Wang and Ren, 2013). Bioanode syntrophic associations are similar to those encountered in anaerobic digestion, where complex substrates are fermented to simple molecules for their use in methanogenesis. Diverse microbial communities with exoelectrogenic and non-exoelectrogenic species are usually found in bioanodes fed with complex substrates. Studies have reported species and activities associated with sulfate reduction, methanogenesis, and fermentation in bioanodes (Ishii et al., 2013; Lu et al., 2012). A diverse community has the potential to use a wide variety of substrates, but the presence of sulfate-reducing and methanogenic pathways diverts electrons away from the anode and thus lowers the MEC Coulombic efficiency (Borole et al., 2011).

### 2.2.3 MEC Performance and Anode Substrates

The performance of MEC is typically reported using both rate and efficiency parameters. Rate parameters include current density and H<sub>2</sub> production rate. The current density can be expressed as per surface area of the anode electrode or the ion exchange membrane, or per reactor liquid volume. The H<sub>2</sub> production rate is proportional to the current density. In addition to rate parameters, several efficiency parameters are used to evaluate MEC performance. Chemical oxygen demand (COD) removal efficiency indicates the extent of degradation of anode substrates. Coulombic efficiency characterizes the efficiency of electron transfer from the degrade substrate to the anode electrode (i.e., electrical circuit). H<sub>2</sub> yield is positively correlated to the Coulombic efficiency. Energy efficiency evaluates the energy recovery by the H<sub>2</sub> production from the chemical and electric energy input (Logan et al., 2008). Calculations of the above-mentioned parameters are included in Chapter 3, Section 3.3.

MEC performance is collectively affected by a number of factors, such as reactor material and configuration, bioanode microbial community, and operational conditions (Logan et al., 2015). In addition, the performance of MECs fed with different anode substrates can vary significantly. As shown in Table 2.3, MECs fed with acetate usually achieve the highest H<sub>2</sub> production rate and yield among all anode substrates. The performance of MEC fed with more complex compounds and wastewater streams is related to the biodegradability and concentration of the feedstock. Although reactor size, electrode material, and applied voltage are not included in Table 2.3, these factors can significantly affect MEC performance. For example, small-size reactors (< 50 mL) with a relatively high voltage (> 0.6 V) generally result in higher H<sub>2</sub> production rate.

**Table 2.3.** Performance of MECs fed with various types of substrates.

Substrate	Specific compounds or source	H <sub>2</sub> production rate (L/L-d)	H <sub>2</sub> yield <sup>a</sup> (%)	References
Acetate		1.1-6.3	90 - 91	(Tartakovsky et al., 2009) (Cheng and Logan, 2007)
VFAs (other than acetate)	Propionic, butyric, valeric, lactic acids	0.14 – 1.04	67-91	(Cheng and Logan, 2007)
Sugars	Glucose, xylose, maltose	0.02 - 1.23	20-88	(Catal, 2016; Cheng and Logan, 2007)
Fermentation effluent	Sugar beet juice fermentation, cellulose fermentation, corn stalk fermentation	0.3 – 3.4	53 - 60	(Dhar et al., 2015) (Lalaurette et al., 2009; Li et al., 2014; Wang et al., 2011)
Wastewater	Domestic, winery, swine	0.17 – 2.6	28 - 60	(Cusick et al., 2010; Ditzig et al., 2007; Escapa et al., 2012; Gil-Carrera et al., 2013; Wagner et al., 2009)
Biomass-derived streams	Switchgrass pyrolysis aqueous phase, straw hydrolysate	0.6 - 4.3	64 - 76	(Lewis et al., 2015; Ren et al., 2013a)

<sup>a</sup> Calculated based on electron equivalents of H<sub>2</sub> produced and substrates converted



The high yield of H<sub>2</sub> makes MEC technology advantageous over dark fermentation for H<sub>2</sub> production. As discussed in Section 2.2.1, the stoichiometric H<sub>2</sub> production from glucose in dark fermentation is 4 mol H<sub>2</sub>/mol glucose, while 2 mol H<sub>2</sub>/mol glucose (or 17% based on electron equivalents) is a typical yield in dark fermentation (Lee et al., 2010). In comparison, MECs can stoichiometrically produce 12 mol H<sub>2</sub>/mol glucose, and have achieved 90% H<sub>2</sub> yield from glucose (Cheng and Logan, 2007), although the H<sub>2</sub> production rate is usually lower than that of dark fermentation (Ren et al., 2009). Another advantage of MEC is the potential to reduce or overcome microbial inhibition, which is greatly suffered in dark fermentation. The fact that MEC produces H<sub>2</sub> in an abiotic cathode eliminates the need for H<sub>2</sub>-producing bacteria, which are highly susceptible to inhibition by various compounds, including furanic and phenolic compounds (Klinke et al., 2004b; Monlau et al., 2014). Comparing with water electrolysis, MEC uses much lower voltage input, as low as 0.3 V versus 1.7 V for typical water electrolysis (Logan and Rabaey, 2012).

## CHAPTER 3

### MATERIALS AND METHODS

#### 3.1 Chemicals

Furfural (FF, 99%), 5-hydroxymethyl furfural (HMF,  $\geq 99\%$ ), syringic acid (SA,  $\geq 95\%$ ), vanillic acid (VA,  $\geq 99\%$ ), and 4-hydroxybenzoic acid (HBA,  $\geq 99\%$ ) were used as bioanode substrates. Properties of the parent compounds are listed in Table 2.1. The five compounds are soluble in water (1.5-364 g/L at 25°C), nonvolatile (Henry's law constant =  $10^{-14}$  -  $10^{-6}$  atm-m<sup>3</sup>/mol), and have a low hydrophobicity ( $\log K_{ow}$  = -0.09 to 1.58). The standard potential at pH 7.0 ( $E^{0'}$ ) of the five compounds is from -0.388 to -0.303 V (Table 2.2) compared to the  $E^{0'}$  value of -0.414 V for proton reduction to H<sub>2</sub>.

Analytical standards of 2,5-bis(hydroxymethyl)furan (HMF-OH), 2,5-furandicarboxylic acid (FdiCA), furfuryl alcohol (FF-OH), 2-furoic acid (FF-A), 3,4-dihydroxy-5-methoxybenzoic acid (DHMBA), gallic acid (GA), protocatechuic acid (PA), pyrogallol, catechol, phenol, phloroglucinol, resorcinol, and benzoic acid were used as references for the identification of furanic and phenolic metabolites.

All chemicals were purchased from Alfa Aesar (Ward Hill, MA) and Sigma-Aldrich (St. Louis, MO).

## 3.2 Analytical Methods

### 3.2.1 pH

All pH measurements were performed using the potentiometric method with a ATI Orion Model 370 digital pH meter (Orion Research Inc., Boston, MA) and a gel-filled combination pH electrode (VWR International, West Chester, PA). The meter was calibrated periodically with pH 4.0, 7.0, and 10.0 standard buffer solutions (Fisher Scientific, Pittsburg, PA).

### 3.2.2 Chemical Oxygen Demand (COD)

COD was measured using the closed reflux, colorimetric method as described in *Standard Methods* (Rice et al., 2012). The digestion solution was made of 4.9 g  $K_2Cr_2O_7$ , 6 g  $HgSO_4$ , 6 g  $Ag_2SO_4$  and 500 mL  $H_2SO_4$ . An aliquot of 3 mL digestion solution was transferred to COD digestion vials and then 2 mL of sample was added to the vial. After tumbling the vial 4 to 8 times, the vial content was digested at 150°C for 2 hours and then cooled down to room temperature. The absorbance was measured at 620 nm with a UV/Visible spectrophotometer (Hewlett-Packard Model 8453, Palo Alto, CA) equipped with a diode array detector, deuterium and tungsten lamps and a 1 cm path length. Samples were filtered through a 0.2  $\mu m$  polycarbonate membrane filter if the soluble COD (sCOD) was measured; otherwise, well-mixed samples were used after appropriate dilution for total COD measurements. All samples were prepared in duplicate and a calibration curve was prepared using 1 g/L standard solution of potassium hydrogen phthalate (KHP).

### 3.2.3 Gas Production and Composition

Total gas production was measured by acid brine solution (10% NaCl w/v, 2% H<sub>2</sub>SO<sub>4</sub> v/v) displacement in the burettes, equilibrated to 1 atm. Headspace gas composition (i.e., H<sub>2</sub>, CO<sub>2</sub>, and CH<sub>4</sub>) was determined with a gas chromatography (GC) unit (Agilent Technologies, Model 6890N; Agilent Technologies, Inc., Palo Alto, CA) equipped with two columns and two thermal conductivity detectors. Methane (CH<sub>4</sub>) and hydrogen (H<sub>2</sub>) were separated with a 15 m HP-Molesieve fused silica, 0.53 mm i.d. column (Agilent Technologies, Inc.), using nitrogen as the carrier gas at a constant flow of 6 mL/min. Carbon dioxide (CO<sub>2</sub>) was separated with a 25 m Chrompac PoraPLOT Q fused silica, 0.53 mm i.d. column (Varian, Inc., Palo Alto, CA), using Helium as the carrier gas at a constant flow rate of 6 mL/min. The 10:1 split injector was maintained at 150°C, the oven was set at 40°C and the detector temperature was set at 150°C.

### 3.2.4 Furanic and Phenolic Compounds

The furanic and phenolic compounds were quantified using a high performance liquid chromatography (HPLC) unit equipped with a UV-Vis detector (Agilent 1100, Santa Clara, CA). A HPX-87H column (BioRad, Hercules, CA) was used with an eluent of 15% acetonitrile in 5 mM H<sub>2</sub>SO<sub>4</sub> (v/v) at a flow rate of 0.6 mL/min. The wavelength of 280 nm and 210 nm was used for the furanic and phenolic compounds, respectively. Samples were passed through 0.2 µm membrane filters before injection into the HPLC.

### 3.2.5 Volatile Fatty Acids

Acetate and other volatile fatty acids were quantified by the same HPLC method as described in Section 3.2.4 above at the wavelength of 210 nm, except that the eluent was 5 mM H<sub>2</sub>SO<sub>4</sub> without any organic solvent.

### 3.2.6 Biotransformation Products

Metabolites of the five compounds were identified using an LC/MS-MS unit (Agilent 1260 Infinity LC system, 6410 Triple Quad MSD) equipped with a Kinetex biphenyl column (3×150 mm, 5 μm; Phenomenex, Torrance, CA). The eluent consisted of (A) 5 mM ammonium acetate with 0.5% acetic acid in acetonitrile (v/v) and (B) 5 mM ammonium acetate in 0.5% acetic acid (v/v) at a flow rate of 0.5 mL/min, using gradient elution as follows: eluent A was increased from 2% to 30% in 2.3 min and to 90% in 1.2 min, and then was maintained at 90% for 2.5 min. The mass spectrometer was operated in both positive and negative electrospray ionization (ESI) mode with a resolution of 0.1 Da. Selective ion mode (SIM) was first used to screen for the presence of assumed metabolites, by setting m/z values at [MW-1] in the negative mode and [MW+1] in the positive mode. A confirmation step was then performed by operating the MS-MS in product ion mode. The resulting fragments of precursor ions were compared to those of pure chemicals.

A GC/MS unit (Agilent 7890) equipped with a Zebron ZB-5HT column (Phenomenex, Torrance, CA) was used as a supplementary method for metabolite identification. Samples used for the GC/MS analysis were passed through 0.2 μm PTFE membrane filters and extracted with ethyl acetate. The oven temperature was held at

80 °C for 4 min, then ramped up to 150 °C at a rate of 10 °C/min. The mass spectrometer was set at an electron multiplier voltage (EMV) with a gain factor of 1.0 (1424 V) and a m/z range of 20 – 150. The obtained MS spectra were compared to those in the NIST library for identification.

### 3.2.7 Protein

The protein concentration of the MEC anode biofilm and planktonic biomass was measured and used for biomass quantification. For each biofilm sample, two pieces of 0.5 × 0.5 × 0.5 inch anode electrode were removed from the MEC. Protein was extracted by bead beating followed by 30 min heating at 100 °C in 0.1 N NaOH. To quantify the planktonic protein, 60 mL of bioanode liquid was centrifuged at 10,000 rpm for 15 min. The pellet was then washed three times with clean anolyte followed by centrifugation. The pellet was re-suspended in 0.1 N NaOH, followed by 30 min heating at 100 °C. The extracted protein was quantified using the Pierce™ BCA protein assay kit (Thermo Scientific, Waltham, MA) following the microplate procedure in the manufacturer's instructions. The absorbance at 562 nm wavelength was measured by a microplate spectrometer (Synergy HT, BioTek Instruments, Winooski, VT).

### 3.2.8 Microbial Community Analysis

The structure of biofilm-associated microbial communities was examined by performing 16S rRNA gene based phylogenetic analyses. A piece of anode electrode with attached biofilm (approximately 1 cm × 1cm × 3 cm) was washed several times with the anolyte and then cut into small pieces (< 0.5 cm). The genomic DNA was extracted with the

PowerSoil DNA isolation Kit (MO BIO Laboratories, Carlsbad, CA), according to the manufacturer's instructions. The concentration and purity of the DNA sample were determined with a ND-1000 spectrophotometer (NanoDrop Technologies, Wilmington, DE). The 16S rRNA gene was sequenced using an Illumina MiSeq system (LC Science, Houston, TX; Research and Testing Laboratory, Lubbock, TX). Universal bacterial and archaeal primers were used to amplify partial 16S rRNA genes. The primer sequences used in different analyses are described in respective chapters. The obtained sequences were clustered into Operational Taxonomic Units (OTUs), and the representative sequence of each OUT was used for taxonomic classification. The sequence-based phylogenetic tree of the abundant bacteria (>1% abundance) was constructed by applying the neighbor-joining algorithm using the program MEGA 6.06.

### 3.2.9 Electric Current

Electric current is a measure of the exoelectrogenic activity of the MEC and directly related to the cathodic H<sub>2</sub> production. The electric current was measured by performing chronoamperometry using a potentiostat (Interface 1000, Gamry Instruments, Warminster, PA). The working electrode lead of the potentiostat was connected to the anode, and counter and reference electrode leads were connected to the cathode. The potential of the working electrode (i.e., anode) was fixed at 0.6 V versus the reference electrode (i.e., cathode) for 3 min, and the current measured at the end of the 3 min was recorded. The potential used in the chronoamperometry (0.6 V) was the same as the anode potential during the normal MEC operation, to represent the real-time MEC current.

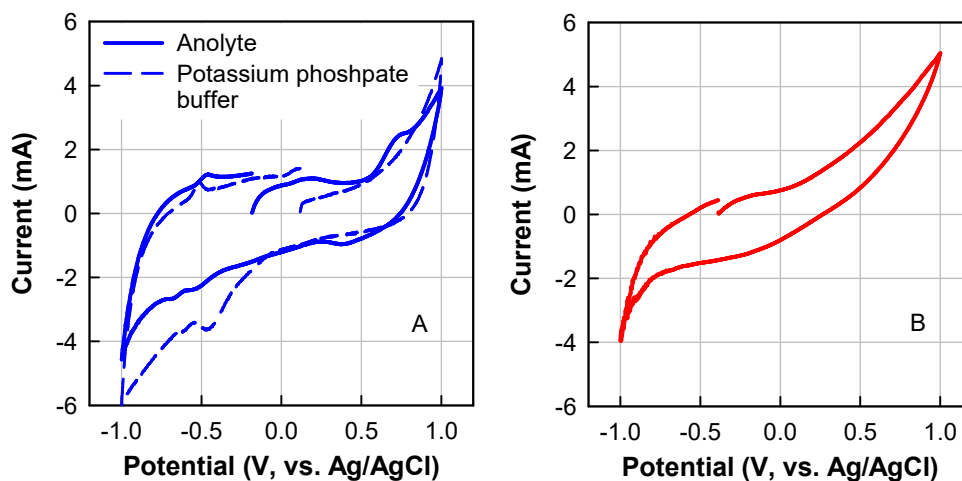
### 3.2.10 Cyclic Voltammetry

Cyclic voltammetry (CV), which depicts the response of current to a varying potential, is a widely used electrochemical technique to study electrode reaction mechanisms. The CV of the MEC anode was performed by using a 6 mm diameter Ag/AgCl reference electrode (0.199 V SHE; BASi, West Lafayette, IN), which was immersed into the anolyte near the anode electrode. The potentiostat was connected to the MEC in a three-electrode setup. The working electrode lead was connected to the MEC anode, the counter electrode lead connected to the MEC cathode, and the reference electrode lead connected to the Ag/AgCl electrode. The anolyte and catholyte was not mixed during the cyclic voltammetry. The potential scan started from - 0.7 to + 0.3 V, and then to -0.7 V at a scan rate of 5 mV/s. Slow scan rates around 1 mV/s are commonly used in bioanode studies (Rimboud et al., 2014). The scan range and direction were determined based on the analyses described below.

In order to select a potential scan range, an anode CV was conducted at a large potential range of -1.0 ~ +1.0 V (vs. Ag/AgCl), using an un-inoculated carbon felt anode electrode and then a starved, non-fed biofilm-attached anode electrode (non-active bioanode), in the presence of only anolyte. In this test, the initial potential of the scan was the open circuit potential ( $E_{oc}$ ), which measured with a stability of 0.05 mV/s before the CV was started. Using the un-inoculated electrode, water electrolysis was observed at > 0.5 V and < - 0.7 V (Figure 3.1A). Several other redox peaks were observed, which could be attributed to the dissolved salts, metal ions and vitamins in the anolyte (see anolyte composition in Section 4.2.1 and Table 4.1). The three redox peaks around -0.5 V likely resulted from phosphate ions in the anolyte, evidenced by the voltammogram obtained



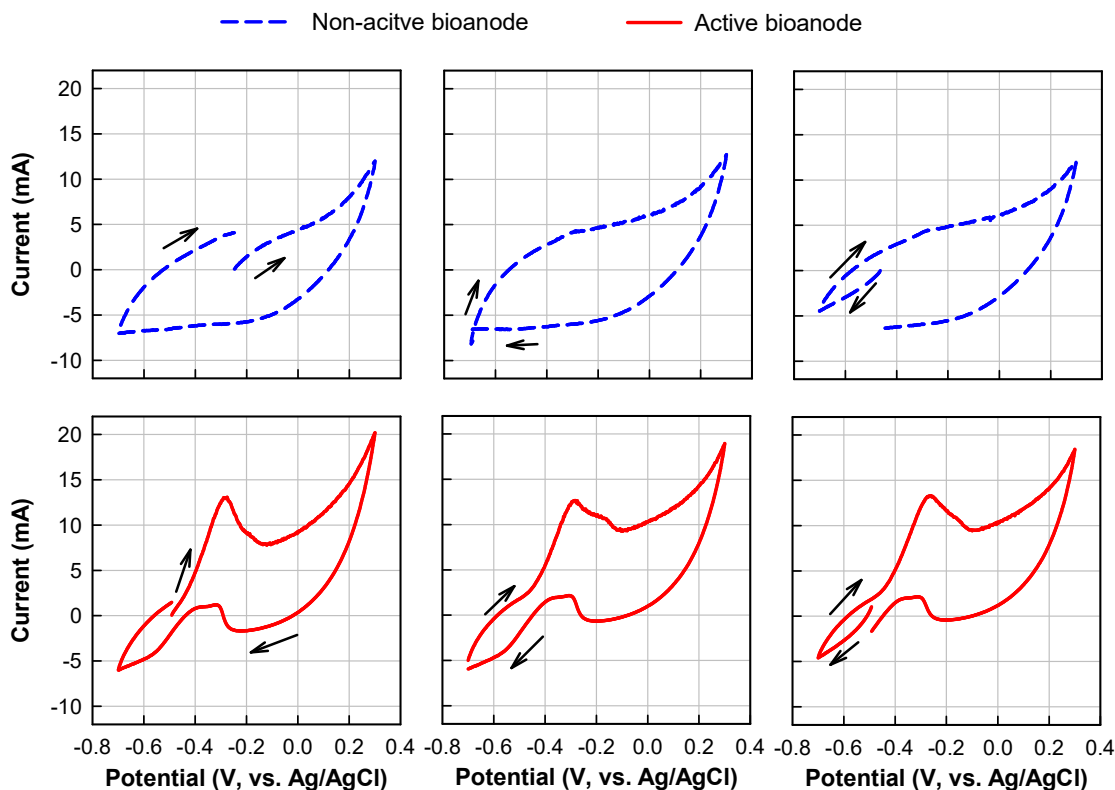
with the un-inoculated electrode in potassium phosphate buffer (Figure 3.1A). However, when a non-active bioanode was used for the CV, the on-set potential for water oxidation was less positive (around + 0.3 V; Figure 3.1B) than that observed with the carbon felt electrode (+ 0.5 V), which is attributed to the effect of biofilm, attached on the carbon felt electrode. Therefore, a scan range of - 0.7 ~ + 0.3 V was selected for CV analyses in this study, unless otherwise stated due to further change of the biofilm-attached electrode.



**Figure 3.1.** Cyclic voltammograms of a carbon felt anode electrode (A) and a non-active biofilm-attached anode electrode (B) in anolyte.

Three different scan directions were experimented with a non-active bioanode and an active bioanode: (1)  $E_{oc} \rightarrow + 0.3 \text{ V} \rightarrow - 0.7 \text{ V}$ ; (2)  $- 0.7 \text{ V} \rightarrow + 0.3 \text{ V} \rightarrow - 0.7 \text{ V}$ ; and (3)  $E_{oc} \rightarrow - 0.7 \text{ V} \rightarrow + 0.3 \text{ V}$ . As shown in Figure 3.2, all three scan methods resulted in similar voltammograms of both non-active and active bioanodes, except the slight difference in the capacitance current observed at the start and end of the scan. Thus, the scan direction of  $- 0.7 \text{ V} \rightarrow + 0.3 \text{ V} \rightarrow - 0.7 \text{ V}$  was used throughout this study, which is

commonly practiced in studies of bioelectrochemical systems (Baron et al., 2009; Marsili et al., 2010; Zhang et al., 2014).



**Figure 3.2.** Non-active and active bioanode voltammograms conducted with different scan directions. Left column:  $E_{oc} \rightarrow +0.3 \text{ V} \rightarrow -0.7 \text{ V}$ ; middle column:  $-0.7 \text{ V} \rightarrow +0.3 \text{ V} \rightarrow -0.7 \text{ V}$ ; right column:  $E_{oc} \rightarrow -0.7 \text{ V} \rightarrow +0.3 \text{ V}$ .

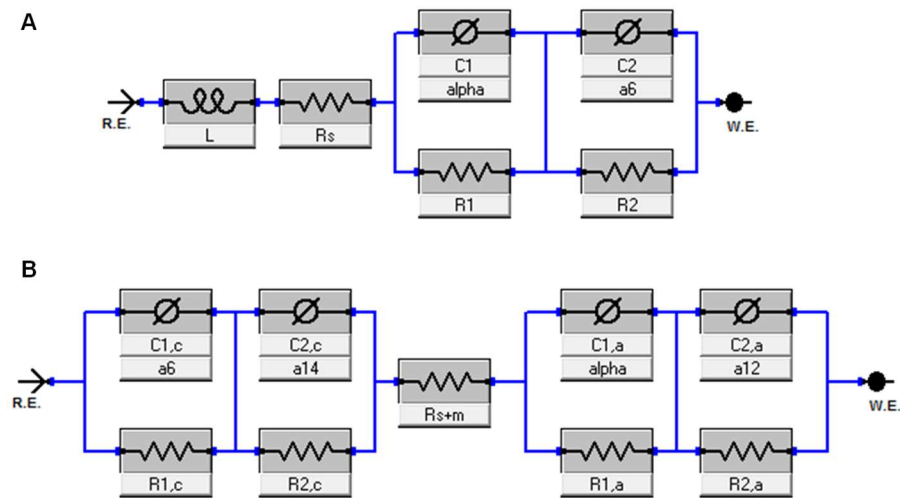
### 3.2.11 Electrochemical Impedance Spectroscopy

Electrochemical impedance spectroscopy (EIS) is an advanced electrochemical technique for measuring total internal resistance and resistance associated with specific components of an electrochemical cell (He et al., 2009). In the present study, EIS was conducted with

the MEC whole cell as well as anode and cathode half cells at a frequency range of 100 kHz to 5 MHz and an AC signal of 10 mV amplitude, using a Gamry Interface 1000 potentiostat and an EIS300<sup>TM</sup> software (Gamry Instruments, Warminster, PA). In whole-cell EIS, the potentiostat was connected to the MEC in a two-electrode setup, with the anode as the working electrode and the cathode as both the counter and reference electrode; the DC potential was +0.6 V (i.e., the same as the normal MEC operation; see Section 5.2.1). For the half-cell EIS, the potentiostat was connected to the MEC in a three-electrode setup, with the anode or cathode as the working electrode, the other electrode as the counter electrode, and a Ag/AgCl electrode placed next to the working electrode as the reference electrode. The DC potential for the half-cell EIS was set at the electrode potential (vs. Ag/AgCl) measured *in-situ*.

The obtained EIS spectra were fitted to equivalent electric circuits using the Simplex Method of the Gamry Analyst software. Among literature-reported equivalent circuits commonly used to describe MECs, as reviewed by Dominguez-Benetton et al. (2012), the circuit in Figure 3.3A resulted in the best fit with EIS data of the anode and cathode half-cells in the present study and was thus selected as the equivalent circuit. The equivalent circuit consisted of two sets of constant phase elements (C1, C2) in parallel with resistors (R1, R2). The resistors (R1 and R2) represent resistance associated with charge-transfer and biofilm formation, while the constant phase elements represent capacitance of a rough electrode surface, associated with electrolyte double layer and biofilm. Inductor “L” represents the contribution of the inductive coupling in the high-frequency range of the wire. Resistor “R<sub>s</sub>” represents the anolyte or catholyte solution resistance (Dominguez-Benetton et al., 2012; He et al., 2006).

Based on the selected equivalent circuit for the half-cells, an equivalent circuit representing the MEC whole-cell was developed (Figure 3.3B). Resistor “ $R_{s+m}$ ” represents resistance associated with the electrolyte and the cation exchange membrane between the anode and the cathode. Inductor “ $L$ ” was not included in the whole-cell equivalent circuit, because inductance was not observed at the high-frequency range, probably due to the different wiring method in the two-electrode setup for whole-cell EIS.



**Figure 3.3.** Equivalent circuit used in EIS representative of anode or cathode half-cell (A), and the MEC whole-cell (B).

### 3.3 Calculations

#### 3.3.1 Current Density

Current density was normalized to either the empty bed volume of the anode chamber (mA/cm<sup>3</sup>) for comparison with single-chamber MECs, or the projected surface area of the Nafion membrane (mA/cm<sup>2</sup>), assuming the membrane surface area was limiting, due to the narrow channel of the H-type reactor.

#### 3.3.2 Coulombic Efficiency

Coulombic efficiency (CE) was calculated based on the number of electrons recovered as electrical current per electron equivalent of COD removed, as follows:

$$CE (\%) = \frac{8 \int_0^t I dt}{F V_a \Delta COD} \times 100 \quad 3.1$$

where I is the current (A), F is the Faraday constant (96485 C/mol), V<sub>a</sub> is the anode liquid volume (L), t is time (s), and the factor of 8 is for the conversion from g COD to mol e<sup>-</sup>.

#### 3.3.3 Anode Efficiency

Anode efficiency was defined in this study as the ratio of electron equivalents recovered as electrical current to those of substrate added.

$$\eta_a = \frac{\int_0^t I dt / F}{n \times eeq} \quad 3.2$$

where I is the current (A), F is the Faraday constant (96485 C/mol), t is time (s), n is the moles of substrate added to the anode (mol), and eeq is the electron equivalence of the

substrate (i.e., eq/mol). Alternatively, anode efficiency is calculated based on the COD removal and Coulombic efficiency, as follows:

$$\eta_a = CE \times \frac{\Delta COD}{COD_{in}} \quad 3.3$$

where  $COD_{in}$  is the COD of the substrate added (g).

### 3.3.4 Cathode Efficiency

Cathode efficiency was calculated as the ratio of electron equivalents of cathodic H<sub>2</sub> measured to total electrons represented by the current.

$$\eta_c = \frac{2m_{H_2}}{\int_0^t I dt / F} \quad 3.4$$

where  $m_{H_2}$  is the moles of cathodic H<sub>2</sub> produced (mol), the factor of 2 is for the conversion from mol H<sub>2</sub> to mol e<sup>-</sup>, I is the current (A), t is time (s), and F is the Faraday constant (96485 C/mol).

### 3.3.5 H<sub>2</sub> Yield

H<sub>2</sub> yield was calculated based on the electron equivalents of cathodic H<sub>2</sub> measured per electron equivalent of COD removed, as follows:

$$H_2 \text{ Yield} = \frac{2m_{H_2}}{\frac{\Delta COD \times V_a}{8}} \quad 3.5$$

where  $m_{H_2}$  is moles of cathodic H<sub>2</sub> produced (mol),  $\Delta COD$  is the COD removed (g/L), and  $V_a$  is the anode working volume (L). The factor of 2 or 8 is for the conversion from mol H<sub>2</sub> or g COD to mol e<sup>-</sup>. Alternatively, the H<sub>2</sub> yield can be calculated based on the Coulombic efficiency and cathode efficiency, as follows:

$$H_2 \text{ Yield} = CE \times \eta_c \quad 3.6$$

### 3.3.6 Electrical Energy Efficiency

Electrical energy efficiency ( $\eta_e$ ) was defined as the ratio of energy recovered as H<sub>2</sub> to the electrical energy input.

In a batch system,  $\eta_e$  was calculated as follows:

$$\eta_e \% = \frac{W_{H_2}}{W_e} \times 100 \quad 3.7$$

where  $W_{H_2}$  (J) is the energy content of the cathodic H<sub>2</sub> produced, and  $W_e$  (J) is the electrical energy input (J).

$W_{H_2}$  was calculated as the follows:

$$W_{H_2} = -\Delta H \times m_{H_2} \quad 3.8$$

where  $\Delta H$  is the higher heating value of H<sub>2</sub>,  $-285.8 \times 10^3$  J/mol (Lide, 1995), and  $m_{H_2}$  is moles of cathodic H<sub>2</sub> produced (mol).

$W_e$  was calculated as the follows:

$$W_e = \int_0^t IU dt \quad 3.9$$

where  $I$  is the current (A),  $U$  is the voltage between the anode and the cathode (V), and  $t$  is time (s).

In a continuous-flow system,  $\eta_e$  was calculated as follows:

$$\eta_e \% = \frac{P_{H_2}}{P_e} \times 100 \quad 3.10$$

where  $P_{H_2}$  is the H<sub>2</sub> energy recovery rate (J/s), and  $P_e$  is the electrical energy input rate (J/s).

$P_{H_2}$  was calculated as follows:

$$P_{H_2} = -\Delta H Q_{H_2} \quad 3.11$$

where  $\Delta H$  is as defined above, and  $Q_{H_2}$  is the  $H_2$  production rate during stable operation (mol/s).

$P_e$  was calculated as follows:

$$P_e = IU \quad 3.12$$

where  $I$  is the steady-state current (A) and  $U$  is the voltage between the anode and cathode (V).

### 3.3.7 Overall Energy Efficiency

Overall energy efficiency ( $\eta_{e+s}$ ) was calculated as the ratio of energy recovered as  $H_2$  to the sum of electrical and substrate energy input.

In a batch system,  $\eta_{e+s}$  was calculated as follows:

$$\eta_{e+s} \% = \frac{W_{H_2}}{W_e + W_s} \times 100 \quad 3.13$$

where  $W_{H_2}$  and  $W_e$  are as defined in Section 3.3.6 above, and  $W_s$  is substrate energy input (J) defined as follows:

$$W_s = \Delta COD \times V_a \times \Delta H_s \quad 3.14$$

where  $\Delta COD$  is the COD removal during the batch run (g/L),  $V_a$  is the anode working volume (L), and  $\Delta H_s$  is estimated heat of combustion of COD (14700 J/g COD) (Logan et al., 2008).

In a continuous-flow system,  $\eta_{e+s}$  was calculated as follows:



$$\eta_{e+s}\% = \frac{P_{H_2}}{P_e + P_s} \times 100 \quad 3.15$$

where  $P_{H_2}$  and  $P_e$  are as defined in Section 3.3.6 above, and  $P_s$  is substrate energy input rate (J/s) defined as follows:

$$P_s = \frac{V_a}{HRT} (sCOD_{inf} - sCOD_{eff}) \Delta H_s \quad 3.16$$

where  $V_a$  and  $\Delta H_s$  are as defined above, HRT is hydraulic retention time (s),  $sCOD_{inf}$  and  $sCOD_{eff}$  are influent and effluent soluble COD concentration (g/L), respectively.

## CHAPTER 4

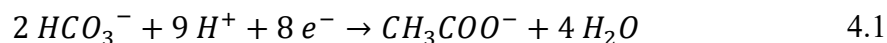
### ENRICHMENT OF ANODE MICROBIAL COMMUNITY

#### 4.1 Introduction

A microbial electrolysis cell (MEC) for hydrogen (H<sub>2</sub>) production typically consists of a bioanode, where microbial utilization of organic substrates takes place, and an abiotic cathode where protons are reduced to H<sub>2</sub>. An important step in the development of MEC is to establish an anode microbial community, which can perform effective exoelectrogenesis, i.e., produce and transport electrons to the anode electrode. In addition, because furanic and phenolic compounds were used as anode substrates in this study, the anode microbial community should also demonstrate the capacity to utilize the furanic and phenolic compounds as the sole carbon and energy source.

Microbial fuel cell (MFC) is another type of bioelectrochemical system, which has the same anode reactions as MEC. However, the MFC does not require an anoxic cathode environment or an external voltage supply, as is the case of MEC. Thus, for the advantage of simple configuration and operation, a MFC was used in this study to pre-enrich an anode microbial community, which could then be transferred to a MEC.

In both MFC and MEC anodes, the electron-producing half reaction is oxidation of organic substrate, in the absence of soluble terminal electron acceptors (e.g., O<sub>2</sub>, NO<sub>3</sub><sup>-</sup>, and SO<sub>4</sub><sup>2-</sup>). Assuming acetate is the exoelectrogenic substrate, the same anode half reaction applies to both MFC and MEC; the reaction and biological standard reduction-oxidation potential ( $E^{\circ}$ , pH 7.0) are as shown in Equation 4.1.



$$E_{HCO_3^-/CH_3COO^-}^{0'} = -0.278 V$$

However, the cathode half reaction of a MFC with an air cathode is oxygen reduction to water (Equation 4.2), with a much more positive reduction-oxidation potential than the reaction of proton reduction in a MEC (Equation 4.3).



Thus, the biological standard reduction-oxidation potential change of the overall reactions of MFC and MEC can be calculated in Equation 4.4 and 4.5.

$$\text{MFC} \quad \Delta E^{0'} = E_{O_2/H_2O}^{0'} - E_{HCO_3^-/CH_3COO^-}^{0'} = 1.083 V > 0 \quad 4.4$$

$$\text{MEC} \quad \Delta E^{0'} = E_{H^+/H_2}^{0'} - E_{HCO_3^-/CH_3COO^-}^{0'} = -0.136 V < 0 \quad 4.5$$

Thus, the overall reaction of a MFC under standard conditions is spontaneous, whereas the MEC overall reaction requires voltage input greater than 0.136 V. Because of the different reactions, the MFC cathode is in contact with air, whereas the MEC cathode is under strictly anoxic conditions. Also, the voltage supply in the MEC is not needed for a MFC.

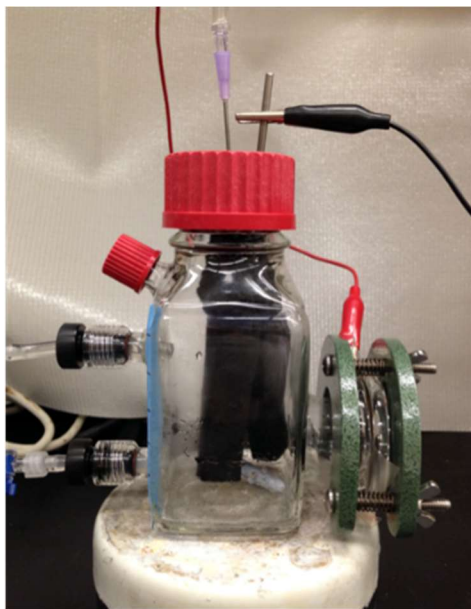
The objective of the work reported in this chapter was to establish an anode microbial community, which can utilize furanic and phenolic compounds and produce current in a MFC.

## 4.2 Materials and Methods

### 4.2.1 MFC

An air-cathode MFC was developed for enriching the anode microbial community (Figure 4.1). The anode chamber was a modified square glass bottle with an open channel

on one side. The liquid volume was 200 mL with a 60 mL headspace. The anode electrode was porous carbon felt (5 stripes, 1 cm × 1 cm × 10 cm each; Alfa Aesar, Ward Hill, MA) tied to a stainless steel rod. The cathode was a membrane-electrode assembly with a surface area of 5.7 cm<sup>2</sup> purchased from Fuel Cells Etc (College Station, TX), which was made of a cation exchange membrane (Nafion 115) and carbon cloth containing 0.5 mg/cm<sup>2</sup> Pt. The cathode was clamped to the side channel extended from the anode chamber and exposed to air on one side. Conductive wires were used to connect the anode, the cathode and a variable resistor. The voltage across the resistor was measured by a multimeter (RadioShack, Fort Worth, TX), and the current was then calculated according to Ohm's law ( $V = I \times R$ ).



**Figure 4.1.** MFC Setup.

#### 4.2.2 Inoculation and Enrichment Procedures

The bioanode inoculum was a piece of biofilm-attached carbon felt (approximately 1 cm × 1 cm × 3 cm) from a MFC anode developed at the Oak Ridge National Laboratory (Oak Ridge, TN), which over time had been fed with corn stover hydrolysates and switchgrass pyrolysis aqueous stream, bearing levoglucosan, ketones, volatile fatty acids, as well as furanic and phenolic compounds (Borole et al., 2009; Borole et al., 2013; Lewis et al., 2015). The original inoculum of this MFC was a sample collected from a municipal anaerobic digester.

The inoculum was placed in the center of the MFC anode carbon felt electrode, which was pre-autoclaved and flushed with N<sub>2</sub>. The anolyte, used as mineral microbial growth medium, was then anaerobically transferred to the anode chamber. The anolyte consisted of (in g/L): NH<sub>4</sub>Cl, 0.31 g/L; KCl, 0.13 g/L; NaH<sub>2</sub>PO<sub>4</sub>·H<sub>2</sub>O, 2.45 g/L; Na<sub>2</sub>HPO<sub>4</sub>, 4.58 g/L, along with trace metal (12.5 mL/L) and vitamin solutions (2.5 mL/L). The composition of the trace metal and vitamin stock solutions is shown in Table 4.1

**Table 4.1.** The vitamin stock solution was added after the anolyte was autoclaved, flushed with N<sub>2</sub> for 30 min, and cooled to room temperature. A mixture of the five compounds at equal electron equivalents (each at 62.5 mg COD/L) and a total concentration of 200 mg/L (312 mg COD/L) was fed to the MFC following the schedule shown in Table 4.2. During the first ten feeding cycles (~70 days), glucose (200 mg/L) was added along with the five compounds to enhance microbial growth. Between each feeding cycle, the MFC was drained and fresh anolyte was added. Partial or no replacement of anolyte was practiced for the first five feeding cycles, in order to

minimize biomass washout. The external resistor was gradually reduced from 500 to 250 and then to 100  $\Omega$ , in order to promote the growth of exoelectrogens.

**Table 4.1.** Composition of Trace Metal and Vitamin Stock Solutions.

<b>Compound</b>	<b>Concentration (g/L)</b>
<i>Trace metal stock solution</i>	
Nitrilotriacetic Acid	1.5
MgSO <sub>4</sub> · 7H <sub>2</sub> O	3.0
MnSO <sub>4</sub> · H <sub>2</sub> O	0.5
NaCl	1.0
Fe SO <sub>4</sub> · 7H <sub>2</sub> O	0.1
CoCl <sub>2</sub> · 6H <sub>2</sub> O	0.1
CaCl <sub>2</sub>	0.1
ZnSO <sub>4</sub> · 7H <sub>2</sub> O	0.1
CuSO <sub>4</sub> · 5H <sub>2</sub> O	0.01
AlK(SO <sub>4</sub> ) <sub>2</sub> · 12H <sub>2</sub> O	0.01
Na <sub>2</sub> MnO <sub>4</sub> · 2H <sub>2</sub> O	0.01
<i>Vitamin stock solution</i>	
Folic acid	0.01
Pyridoxine hydrochloride	0.05
Riboflavin	0.025
Biotin	0.01
Thiamine	0.025
Nicotinic acid	0.025
Calcium Pantothenate	0.025
Vitamin B12	0.0005
p-Aminobenzoic acid	0.025
Thioctic acid	0.025

**Table 4.2.** MFC Operation Schedule during Startup.

Incubation period	Substrate		Feeding frequency	Anolyte replacement	External resistance ( $\Omega$ )
	Furanic and phenolic mixture (mg/L)	Glucose (mg/L)			
0-14 d	200	200	weekly	200 mL, every 2 weeks	500
14-35 d	200	200	Twice a week	100 mL, twice a week	500
35-42 d	200	200	weekly	200 mL, weekly	250
42-70 d	200	200	weekly	200 mL, weekly	100
70-134 d	200	0	weekly	200 mL, weekly	100

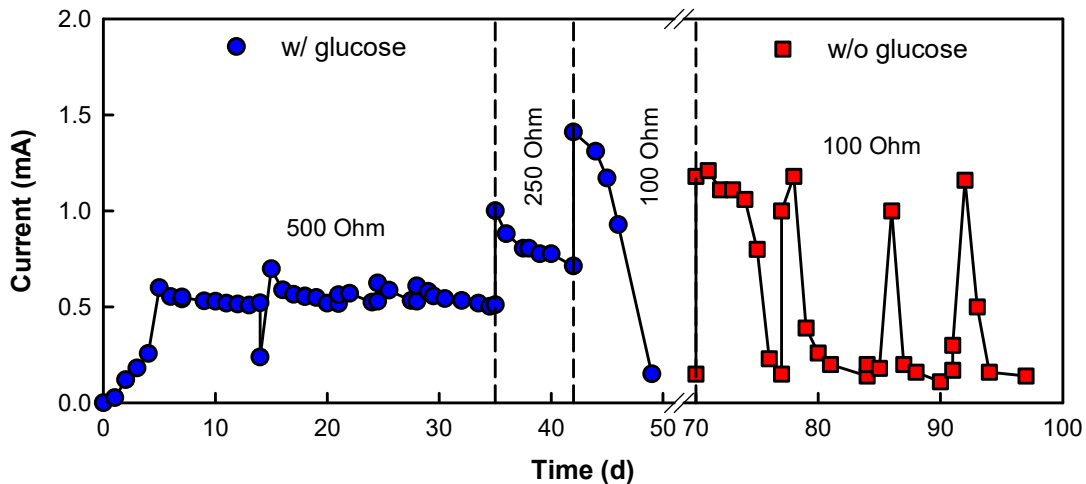
#### 4.2.3 Bioanode Microbial Community Analysis

Microbial community analysis of the MFC anode was performed after 6 months of enrichment. The genomic DNA was extracted and checked for purity as described in Section 3.2.8 above. 16S rRNA gene was sequenced using an Illumina MiSeq system (LC Science, Houston, TX). Bacterial primers 319F (5'-ACTCCTACGGGAGGCAGCAG-3') and 806R (5'-GGACTACHVGGGTWTCTAAT-3') were used to amplify the V3-V4 hypervariable regions of the 16S rRNA gene. The obtained sequences were clustered into Operational Taxonomic Units (OTUs) with 97% similarity. The longest read in each OTU was used as the representative sequence for taxonomic classification using the RDP classifier Version 2.7.

### 4.3 Results and Discussion

#### 4.3.1 MFC Fed with Furanic and Phenolic Compounds Along with Glucose

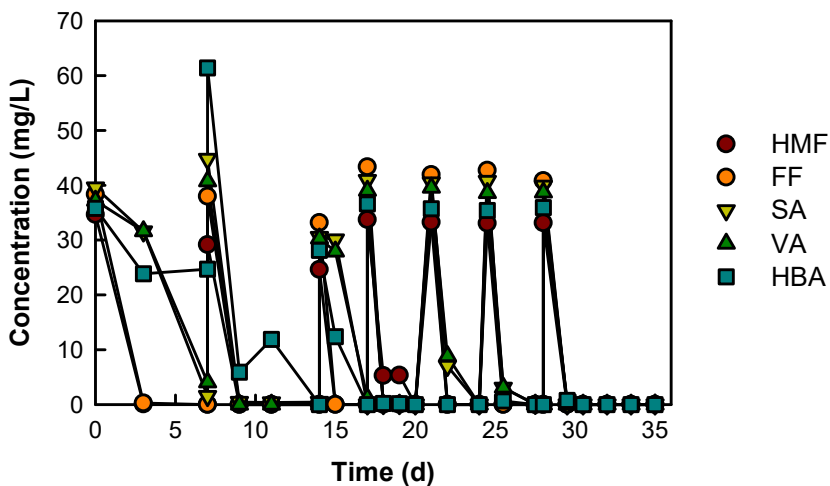
During the MFC startup, glucose (200 mg/L) was added to the MFC along with the furanic and phenolic mixture (200 mg/L) to facilitate the initial microbial growth. During the first week of incubation, current was produced, gradually reaching 0.6 mA in 7 days (Figure 4.2). The same level of current production was sustained in the subsequent feeding cycles (7-35 d) at an external resistance of 500  $\Omega$ . When the external resistance was reduced from 500 to 250  $\Omega$ , the current increased to 1.1 mA, and increased further to 1.4 mA when the resistance was reduced to 100  $\Omega$  (Figure 4.2). The decline of current observed during each feeding cycle is attributed to the depletion of degradable substrate. At the external resistance of 100  $\Omega$ , multiple feeding cycles were conducted, and repeated MFC activity was observed (not shown in Figure 4.2 for clarity).



**Figure 4.2.** MFC current production in batch runs conducted with 200 mg/L furanic and phenolic mixture in the presence or absence of glucose at different external resistance.



During each feeding cycle, glucose was completely removed within 5 h. Complete transformation of the five furanic and phenolic parent compounds was also observed within 24 h starting on day 18 (Figure 4.3). Gas production was very low (ca. 6 mL at 22°C and 1 atm) and consisted of 2.5% CO<sub>2</sub>. Methane was not detected. The removal of soluble COD (sCOD) varied from 17 to 41%, with Coulombic efficiency ranging from 32 to 87%. Two persistent metabolites were detected in the HPLC-UV spectra, which were later identified as catechol and phenol (as detailed in Chapter 6). The persistence of metabolites indicates incomplete or low extent of biotransformation of the furanic and phenolic compounds.



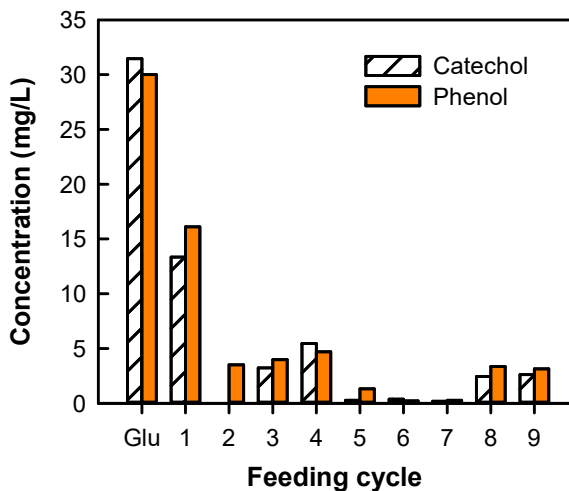
**Figure 4.3.** Time course of five parent compounds during MFC startup. Abbreviations: HMF, 5-hydroxymethylfurfural; FF, furfural; SA, syringic acid; VA, vanillic acid; HBA, 4-hydroxybenzoic acid.

In order to determine how much COD removal was due to glucose degradation, glucose at 200 mg/L was re-spiked at the end of a feeding cycle after the parent model compounds had disappeared and the sCOD had reached a plateau. Within 2 days, the sCOD concentration declined and reached a value approximately at the level observed before the glucose addition, whereas the persistent metabolites were not further transformed. Thus, the sCOD removal observed during normal feeding cycles was primarily due to glucose degradation, and the contribution of the degradation of furanic and phenolic compounds was insignificant.

#### 4.3.2 MFC Fed with Furanic and Phenolic Compounds without Glucose

In order to improve the biodegradation extent and to achieve further removal of the persistent metabolites, the MFC was fed with the five furanic and phenolic compounds as the sole energy and carbon source (i.e., glucose was excluded) from day 70 to 134 (Table 4.2, above). In each repetitive feeding cycle, the MFC produced a maximum current of  $1.25 \pm 0.24$  mA during the first day of incubation. The current declined in the following days due to substrate depletion (Figure 4.2 above; 70-98 d). The parent compounds were completely transformed during each feeding cycle, similar to that observed when glucose was added. However, the levels of metabolites measured at the end of the feeding cycles decreased significantly over time, compared to those when glucose was also added (Figure 4.4). In addition, the sCOD removal ranged from 50 to 60%, whereas in the glucose-amended feeding cycle the observed sCOD removal was only from glucose degradation, rather than from the furanic and phenolic compounds. Thus, the extent of biotransformation extent the five furanic and phenolic compounds was improved over the

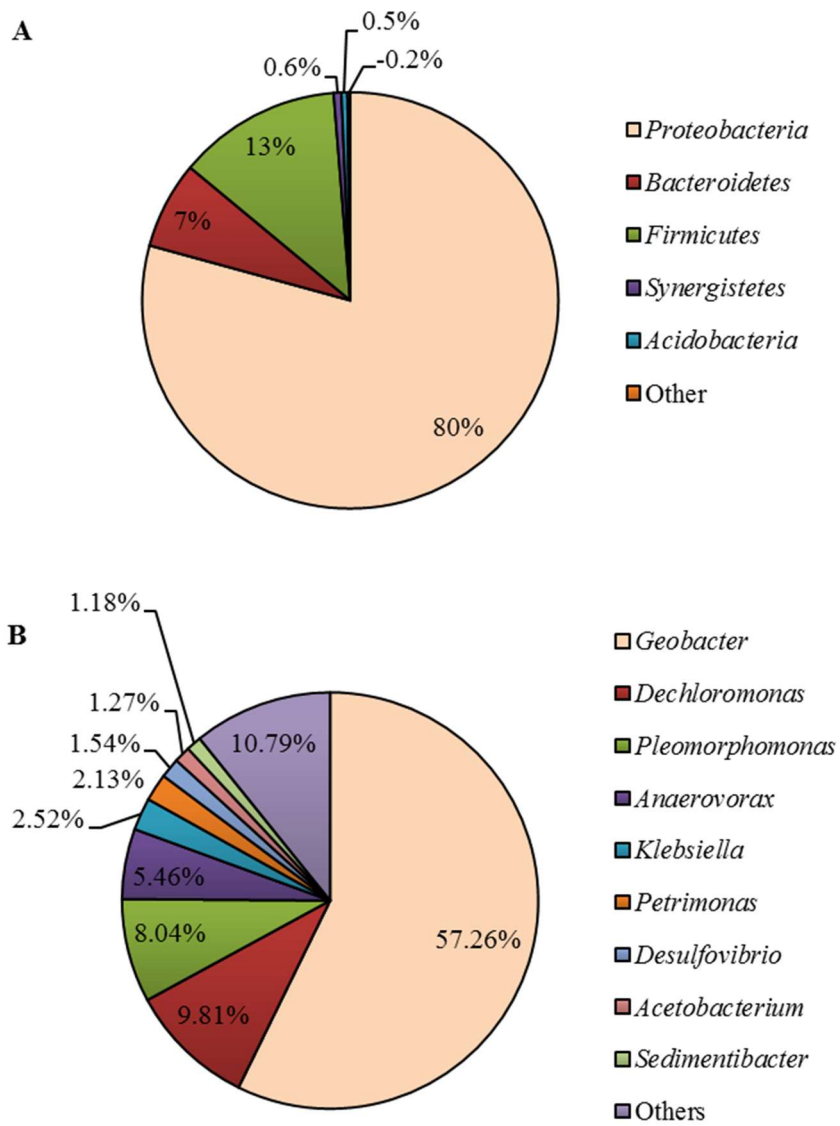
enrichment period by excluding glucose from the feed. The Coulombic efficiency was 40-60%, which was comparable to that achieved in glucose-amended feeding cycles (32 - 87%).



**Figure 4.4.** Catechol and phenol measured at the end of feeding cycles conducted with glucose (Glu) and furanic and phenolic compounds as the sole carbon and energy source (1-9).

#### 4.3.3 Microbial Community Structure

After 6 months of enrichment, the microbial community of the MFC anode biofilm was analyzed based on 16S rRNA gene sequences. As shown in Figure 4.5, about 80% of the microbial community belonged to the phylum of *Proteobacteria*. At the genus level, the microbial community was dominated by *Geobacter*, which has been reported as one of the most efficient exoelectrogens in bioelectrochemical systems (Logan, 2009). Other microbial species present can be related to the biotransformation of furanic and phenolic compounds, which is further discussed in Chapter 5.



**Figure 4.5.** MFC anode microbial community structures at the phylum (A) and genus (B) level.

#### **4.4 Summary**

A bioanode microbial community was developed in a MFC by feeding the five furanic and phenolic compounds, as well as glucose in the initial enrichment phase. The microbial community showed promising exoelectrogenic activity and the ability to transform the five furanic and phenolic compounds. With glucose excluded from the feed, the microbial community was adapted to use furanic and phenolic compounds as the sole carbon and energy source. Decreased levels of persistent transformation products and higher overall extent of biotransformation were also achieved with prolonged enrichment. With the demonstrated exoelectrogenic acidity and promising capacity to transform furanic and phenolic compounds, the anode microbial community described in this chapter provided an appropriate inoculum to start a MEC.

# CHAPTER 5

## HYDROGEN PRODUCTION IN MEC

### USING FURANIC AND PHENOLIC COMPOUNDS

#### 5.1 Introduction

As MEC is being recognized as a promising technology for waste, water and energy management in biofuel production, lignocellulosic effluent, refinery wastewater and switchgrass-derived bio-oil aqueous phase have been investigated in MECs for treatment and H<sub>2</sub> production (Lalaurette et al., 2009; Lewis et al., 2015; Ren et al., 2013b). In these complex streams, readily biodegradable carbohydrates (e.g., sugars and acetic acid) are usually present and likely major contributors to H<sub>2</sub> production (Lalaurette et al., 2009; Lewis et al., 2015). In contrast, furanic and phenolic compounds derived from lignocellulose are problematic components due to their inhibitory effect (Piotrowski et al., 2014). The contribution, effect, and fate of furanic and phenolic compounds on H<sub>2</sub> production in MEC has been poorly understood.

Two previous studies used furanic and phenolic compounds as the substrate in the anode of a MFC, but had mixed results. Catal et al. (2008) reported that, with the exception of HMF, use of nine individual furanic and phenolic compounds (2-furaldehyde, syringaldehyde, vanillin, *trans*-cinnamic acid, *trans*-4-hydroxy-3-methoxy-cinnamic acid, 4-hydroxy-cinnamic acid, 3,5-dimethoxy-4-hydroxy-cinnamic acids, benzyl alcohol and acetophenone) did not generate voltage. In contrast, Borole et al. (2013) demonstrated that a MFC anode microbial consortium was able to convert furfural, HMF, 4-hydroxybenzaldehyde, hydroxyacetophenone, and vanillic acid to

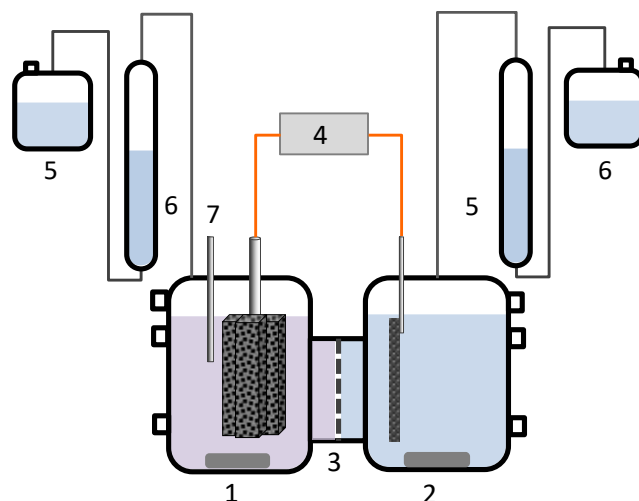
electricity. Thus, the question remains whether a MEC anode microbial community can use furanic and phenolic compounds as the sole carbon and energy source to produce H<sub>2</sub> in the cathode.

The specific objective of the work presented in this chapter was to assess the capacity of a MEC to produce hydrogen gas (H<sub>2</sub>) using a mixture of two furanic (furfural, FF; 5-hydroxymethyl furfural, HMF) and three phenolic (syringic acid, SA; vanillic acid, VA; and 4-hydroxybenzoic acid, HBA) compounds as the substrate in the bioanode.

## 5.2 Materials and Methods

### 5.2.1 MEC

An H-type MEC was developed with two square glass bottles separated by a cation exchange membrane (Nafion 117, 5.7 cm<sup>2</sup>; Dupont, Wilmington, DE) and maintained at room temperature (20-22°C). Both chambers and the anode electrode had the same configuration as the MFC anode described in Section 4.2.1, above. The cathode electrode was a carbon cloth containing 0.5 mg/cm<sup>2</sup> of Pt (5 cm × 6 cm; Fuel Cell Etc, College Station, TX). The anolyte composition was the same as the MFC anolyte described in Section 4.2.2, above. The catholyte was 100 mM buffer made of Na<sub>2</sub>HPO<sub>4</sub> and NaH<sub>2</sub>PO<sub>4</sub> · H<sub>2</sub>O. The anolyte and the catholyte were both mixed magnetically. A gas collection burette using displacement of an acid brine solution was connected to each chamber headspace for gas volume measurement (Figure 5.1). A potentiostat (Interface 1000, Gamry Instruments, Warminster, PA) was used to set a voltage of 0.6 V at the anode against the cathode using the two-electrode setup, with the anode as the working electrode and the cathode as both the counter and reference electrode.



**Figure 5.1.** MEC Setup. 1, anode chamber; 2, cathode chamber; 3, cation exchange membrane; 4, potentiostat; 5, displacement reservoir; 6, glass burette. 7, Ag/AgCl reference electrode.

### 5.2.2 MEC Operation

The MEC anode was inoculated with a microbial community sample taken from the MFC bioanode, which had been enriched with the mixture of the five furanic and phenolic compounds for 6 months (see Chapter 4). A piece of biofilm-attached carbon felt electrode (approximately 1 cm × 1 cm × 3 cm) of the MFC bioanode was cut using sterile scissors and anaerobically transferred to the center of the MEC anode electrode. During the startup, the bioanode was fed weekly with 200 mg/L of the five compounds mixture. Both the anolyte and catholyte were replaced at the beginning of each feeding cycle. After the startup, which lasted for 9 weeks, the total initial concentration of the substrate mixture was increased from 200 to 400, 800, and then to 1200 mg/L. The anode and cathode headspaces were initially filled with N<sub>2</sub>. The current was recorded every 4 hours. The duration of each feeding cycle was 6-7 days until the current decreased below 0.2



mA. Gas production ( $\text{H}_2$ ,  $\text{CO}_2$ ,  $\text{CH}_4$ ) in both anode and cathode headspaces was monitored. Liquid samples were taken periodically and analyzed for pH, as well as concentrations of the furanic and phenolic parent compounds, metabolites, and sCOD. Current density, Coulombic efficiency, and  $\text{H}_2$  yield were calculated to assess the effect of initial concentration of furanic and phenolic substrates on the MEC performance. Additional batch runs were conducted with 200, 400 and 800 mg/L sodium acetate (NaAc) to further understand the exoelectrogenic process of the MEC bioanode. During these batch runs, cyclic voltammetry was conducted, in addition to the above-mentioned measurements performed for the furanic and phenolic batch runs.

### 5.2.3 Experimental Controls

Two controls were evaluated. Control 1, setup with a biomass-free anode electrode in the MEC, was used to evaluate the potential contribution of the applied voltage on current production and transformation of the five compounds in the absence of microbial activity. Control 2 was used to investigate the stability of the five compounds in the presence of the porous carbon felt and anolyte. Four serum bottles, each containing 100 mL anolyte and 200 mg/L compound mixture, were kept under  $\text{N}_2$  headspaces. Two of the bottles contained carbon felt with equivalent quantity (v/v) as in the MEC anode. The concentration of the five compounds was monitored for 7 days.

### 5.2.4 Anode Microbial Community Analysis

Microbial community analysis of the MEC anode was performed after 9 weeks (9 feedings) from the startup. A piece of anode electrode with attached biofilm

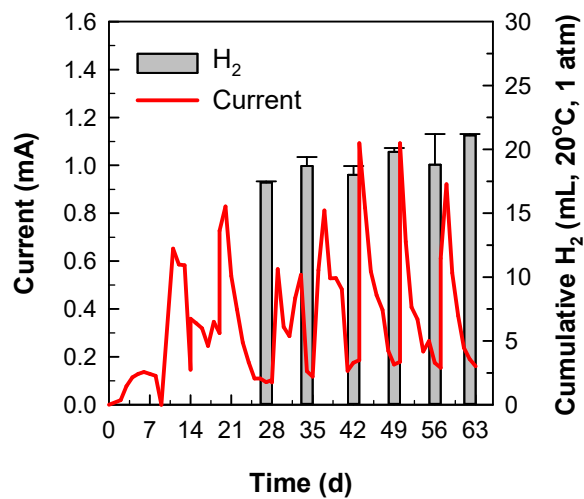
(approximately 1 cm × 1 cm × 3 cm) was washed several times with the anolyte and then cut into small pieces (< 0.5 cm). The genomic DNA was extracted and checked for purity as described in Section 3.2.8. 16S rRNA gene was sequenced using an Illumina MiSeq system (LC Science, Houston, TX). Bacterial primers 319F (5'-ACTCCTACGGGAGGCAGCAG-3') and 806R (5'-GGACTACHVGGGTWTCTAAT-3') were used to amplify the V3-V4 hypervariable regions of the 16S rRNA gene. The obtained sequences were clustered into Operational Taxonomic Units (OTUs) with 97% similarity. The longest read in each OTU was chosen as the representative sequence for taxonomic classification using the RDP classifier Version 2.7. The sequence-based phylogenetic tree of the abundant bacteria (>1% abundance) was constructed by applying the neighbor-joining algorithm using the program MEGA 6.06. The tree topology was evaluated by bootstrap resampling analysis of 1000 data sets. The representative sequences of the abundant species have been deposited to GenBank, National Center for Biotechnology Information (NCBI; [www.ncbi.nlm.nih.gov/](http://www.ncbi.nlm.nih.gov/)) with sequence accession numbers from KT124613 to KT124626.

## **5.3 Results and Discussion**

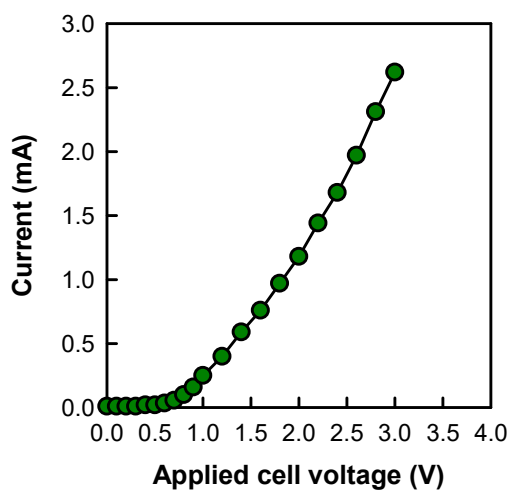
### **5.3.1 MEC Startup**

During the MEC startup period, fed-batch addition of 200 mg/L compound mixture was conducted in repetitive 7-day feeding cycles. Stable maximum current and H<sub>2</sub> production was observed by day 28 (Figure 5.2) and the startup period continued for another 35 days (5 feeding cycles) to confirm stable performance. During the MEC operation, the anolyte and catholyte pH was in the range of 6.7-7.0 and 7.0-7.3, respectively. The maximum

current density ( $I_{\max}$ ) was  $0.16 \pm 0.04$  mA/cm<sup>2</sup> or  $3.6 \pm 0.9$  A/m<sup>3</sup>, cumulative H<sub>2</sub> production was  $19.3 \pm 1.2$  mL (20°C, 1 atm), and Coulombic efficiency was  $44 \pm 12\%$  over the last 5 feeding cycles. The five compounds were completely transformed, with sCOD removal of  $57 \pm 10\%$  during each feeding cycle. An abiotic control assay (Control 1), conducted under the same MEC conditions, with the exception that the anode was not inoculated, resulted in negligible current ( $<0.12$  mA) and H<sub>2</sub> production ( $< 3$  mL) over 7 days, confirming that the current and H<sub>2</sub> production in the inoculated MEC was due to the bioactivity. Further examination of the current produced under abiotic conditions at an increasing voltage from 0.1 to 3.0 V resulted in an overpotential of the un-inoculated MEC of ca. 0.6 V (Figure 5.3), which is the voltage applied under normal MEC conditions. These results explain the very low current observed in the un-inoculated MEC.



**Figure 5.2.** Current and cumulative H<sub>2</sub> production during the MEC startup.

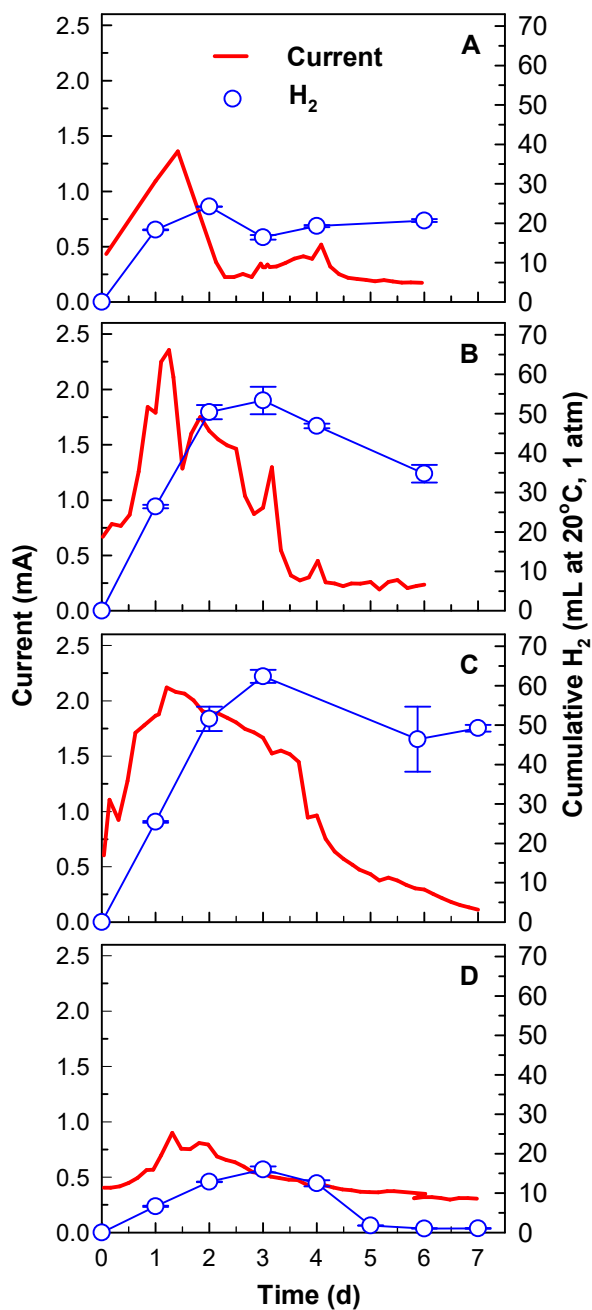


**Figure 5.3.** Current production in an un-inoculated, abiotic MEC at increasing applied voltage.

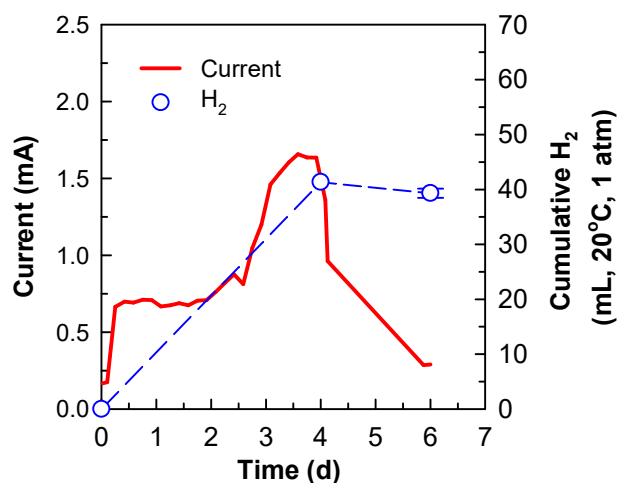
### 5.3.2 MEC Performance with Increased Substrate Concentration

After demonstrating H<sub>2</sub> production occurred during the MEC startup period, four consecutive batch assays were carried out with increasing initial anode substrate concentration, in order to assess the capacity of the bioanode to transform the five compounds at higher concentrations, as well as any potential inhibitory effect of these compounds or their transformation products on current and H<sub>2</sub> production (Figure 5.4). When the initial anode substrate concentration was increased from 200 to 400 mg/L, the I<sub>max</sub> almost doubled from 1.36 mA to 2.36 mA. As a result, the maximum H<sub>2</sub> production rate in the cathode increased from 18.3 to 26.5 mL/d. H<sub>2</sub> in the anode headspace was negligible (< 1 mL). Electric current of 1 mA corresponds to a maximum H<sub>2</sub> production rate of 11 mL/d (20°C, 1 atm) or 0.45 mmol/d, based on the fact that production of 1 mole of H<sub>2</sub> requires at least 2 moles of electrons (2 × 96585 coulombs). The current magnitude is also indicative of the rate of exoelectrogenesis. Thus, increasing the initial substrate concentration from 200 to 400 mg/L resulted in faster exoelectrogenesis, by providing higher concentration of the electron donor and/or enhancing the substrate mass transfer from the bulk solution into the biofilm. When the substrate concentration was further increased to 800 mg/L, although the I<sub>max</sub> did not increase, high current was sustained for a longer time resulting in a higher cumulative H<sub>2</sub> production than in the 400 mg/L run (49 mL vs. 35 mL). However, when the initial substrate concentration was increased to 1,200 mg/L, both the current and H<sub>2</sub> production were severely inhibited (Figure 5.4). The anode pH was 6.7 on day 3, which ruled out the possibility that low pH inhibited the bioanode activity. In fact, the 1,200 mg/L concentration is comparable to what has been reported for the inhibition of H<sub>2</sub> and ethanol fermentation by mixed cultures, typically around

1,000 mg/L (Klinke et al., 2004a; Monlau et al., 2014; Piotrowski et al., 2014). In order to determine whether the observed inhibition was reversible or not, the analyte was replaced with fresh medium and the compound mixture at 200 mg/L was added. Both current and H<sub>2</sub> production were restored to the previous levels within 2 days (Figure 5.5). The inhibitory effect of furanic and phenolic compounds on exoelectrogenesis was further investigated as reported in Chapter 7. Although inhibition was observed at 1,200 mg/L total substrate concentration, the MEC in the present study demonstrated its capacity to use furanic and phenolic compounds (up to 800 mg/L) as the sole carbon and energy source to produce H<sub>2</sub>. For comparison, a mixed fermentative culture produced only 0.58 mL/L of H<sub>2</sub> from HMF and no H<sub>2</sub> from furfural at 10-1000 mg/L (Liu et al., 2015b).



**Figure 5.4.** Current and cumulative H<sub>2</sub> production during four batch runs conducted at increased initial substrate concentrations in the MEC anode (A, 200 mg/L; B, 400 mg/L; C, 800 mg/L; D, 1200 mg/L). Error bars represent mean  $\pm$  standard deviation,  $n = 3$ .



**Figure 5.5.** Current and H<sub>2</sub> production at 200 mg/L initial substrate concentration after the observed inhibition during the 1200 mg/L batch run.

Efficiency parameters were calculated for the MEC batch runs performed with 200-800 mg/L initial substrate concentration (Table 5.1). The sCOD removal (49 - 61%) was lower than that of the 200-800 mg/L NaAc batch runs (76 - 87%), demonstrating that the extent of biodegradation of the furanic and phenolic compounds was lower than that of acetate in the MEC anode. The observed biotransformation products contributing to the residual COD are discussed in Section 5.3.3. From the electron equivalents removed, 44-69% were converted to current (i.e., Coulombic efficiency), and 26-42% were captured as H<sub>2</sub> (i.e., H<sub>2</sub> yield). Both the Coulombic efficiency and H<sub>2</sub> yield were lower than those of the NaAc batch runs (84-95%, 55-58%, respectively), suggesting that a larger portion of electron equivalents were used for biomass synthesis when furanic and phenolic substrates were used. The H<sub>2</sub> yield in the MEC was higher than reported values for dark fermentation of glucose using mixed cultures (~2 mol H<sub>2</sub>/mol glucose or 17% based on electron equivalence)(Lee et al., 2010; Ren et al., 2009). The H<sub>2</sub> yield, sCOD



removal and Coulombic efficiency achieved in the present study are comparable to those achieved with wastewater-fed MECs. Both H<sub>2</sub> yield and production rate were significantly improved at increasing initial substrate concentration from 200 to 400 mg/L (P<0.05), but the improvement was not as significant when the substrate concentration was further increased to 800 mg/L (P>0.05). The maximum H<sub>2</sub> production rate (0.1 L/L-d) was lower than that observed with domestic wastewater-fed MECs (0.3 L/L-d) (Cusick et al., 2010; Ditzig et al., 2007; Escapa et al., 2012). The relatively low H<sub>2</sub> production rate can be partially explained by the H-type reactor used in the present study, which has higher internal resistance than other optimized reactor designs (Call and Logan, 2008; Wang et al., 2010). On the other hand, furanic and phenolic compounds are less biodegradable than domestic wastewater. As discussed in Section 5.3.3, not all of the transformation products of the parent furanic and phenolic compounds were effectively used by the exoelectrogens.

While five specific furanic and phenolic compounds were assessed in the present study, in practice, use of a more complex mixture of substrates (e.g., lignocellulosic hydrolysates) is anticipated. Such feedstocks contain easily degradable compounds (e.g., carbohydrates) and thus can result in higher H<sub>2</sub> production rate in full scale MECs. A recent study on the utilization of switchgrass pyrolysates in MEC at a loading rate of 10 g COD/L-d achieved a H<sub>2</sub> production rate of 4.3 L/L-d without any inhibition (Lewis et al., 2015). Because the H<sub>2</sub> production rate is proportional to current density (A/m<sup>2</sup>), a more effective exoelectrogenesis with a higher biofilm density and a higher extent of transformation of furanic and phenolic compounds will improve the H<sub>2</sub> production rate of the MEC.

**Table 5.1.** Efficiency parameters of the MEC fed with the mixture of the five compounds.

Parameter	Initial substrate concentration (mg/L)		
	200	400	800
H <sub>2</sub> yield			
(mol/mol) <sup>a</sup>	2.9 ± 0.2 <sup>e</sup>	2.5 ± 0.2	1.7 ± 0.03
(%) <sup>b</sup>	38 ± 0.2	42 ± 7	26 ± 0.4
sCOD removal (%)	49 ± 0.1	49 ± 8	61 ± 4
CE (%) <sup>c</sup>	58 ± 1	69 ± 8	44 ± 0.1
H <sub>2</sub> production rate (L/L-d) <sup>d</sup>	0.07 ± 0.0004	0.10 ± 0.002	0.10 ± 0.001

<sup>a</sup> Moles of H<sub>2</sub> collected per mole of the compound mixture transformed

<sup>b</sup> H<sub>2</sub>-COD per COD removed during each batch run

<sup>c</sup> Electrons recovered as electrical current per electron equivalent of COD removal during each batch run

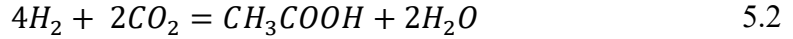
<sup>d</sup> Maximum production rate, observed on day 1 during each feeding cycle (20°C and 1 atm) normalized to the empty bed volume of the anode chamber

<sup>e</sup> Mean ± standard deviation; *n* = 3

Effective collection of H<sub>2</sub> was a challenge in the present study, which negatively impacted the H<sub>2</sub> production rate. The cumulative H<sub>2</sub> volume declined noticeably during the latter part of each batch run when anode bioactivity was lower (Figure 5.4). The difference between the maximum cumulative H<sub>2</sub> on day 3 (day 2 for the 200 mg/L run) and the total H<sub>2</sub> collected at the end of each run was considered to be the minimum H<sub>2</sub> loss. Thus, at least 3.5 - 18.6 mL (15-35%) of the produced H<sub>2</sub> was not captured during the 200-800 mg/L runs, and 93% was lost during the 1200 mg/L run, when overall H<sub>2</sub> production was very low. According to the Henry's law constant for H<sub>2</sub> at 20°C (8.03×10<sup>-4</sup> mol/L/atm; (Sander, 2014)) and the maximum partial pressure of H<sub>2</sub> in the cathode headspace (0.34 atm on day 3 in the 800 mg/L run), the dissolved H<sub>2</sub> in 250 mL catholyte at equilibrium was 0.017 mL at 20°C. The displacement solution of acid brine should have even less dissolved H<sub>2</sub> than the catholyte. Therefore, H<sub>2</sub> dissolution was negligible in the cathode.

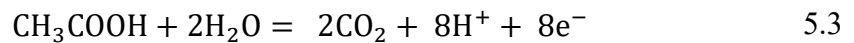
A control test revealed that 6% of H<sub>2</sub> added to the cathode headspace diffused through the cation exchange membrane to the anode headspace of an un-inoculated MEC with an open circuit tested for 7 days (Figure 5.6). Cathode H<sub>2</sub> diffusion through the cation exchange membrane to the anode has been previously acknowledged (Lee et al., 2009a; Rozendal et al., 2008). Under MEC conditions with an active bioanode and in the absence of external electron acceptors (e.g., O<sub>2</sub>, NO<sub>3</sub><sup>-</sup>, etc.), the H<sub>2</sub> diffused to the anode can readily be used by exoelectrogens as an electron donor (Equation 5.1) or by homoacetogens to form acetate (Equation 5.2)(Caccavo et al., 1994; Freguia et al., 2008; Kiely et al., 2011b).



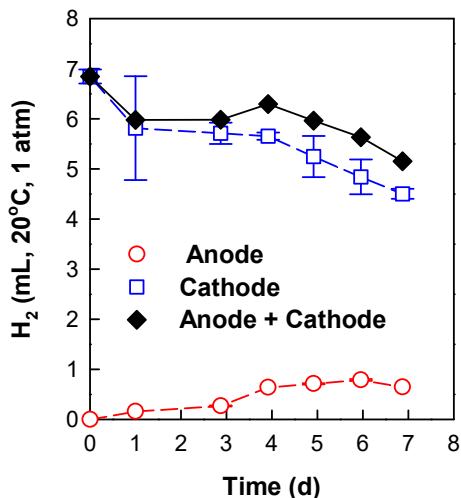


Thus, the diffusion of H<sub>2</sub> from the cathode to the anode could be higher than 6% during the normal 7-day MEC operation. The amount of H<sub>2</sub> diffusion could vary, depending on the in-situ rate of H<sub>2</sub> consumption by exoelectrogens and/or homoacetogens in different batch runs, which might be related to the acetate concentration in the bioanode. Two other factors, the total pressure and the H<sub>2</sub> partial pressure of the cathode headspace, which increased by 0.1 atm and 0.34, respectively, over the incubation period, might also have contributed to the H<sub>2</sub> transport to the anode. Active H<sub>2</sub> harvesting can be used to reduce the H<sub>2</sub> diffusion, as demonstrated in a recent study using a gas-permeable hydrophobic membrane and vacuum to rapidly extract cathodic H<sub>2</sub> (Lu et al., 2016a).

Another effect caused by H<sub>2</sub> diffusion and utilization in the anode can be pseudo-current production by recycling H<sub>2</sub> between cathode and anode. In addition to the current generation in Equation 5.1, acetate generated as shown in Equation 5.2 can also be used as electron donor by exoelectrogens (Equation 5.3)(Freguia et al., 2008; Kiely et al., 2011b).



Adding Equation 5.2 and 5.3 results in Equation 5.1. Therefore, regardless of the pathways (direct exoelectrogenesis using H<sub>2</sub> or homoacetogenesis), every 1 mole of H<sub>2</sub> utilized in the anode will contribute at most 2 moles of e<sup>-</sup> to the current. Taking this effect into consideration, the corrected Coulombic efficiency was 35-52%, about 10% lower than the values reported in Table 5.1.

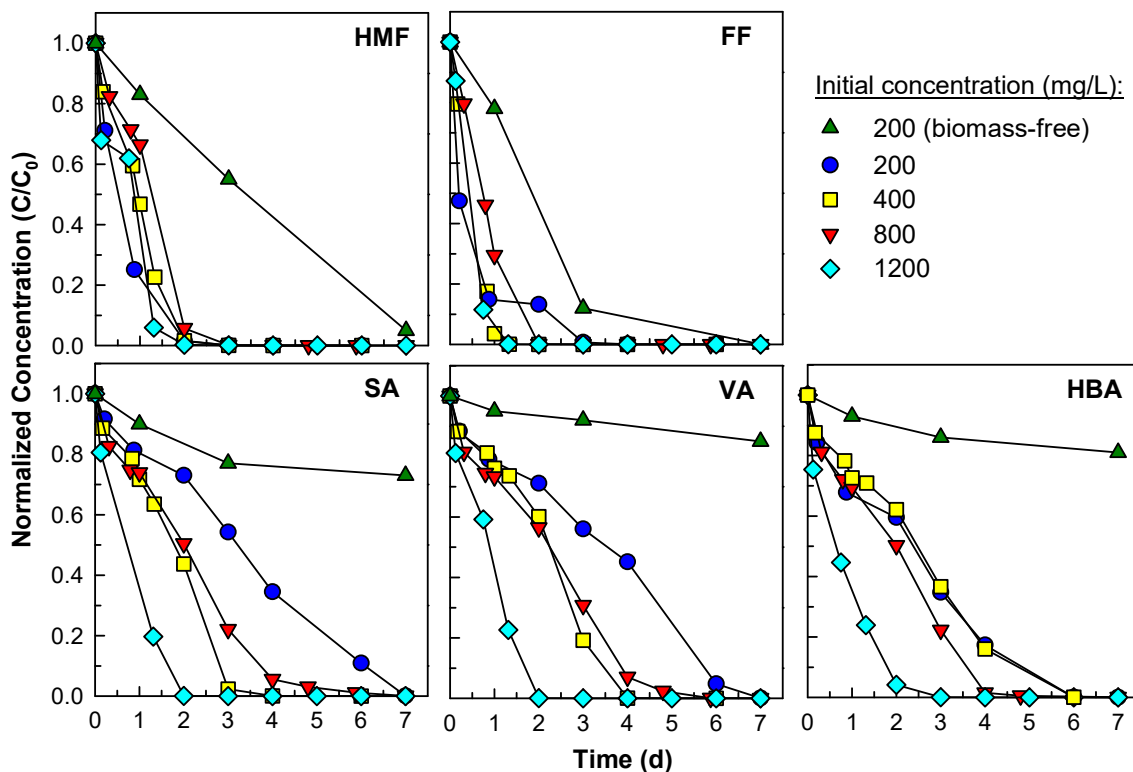


**Figure 5.6.** H<sub>2</sub> diffusion from the cathode to the anode headspace in a biomass-free MEC with an open circuit.

### 5.3.3 Biotransformation of the Furanic and Phenolic Compounds

All five compounds were completely transformed within 7 days at all initial concentrations tested (200-1,200 mg/L) (Figure 5.7). The results from Control 2 (biomass free, non-electrochemical condition) showed no detectable adsorption of the five compounds to the carbon felt, which was expected because the five compounds have  $\log K_{ow} < 2.0$  (Table 2.1). In addition, analysis of the catholyte showed no detectable compounds, confirming the selectivity of the cation exchange membrane. Thus, the disappearance of the five compounds was attributed to electrochemical reactions and/or microbial metabolism in the anode. As demonstrated in Control 1 (i.e., un-inoculated carbon felt), the concentration of the phenolic compounds decreased by about 20% within 7 days (Figure 5.7). It is not clear what products were formed, but none of the identified biotransformation products from the three phenolic compounds (discussed below) was detected. The two furanic compounds were completely transformed in Control 1. Furoic

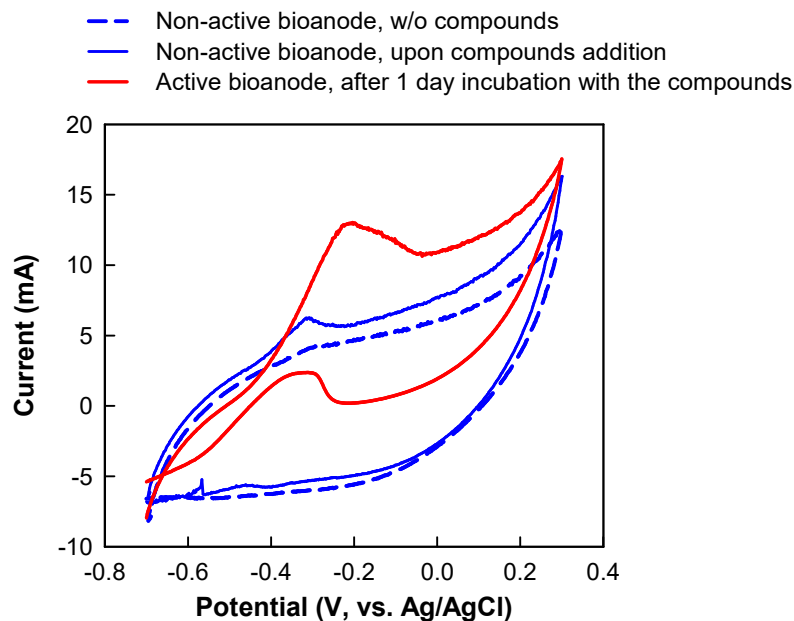
acid (FA) and 2,5-Bis(hydroxymethyl)furan (HMF-OH) were observed as the oxidized product of furfural and reduced product of HMF, respectively. It has been reported that a mixture of products could be generated from electrolysis of furfural and 5-HMF, including oxidized and reduced furan derivatives, open-ring products, and dimers, depending upon the type of electrode and electrolysis condition (Parpot et al., 2004; Vuyyuru and Strasser, 2012).



**Figure 5.7.** Normalized concentration profiles of the five compounds fed to the MEC anode at various initial concentrations (200 to 1200 mg/L total concentration).

However, it is important to note that the transformation rate of all five compounds substantially increased when the bioanode was used (Figure 5.7). The biomass on the bioanode could have added two levels of effect on the carbon felt electrode. First, the

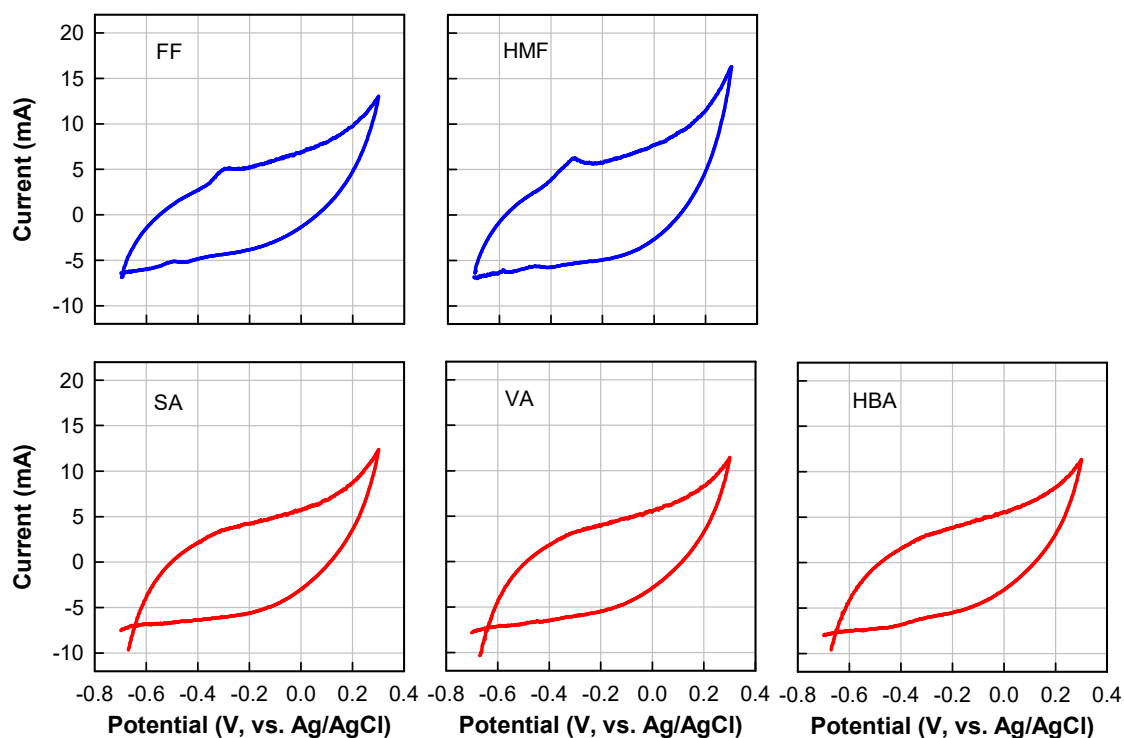
formation of biofilm on the surface of the electrode could have modified the electrode-analyte interface. Second, microbial activity could have introduced additional electrode reaction(s) (i.e., exoelectrogenesis). In order to distinguish such effects, CV was conducted with a non-active bioanode, which had been starved and shown minimal microbial activity, upon the addition of the compounds mixture at 200 mg/L and after mixing for 5 min. As shown in Figure 5.8, except for one small peak observed around  $-0.35$  V, the voltammogram of the non-active bioanode upon the addition of the compounds mixture was almost identical to that of the non-active bioanode in the absence of the compounds. Thus, the formation of biofilm (without bioactivity) did not have a significant effect on the transformation of the compounds or the observed current production. In contrast, the CV conducted with the bioanode after 1 day of incubation with the five compounds, when the bioanode produced significant current (see Section 5.3.2; Figure 5.4), resulted in a significant oxidation peak (Figure 5.8). Therefore, the bioactivity of the biofilm contributed much more significantly to the observed current production and the transformation of the furanic and phenolic compounds, than the modification of the electrode surface by biofilm attachment. Further examination of the active bioanode voltammogram is discussed in Section 5.3.4.



**Figure 5.8.** Cyclic voltammograms of a non-active bioanode in the absence and presence of a mixture of the five compounds, as well as an active bioanode after 1 d of incubation with the compounds mixture.

Cyclic voltammograms of the non-active bioanode in the presence of individual furanic and phenolic compounds were compared (Figure 5.9). Both furanic compounds resulted in small oxidation peaks in the voltammograms, while the non-active bioanode in the presence of phenolic compounds showed only capacitance current. Therefore, the above-mentioned oxidation peak observed in the non-active bioanode voltammogram in the presence of the compounds mixture resulted from the two furanic compounds. The higher electroactivity of furanic compounds is consistent with the observation that furanic compounds were converted by an abiotic carbon felt electrode to a larger extent, than the phenolic compounds (see Figure 5.7, above).





**Figure 5.9.** Cyclic voltammograms of a non-active bioanode in the presence of individual furanic and phenolic compounds.

As concluded above, the observed transformation of the five compounds in Figure 5.7 was mostly due to biotransformation. There was a clear trend for the transformation rate of the five compounds, which increased with increasing initial substrate concentration from 200 to 1,200 mg/L (Figure 5.7; Table 5.2). Increasing the initial concentration of the substrate mixture from 200 to 1,200 mg/L resulted in the following range of volumetric transformation rates (mM/d): 0.333-2.343 for FF; 0.197-1.029 for HMF; 0.047-0.917 for SA; 0.052-0.854 for VA; and 0.085-0.965 for HBA. The increase of the transformation rates, with increasing initial substrate concentration, implies that the five compounds were not inhibitory to the initial biotransformation step(s) even at the

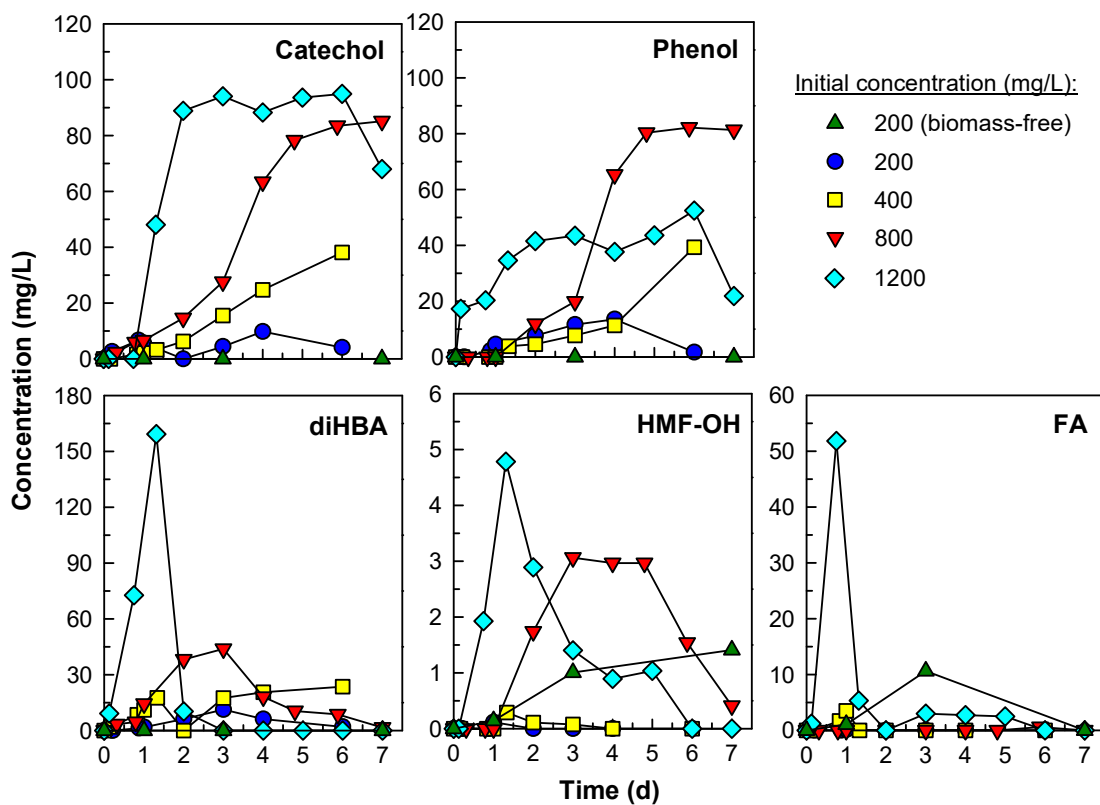
1200 mg/L run. In contrast, as discussed above, the current and H<sub>2</sub> production during the 1200 mg/L run were severely inhibited (Figure 5.4). The observation that the transformation rate of the five compounds increased, while current and H<sub>2</sub> production decreased, indicates that the five compounds were not the direct substrates for exoelectrogens and current generation. Previous studies have suggested that electricity generation was carried out primarily via fermentation products, like acetate and H<sub>2</sub>, when fermentable substrates were used in bioelectrochemical systems (Freguia et al., 2008; Kiely et al., 2011b). Because there was no external electron acceptor available in the anode medium in the present study, the initial biotransformation process of the five compounds in the MEC bioanode is assumed to be fermentation.

**Table 5.2.** Volumetric transformation rate of the furanic and phenolic compounds tested at various initial concentrations in the MEC bioanode.

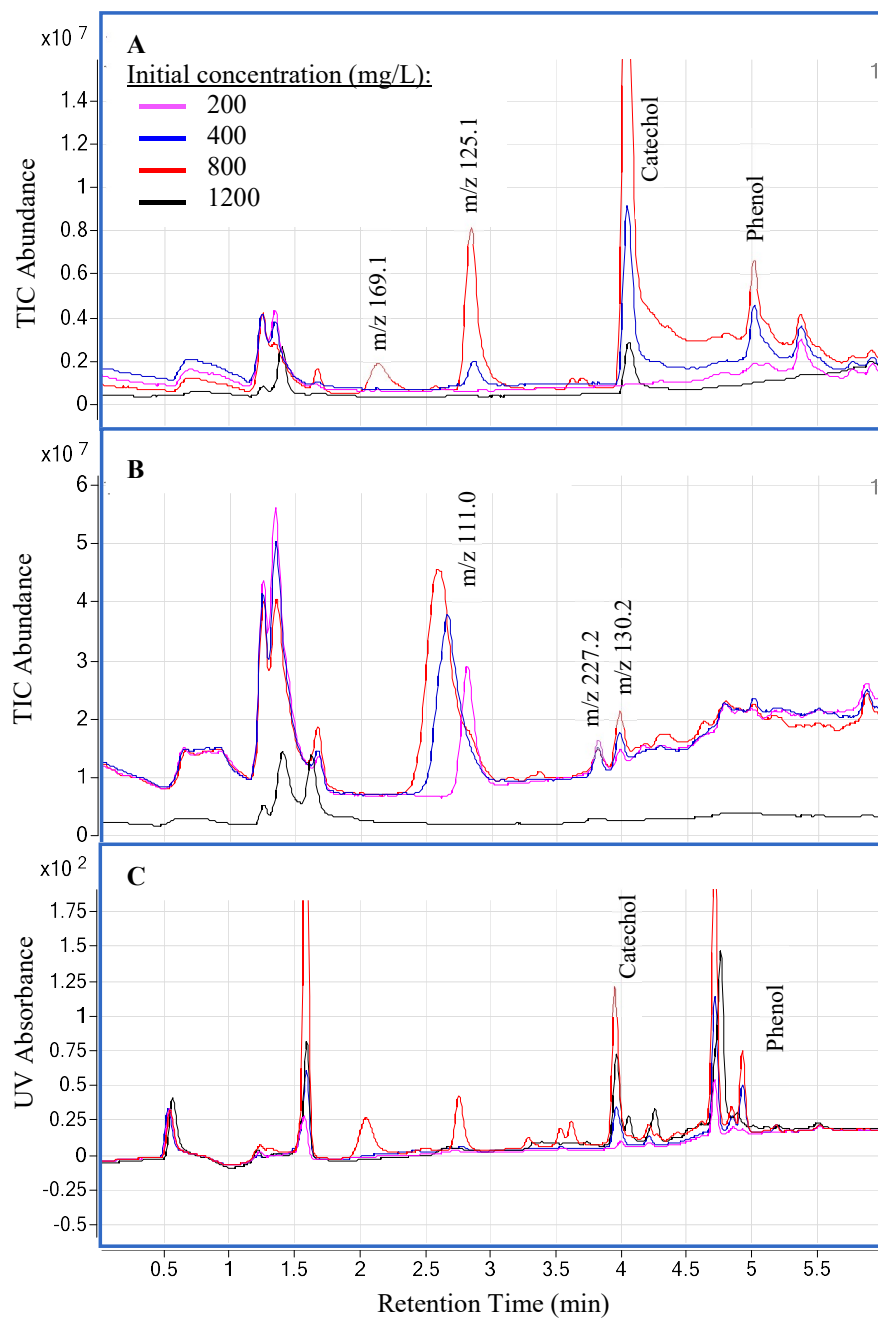
Compound	Initial Conc. (mg/L)		Rate <sup>a</sup>		R <sup>2</sup>	P Value
	Mixture	Individual	mg/L-d	mM/d		
		Compound				
Furfural (FF)	200	33.6	32.0 ± 4.9 <sup>b</sup>	0.333 ± 0.051	0.768	0.0072
	400	65.9	64.5 ± 1.3	0.671 ± 0.014	0.997	<0.0001
	800	113.4	78.7 ± 1.0	0.819 ± 0.010	0.999	<0.0001
	1,200	191.5	225.1 ± 3.4	2.343 ± 0.035	0.999	0.0002
5-hydroxymethyl furfural (HMF)	200	27.5	24.8 ± 2.1	0.197 ± 0.017	0.976	0.0123
	400	57.5	28.3 ± 1.9	0.224 ± 0.015	0.981	0.0001
	800	102.6	46.8 ± 5.3	0.371 ± 0.042	0.963	0.0030
	1,200	178.9	129.8 ± 19.9	1.029 ± 0.158	0.837	0.0073
Syringic acid (SA)	200	42.9	9.4 ± 0.2	0.047 ± 0.001	0.994	<0.0001
	400	86.7	24.2 ± 1.0	0.122 ± 0.005	0.975	<0.0001
	800	180.0	47.0 ± 2.2	0.237 ± 0.011	0.969	<0.0001
	1,200	292.9	181.7 ± 18.4	0.917 ± 0.093	0.961	0.0101
Vanillic acid (VA)	200	39.6	8.8 ± 0.5	0.052 ± 0.003	0.955	<0.0001
	400	81.4	20.0 ± 0.8	0.119 ± 0.005	0.972	<0.0001
	800	166.8	39.0 ± 1.7	0.232 ± 0.010	0.967	<0.0001
	1,200	270.0	143.6 ± 8.5	0.854 ± 0.051	0.963	<0.0001
4- hydroxybenzoic acid (HBA)	200	33.9	11.8 ± 0.8	0.085 ± 0.006	0.948	0.0001
	400	69.8	14.8 ± 0.6	0.107 ± 0.004	0.970	<0.0001
	800	133.4	34.1 ± 1.5	0.247 ± 0.011	0.969	<0.0001
	1,200	212.4	133.3 ± 15.9	0.965 ± 0.115	0.885	0.0036

<sup>a</sup> Rates estimated by linear regression; <sup>b</sup> Mean ± standard error ( $n \geq 5$ )

Transformation products identified using LC/MS/MS include furoic acid (FA), 2,5-Bis(hydroxymethyl)furan (HMF-OH), 3,4-dihydroxybenzoic acid (diHBA), catechol, phenol and acetate (Figure 5.10). These identified transformation products accounted for ca. 50% of the residual sCOD measured during the four batch assays. Thus, half of the transformation products on the basis of electron equivalents have not been identified, which is also indicated by the unknown peaks in the UV and TIC chromatograms at the end of the four batch assays (Figure 5.11). Nevertheless, ethanol, pyruvate, lactate and propionate were not detected at the end of the batch runs. Among the identified transformation products, catechol and phenol accumulated during all batch runs, while the other compounds were transient (Figure 5.10). Acetate accumulated only during the 1200 mg/L run (maximum acetate at 326 mg/L). The transformation products detected in Control 1 (biomass-free anode) include HMF-OH and FA, but no phenolic products (Figure 5.10). Thus, FA and HMF-OH could be produced from electrochemical reactions in the absence of bioactivity, whereas the formation of the detected phenolic products (catechol, phenol and diHBA) was the result of biotransformation.



**Figure 5.10.** Transformation products detected during the four batch assays at increased initial substrate concentrations in the MEC anode (200-1200 mg/L).



**Figure 5.11.** LC/MS chromatograms at the end of four batch assays revealing unidentified metabolites. (A) MS scan in negative mode; (B) MS scan in positive mode; (C) UV absorbance at 254 nm.

It has been widely accepted that fermentation is an important metabolic process, in addition to exoelectrogenesis, when fermentable substrates are used in bioanodes. Fermentation first transforms relatively complex substrates to lower molecular weight molecules (e.g., acetate and H<sub>2</sub>) which are then used as electron donors for exoelectrogenesis (Freguia et al., 2008; Kiely et al., 2011b). This syntrophic interaction was also observed in the present study. Acetate accumulated at 326 mg/L (5.4 mM) in the 1,200 mg/L run, but was not detected in the 200-800 mg/L runs. In the 1200 mg/L run, fast transformation of the five parent compounds resulted in fast production of acetate, but exoelectrogenesis was inhibited by either the five compounds or their transformation products (as discussed above), and thus contributed to a very low acetate utilization (Figure 5.4 and Figure 5.7). In contrast, in the 200-800 mg/L runs, active exoelectrogenesis occurred (Figure 5.4), resulting in rapid consumption of acetate produced by fermentation.

Stoichiometrically, 1200 mg/L of the five compounds could result in a maximum acetate level of 29.3 mM. It is possible that the acetate was partially produced by homoacetogenesis using CO<sub>2</sub> resulting from fermentation and H<sub>2</sub> diffused from the cathode. Yet, as discussed above, homoacetogenesis could contribute 2 mM acetate at the most, if the current production during the 1200 mg/L run was fully converted to H<sub>2</sub> (reverse of Equation 5.1) and then to acetate (Equation 5.2). In addition, the accumulated acetate at the end of the 1200 mg/L run could have resulted in the production of 105 mL of H<sub>2</sub> (1 mol acetate = 4 mol H<sub>2</sub>, based on electron equivalence) if inhibition had not occurred. Compared to the cumulative H<sub>2</sub> production during the 200, 400 and 800 mg/L runs (21, 35 and 49 mL, respectively), 105 mL would have been proportional to the initial

substrate concentration. Therefore, acetate is considered to be the direct substrate for exoelectrogenesis in the present study.

Other significant fermentation products detected and which accumulated were catechol and phenol. These two compounds are both reduced alcohols with higher electron equivalents (0.24 and 0.30 eeq/g) than the five parent compounds (0.18-0.21 eeq/g; Table 2.1). Therefore, catechol and phenol could be electron sinks of fermentation as opposed to the oxidized products resulting from exoelectrogenesis. Previous studies have reported catechol and phenol as biotransformation products from phenolic compounds under fermentative, anaerobic conditions (Evans and Fuchs, 1988; Phelps and Young, 1997). To understand why catechol and phenol were not rapidly transformed, as was the case of the other identified intermediates (i.e., FA, HMF-OH and diHBA), the free energy of putative fermentation reactions was analyzed (Table 5.3). It is assumed that these compounds undergo fermentation, instead of exoelectrogenesis, because they have not been reported as suitable electron donors for exoelectrogens. The standard Gibbs free energy ( $\Delta G^{0'}$ ) values of catechol and phenol fermentation are much more positive than those of FA, HMF-OH and diHBA (Table 5.3). Thus, fermentation of phenol and catechol is expected to be less favorable than that of the other detected transformation products. The limited biotransformation extent of the furanic and phenolic compounds, as well as the relatively low rate of metabolite transformation, may have contributed to the relatively low H<sub>2</sub> production.



**Table 5.3.** Possible fermentation of the identified transformation products to acetate and other products ( $\Delta G^{0'}$ ; Gibbs free energy at pH 7 and 298 K).

Compound	Reaction	$\Delta G^{0'}$ (kJ/mol)
Catechol <sup>a</sup>	$C_6H_6O_2 + 4H_2O = 3CH_3COO^- + H_2 + 3H^+$	-69.12
Phenol <sup>a</sup>	$C_6H_6O + 5H_2O = 3CH_3COO^- + 2H_2 + 3H^+$	+8.46
FA <sup>b</sup>	$2 C_5H_4O_3 + 6 H_2O \rightleftharpoons HCO_3^- + \frac{9}{2}CH_3COO^- + \frac{11}{2} H^+$	-763.66
HMF-OH <sup>b</sup>	$C_6H_8O_3 + 3 H_2O \rightleftharpoons 3CH_3COO^- + H_2 + 3 H^+$	-215.76
diHBA <sup>b</sup>	$2 C_7H_6O_4 + 8 H_2O \rightleftharpoons HCO_3^- + \frac{13}{2}CH_3COO^- + \frac{15}{2} H^+$	-257.66

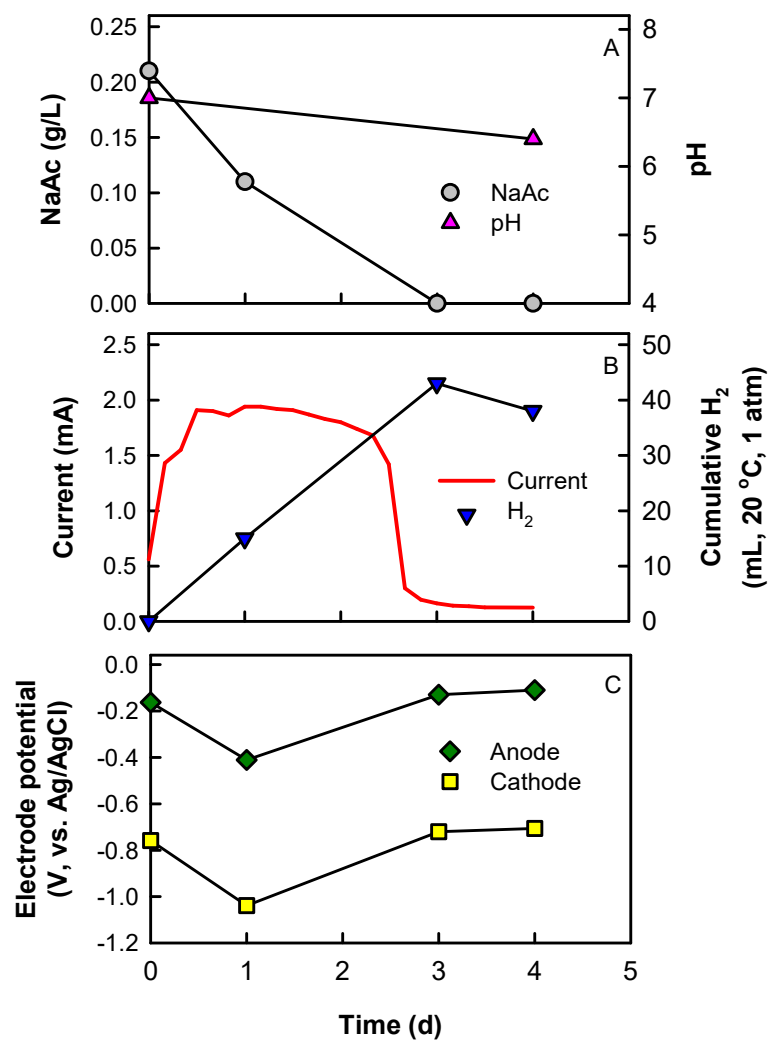
<sup>a</sup>  $G_f^0$  value from (Yaws, 2003)

<sup>b</sup>  $G_f^0$  value calculated based on the group contribution method (Mavrouniotis, 1990)

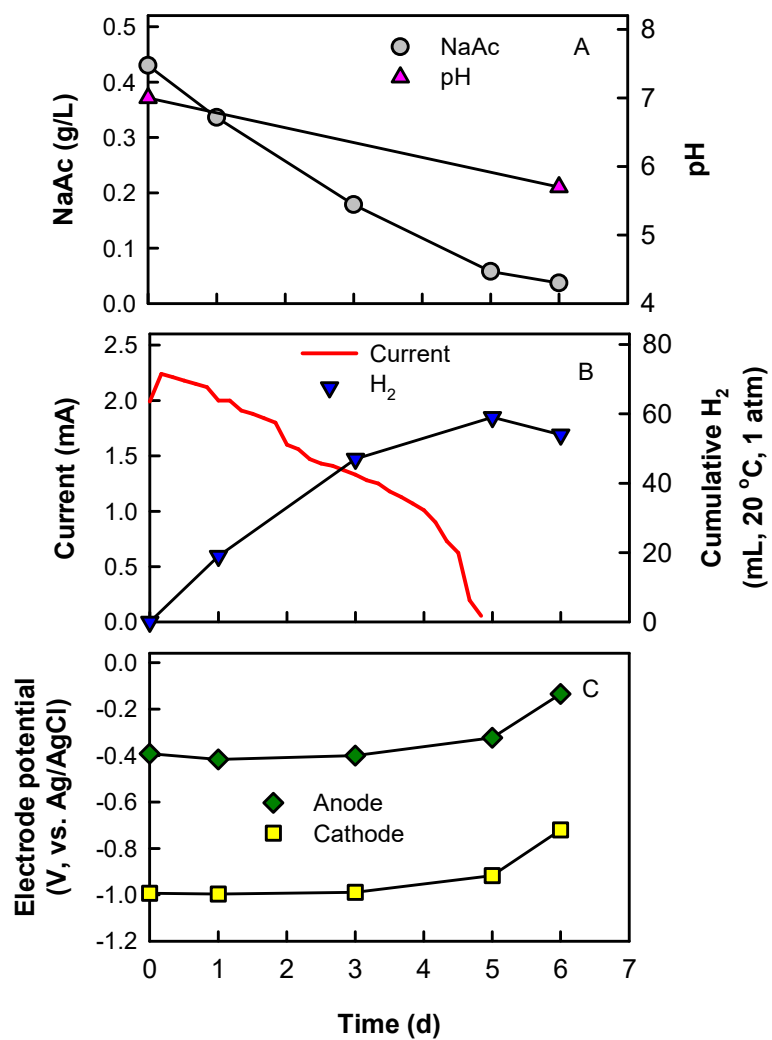
#### 5.3.4 Exoelectrogenesis in MEC Bioanode

As discussed above, the biotransformation of the furanic and phenolic compounds occurred via fermentation followed by exoelectrogenesis. The fermentative transformation involves non-electrochemical reactions, resulting in acetate for use in exoelectrogenesis. In contrast, exoelectrogenesis relies on electrochemical half-reaction(s) to generate current and then cathodic H<sub>2</sub>. To further understand the exoelectrogenic process in this study, the MEC bioanode was fed with NaAc at 200, 400 and 800 mg/L, and its electrochemical characteristics were examined.

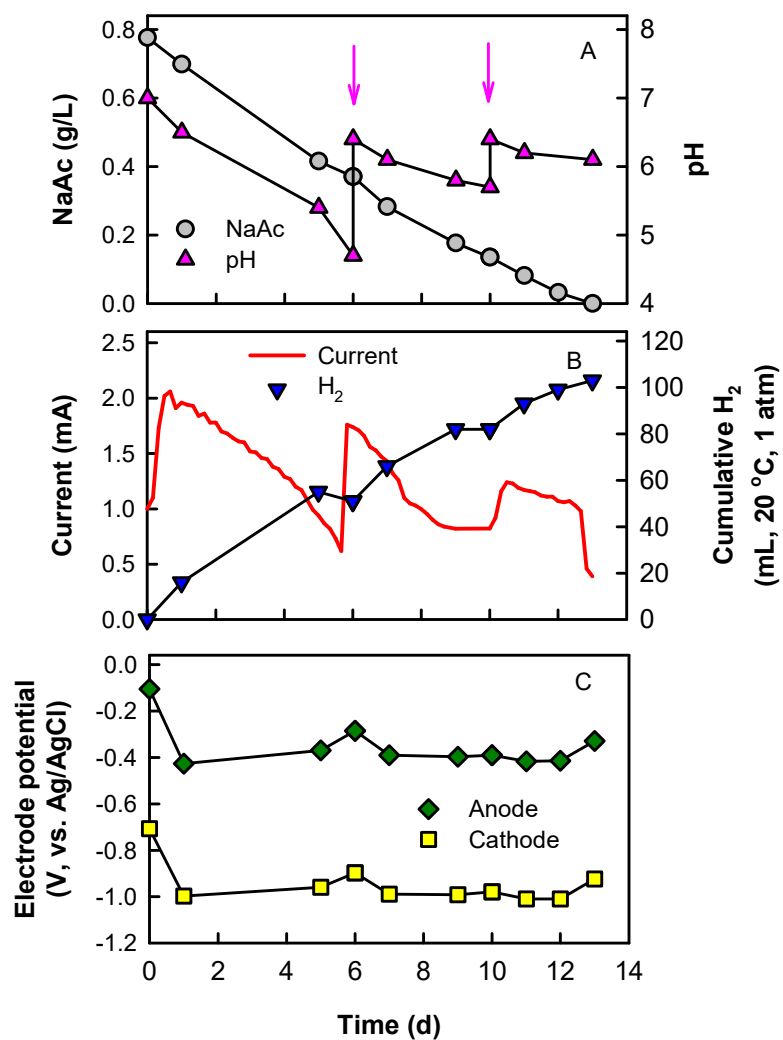
In these batch runs, NaAc was completely converted in 3-13 days, depending on the initial concentration (Figure 5.12A, Figure 5.13A, Figure 5.14A). While acetate being actively consumed, the anode bulk pH decreased over time, with the greatest decrease to below 6.0 observed in the 800 mg/L run. The cathode pH increased from 7.0 to 10 by the end of the 800 mg/L run. The H-type MEC reactor used a relatively narrow channel between the anode and cathode chambers, allowing a limited surface area of the cation exchange membrane. Thus, the quantity of proton transported per unit time is limited. When a high concentration of acetate was used, the protons produced in the anode could not be immediately transported to the cathode, which over time caused proton accumulation and thus pH decrease in the anode and increase in the cathode.



**Figure 5.12.** NaAc concentration and pH (A), current and H<sub>2</sub> production (B), as well as electrode potential (C) measured during the batch run conducted with 200 mg/L NaAc.

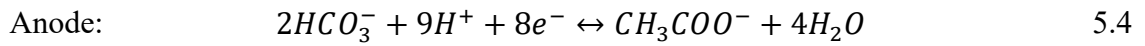


**Figure 5.13.** NaAc concentration and pH (A), current and H<sub>2</sub> production (B), as well as electrode potential (C) measured during the batch run conducted with 400 mg/L NaAc.

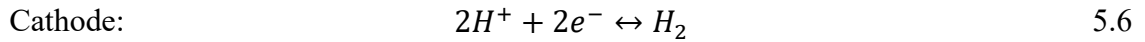


**Figure 5.14.** NaAc concentration and pH (A), current and H<sub>2</sub> production (B), as well as electrode potential (C) measured during the batch run conducted with 800 mg/L NaAc. Arrows indicate pH adjustment.

The observed maximum current was around 2.0 mA, the same for all three batch runs regardless of the increased initial acetate concentration (Figure 5.12B, Figure 5.13B, Figure 5.14B). Cumulative H<sub>2</sub> production was positively correlated to the current. H<sub>2</sub> loss discussed above was also observed at the end of the 200 and 400 mg/L batch runs. Decreasing current was observed during the 800 mg/L batch run, following the decrease of pH, even though acetate was abundantly present. Adjustment of pH resulted in immediate increase of current on day 6 and 10 (Figure 5.14B). The effect of pH on the current is discussed below. The equilibrium half potentials of the anode and cathode reactions can be calculated using the Nernst equation as follows:



$$E_a = E_a^0 - \frac{RT}{nF} \ln \frac{[\text{CH}_3\text{COO}^-]}{[\text{HCO}_3^-]^2 [\text{H}^+]^9} \quad 5.5$$



$$E_c = E_c^0 - \frac{RT}{nF} \ln \frac{p_{\text{H}_2}}{[\text{H}^+]^2} \quad 5.7$$

$$\text{Overall:} \quad E_{eq} = E_c - E_a \quad 5.8$$

where  $E_a^0$  is equal to 0.187 V,  $E_c^0$  is equal to 0 by convention, R is the ideal gas law constant, T is the absolute temperature, n is the number of electrons transferred, and F is the Faraday's constant.

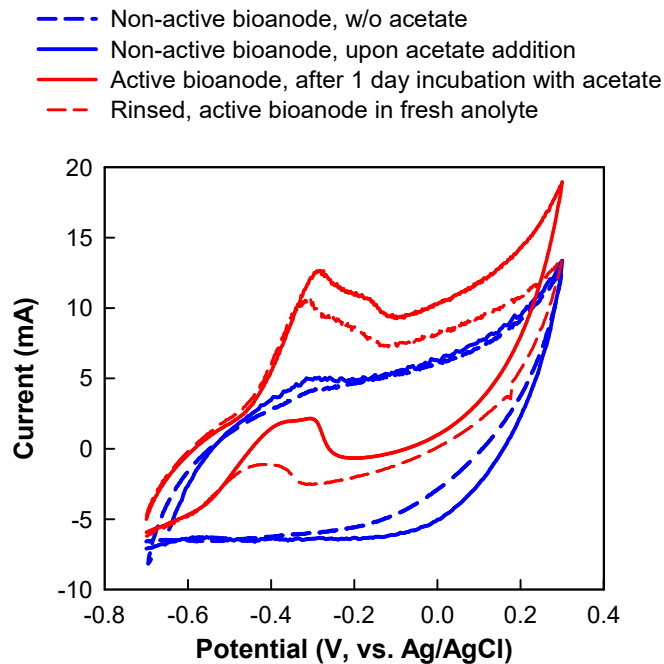
Based on Equation 5.5 and 5.7, the equilibrium anode potential increased with decreasing anode pH, while the equilibrium cathode potential decreased with increasing cathode pH. Consequently, the equilibrium potential of the overall reaction ( $E_{eq}$ ) became more negative (Equation 5.8), meaning that a higher applied voltage is required for compensating the negative  $E_{eq}$ . In theory, every pH unit difference between the anode

and the cathode chamber will decrease  $E_{eq}$  by 0.06 V (Logan et al., 2008). In this study, a fixed voltage (0.6 V) was supplied, part of which is expected to be used for internal losses (i.e., overpotentials and Ohmic losses)(Logan et al., 2008). Therefore, when  $E_{eq}$  decreased to a level which the applied voltage can no longer compensate, the current production decreased. The decrease of current due to pH change was observed on day 6 and 10 during the 800 mg/L batch run (Figure 5.14B). After 13 days in the 800 mg/L batch run, acetate was depleted (Figure 5.14A), while pH was above 6.0. The decreased current at this time was due to substrate depletion, same as at the end of the 200 and 400 mg/L runs.

In the batch runs conducted with furanic and phenolic mixture (discussed in Section 5.3.2), the pH was maintained above 6.7 during the 7-d run. Thus, the pH effect was not the cause of the observed low current at the end of the batch runs. Instead, acetate depletion resulted in the low current. Although up to 1.2 g/L furanic and phenolic mixture was used, the maximum acetate produced was 0.326 g/L (i.e., 0.45 g/L NaAc), lower than the concentration that resulted in severe pH drop within 7 days.

The measured anode potential was stable at -0.4 V (vs. Ag/AgCl) during active exoelectrogenesis, but it increased when a low current was produced (Figure 5.12C, Figure 5.13C, Figure 5.14C). The measured cathode potential is always -0.6 V relative to the anode potential. Because the electrode potential was measured using a voltmeter, which introduces a secondary circuit to the MEC already connected to the potentiostat, interference between the circuits could result in inaccuracy of the potential measurements.

Cyclic voltammetry was conducted to examine the exoelectrogenic activity of the bioanode fed with 200 mg/L NaAc. As shown in Figure 5.15, the non-active bioanode produced only capacitance current, either in the presence or absence of acetate. In contrast, after 1 day of incubation with acetate, when the maximum current was observed in the 200 mg/L NaAc batch run (see Figure 5.12, above), the voltammogram of the bioanode showed a significant oxidation peak at around  $-0.3$  V (Figure 5.15). Thus, the oxidation peak was not associated with abiotic acetate oxidation, but rather resulted from the exoelectrogenic activity.



**Figure 5.15.** Cyclic voltammograms of the bioanode fed with 200 mg/L NaAc at the beginning of a batch run (non-active), after 1 day of incubation (active) and after the anode was rinsed with fresh anolyte.

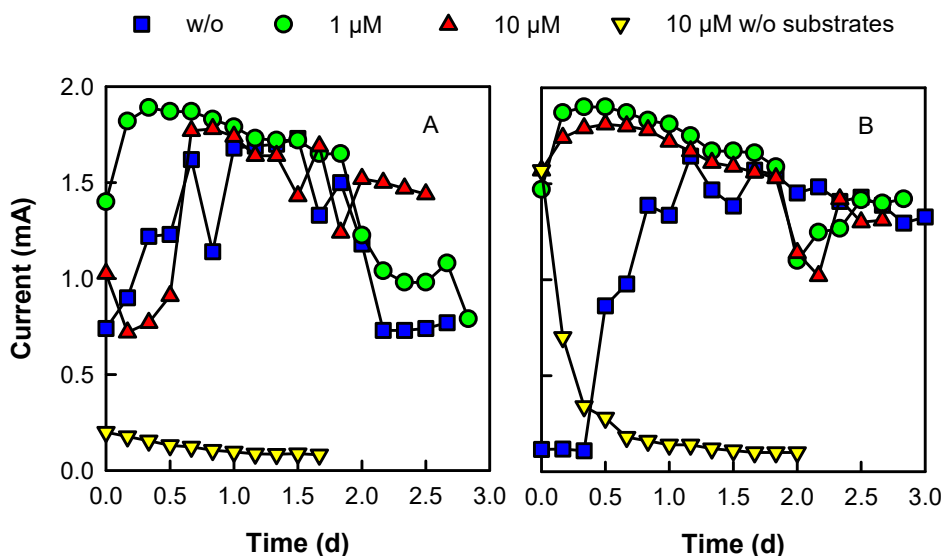


Depending on the mechanism of extracellular electron transfer (EET) used by the exoelectrogens in the bioanode, the oxidation peak in the forward scan could be attributed to outer-membrane bound c-type cytochromes and/or nanowires, if a direct electron transfer mechanism was used, or soluble electron transfer mediators, if an indirect electron transfer mechanism was used (Bond et al., 2012; Marsili et al., 2008). An oxidation peak was observed in backward scan (around -0.4 V), which is not common but has been shown in bioanode voltammograms of other studies, without a mechanistic interpretation (Marsili et al., 2010; Zhang et al., 2014). One possible interpretation of the oxidation peak is the presence of membrane-bound proteins performing bi-directional EET between the electrode and microbial cells. In spite of a few reports on the EET of bi-directional proteins, the mechanism is largely unknown (Nealson and Rowe, 2016; Ross et al., 2011).

The fundamentals of direct and indirect EET are discussed in Section 2.2.2, above. In order to identify which EET mechanism was at play, the active bioanode was anaerobically rinsed with anolyte to remove any soluble electron transfer mediators, and CV was conducted again with the bioanode in fresh anolyte. It is noteworthy that the same oxidation peak was observed in the voltammogram of the rinsed bioanode at a comparable height to that in the active bioanode, despite the slight shift of the baseline capacitance current (Figure 5.15). Therefore, direct EET was the primary electron transfer mechanism used by the exoelectrogens in the present study.

To provide further evidence supporting the direct EET mechanism, the effect of soluble electron transfer mediators, riboflavin (RF) and anthraquinone-2,6-disulfonate (AQDS), on the current production in the MEC fed with the five furanic and phenolic

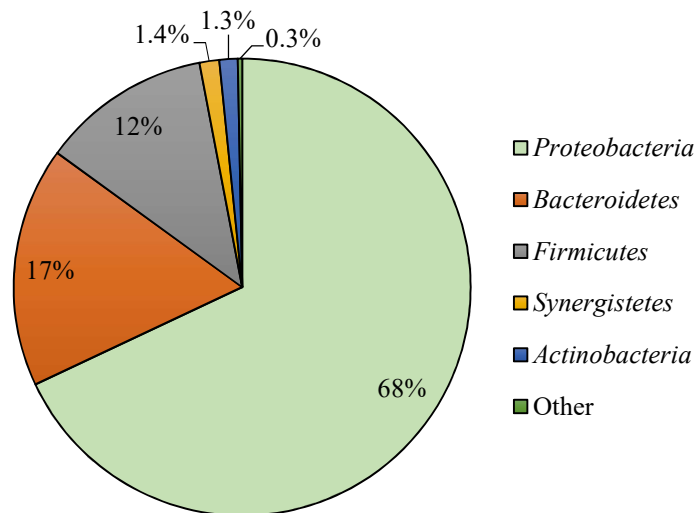
compounds was examined. RF is a dominant electron shuttling compound secreted by exoelectrogens to mediate indirect electron transfer (Marsili et al., 2008), while AQDS is a widely used exogenous electron shuttle (Esteve-Núñez et al., 2008). These two selected mediators represent endogenous and exogenous electron mediators. However, the current produced in the MEC fed with 0.5 g/L furanic and phenolic mixture was not significantly improved by adding RF or AQDS at concentrations of 1 and 10  $\mu\text{M}$ , except the earlier onset of the maximum current on the first day of several batch runs (Figure 5.16). Adding 10  $\mu\text{M}$  RF without the furanic and phenolic substrates resulted in negligible current, whereas 10  $\mu\text{M}$  AQDS alone resulted in an immediate but short production of current up to 1.5 mA. Overall, the addition of soluble electron transfer mediators did not improve the MEC current production, which further indicates that direct EET was the major mechanism of exoelectrogenesis in the present study.



**Figure 5.16.** Current production of MEC fed with furanic and phenolic substrates and amended with RF (A) and AQDS (B) at 1 and 10  $\mu\text{M}$ .

### 5.3.5 Anode Microbial Community

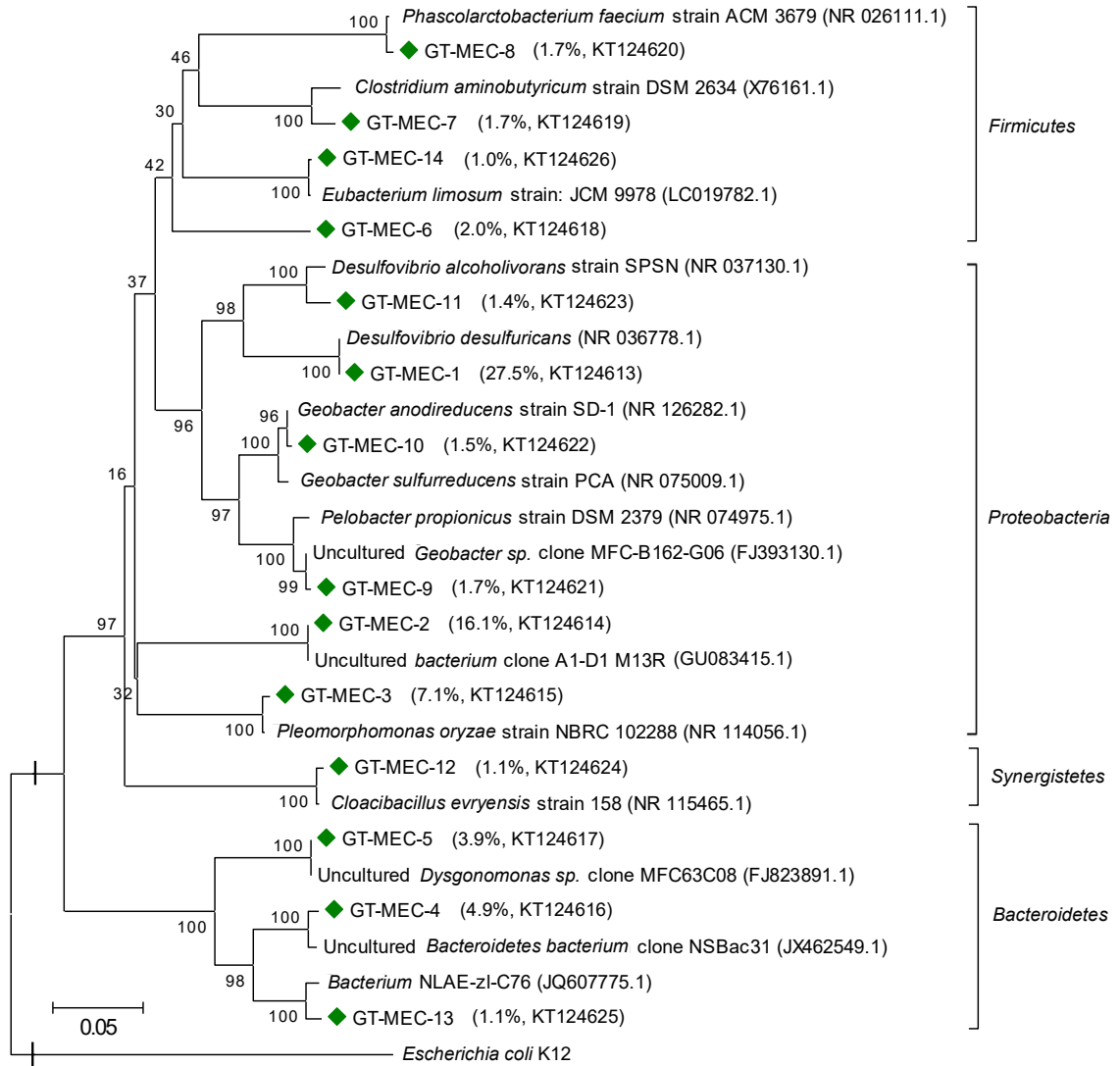
The 16S rRNA gene sequencing analysis revealed that after 9 weeks of MEC operation 14 dominant OTUs (each greater than 1% abundance out of 38020 clean sequences obtained) were present. The anode microbial community was dominated by species of the *Proteobacteria* phylum, representing 68% of the community (Figure 5.17). The abundant genera belonging to this phylum were *Desulfovibrio* (39% of the total 16S rRNA gene sequences), *Pleomorphomonas* (11%), and *Geobacter* (5%). The second abundant phylum was *Bacteroidetes* (17%), comprised of *Petrimonas* (10%) and *Dysgonomonas* (7%) genera, followed by *Firmicutes* (12%) with the major genera of *Anaerovorax* (3%), *Phascolarctobacterium* (3%), and *Clostridium XIVa* (3%). Other phyla present with abundance less than 2% were *Synergistetes* and *Actinobacteria*. At the phylum level, the structure of the anode microbial community was similar to that of the MFC anode from which the inoculum was taken to start the MEC (Figure 4.5).



**Figure 5.17.** Composition of the MEC anode microbial community at phylum level.

The phylogenetic relationships of the abundant microorganisms (>1% abundance) detected in the MEC bioanode are shown in Figure 5.18. *Desulfovibrio desulfuricans* is a sulfate-reducing bacterium, which is able to perform exoelectrogenesis through cytochrome c (Kang et al., 2014). In addition, the major known degraders of furfural and 5-HMF under anaerobic conditions belong to *Desulfovibrio* genus (Wierckx et al., 2011b). *Geobacter* spp. are well studied exoelectrogens, using acetate and H<sub>2</sub> as primary electron donors (Caccavo et al., 1994; Sun et al., 2014). *Eubacterium limosum* is known to grow on methoxylated aromatic compounds, such as syringic acid and vanillic acid (Sharak Genthner and Bryant, 1987). *E. limosum* is also a homoacetogen, which could consume H<sub>2</sub> formed during fermentation and produce acetate for exoelectrogens (Genthner et al., 1981). *Pelobacter propionicus* is not known to perform exoelectrogenesis or to use acetate as the electron donor, but is thought to be involved in syntrophic interactions with exoelectrogens fermenting initial substrates to acetate (Kiely et al., 2011a; Parameswaran et al., 2010). *Clostridium populeti* and *Clostridium aminobutyricum* are known mixed-acids fermenters, and the latter has been found in acetate- and glucose-fed MFC anodes (Sleat and Mah, 1985; Xing et al., 2009). *Phascolarctobacterium faecium* can convert succinate to propionate (Del Dot et al., 1993). Therefore, *E. limosum*, *P. propionicus*, *P. faecium* and *Clostridium* spp. could be syntrophic partners with exoelectrogens by converting the furanic and phenolic compounds or their biotransformation products to readily available substrate (e.g., acetate) for exoelectrogenesis. Several detected species in the present study are closely related to bacteria, such as *Dysgonomonas* spp. (Borole et al., 2009), *Pleomorphomonas oryzae* (Yamamuro et al., 2014), and the uncultured bacterium clones (JX462549.1 and

GU083415.1)(Kiely et al., 2011a; Kobayashi et al., 2013) previously found in bioelectrochemical systems, but their functions are unknown. Other phylotypes related to the OTUs detected in the present study are *Cloacibacillus evryensis*, an amino-acid degrading bacterium found in anaerobic digesters (Ganesan et al., 2008), and a bacterial species found in cellulose and xylan-pectin enrichments of cow feces (Ziemer, 2014). These species may have been carried over from the original inoculum, which came from a municipal anaerobic digester. In summary, the abundant species in the bioanode are mainly related to exoelectrogens, putative degraders of the furanic and phenolic compounds, and potential syntrophic partners with exoelectrogens.



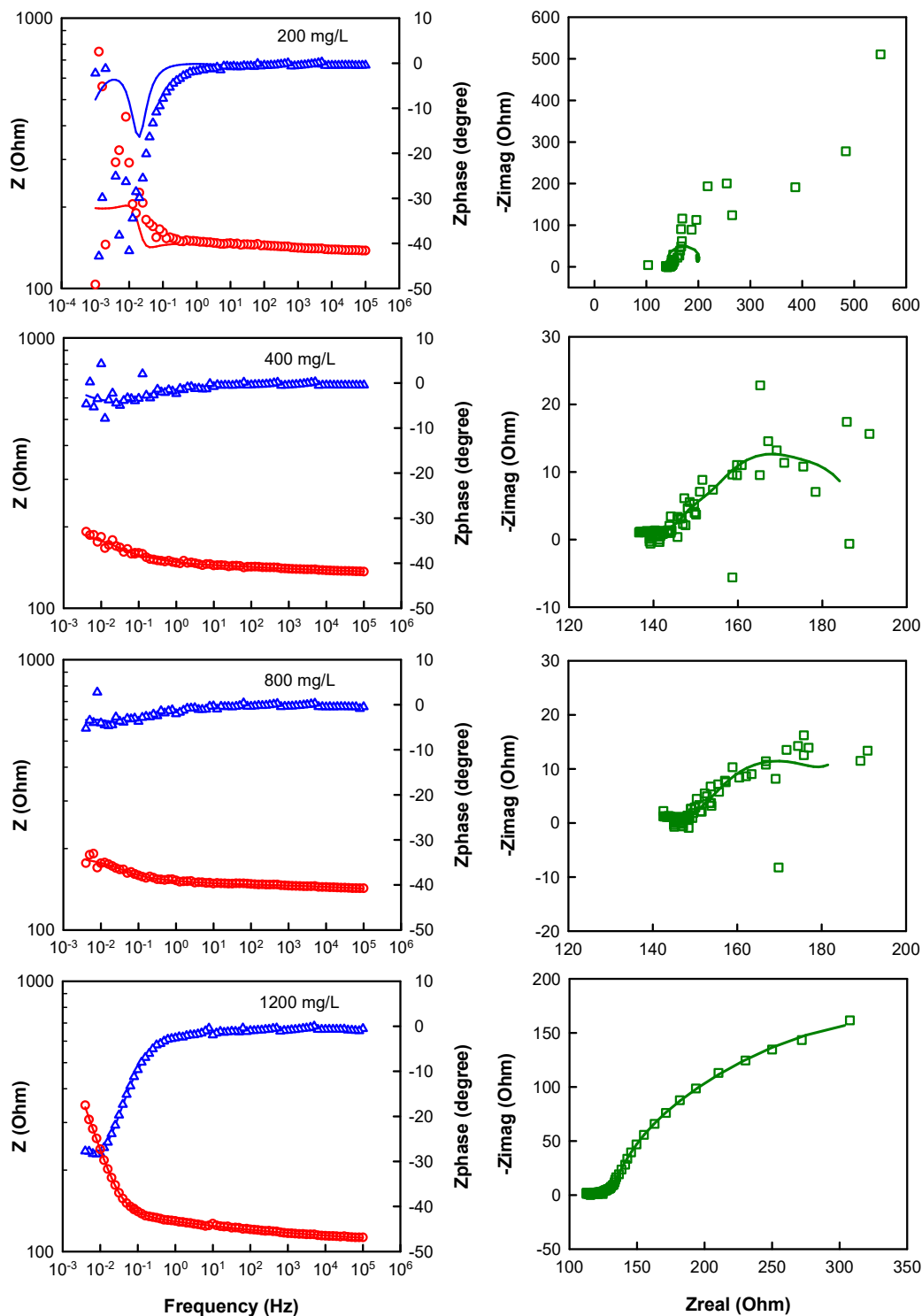
**Figure 5.18.** Phylogenetic tree of the dominant bacteria identified in the MEC anode.

Fraction of bacterial population and GenBank accession numbers shown in parentheses.

*Escherichia coli* K12 was used as the outgroup.

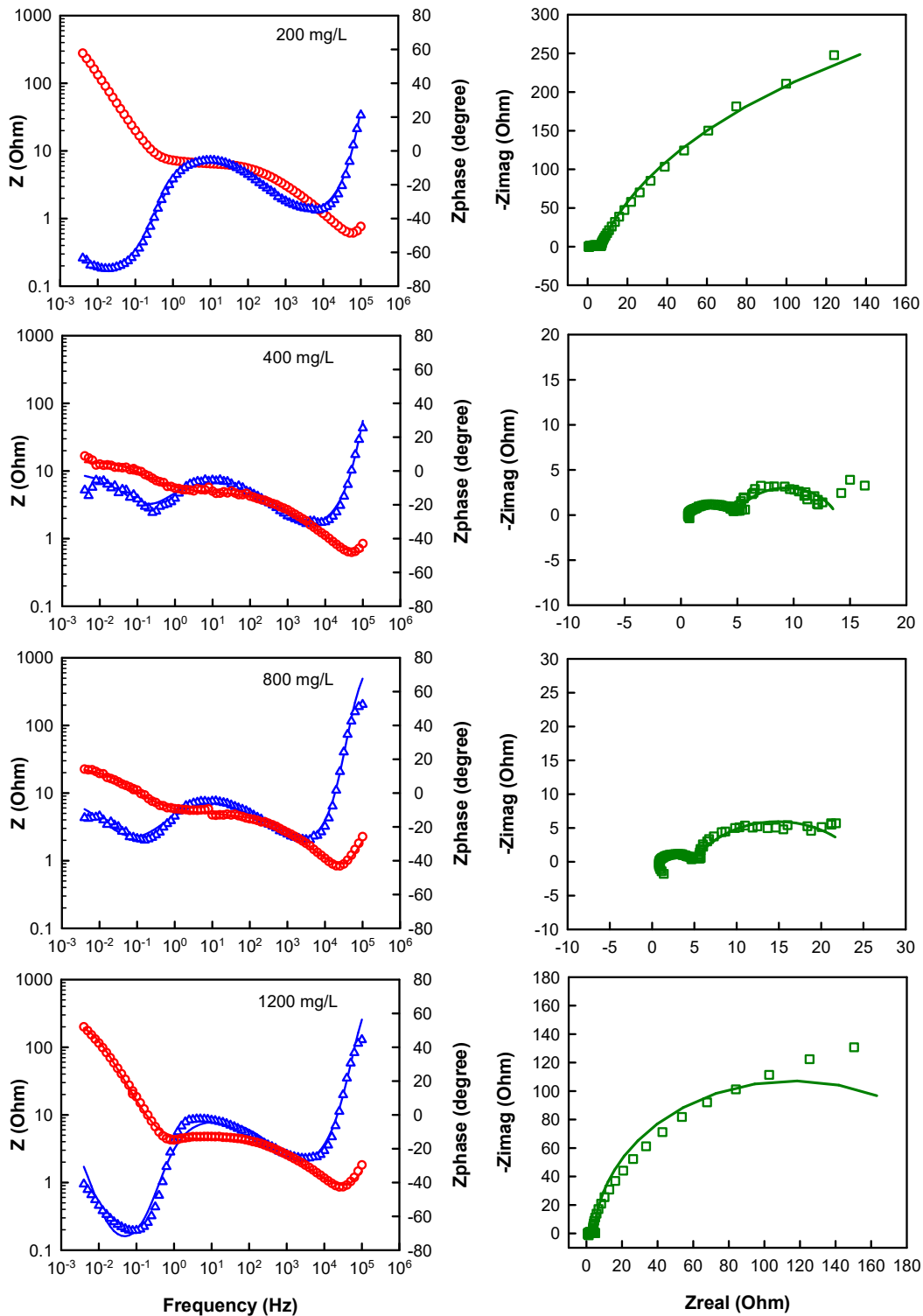
### 5.3.6 MEC Internal Resistance

The MEC internal resistance was measured using electrochemical impedance spectroscopy (EIS, see Section 3.2.11) at the end of each batch run conducted with 200-1200 mg/L furanic and phenolic compounds. Fitting the EIS spectra of the whole-cell to the selected equivalent circuit, shown in Figure 3.3B, resulted in poor goodness of fit ( $10^{-3}$  -  $10^{-2}$ ) and large error of the estimated parameters for all datasets obtained from the four batch runs (Figure 5.19). However, half-cell EIS spectra were fitted reasonably well to the equivalent circuit (Figure 3.3B), resulting in goodness of fit  $\leq 10^{-3}$ , and relatively small standard deviations (Figure 5.20; Figure 5.21). Thus, the resistance associated with the anode or cathode processes was calculated based on the half-cell EIS spectra, while the resistance associated with the anolyte/catholyte plus the cation exchange membrane was obtained from the whole-cell EIS data.

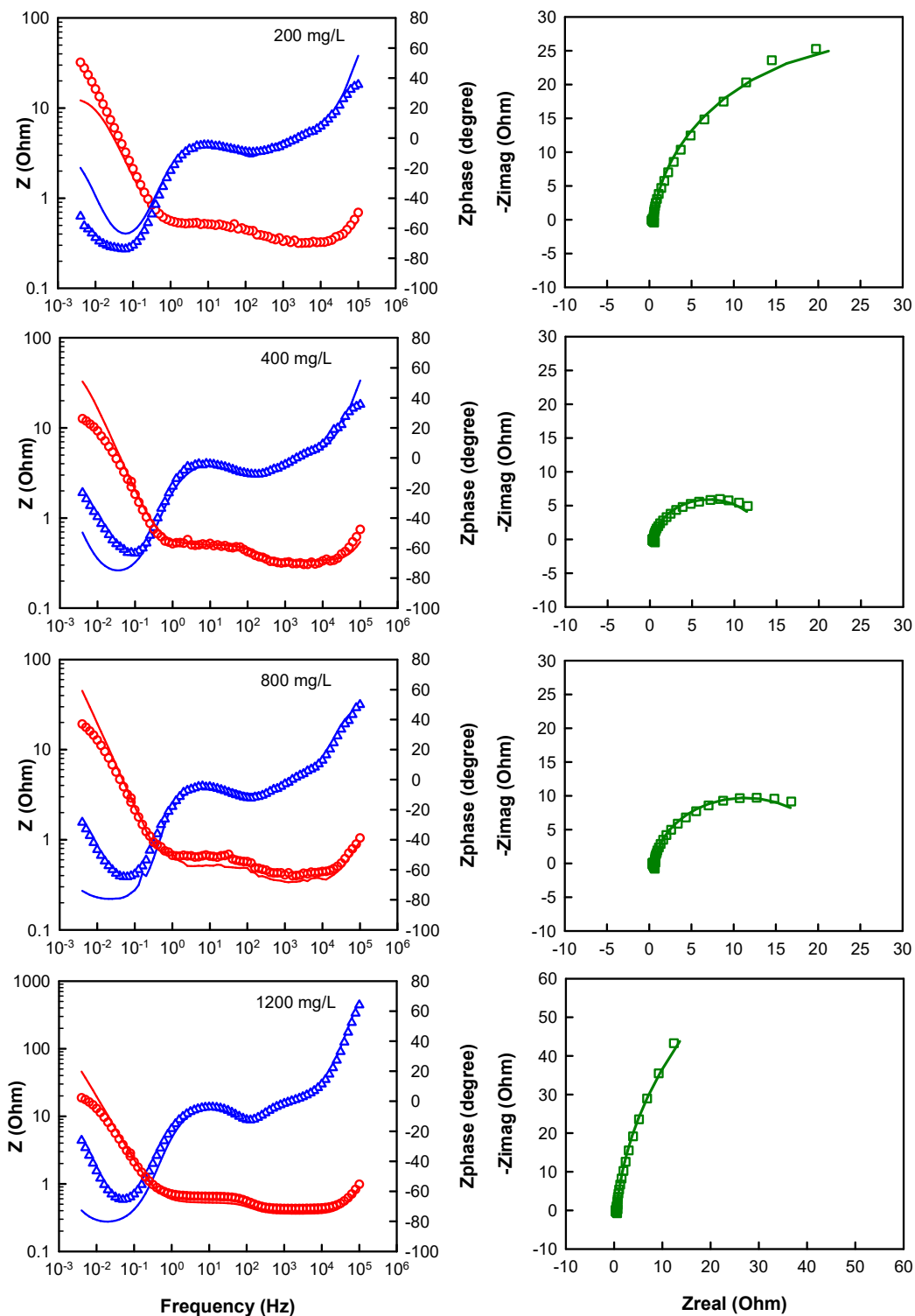


**Figure 5.19.** Bode (left column) and Nyquist (right column) plots of electrochemical impedance spectra of MEC whole-cell in batch runs conducted with 200-1200 mg/L initial concentration of furanic and phenolic compounds. Lines represent data fit using the equivalent circuit shown in Figure 3.3B.





**Figure 5.20.** Bode (left column) and Nyquist (right column) plots of electrochemical impedance spectra of MEC anode half-cell in batch runs conducted with 200-1200 mg/L initial concentration of furanic and phenolic compounds. Lines represent data fit using the equivalent circuit shown in Figure 3.3A.



**Figure 5.21.** Bode (left column) and Nyquist (right column) plots of electrochemical impedance spectra of MEC cathode half-cell in batch runs conducted with 200-1200 mg/L initial concentration of furanic and phenolic compounds. Lines represent data fit using the equivalent circuit shown in Figure 3.3A.

The anode and cathode resistance ( $R_a$  and  $R_c$ ), each consisting of charge transfer and diffusion resistance, were generally comparable, except for the 200 mg/L batch run, in which  $R_a$  was significantly larger than  $R_c$  (Table 5.4). It is noteworthy that both  $R_a$  and  $R_c$  varied considerably from less than 100  $\Omega$  to several hundred  $\Omega$  in different batch runs. A high  $R_a$  was expected in the 1200 mg/L batch run, because of the observed inhibition of exoelectrogenesis, as discussed in Section 5.3.2. However, the increased  $R_c$  in the 1200 mg/L batch run and the extremely high  $R_a$  in the 200 mg/L were not fully understood. In contrast to the varying  $R_a$  and  $R_c$ , the resistance associated with the electrolyte and the membrane was relatively consistent at 100-140  $\Omega$ , and was the major resistance component in the 400 and 800 mg/L batch runs (Table 5.4 **Table 5.4**). In most previously reported studies, the membrane resistance is usually dominant over electrolyte resistance (Manohar et al., 2008; Sleutels et al., 2009). Thus, the cation exchange membrane is a significant contributor to the MEC internal resistance in this study.

The use of EIS to characterize bioelectrochemical systems is an active area of research, currently under exploration (Dominguez-Benetton et al., 2012). In the present study, the EIS analysis did not provide conclusive information on the specific resistance components of the MEC. The equivalent circuits were selected based on generic processes in MEC and the goodness of fit to the experimental data. However, further assessment and optimization of the equivalent circuit are needed for the justification of geometric characteristics, reaction sequences, mass transfer, adsorption, and other physical phenomena taking place in the MEC (Dominguez-Benetton et al., 2012).

**Table 5.4.** MEC internal resistance ( $R_{\text{total}}$ ) associated with the anode ( $R_{\text{a}}$ ), cathode ( $R_{\text{c}}$ ), and the solution plus cation exchange membrane ( $R_{\text{s+m}}$ ) at the end of batch runs conducted with various initial concentrations of furanic and phenolic compounds.

Resistance components ( $\Omega$ )	Initial substrate concentration (mg/L)			
	200	400	800	1200
$R_{\text{a}}$	$882 \pm 71^{\text{a}}$	$13.8 \pm 0.3$	$24.8 \pm 0.7$	$228 \pm 5.5$
$R_{\text{c}}$	$56.5 \pm 2.2$	$13.5 \pm 0.3$	$22.0 \pm 0.5$	$211 \pm 24.2$
$R_{\text{s+m}}$	$139 \pm 2.2$	$133 \pm 39$	$140 \pm 21$	$106.6 \pm 130$
$R_{\text{total}}$	1078	160	187	546

<sup>a</sup> Mean  $\pm$  standard error

## 5.4 Summary

Furanic and phenolic compounds, which are a great challenge in dark fermentation of lignocellulosic hydrolysates, were productively utilized in the MEC to produce H<sub>2</sub>. The five compounds were completely transformed within 7-day batch runs and their biotransformation rate increased with increasing initial concentration. At an initial concentration of 1200 mg/L (8.7 mM) of the mixture of the five compounds, their biotransformation rate ranged from 0.85 to 2.34 mM/d. The anode Coulombic efficiency was 44–69%, which is comparable to that of wastewater-fed MECs. The H<sub>2</sub> yield varied from 0.26 to 0.42 g H<sub>2</sub>-COD/g COD removed in the anode, and the bioanode volume normalized H<sub>2</sub> production rate was 0.07–0.1 L/L-d.

The biotransformation of the five compounds took place via fermentation followed by exoelectrogenesis. The major identified fermentation products that did not transform further were catechol and phenol. Acetate was the direct substrate for exoelectrogenesis. Microbial species closely related to exoelectrogens, furanic and phenolic degraders, as well as putative syntrophic acetogens were detected in the MEC bioanode, which supports the proposed fermentation-exoelectrogenesis processes in the biotransformation of furanic and phenolic compounds. The biotransformation fate of furanic and phenolic compounds shown in the present study provides mechanistic insights into bioprocesses taking place in MEC and fermentation systems which use complex, lignocellulose-derived feedstocks.

The MEC H<sub>2</sub> production is an alternative to the currently used process of reforming natural gas to supply H<sub>2</sub> needed to upgrade bio-oils to stable hydrocarbon fuels. The demonstrated MEC capacity to use problematic furanic and phenolic

compounds in lignocellulose-related streams for H<sub>2</sub> production, strengthens the benefit and promise of integrating MEC technology in biorefinery platforms.

# CHAPTER 6

## BIOTRANSFORMATION OF FURANIC AND PHENOLIC COMPOUNDS IN MEC BIOANODE

### 6.1 Introduction

The problematic furanic and phenolic compounds can be utilized as MEC bioanode substrates for cathodic H<sub>2</sub> production, as discussed in Chapter 5. However, the fate of the individual compounds and their respective contribution to MEC H<sub>2</sub> production is largely unknown. MEC relies on microbial oxidation of organic substances in the anode for the production of electrons (and protons), which are then used in the reduction reaction in the cathode for H<sub>2</sub> production. Thus, the quantity of electrons that the bioanode can generate from the substrate, which is related to the extent of biotransformation of furanic and phenolic compound in this case, is crucial for the cathodic H<sub>2</sub> production.

It is generally accepted that when the bioanode substrate is a complex organic compound, fermentation is required to convert the complex compound to mainly acetate, which can then be used in exoelectrogenesis to produce current (Kiely et al., 2011b; Ren et al., 2007). The work reported in Chapter 5 demonstrated that the five furanic and phenolic compounds were not directly utilized by bioanode exoelectrogens. Instead, fermentation in the bioanode produced acetate, which was then used as an exoelectrogenic substrate. Although several metabolites were reported in Chapter 5, the extent of fermentative transformation of the individual compounds was not understood, because the furanic and phenolic compounds were used as a mixture. Very limited information is available on the transformation of furanic compounds in bioanodes, except

for the observed disappearance of the parent compounds reported by Catal et al. (2008) and Borole et al. (2013). Removal of phenolic compounds in microbial fuel cell (MFC) bioanodes has been reported in several studies (Borole et al., 2009; Friman et al., 2013; Huang et al., 2011; Song et al., 2014), but the biotransformation extent and pathways of individual compounds were not examined in these studies. Marone et al. (2016) reported the removal of hydroxytyrosol and tyrosol from table olive brine processing wastewater treated by a bioelectrochemical system, with the detection of 3,4-hydroxyphenyl acetic acid, 3,4-dihydroxybenzaldehyde, and *p*-hydroxyphenyl acetic acid as biotransformation products. A MFC study conducted by Hedbavna et al. (2016) showed that phenol, cresols and xylenols in groundwater were biotransformed to 4-hydroxybenzoic acid and 4-hydroxy-3-methylbenzoic acid. In this case, oxygen, nitrate, iron (III), and sulfate were present as electron acceptors in addition to the bioanode electrode.

Despite the knowledge gained from previous studies, important questions remain unanswered relative to the fate of furanic and phenolic compounds in bioanodes: (1) To what extent are these compounds transformed (e.g., furanic or aromatic rings cleaved or not)? (2) What are the biotransformation pathways? (3) Are there any limiting steps in the biotransformation pathways of these compounds in bioanodes impacting exoelectrogenic activity? To address these questions, the objective of the work reported in this chapter was to assess the extent of biotransformation and metabolic pathways of the five furanic and phenolic compounds, as well as their individual contribution to exoelectrogenesis in a MEC bioanode.



## 6.2 Materials and Methods

### 6.2.1 MEC

The MEC used for the work reported in this chapter was developed as described in Chapter 5, and consistently fed with a mixture of the five furanic and phenolic compounds, maintained at room temperature (20-22°C) for almost 2 years. Over the course of operation, the total biomass concentration in the anode chamber increased from  $52.7 \pm 0.9$  to  $352 \pm 10$  mg/L measured as protein, approximately 90% of which was associated with the biofilm. The MEC bioanode biofilm-associated microbial community was analyzed at 7 and 13 months of operation, as described in Section 5.3.5 and 8.2.4, respectively.

### 6.2.2 Fermentative Culture

In order to evaluate the fermentative activity in the bioanode under non-exoelectrogenic conditions, a fermentative culture was developed using an inoculum from the MEC bioanode, which had been maintained with the mixture of furanic and phenolic compounds for more than 1 year. Autoclaved carbon-felt (i.e., the same material as the MEC anode electrode) was placed in a 1-L glass reactor to support biofilm development. The ratio of the carbon-felt to liquid phase (1:4 v/v) was kept the same as that in the MEC bioanode. To inoculate the culture, two pieces of biofilm-attached carbon felt electrode (1 × 1 × 3 cm, each) along with 100 mL suspension removed from the MEC bioanode were anaerobically transferred to the reactor. The MEC anolyte, used as microbial growth medium, was then added to the reactor to reach a final liquid volume of 600 mL, leaving a 490 mL headspace which was filled with N<sub>2</sub> (ca. 0.1 bar). The culture was maintained

at room temperature (20-22°C). Weekly feedings were conducted with 1 mM SA for 1 month, a mixture of SA, VA and HBA (1 mM each) for 2 months, and then a mixture of the above-mentioned two five furanic and three phenolic compounds (0.5 mM each) for 1 month. Glucose (1 mM) was added for the first feeding only. Before each weekly feeding, 200 mL of liquid was wasted from the culture and fresh anolyte added, resulting in a hydraulic retention time of 21 d. The pH was maintained at 6.8-7.0 during each feeding cycle. CO<sub>2</sub> was detected in the headspace, but not H<sub>2</sub> or CH<sub>4</sub>. The total biomass concentration measured as protein was  $47.2 \pm 1.5$  mg/L, with 95% of the biomass residing on the carbon felt-attached biofilm. The biofilm-associated microbial community was analyzed at the completion of the batch runs reported in Section 6.2.3 (i.e., after 6 months from startup), following the procedure described in Section 6.2.7.

### 6.2.3 Batch Runs in MEC Bioanode and Fermentative Culture

Consecutive batch runs were conducted with SA, VA, HBA, FF, or HMF at an initial concentration of 1 mM in both the MEC bioanode and the fermentative culture, which were developed as described in Sections 6.2.1 and 6.2.2, respectively. The headspace of the MEC and the fermentative culture were filled with N<sub>2</sub> (ca. 0.1 bar) at the start of each batch run. During the batch runs, the MEC anolyte and catholyte, as well as the fermentative culture, were continuously mixed magnetically. The pH, concentration of each parent compound, current and cathodic H<sub>2</sub> were monitored; metabolites were identified and quantified as described in Section 6.2.6, below. Each batch run lasted for 6 days. Between each bioanode batch run, the MEC anode chamber was drained and washed with clean anolyte to avoid residuals being carried over to the next batch run;

then fresh anolyte and catholyte added. Between each fermentative batch run, the fermentative culture was drained and washed with fresh anolyte following the same procedure as for the MEC batch runs, while retaining the carbon felt-attached biofilm. Replicate batch runs were conducted to confirm reproducibility.

#### 6.2.4 Fermentative Transformation by Different Microbial Communities

Both the MEC bioanode and the fermentative culture are related to the same, original inoculum obtained from ORNL (see Section 4.2.2). In order to assess whether the observed extent of biotransformation is unique to these two microbial communities, biotransformation assays were conducted with four different microbial communities. Two microbial communities were developed with environmental samples from a pulp and paper mill lagoon sediment (PPS; Dykstra et al. 2015) and a contaminated estuarine sediment (CS; Gess and Pavlostathis, 1997). Two more microbial communities were developed with mixed fermentative/methanogenic cultures enriched from samples obtained from a mesophilic, municipal anaerobic digester (METH), and from the pulp and paper mill lagoon sediment (PPC). All above-mentioned inocula samples and cultures used in this phase of the study were developed and maintained at room temperature (20 - 22 °C).

With each microbial community, a batch assay was conducted with 160-mL serum bottles (100 mL liquid volume) sealed with rubber stoppers and aluminum crimps. Each assay included five series, each in triplicate. The test series (TEST) consisted of microbial seed (5 mL suspension), growth medium (i.e., MEC anolyte), as well as furanic and phenolic compounds mixture at 200 mg/L. A glucose-amended series (GLU)

included 200 mg/L glucose as a co-substrate in addition to the components in TEST series. A seed blank series (SB) did not contain furanic and phenolic compounds, and was used as a control of background microbial activity. A reference series (RF) was amended with glucose, but not furanic and phenolic compounds. An abiotic series (AB) was set up as the TEST series, except that the microbial seed was not added. Deionized water was used to bring the total liquid volume of all series to 100 mL. The concentrations of the parent compounds and their transformation products, as well as gas production in the headspace, were measured using the methods described in Chapter 3, Section 3.2.

#### 6.2.5 Microaerophilic Bioanode

The MEC anode was maintained under microaerophilic conditions for one week to explore the possibility of further transformation of persistent metabolites using oxygen as a terminal electron acceptor in addition to the bioanode electrode. The gas collection burette was disconnected from the bioanode headspace, to keep a small headspace of 60 mL. The microaerophilic batch run started at the end of a normal bioanode batch run, when the parent compounds had been removed and metabolites had persisted for days. The bioanode headspace was first flushed with N<sub>2</sub> for 5 min, and air was added using a syringe to reach a total pressure of 0.18 bar, resulting in an initial gas-phase oxygen concentration of 18 % after 30 min of equilibration. Air was added again to the bioanode headspace when the headspace pressure decreased to atmospheric pressure. The oxygen content in the headspace, concentrations of persistent metabolites, COD, current and cathodic H<sub>2</sub> were monitored.


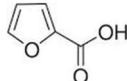
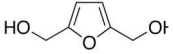
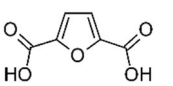
### 6.2.6 Identification of Metabolites

Phenolic and furanic metabolites were identified using the LC/MS-MS method described in Section 3.2.6. The first step in metabolite identification was assuming possible chemical structures resulting from the elimination of functional groups from the parent compounds, as shown in Table 6.1. In the second step, pure chemicals of the assumed metabolites were analyzed by the LC/MS-MS in the scan mode at 100 V fragmentation voltage, in order to determine the chromatographic retention time and  $m/z$  value of the primary ion of each compound (Table 6.1). The retention time and  $m/z$  values were then used to screen for the presence of the corresponding compounds in the samples, by setting the LC/MS-MS in selective ion mode (SIM) at a fragmentation voltage of 100 V and  $m/z$  values determined as described above. Positive ionization was used for furanic compounds detection, while negative ionization was used for phenolic compounds. Isomers with the same  $m/z$  values, such as catechol vs. resorcinol and pyrogallol vs. phloroglucinol, were distinguished by the chromatographic retention time. Samples showing peaks with matched  $m/z$  values and retention time of the assumed metabolites were further analyzed for structure confirmation as described below. In the confirmation step, the LC/MS-MS was operated in the product ion mode at the optimal collision energy determined specifically for each compound (Table 6.1). Then the resulting fragmentation patterns were compared to those of pure chemicals.

**Table 6.1.** Possible metabolites of SA, VA, HBA, FF, and HMF. Parameters listed are based on LC/MS-MS analysis unless otherwise stated.

Compound	Structure	Molecular weight (g/mol)	Primary or precursor ion m/z	Potential Origin	Detection, origin	Retention time (min)	Collision energy (V)
3,4-Dihydroxy-5-methoxybenzoic acid (DHMBA)		184	183	SA	Yes, SA	3.7	2
Gallic acid (GA)		170	169	SA	Yes, SA	2.3	2
Pyrogallol		126	125	SA	Yes, SA	2.8	20
Phloroglucinol		126	125	SA	No, retention time not match	2.2	NA <sup>a</sup>
Protocatechuic acid (PA)		154	153	SA VA	Yes, VA	3.4	10
Catechol		110	109	SA VA	Yes, VA	4.0	20
Resorcinol		110	109	SA VA	No, retention time not match	3.5	NA <sup>a</sup>
4-hydroxybenzoic acid (HBA)		138	137	SA VA	No	4.0	NA <sup>a</sup>
Benzoic acid		122	121	SA VA HBA	No	4.8	NA <sup>a</sup>
Phenol <sup>a</sup>		94	94	SA VA HBA	Yes, HBA	6.2	NA <sup>a</sup>

**Table 6.1. (Continued)**

Compound	Structure	Molecular weight (g/mol)	Primary or precursor ion m/z	Potential Origin	Detection, origin	Retention time (min)	Collision energy (V)
Furfuryl alcohol		98	99	FF	No	3.5	NA <sup>a</sup>
2-furoic acid		112	111	FF	Yes	3.1	10
2,5-Bis(hydroxymethyl)furan		128	129	HMF	Yes	3.1	10
2,5-Furandicarboxylic acid		156	155	HMF	No	1.6	NA <sup>a</sup>

<sup>a</sup> NA, not available (product ion mode not used)

<sup>b</sup> Identified using GC/MS

Phenol, as an exception, was identified using the GC/MS method described in Section 3.2.6, due to its poor ionization in the LC/MS-MS method. Samples used for the GC/MS analysis were passed through 0.2  $\mu\text{m}$  PTFE membrane filters and extracted with ethyl acetate. In a 10 mL glass culture tube sealed with Teflon-lined cap, 4 mL sample and 4 mL ethyl acetate were added and then vortexed for 5 min. The mixture was then transferred to a 30 mL glass separatory funnel, allowed to separate for 30 min. The bottom water phase was drained and the top organic phase was transferred to a clean glass tube, evaporated to dryness under a  $\text{N}_2$  stream. The dried sample was reconstituted in 1 mL ethyl acetate and then 1  $\mu\text{L}$  was injected into the GC/MS. The obtained MS spectra were compared to those in the NIST library for positive identification.

#### 6.2.7 Fermentative Culture Microbial Community Analysis

The microbial community of the fermentative culture carbon felt-attached biofilm was analyzed after 6 months from startup. Genomic DNA was extracted from the carbon felt-attached biofilm of the fermentative culture and analyzed as described in Section 3.2.8. The extracted DNA was sequenced for 16S rRNA gene using Illumina MiSeq (Research and Testing Laboratory; Lubbock, TX) using primer sets of 28F/388R (5'-GAGTTTGATCNTGGCTCAG-3'/5'-TGCTGCCTCCCGTAGGAGT-3'). The obtained sequences were clustered into Operational Taxonomic Units (OTUs) at 4% divergence using the UPARSE algorithm. The centroid sequence of each OTU was used for taxonomic classification using the USEARCH global alignment program. The 16S rRNA sequences of the abundant species (>1 %) were deposited to GenBank, National Center



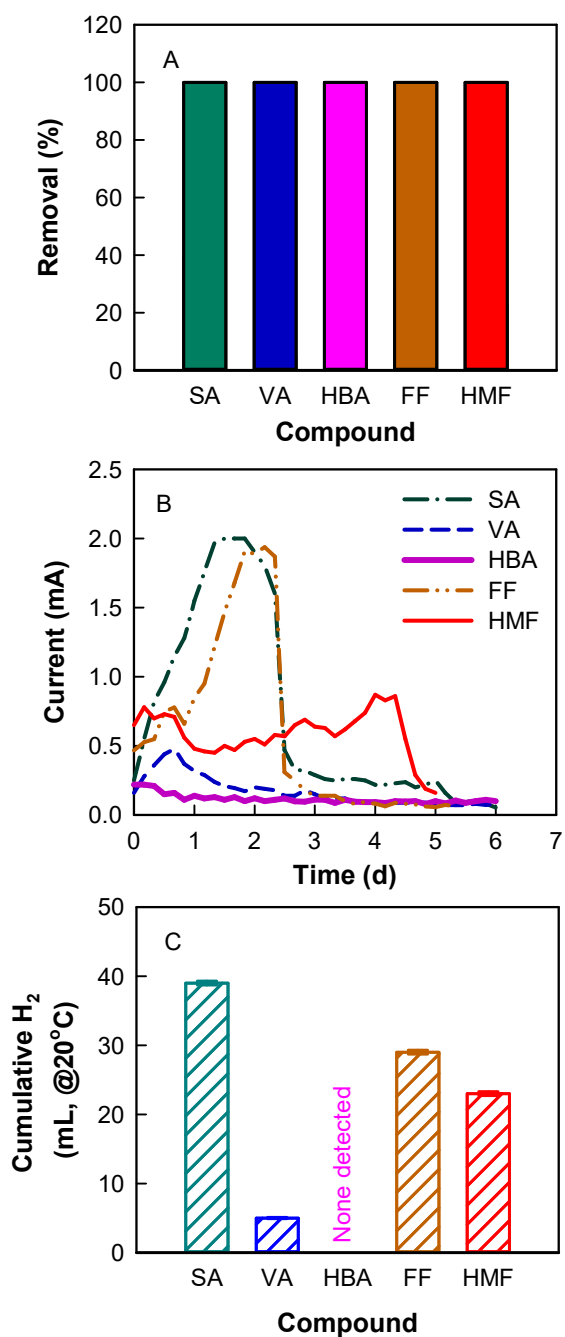
for Biotechnology Information (NCBI; [www.ncbi.nlm.nih.gov/](http://www.ncbi.nlm.nih.gov/)) with sequence accession numbers from KX299014 to KX299022.

## 6.3 Results and Discussion

### 6.3.1 MEC Bioanode Runs with Individual Compounds

Complete removal of the five parent compounds, SA, VA, HBA, FF and HMF, was observed in 6 days in each respective batch run (Figure 6.1A). The disappearance of the five compounds was not due to adsorption to the carbon-felt electrode or diffusion to the cathode compartment, as confirmed by the results reported in Chapter 5. Electrochemical reactions under abiotic conditions accounted for 19 - 22% of the transformation of the phenolic compounds (SA, VA and HBA) and more than 90% of the furanic compounds (FF and HMF), but the reaction rate was considerably lower than that in the active bioanode (Figure 5.7). More importantly, negligible current was observed with the abiotic electrochemical reactions, as reported in Chapter 5. In the tests reported here, the batch runs conducted with SA and FF produced peak current at 2.0 mA around two days (Figure 6.1B). The current in the HMF batch run stayed relatively low around 0.7 mA but lasted over 4 days, longer than in other batch runs. In contrast, VA and HBA batch runs produced much lower current. A peak current of 0.5 mA was observed on day 1 of the VA batch run, and the HBA batch run produced extremely low current ( $< 0.2$  mA), close to background current levels (usually at 0.05-0.1 mA, with the anolyte and catholyte in the absence of any organic substrate). Consistent with the observed current, the highest H<sub>2</sub> production was observed in the SA batch run ( $39 \pm 0.1$  mL, 20°C and 1 atm), followed by FF ( $29 \pm 0.1$  mL) and HMF ( $23 \pm 0.1$  mL), more than 7-fold higher than that in the

VA batch run ( $5 \pm 0.1$  mL); cathodic  $H_2$  was not detected in the HBA batch run (Figure 6.1C). Reproducible current and  $H_2$  production were observed with all five compounds in replicate batch runs (data not shown). The anode pH decreased slightly from 7.0 to 6.8 during the SA, FF and HMF batch run, and remained constant at 7.0 for the VA and HBA runs. The cathode pH remained at 7.0 for all runs conducted with the five compounds. With the voltage between the anode and the cathode controlled by the potentiostat (0.6 V), both anode and cathode potentials changed during the batch runs, ranging from -0.4 to -0.1 V for the anode and from -1.0 to -0.7 V (vs. Ag/AgCl) for the cathode. Although the parent furanic and phenolic compounds may inhibit bioanode activities, especially exoelectrogenesis, the initial concentrations of the five compounds used in the batch runs were below their no-observed-effect-concentration (0.8 g/L), as determined for the same MEC system (see Chapter 7). Thus, inhibition was not an issue or the cause of the difference in the observed exoelectrogenic activity among runs conducted with each of the five parent compounds.



**Figure 6.1.** Removal of parent compounds (A), current (B) and cathodic H<sub>2</sub> production (C) during MEC bioanode batch runs conducted with SA, VA, HBA, FF, or HMF. Error bars represent standard deviations ( $n = 2$ ).

Because the electron equivalence of the five compounds is different (Table 2.1), whereas an equal molar concentration (1 mM) of each parent compound was used in the respective batch run, the electron input of the five batch runs was different (Table 6.2; SA > VA > HBA > HMF > FF). However, the current and cathodic H<sub>2</sub> production did not follow the order of electron equivalents input. The furanic compounds (FF and HMF) had a lower electron equivalents input but resulted in higher current and H<sub>2</sub> than VA and HBA. The difference in electron equivalents cannot account for the observed difference in current and H<sub>2</sub> production from the five compounds, nor the nearly absence of exoelectrogenesis in the HBA run. Based on the electron balance performed for each batch run, the anode efficiency was above 50% for the SA, FF and HMF batch runs, whereas it was as low as 12 and 9% for VA and HBA batch runs, respectively (Table 6.2). In addition, the cathode efficiency was comparable among these batch runs (69-81%), except that the cathode efficiency could not be calculated for the HBA batch run because of the lack of H<sub>2</sub> production. Therefore, the biotransformation of SA, FF or HMF supported exoelectrogenic activity to a much higher degree than VA or HBA, which is mainly attributed to the difference in the bioanode activity, as opposed to the cathode efficiency. The relatively small variation of cathode efficiency may be due the difference in the extent of cathodic H<sub>2</sub> loss due to diffusion to and consumption in the bioanode, as discussed in detail in Section 5.3.2. The results reported in this chapter provide insight into the relative contribution of individual phenolic compounds to exoelectrogenesis, which was not delineated in Chapter 5, in which mixtures of furanic and phenolic compounds were used as bioanode substrates. Moreover, it is clearly that the two furanic compounds (FF and HMF) are favorable substrates for use in the MEC bioanode, leading

to active exoelectrogenesis. The three phenolic compounds (SA, VA and HBA) representing different classes of lignin units (syringyl, guaiacyl and *p*-hydroxyphenyl, respectively) differ significantly in their exoelectrogenic potential.

**Table 6.2.** Electron balance of batch runs conducted with individual furanic and phenolic compounds.

Parameter	Bioanode batch run with:				
	SA	VA	HBA	FF	HMF
Total substrate input (mmol) <sup>a</sup>	7.18	6.38	5.60	4.02	4.94
Electrons recovered as current (e <sup>-</sup> mmol) <sup>b</sup>	3.59	0.76	0.40	2.89	2.75
Electrons recovered as cathodic H <sub>2</sub> (e <sup>-</sup> mmol) <sup>c</sup>	2.92	0.58	ND <sup>f</sup>	2.4	1.9
Anode efficiency (%) <sup>d</sup>	50	12	9	72	56
Cathode efficiency (%) <sup>e</sup>	81	76	NA <sup>g</sup>	83	69

<sup>a</sup> Calculated as the substrate electron equivalence (Table 2.1) multiplied by the molar concentration of substrate (1 mM) and the anode liquid volume (0.2 L)

<sup>b</sup> Calculated as current integrated over time

<sup>c</sup> Calculated as the electron equivalence of H<sub>2</sub> multiplied by the mole of measured cathodic H<sub>2</sub>

<sup>d</sup> Defined in Section 3.3.3; calculated as the ratio of row 2 to row 1

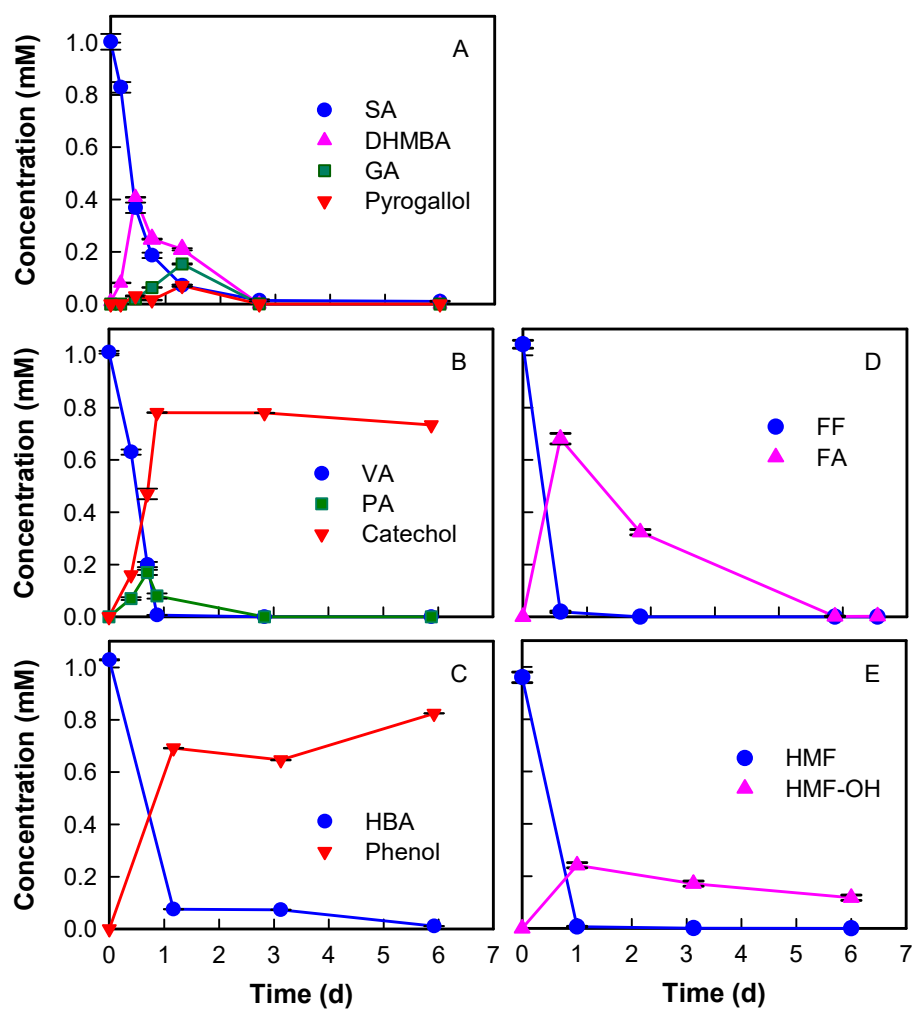
<sup>e</sup> Defined in Section 3.3.4; calculated as the ratio of row 3 to row 2

<sup>f</sup> ND, none detected

<sup>g</sup> NA, not available

### 6.3.2 Metabolic Fate of Parent Compounds in MEC Bioanode

During the SA biotransformation in the bioanode, several compounds were identified as metabolites (Figure 6.2A). The first detected metabolite was 3,4-dihydroxy-5-methoxybenzoic acid (DHMBA), whose chemical structure suggests that one methyl group (-CH<sub>3</sub>) was removed in the first step of SA biotransformation. The DHMBA concentration increased to 0.4 mM within 12 h and then gradually decreased to an undetectable level in the next 2 days. Following the disappearance of DHMBA, gallic acid (GA) and pyrogallol were detected as two metabolites. The chemical structures of GA and pyrogallol indicate that a second demethylation step occurred, removing the -CH<sub>3</sub> group from DHMBA, resulting in GA, followed by a decarboxylation step eliminating the -COOH group from GA, leading to the production of pyrogallol. Both GA and pyrogallol were transient metabolites detected at a maximum concentration of 0.15 and 0.07 mM, respectively, in 1.5 days (Figure 6.2A). Pyrogallol was the last aromatic metabolite detected, and could potentially be the last product before the aromatic ring cleavage. GA and pyrogallol correspond to the unknown peaks (m/z 169 at 2.3 min, and m/z 125 at 2.8 min, respectively) in the LC/MS chromatogram (Figure 5.11) presented in Chapter 5. A long-term operation of the MEC bioanode and the fermentative culture, both fed with 1 mM SA, was conducted for 27 days to ensure complete biotransformation of SA. The above-reported metabolites were also detected during the long-term MEC incubation, and the remaining sCOD accounted for 30% of the initially added COD, indicating un-identified metabolites potentially produced via other minor pathways. Nevertheless, other assumed metabolites, such as catechol, phenol and benzoic acid listed in Table 6.1, were not detected during the biotransformation of SA.



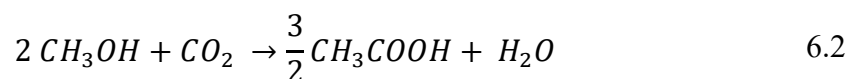
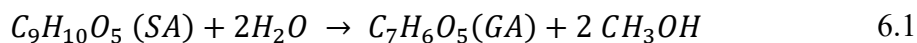
**Figure 6.2.** Biotransformation products of SA (A), VA (B), HBA (C), FF (D), and HMF (E) in MEC bioanode batch runs. Error bars represent standard deviations ( $n = 2$ ).

Abbreviations: SA, syringic acid; DHMBA, 3,4-dihydroxy-5-methoxybenzoic acid; GA, gallic acid; VA, vanillic acid; PA, protocatechuic acid; HBA, 4-hydroxybenzoic acid; FA, furoic acid; HMF-OH, 2,5-Bis(hydroxymethyl)furan.

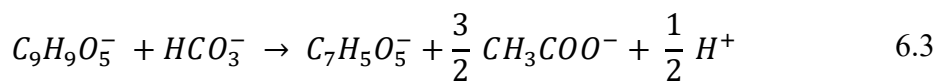


The above-mentioned SA metabolites were also reported by Kaiser and Hanselmann (1982), who studied SA biotransformation in a fermentative/methanogenic culture enriched from a freshwater lake sediment. In addition, the same study reported further fermentation of pyrogallol to acetate at a stoichiometric amount (3 mol) under methanogenesis-inhibited conditions, demonstrating that the aromatic ring of pyrogallol was cleaved by fermentative bacteria, independently from a syntrophic association with methanogens. In this study, acetate was not detected during the SA batch run in the bioanode, as a result of a rapid acetate consumption by the active exoelectrogens, given that acetate is a major substrate used by exoelectrogens (Logan and Rabaey, 2012; Wang and Ren, 2013). The high exoelectrogenic activity in the SA batch run, in turn, indicates that a significant quantity of acetate was produced. As reported in Chapter 5, acetate was detected only with an open circuit (i.e., in the absence of exoelectrogenesis) or when exoelectrogenesis was inhibited. Direct evidence of acetate production from SA is provided by the fermentative batch run, discussed in Section 6.3.3, below.

Acetate can be produced not only from aromatic ring cleavage, but also from the demethylation of methoxy groups. Bache and Pfennig (1981) reported that methoxy carbons on aromatic compounds were first removed from the aromatic ring, resulting in methanol (Equation 6.1), which was subsequently converted to acetate in the presence of bicarbonate (Equation 6.2).



The overall reaction at neutral pH can be written as follows:



The conversion of methoxy carbon to acetate was confirmed in *Acetobacterium woodii*, an acetogenic, fermentative bacterium, growing on methoxy groups of various aromatic compounds, including SA and VA, without cleaving the aromatic rings. For every 1 mol methoxy group removed, 0.75 mol of acetate was produced (Bache and Pfennig, 1981). As stated in Section 6.3.5, below, *Acetobacterium* was present in the MEC bioanode used in the present study. In addition, bicarbonate could be produced by the decarboxylation of GA to pyrogallol, as well as from the oxidation of acetate during exoelectrogenesis. Thus, it is plausible that two demethylation steps of SA could have resulted in 1.5 mM acetate. Based on the electron equivalence of acetate (8 e<sup>-</sup> mol/mol) and the current produced during the SA batch run, the amount of acetate used for the exoelectrogenesis was back calculated as 2.8 mM, assuming 90% Coulombic efficiency of the acetate-fed bioanode (see Chapter 5, Section 5.3.2). Thus, the acetate produced from the methoxy groups of SA (1.5 mM maximum) was not enough to support the observed exoelectrogenesis. Instead, aromatic ring cleavage must have contributed to the calculated acetate production.

VA biotransformation resulted in two aromatic metabolites, protocatechuic acid (PA) and catechol (Figure 6.2B). Similar to SA, demethylation occurred, removing the methoxy carbon from VA, resulting in PA production. Subsequently, decarboxylation of PA led to the production of catechol. PA was detected at low levels (< 0.2 mM) with a transient appearance in the first 3 days. In contrast, catechol was formed in 1 day reaching a high concentration (0.8 mM) and was persistent throughout the 6-day batch run. Because VA and catechol are both mono-aromatic compounds, 1 mM VA is

expected to produce 1 mM catechol at most. Thus, the detected catechol (0.8 mM) accounted for 80% of the VA added, making catechol a major dead-end product. The conversion of VA to PA and then to catechol has been reported in a fermentative/methanogenic culture enriched from a freshwater sediment (Kaiser and Hanselmann, 1982). The same study reported that catechol was persistent throughout the 2-week incubation, and suggested that only aromatic compounds with three hydroxyl or methoxy substituents are degraded via ring cleavage. These previous findings are in agreement with the observations during SA and VA biotransformation in the present study.

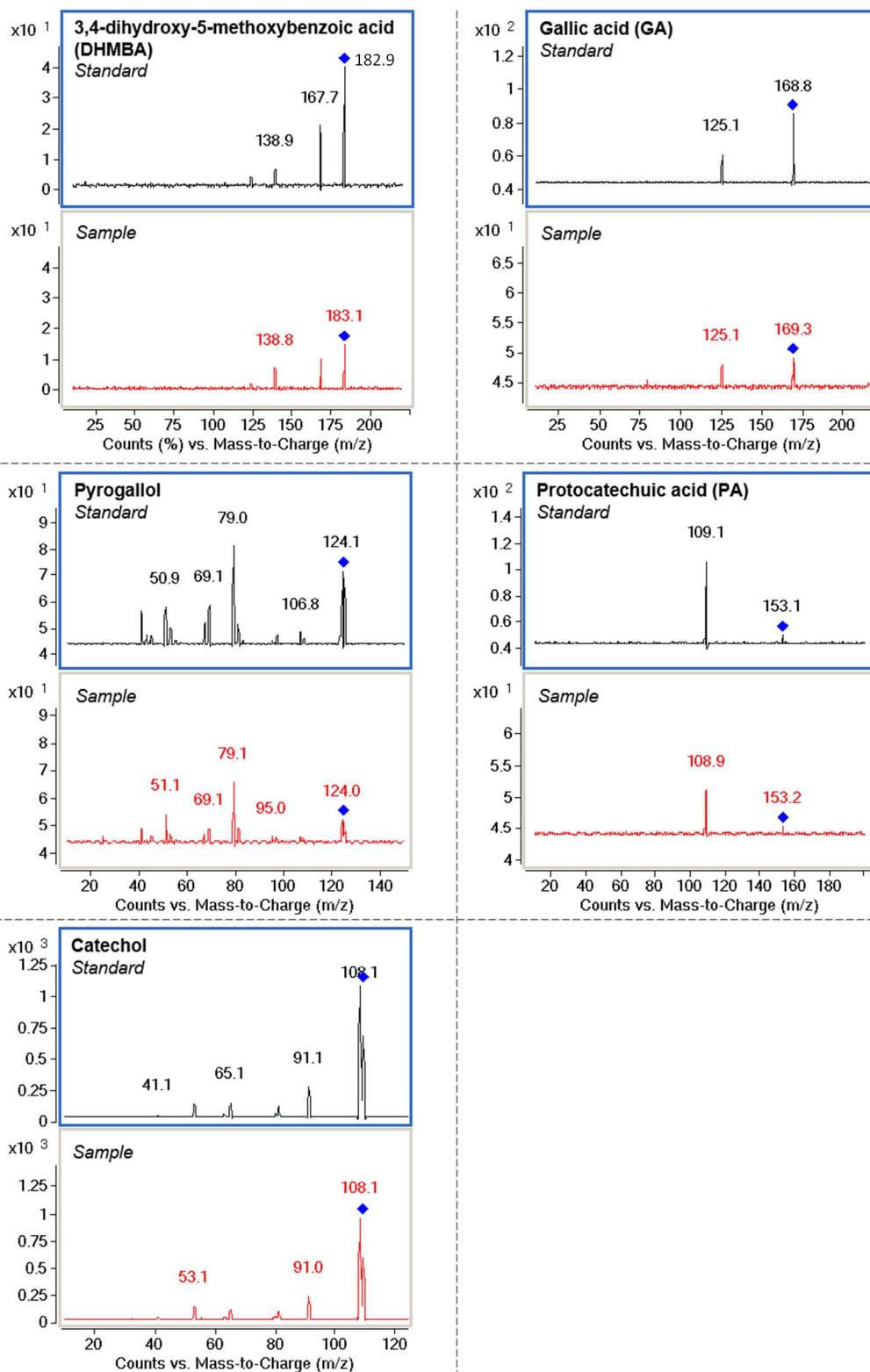
As discussed above, methoxy carbons on methoxylated aromatic compounds can be converted to acetate with a stoichiometric coefficient of 0.75 mol-acetate/mol-methoxy group. Acetate produced by the demethylation of VA, in spite of an intact aromatic ring, may explain the small peak current observed on day 1 during the VA biotransformation (Figure 6.1A). The total current observed during the VA batch run requires at least 0.53 mM of acetate, back calculated based on the above-mentioned electron equivalence of acetate. This minimum acetate demand is close to the concentration that can be produced from the methoxy group of VA (0.75 mM). In comparison, SA has twice the amount of methoxy carbons (Table 2.1), but its exoelectrogenic capacity was 7-fold higher than that of VA. Thus, the number of methoxy groups in SA and VA cannot fully explain the difference in their exoelectrogenic capacity measured in the batch runs.

Catechol is a dihydroxylated metabolite produced from VA, analogous to pyrogallol, a trihydroxylated benzene derived from SA. However, the persistence of

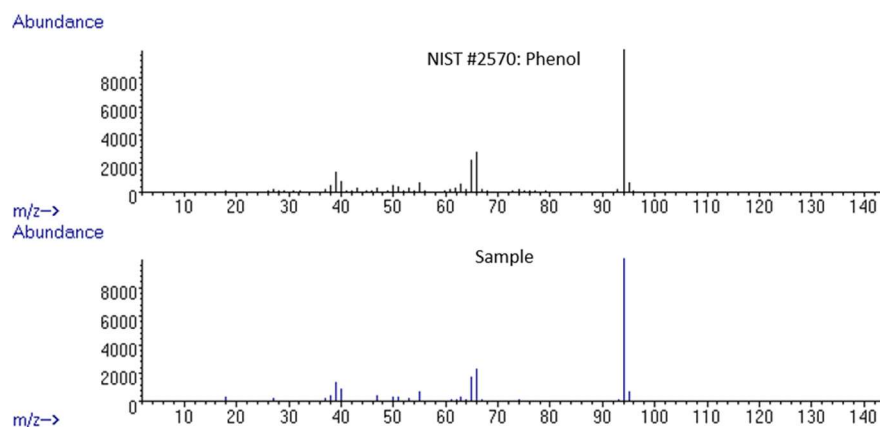
catechol is in contrast to the transient fate of pyrogallol. Thus, the biotransformation pathway of SA and VA becomes significantly different after the initial, common steps of demethylation and decarboxylation. The relatively low extent of VA fermentative biotransformation is consistent with the observed low exoelectrogenic activity, while the higher extent of SA biotransformation resulted in a higher exoelectrogenic activity. Therefore, the difference in the exoelectrogenic capacity of SA and VA is not only related to the number of methoxy groups, but more importantly to the extent of the fermentative biotransformation, i.e., aromatic ring cleavage or not.

HBA biotransformation resulted in phenol as the only detected metabolite (Figure 6.2C), resulting from the decarboxylation of HBA. Phenol was detected at high levels (0.7-0.8 mM) and was persistent throughout the 6-day batch run. Thus, as in the above-discussed VA biotransformation, HBA was biotransformed mainly to a dead-end product representing 80% of the HBA added. Moreover, HBA does not contain any methoxy substituent which could lead to the production of acetate. The combination of the low extent of biotransformation and the lack of a methoxy group led to an extremely low exoelectrogenic activity in the HBA-fed bioanode (Figure 6.1). Benzoic acid, an assumed metabolite, was not consistently detected in all samples and its concentration was negligible ( $< 0.02$  mM). Therefore, benzoic acid is not considered an important metabolite of HBA under the experimental conditions of the present study. The biotransformation of HBA to phenol has been reported in an enriched fermentative/methanogenic culture (Tschech and Schink, 1986), anoxic aquifer samples (Kuhn et al., 1989), and a pure culture of *Clostridium* strain JW/Z-1 (Zhang and Wiegel, 1990).

Transient pyrogallol levels, as well as persistent catechol and phenol, were observed in repeated consecutive batch runs conducted with SA, VA or HBA (data not shown), confirming the reproducibility of the above-discussed results of the first round batch runs. The chemical structures of the above-mentioned metabolites were confirmed by their mass spectra obtained from LC/MS-MS (Figure 6.3). All identified compounds had fragmentation patterns identical to those of the analytical standards. Phenolic acids, such as DHMBA, GA and PA, mainly yielded fragments at  $m/z$  of  $[M-1]$  and  $[M - 45]$ , representing the loss of a  $H^+$  and a  $-COOH$ , respectively. In the mass spectra of pyrogallol and catechol, large fragment peaks appeared at  $m/z$  of  $[M-1]$  and  $[M-2]$ , along with other small peaks. The abundant  $[M-1]$  or  $[M-2]$  peak was attributed to the elimination of  $H^+$  from one or two  $-OH$  group(s). The phenol mass spectrum in GC/MS showed a strong molecular peak ( $m/z = 94$ ) and a fragment peak at  $m/z$  of  $[M-28]$ , resulting from the loss of a carbon monoxide (Figure 6.4).



**Figure 6.3.** Mass spectra of metabolites identified in LC/MS-MS. Blue diamond symbols indicate m/z of precursor ions.



**Figure 6.4.** Phenol GC/MS mass spectra in the NIST Standard Reference Database and in sample resulting from the biotransformation of 4-hydroxybenzoic acid (HBA).

In the FF-fed bioanode, FF was rapidly transformed within 1 day, with the production of 2-furoic acid (FA) at 0.69 mM, which was then further transformed in the next 4 days (Figure 6.2D). The formation of FA suggests that the carbonyl group (C=O) of FF was oxidized, converting the aldehyde to the corresponding carboxylic acid. *Desulfovibrio furfuralis* (also referred to as *Desulfovibrio* sp. strain F1), which is the major anaerobic bacterial FF degrader, was reported to transform FF to FA and/or furfuryl alcohol, and then eventually to acetate as the end fermentation product (Folkerts et al., 1989). In the present study, although acetate was not detected during the bioanode batch run conducted with FF, likely due to rapid consumption by exoelectrogens, further transformation of FA and the high current production indicate a high extent of FF biotransformation. In fact, 72% of the FF added was eventually converted to electric current (Table 6.2), representing the highest anode efficiency achieved among the five parent compounds used in the MEC bioanode batch runs.

During the HMF biotransformation, the carbonyl group of HMF was reduced to a hydroxyl group, resulting in the corresponding alcohol of HMF (2,5-bis(hydroxymethyl)furan, HMF-OH; Figure 6.2E). A relatively low level of HMF-OH was detected (0.24 mM), and un-identified metabolites could have been present. In agreement with the study, anaerobic conversion of HMF to HMF-OH via a  $2e^-$  reduction was reported in cultures of *Clostridium acetobutylicum* (Zhang et al., 2012) and enteric bacteria (Boopathy et al., 1993).

Among the biotransformation products identified in the work reported in this chapter, catechol, phenol, PA, FA and HMF-OH were detected in the MEC bioanode fed with the mixture of furanic and phenolic mixture, as reported in Chapter 5. The persistence of catechol and phenol, as well as the transient fate of PA, FA and HMF-OH, were consistently observed. In addition, the origin of these metabolites, which was unclear in the results reported in Chapter 5, was delineated based on the results reported in this chapter.

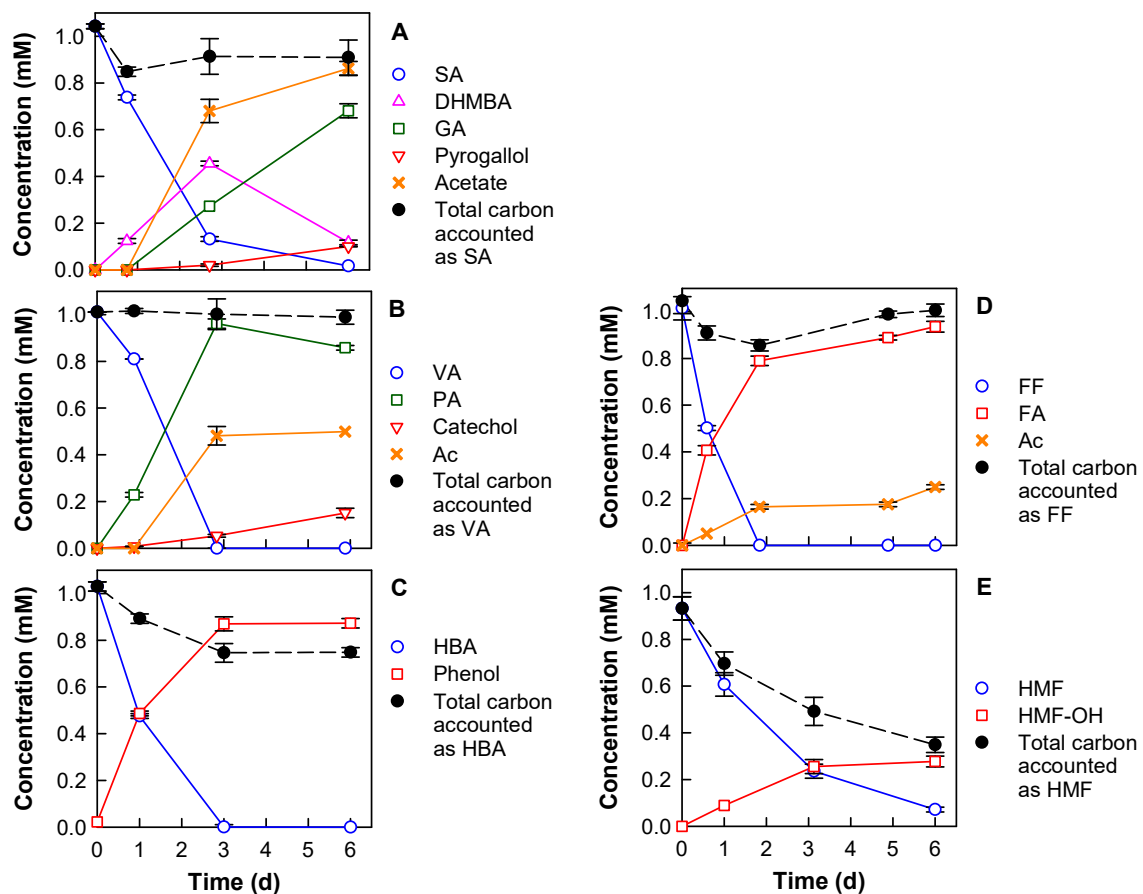
### 6.3.3 Metabolic Fate in Parent Compounds in Fermentative Culture

In order to further delineate the role of fermentative biotransformation in the MEC bioanode, the biotransformation of SA, VA, HBA, FF and HMF was also evaluated in consecutive batch runs conducted using the fermentative culture. This culture, which was inoculated with the microbial community from the MEC bioanode (see Section 6.2.2), represents an open circuit control under non-exoelectrogenic conditions.

SA biotransformation resulted in the production of DHMBA, GA, pyrogallol and acetate (Figure 6.5A). The detected metabolites represented a carbon recovery of 85-



90%, while a small fraction of carbon could have been used for biomass synthesis. The detected aromatic metabolites were identical to those found in the MEC bioanode batch runs, except for acetate, which was not detected in the bioanode but accumulated to a high level (0.86 mM) in the fermentative culture. Because there was no acetate-consuming process in the fermentative culture, such as exoelectrogenesis or methanogenesis, acetate accumulated as an end product. The observed acetate level (0.86 mM) was lower than the calculated acetate demand (2.5 mM) corresponding to the observed exoelectrogenic activity in the SA bioanode batch run. This discrepancy is attributed to the different rate of biotransformation in the bioanode and the fermentative culture, resulting in a different extent of biotransformation. The biomass concentration in the fermentative culture was 7-fold lower than that in the bioanode (47.2 vs. 352 mg/L as protein; see Sections 6.2.1 and 6.2.2, above). Consequently, the biotransformation rate was lower in the fermentative batch run (Figure 6.2A vs. Figure 6.5A). Thus, for the same incubation time of 6 days, a lower extent of biotransformation was achieved in the runs conducted with the fermentative culture, resulting in a relatively lower acetate concentration at the end of the batch run. To achieve complete SA biotransformation, long-term batch runs for 27 days were conducted with the fermentative culture and MEC bioanode, as mentioned in Section 6.3.2, above. After the long-term incubation of the fermentative culture, the acetate concentration reached 3.3 mM, consistent with the calculated amount of acetate needed for the observed exoelectrogenesis (2.8 mM; Section 6.3.2, above). Due to the long-term incubation of the fermentative culture, a higher extent of microbial decay and fermentation may have contributed to the observed higher acetate level.



**Figure 6.5.** Biotransformation products of SA (A), VA (B), HBA (C), FF (D), and HMF (E) in batch runs conducted with the fermentative culture. Error bars represent standard deviations ( $n = 2$ ). Abbreviations: SA, syringic acid; DHMBA, 3,4-dihydroxy-5-methoxybenzoic acid; GA, gallic acid; VA, vanillic acid; PA, protocatechuic acid; HBA, 4-hydroxybenzoic acid; FA, furoic acid; HMF-OH, 2,5-Bis(hydroxymethyl)furan.

VA biotransformation in the fermentative culture resulted in the production of PA and catechol (Figure 6.5B), the same metabolites detected in the VA bioanode batch run. As discussed above, due to the lower biomass concentration in the fermentative culture compared to that in the bioanode, the concentrations of the observed metabolites were lower than those in the MEC bioanode run. For instance, catechol did not reach a level as high as in the bioanode run for the same incubation time (6 d). Nevertheless, a nearly 100% carbon balance was achieved. Acetate was produced and remained at 0.5 mM after VA was completely transformed. As discussed above, the methoxy carbon on VA can be converted to acetate at a stoichiometric amount of 0.75 mM/mM VA, which is slightly higher than the measured acetate concentration.

HBA biotransformation in the fermentative culture resulted in the production of phenol as the only detected metabolite, representing 75% of the HBA added. Acetate was not detected throughout the 6-d incubation period (Figure 6.5C). The persistence and dominance of phenol during the HBA biotransformation is consistent with the observed low exoelectrogenic activity of the MEC bioanode batch run. The lack of acetate production in this fermentation run also agrees with the observed negligible exoelectrogenesis during the MEC bioanode run. Carbon balance analysis showed that 25% of the initially added carbon was not accounted for by the detected metabolite (i.e., phenol). It is noteworthy that 1 mM HBA converted to phenol by decarboxylation can result in 1 mM bicarbonate, representing 12.5% of the total added carbon. The remaining 12.5% of the unaccounted carbon might be attributed to un-identified metabolites formed in minor biotransformation pathways and/or microbial growth.

FF biotransformation in the fermentative culture resulted in FA and acetate, with a total carbon recovery up to 99% (Figure 6.5D). A high concentration of FA was detected (0.92 mM), representing 92% of the initial FF concentration. In comparison, FA resulting from abiotic electrochemical reaction accounted for only 25% of the initial FF concentration, as reported in Chapter 5. Thus, microbial metabolism dominated over abiotic electrochemical reactions for the transformation of FF to FA in the bioanode. FF and acetate were previously reported as intermediates of FF biotransformation in a culture of *Desulfovibrio furfuralis* under sulfate-reducing conditions (Folkerts et al., 1989).

HMF biotransformation in the fermentative culture resulted in HMF-OH as the only identified metabolite (Figure 6.5E), consistent with the observation in the MEC bioanode run, as discussed in Section 6.3.2, above. Acetate was not detected in the HMF batch run with the fermentative culture, even though active exoelectrogenesis was observed in the MEC bioanode fed with HMF (see Figure 6.1B). It is possible that acetate production was relatively slow during the HMF fermentation, and thus acetate was not detected within the 6-d batch run, which is also consistent with the relative low (but long-lasting) current observed during the HMF bioanode batch run. The detected HMF-OH in 6 days of incubation accounted for only 38% of the FF added to the fermentative culture (Figure 6.5E). Thus, un-identified metabolites could have been present. Nevertheless, the MEC anode efficiency during the HMF batch run was relatively high (56%; Table 6.2), which means that a significant fraction of un-identified metabolites was eventually transformed, resulting in electric current.

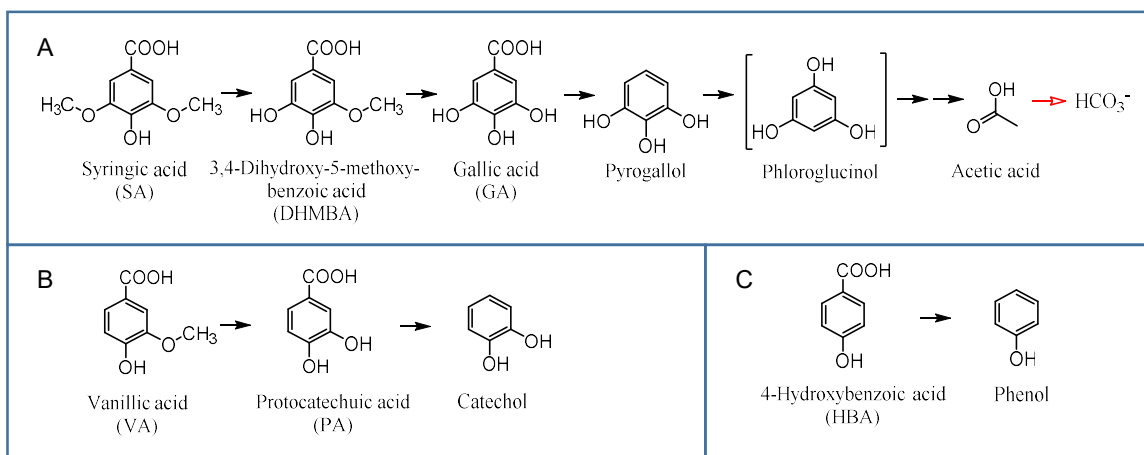
Considering that the main metabolic processes in a bioanode are fermentation followed by exoelectrogenesis, acetate production through fermentation is critical to the exoelectrogenic capacity of the phenolic substrates. Nevertheless, it is noteworthy that the measured acetate concentration does not represent the ultimate acetate-producing capacity of these compounds because of the limited duration of the fermentative batch runs, which in turn resulted in limited extent of biotransformation. Qualitatively, the fermentative transformation of the five compounds using the fermentative culture resulted in the production of aromatic and furanic metabolites identical to those detected in the MEC bioanode batch runs. Therefore, the fermentative transformation of the furanic and phenolic compounds in the MEC bioanode took place independently of exoelectrogenesis.

#### 6.3.4 SA, VA and HBA Biotransformation Pathways

As discussed in Section 6.3.1, above, the two furanic compounds (FF and HMF) were favorable MEC substrate resulting in > 50% anode efficiency. However, the three phenolic compounds (SA, VA and HBA), belonging to three different classes (syringyl, guaiacyl and *p*-hydroxyphenyl, respectively), differ significantly in their exoelectrogenic potential, resulting in anode efficiency ranging from 9% to 50% (Table 6.2). Thus, further investigation on the biotransformation pathways was focused the three phenolic compounds, to identify the limitations and to explain the difference in the exoelectrogenic potential of SA, VA and HBA.

Based on the chemical structures and the sequence of detected metabolites, biotransformation pathways of SA, VA and HBA in the MEC bioanode are proposed

(Figure 6.6). Demethylation and decarboxylation were common reactions employed to remove the  $-CH_3$  from  $-O-CH_3$  groups and the  $-COOH$  substituents from aromatic rings, resulting in hydroxylated analogs of SA, VA and HBA (i.e., pyrogallol, catechol and phenol, respectively). As demonstrated in fermentative batch runs (Section 6.3.3), these reactions could occur through fermentation, independent of exoelectrogenesis. Enzymes catalyzing the abovementioned demethylation and decarboxylation reactions have been found and characterized in fermentative bacteria. *O*-demethylase, a tetrahydrofolate- and ATP-dependent enzyme cleaving phenylmethylether bonds via methyl transfer, has been reported in *Acetobacterium* spp. (Berman and Frazer, 1992; Kaufmann et al., 1998). Gallate decarboxylase, a specific,  $Mg^{2+}$ -dependent enzyme, was found in a fermentative bacterium *Pelobacter acidigallici*, involved in the conversion of gallic acid to pyrogallol (Brune and Schink, 1992). 4-hydroxybenzoate and 3,4-dihydroxybenzoate decarboxylases, purified from *Clostridium hydroxybenzoicum*, are oxygen-sensitive and ATP-independent enzymes catalyzing the decarboxylation of HBA and PA and the reverse reactions (He and Wiegel, 1995). As discussed in Section 6.3.5, below, *Acetobacterium*, *Pelobacter*, and *Clostridium* were detected in the MEC bioanode and the fermentative culture biofilm microbial communities.



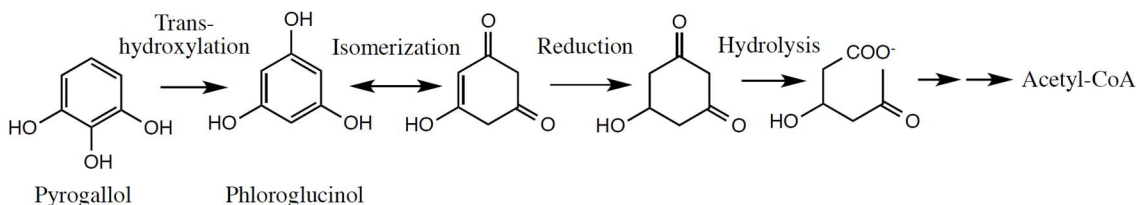
**Figure 6.6.** Proposed biotransformation pathways of SA (A), VA (B) and HBA (C) under MEC bioanode conditions based on identified metabolites. Solid arrows denote fermentative steps; hollow arrow denotes exoelectrogenic step. Phloroglucinol in brackets is a hypothetical intermediate.

After the common demethylation and decarboxylation steps, subsequent reactions in the biotransformation pathways after the production of pyrogallol, catechol and phenol differed. As discussed in Sections 6.3.2 and 6.3.3, above, the aromatic ring of pyrogallol was cleaved, resulting in the production of acetate under both bioanode and fermentative conditions. However, catechol and phenol remained intact as major and persistent metabolites. Consistent with the results reported in this chapter, during the enrichment of the bioanode and the fermentative culture, when mixtures of SA, VA, HBA, FF and HMF were used as bioanode substrates, the removal of parent phenolic compounds, as well as the accumulation of catechol and phenol were observed (see Chapter 5). Although SA has a higher extent of biotransformation than VA and HBA, as shown by the results reported in this chapter, preferential substrate utilization was not observed when these compounds were added to the MEC bioanode as a mixture (see Chapter 5; Figure 5.7).

Aromatic ring cleavage under anoxic conditions is possible by reductive reactions, which requires the formation of central intermediates possessing strong electron-withdrawing substituents, thus facilitating electron transfer to the ring (Fuchs et al., 2011). One group of such central intermediates is aromatic compounds with two or more hydroxyl groups in the *meta* position relative to each other, such as resorcinol (1,3-dihydroxybenzene) and phloroglucinol (1,3,5-trihydroxybenzene), which have mesomeric non-aromatic structures and weakened aromatic stability (Schink et al., 2000). Another group of central intermediates is CoA-thioester substituted aromatic compounds, such as benzoyl-CoA. The aromatic ring of such central intermediates can be cleaved by reduction and/or hydrolysis (Schink et al., 2000). Pyrogallol (1,2,3-trihydroxybenzene) detected in the present study could not be hydrolyzed or directly reduced (Schink et al., 2000). However, through a transhydroxylation reaction, pyrogallol can be isomerized to phloroglucinol (Brune and Schink, 1990), which can then be easily reduced by a conventional NADPH-dependent reductase and hydrolyzed to yield 3 mol of acetate (Figure 6.7) (Schink et al., 2000). The reaction of pyrogallol-to-phloroglucinol isomerization ( $\Delta G^{\circ} = -15.5$  kJ/mol) is a well-established pyrogallol degradation mechanism in fermentative bacteria, such as *Eubacterium oxidoreducens* and *Pelobacter acidigallici* (Brune and Schink, 1992; Brune and Schink, 1990; Haddock and Ferry, 1989). In this study, the detection of both *Eubacterium* and *Pelobacter* species in the MEC bioanode microbial community (see Section 6.3.5, below), and acetate as a fermentation product, supports the phloroglucinol pathway in the pyrogallol degradation. Although phloroglucinol was not detected, which might be due to a fast consumption



rate, it is included in the SA biotransformation pathway as a hypothetical intermediate (Figure 6.6A).



**Figure 6.7.** Transhydroxylation of pyrogallol to phloroglucinol and subsequent ring cleavage reactions (Schink et al., 2000).

Catechol and phenol cannot undergo transhydroxylation reactions to form phloroglucinol or resorcinol, as is the case of pyrogallol (Brune and Schink, 1990). Thus, an alternative route for anaerobic ring cleavage (i.e., benzoyl-CoA pathway) is required for catechol and phenol degradation. The benzoyl-CoA pathway has been demonstrated in sulfate- and nitrate-reducing bacteria (*Desulfobacterium*, *Thauera aromatica* and *Azoarcus* spp.) for catechol and phenol degradation. In this pathway, a carboxylation step is required to convert catechol and phenol to protocatechuic acid (PA) and 4-hydroxybenzoic acid (HBA), respectively, prior to the addition of CoA thioesters (Gorny and Schink, 1994; Tschuch and Fuchs, 1989; van Schie and Young, 1998). However, the biotransformation observed in the present study occurred in the opposite direction (i.e., PA to catechol and HBA to phenol; Figure 6.6). Thus, the benzoyl-CoA pathway was not used or was of minor importance in the present study. Otherwise, PA and HBA would have been converted to protocatechuy-CoA and 4-hydroxybenzoyl-CoA, instead of catechol and phenol. The reason why VA (or PA) and HBA were not converted to

benzoyl-CoA is unclear, but plausible explanations are discussed below. The benzoyl-CoA pathway is energy intensive. Benzoyl-CoA degradation yields 3 ATP equivalents, but the formation of benzoyl-CoA consumes 2 ATP equivalents and the ring reduction consumes another 2 ATP equivalents (Fuchs et al., 2011). Thus, it is particularly difficult for fermentative bacteria, which do not have a respiratory chain as do nitrate and sulfate reducers, to generate the ATP equivalents needed for the benzoyl-CoA pathway, unless an ATP-independent ring reduction mechanism is used (Fuchs et al., 2011). Furthermore, the carboxylation of catechol to PA or phenol to HBA requires additional ATP, making the overall energy balance extremely demanding (Fuchs et al., 2011; Schink et al., 2000). In comparison, decarboxylation reactions (i.e., PA to catechol and HBA to phenol) can generate ATP by creating a proton gradient across the cell membrane (Schie and Young, 2000). The free energy change in the reaction of HBA decarboxylation to phenol was estimated as -19 to -21 kJ/mol (Brune and Schink, 1992). Thus, the decarboxylation reaction is more physiologically advantageous than the benzoyl-CoA pathway, which may partially explain the persistence of catechol and phenol in the present study.

Table 6.3 lists the standard Gibbs free energy change ( $\Delta G^\circ$ , pH 7 and 298 K) of potential fermentation reactions of SA, VA, HBA, pyrogallol, catechol and phenol. Fermentation products of SA, VA, and HBA were hypothesized based on the stoichiometry of demethylation (0.75 mol-acetate/mol-methoxy group), decarboxylation (1 mol  $\text{HCO}_3^-$ /mol-carboxyl group), and aromatic ring cleavage (3 mol-acetate/mol-aromatic ring).  $\text{H}_2$  and  $\text{H}_2\text{O}$  were added accordingly to balance the reactions. Fermentation reactions of pyrogallol, catechol and phenol were written using different electron sinks (propionate, butyrate, ethanol, and  $\text{H}_2$ ) based on the oxidation state of each

compound (Table 6.3). The calculated  $\Delta G^{\circ}$  values are negative for all reactions, except for phenol fermentation to acetate and  $H_2$  (+ 8.46 kJ/mol; Equation 12 in Table 6.3 ), indicating that the hypothetical fermentation reactions are favorable for SA, VA, HBA, catechol and pyrogallol, without the need of syntrophic  $H_2$ -utilizing partners. To calculate the maximum concentration of fermentation products required to achieve  $\Delta G = 0$  for the fermentation of phenol (Equation 12 in Table 6.3), Equation 6.4 below was used.

$$\Delta G = \Delta G^{\circ} + RT \ln \frac{[CH_3COO^-]^3 [P_{H_2}]^2}{[C_6H_6O]} \quad 6.4$$

Under typical experimental conditions of this study, the phenol concentration was around 1 mM ( $[C_6H_6O] = 0.001 M$ ) and pH was 7.0. Thus, solving Equation 6.4 for  $\Delta G = 0$  resulted in  $[CH_3COO^-]^3 [P_{H_2}]^2 = 10^{-5}$ . Acetate or  $H_2$  was not detected in any of the bioanode batch runs in the present study. Even if trace, undetected acetate and  $H_2$  were present, the acetate concentration would have been far below 0.01 M, and the  $H_2$  partial pressure in the anode would have been  $< 1$  atm, resulting in  $[CH_3COO^-]^3 [P_{H_2}]^2 < 10^{-5}$ . Therefore, the reaction of phenol fermentation to acetate and  $H_2$  was thermodynamically favorable under typical experimental conditions of the present study. Moreover, exoelectrogens can act as syntrophic partners utilizing acetate and  $H_2$  produced from fermentation, as previously demonstrated in a glucose-fed bioanode (Freguia et al., 2008). Homoacetogens, represented by *Acetobacterium*, were also important in the syntrophy as  $H_2$  scavengers (Parameswaran et al., 2010). Therefore, thermodynamics cannot fully explain the persistence of either catechol or phenol observed in the present study.

**Table 6.3.** Hypothetical fermentative reactions of the phenolic compounds ( $\Delta G^{\circ}$ ; Gibbs free energy change at pH 7 and 298 K).

Equation number	Fermentation products	Reaction	$\Delta G^{\circ}$ (kJ/mol)
<i>Syringic acid (SA)</i>			
1	Pyrogallol, acetate	$C_9H_{10}O_5 + H_2O = C_6H_6O_3 + \frac{3}{2}CH_3COO^- + \frac{3}{2}H^+$	-150.79
2	Acetate	$C_9H_{10}O_5 + 4H_2O = \frac{9}{2}CH_3COO^- + \frac{9}{2}H^+$	-309.09
----- <i>Vanillic acid (VA)</i>			
3	Catechol, acetate	$C_8H_8O_4 + H_2O = C_6H_6O_2 + \frac{3}{4}CH_3COO^- + \frac{5}{4}H^+ + \frac{1}{2}HCO_3^-$	-99.06
4	Acetate, H <sub>2</sub> , HCO <sub>3</sub> <sup>-</sup>	$C_8H_8O_4 + 5H_2O = \frac{15}{4}CH_3COO^- + \frac{1}{2}HCO_3^- + \frac{17}{4}H^+ + H_2$	-168.18
----- <i>4-Hydroxybenzoic acid (HBA)</i>			
5	Phenol, HCO <sub>3</sub> <sup>-</sup>	$C_7H_6O_3 + H_2O = C_6H_6O + HCO_3^- + H^+ + H_2$	-23.44
6	Acetate, H <sub>2</sub> , HCO <sub>3</sub> <sup>-</sup>	$C_7H_6O_3 + 6H_2O = 3CH_3COO^- + HCO_3^- + 4H^+ + 2H_2$	-14.98
----- <i>Pyrogallol</i>			
7	Acetate	$C_6H_6O_3 + 3H_2O = 3CH_3COO^- + 3H^+$	-158.31
----- <i>Catechol</i>			
8	Acetate, H <sub>2</sub>	$C_6H_6O_2 + 4H_2O = 3CH_3COO^- + 3H^+ + H_2$	-69.12
9	Acetate, ethanol	$C_6H_6O_2 + \frac{7}{2}H_2O = \frac{1}{2}C_2H_6O + \frac{5}{2}CH_3COO^- + \frac{5}{2}H^+$	-73.95
10	Acetate, propionate	$C_6H_6O_2 + 3H_2O = CH_3CH_2COO^- + \frac{3}{2}CH_3COO^- + \frac{5}{2}H^+$	-93.33
11	Acetate, butyrate	$C_6H_6O_2 + 3H_2O = \frac{1}{2}CH_3CH_2CH_2COO^- + 2CH_3COO^- + \frac{5}{2}H^+$	-93.27
----- <i>Phenol</i>			
12	Acetate, H <sub>2</sub>	$C_6H_6O + 5H_2O = 3CH_3COO^- + 3H^+ + 2H_2$	+8.46
13	Acetate, ethanol	$C_6H_6O + 4H_2O = C_2H_6O + 2CH_3COO^- + 2H^+$	-1.19
14	Acetate, butyrate	$C_6H_6O + 3H_2O = CH_3CH_2CH_2COO^- + CH_3COO^- + 2H^+$	-39.84

### 6.3.5 Microbial Communities

The composition of the bioanode microbial community characterized after 6 months of enrichment (in MFC), as well as after 7 and 13 months (in MEC) is presented in Table 6.4. The analysis results of these bioanode microbial communities are reported and discussed in detail in Chapter 4, Chapter 5 and Chapter 8, respectively. Here, an overview is provided on the bioanode biofilm microbial community established during the long-term bioanode development and use, as compared to the microbial community of the fermentative culture. The three samples of the bioanode microbial community (i.e., MFC-6 month, MEC-7 month, and MEC-13 month) consisted of the same major phyla at comparable relative abundances: *Proteobacteria* (68 – 85%), *Bacteroidetes* (2-17%), and *Firmicutes* (9-12%)(Table 6.4). The *Proteobacteria* phylum was dominated by *Geobacter* or *Desulfovibrio* genera (> 30%), which are considered as putative exoelectrogens (Kang et al., 2014; Logan, 2009). *Desulfovibrio* genus also includes furanic compound degraders (Folkerts et al., 1989). The MEC-7 month sample was less abundant in *Geobacter* spp. and more abundant in *Desulfovibrio* spp., compared to the MFC-6 month sample, possibly as a result of community transfer from the MFC to the MEC bioanode. Nevertheless, after several months of MEC operation, the abundance of *Geobacter* and *Desulfovibrio* spp. observed in the MEC-13 month sample was similar to that in the MFC-6 month sample. *Pelobacter* genus, which includes species degrading pyrogallol (Brune and Schink, 1992), was detected in *Proteobacteria* (0.2-1.7%). In the *Firmicutes* phylum, genera of *Eubacterium*, *Acetobacterium*, *Anaerovorax*, and *Clostridium* were present in the three bioanode samples, at an abundance within the same order of magnitude. As discussed above, *Eubacterium*, *Acetobacterium*, *Clostridium*, and

*Pelobacter* spp. have been reported to anaerobically transform phenolic compounds (Bache and Pfennig, 1981; Brune and Schink, 1992; Brune and Schink, 1990; Haddock and Ferry, 1989; He and Wiegel, 1995; Zhang and Wiegel, 1990). It is noteworthy that the same microbial phlotypes were found in the bioanode at different stages of the present study, although at a variable abundance at the genus level. Thus, the long-term MEC operation with the same substrate mixture as bioanode feed resulted in a well-established bioanode microbial community. Although 6-d batch runs using individual phenolic compounds were conducted, such short-term experiments should not have significantly altered the bioanode biofilm microbial community structure.

The microbial community of the fermentative culture biofilm, characterized 6 months after the startup, was dominated by *Proteobacteria* (60%), *Bacteroidetes* (28%), and *Firmicutes* (12%)(Table 6.4). Abundant species (i.e., > 1% of total sequences) within the *Proteobacteria* phylum belonged to the genera of *Azoarcus* (33%), *Pseudomonas* (24%), and *Magnetospirillum* (2%). In the *Firmicutes* phylum, abundant phlotypes were distributed in genera of *Acetobacterium* (8%), *Anaerovorax* (2%), and *Clostridium* (1%).

**Table 6.4.** Microbial community composition (%) of the MEC bioanode and fermentative culture biofilms at phylum and genus levels.

Species	Biofilm Sample			
	MFC-6 month	MEC-7 month	MEC-13 month	Fermentative culture-6 month
<b><i>Proteobacteria</i></b>	<b>79</b>	<b>68</b>	<b>85</b>	<b>60</b>
<i>Geobacter</i>	57.26	5	66	0.02 ↓
<i>Desulfovibrio</i>	1.54	32	0.6	0.09 ↓
<i>Pelobacter</i>	0.9	1.7	0.2	0.5
<i>Azoarcus</i>	0.9	17	0.3	33
<i>Magnetospirillum</i>	0.05	0.8	1	2
<i>Pleomorphomonas</i>	8.04	11	0.2	0.01 ↓
<i>Pseudomonas</i>	0.03	0.05	0.07	24 ↑
Unclassified <i>Proteobacteria</i>	10	0.5	17	0.4
<b><i>Bacteroidetes</i></b>	<b>6.8</b>	<b>17</b>	<b>2</b>	<b>28</b>
<i>Dysgonomonas</i>	0.02	7	0.6	0.07
<i>Proteiniphilum</i>	0.02	0.04	0.05	2 ↑
Unclassified <i>Bacteroidetes</i>	7	10	1.4	26
<b><i>Firmicutes</i></b>	<b>12</b>	<b>12</b>	<b>9</b>	<b>12</b>
<i>Eubacterium</i>	2	1	0.4	ND <sup>a</sup> ↓
<i>Acetobacterium</i>	1.27	0.3	0.3	8 ↑
<i>Anaerovorax</i>	5.46	3	6	2
<i>Clostridium</i>	0.7	2	1	1
<i>Phascolarctobacterium</i>	0.04	3	0.03	0.1
Unclassified <i>Firmicutes</i>	2.53	2.7	1.27	0.9
<b><i>Synergistetes</i></b>	<b>1.5</b>	<b>1.4</b>	<b>0.03</b>	<b>0.6</b>
<b><i>Actinobacteria</i></b>	<b>0.6</b>	<b>1.3</b>	<b>0.2</b>	<b>0.3</b>
Unclassified <i>Bacteria</i>	<b>0.1</b>	<b>0.3</b>	<b>4</b>	<b>1</b>

<sup>a</sup> ND, not detected

The similarity and dissimilarity between the microbial communities of the bioanode and the fermentative culture biofilms are discussed below. First, the two microbial communities are highly similar at the phylum level, and all genera detected in the fermentative culture were present in the bioanode (Table 6.4). Second, several abundant genera in the bioanode were found at levels order(s) of magnitude lower in the fermentative culture, including *Geobacter*, *Desulfovibrio*, *Eubacterium*, and *Pleomorphomonas*. As mentioned above, *Geobacter* and *Desulfovibrio* are putative exoelectrogens, which were expected to be less predominant in the non-exoelectrogenic, fermentative culture. It is not clear why *Eubacterium* and *Pleomorphomonas* were also considerably less abundant in the fermentative culture biofilm. In contrast, the relative abundance of *Pseudomonas*, *Proteiniphilum*, and *Acetobacterium* spp. was order(s) of magnitude higher in the fermentative culture biofilm than in the bioanode biofilm. The members of *Pseudomonas* genus can use many different organic compounds as carbon and energy sources, both aerobically and anaerobically (Madigan et al., 2009). Such metabolic diversity makes it difficult to identify the reason why *Pseudomonas* spp. were enriched in the fermentative culture. *Proteiniphilum* spp. are proteolytic, obligate anaerobic bacteria (Chen and Dong, 2005), which may have grown on dead cell material in the fermentative culture. *Acetobacterium* spp., which is an important phenolic degrader, as mentioned above (Bache and Pfennig, 1981; Kaufmann et al., 1998), could grow favorably in the fermentative culture. In summary, consistent with the fact that the fermentative culture was inoculated with the MEC bioanode microbial community, common phylotypes were shared between the two microbial communities. However, due to the difference in metabolic conditions (exoelectrogenic vs. non-exoelectrogenic),



putative exoelectrogens were nearly absent in the fermentative culture, and differences were observed in relative abundance at the genus level of other species.

### 6.3.6 Alternative Microbial Communities and Metabolic Conditions

To assess whether the low extent of VA and HBA biotransformation was due to the lack of requisite microbial species, biotransformation assays of VA and HBA were conducted with more diverse microbial communities in environmental samples (PPS, CS) and enriched cultures (PPC, METH) as described in Section 6.2.4. In all four assays, VA and HBA were converted in 30 days after a lag phase of 7-20 days, resulting in catechol and phenol as the predominant metabolites, respectively. However, after more than 2 years of incubation, catechol and phenol were still persistent at the same levels in the PPS, PPC, and METH assays, whereas they were completely transformed in the CS assay. Yeast extract, which supplies a variety of co-factors required for biotransformation, was added at 20 mg/L to one series of the METH assay and the MEC bioanode. However, catechol and phenol persisted in the yeast extract amended series at the same levels as in the control, suggesting that the lack of co-factors was not the cause of the limited extent of biotransformation of VA and HBA.

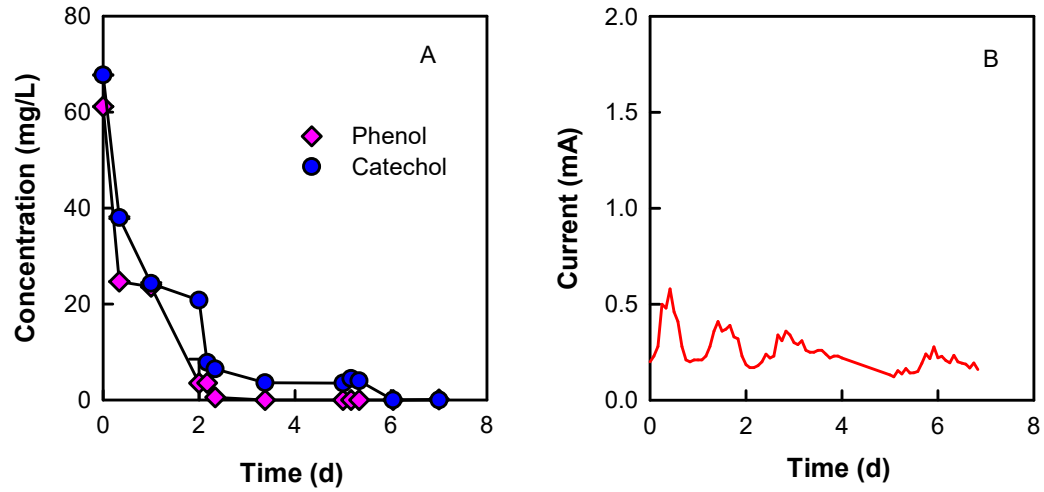
Literature-reported fate of catechol and phenol under fermentative/methanogenic conditions varies from study to study, as discussed below. Kaiser and Hanselmann (1982) and Tschech and Schink (1986) observed persistent catechol produced from VA. In a review by Schink et al. (2000), catechol was regarded as the most slowly degraded divalent phenol under anoxic conditions. Tschech and Schink (1986) reported that phenol, produced from HBA, was slowly degraded in several weeks, whereas Kuhn et al.

(1989) observed a fast degradation of phenol in 4 days. An earlier study reported that all SA, VA, HBA, catechol and phenol were degraded within 34 days, with more than 60% of the carbon converted to CH<sub>4</sub> and CO<sub>2</sub> (Healy and Young, 1979). In contrast to the aforementioned studies, all conducted with pure chemicals, a recent MEC study, which used a complex organic mixture generated during pyrolysis of switchgrass, observed removal of catechol and phenol (Lewis et al., 2015). The presence of readily biodegradable components in the switchgrass-derived stream (e.g., acetate, sugars), may have facilitated the degradation of catechol and phenol. Therefore, the fate of catechol and phenol in the above-mentioned studies varied, depending on microbial communities, metabolic conditions and rates.

The persistence of catechol and phenol in the MEC bioanode presents a biotransformation obstacle for improving the MEC performance. Recognizing that catechol and phenol are highly prone to aerobic biodegradation (Fuchs et al., 2011), the MEC bioanode was tested under microaerophilic conditions for enhancing the biotransformation of catechol and phenol. Although oxygen is usually known for its negative role in bioanodes as a competitive electron acceptor, there is evidence that a slightly oxic condition in the bioanode increases biomass growth and enhances biotransformation of recalcitrant organic compounds, creating an overall positive effect on the current production (Cheng et al., 2015; Lu et al., 2016b). In the present study, with three injections of air to the bioanode headspace (39.1 mg O<sub>2</sub> in total) during the 7-d incubation, catechol and phenol (67.8 and 61.2 mg/L, accumulated from 200 mg/L of furanic and phenolic mixture) were both further transformed (Figure 6.8). CO<sub>2</sub> was detected in the anode headspace (0.3 mmol). The soluble COD removed was 527 mg/L,

compared to 274 mg COD/L corresponding to the removal of catechol and phenol, indicating degradation of other compounds in addition to catechol and phenol. However, the current and cathodic H<sub>2</sub> production was negligible. Thus, the enhanced biotransformation of catechol and phenol in the bioanode under microaerophilic conditions did not lead to an improved exoelectrogenic performance. In contrast to the finding of the present study, a previous study demonstrated improved exoelectrogenesis in a microaerophilic bioanode fed with aniline (Cheng et al., 2015). Because catechol and phenol are not as recalcitrant as aniline, mineralization of catechol and phenol occurred easily under microaerophilic conditions, diverting electron equivalents away from exoelectrogenesis. Thus, controlling the oxygen partial pressure is a challenge for operating a microaerophilic bioanode for the biotransformation of catechol and phenol. In MFCs with air cathodes, where oxygen can diffuse into the bioanode (Zhang et al., 2015), catechol and phenol degradation can be highly favored. The observed decrease of catechol and phenol levels in the MFC reported in Chapter 4 could be attributed to aerobic biotransformation in the bioanode using oxygen diffused from the air cathode. Oxygen diffusion may also have partially accounted for phenol removal reported in previous MFC studies (Friman et al., 2013; Luo et al., 2009; Song et al., 2014). In addition, if the bioanode feed contains significant levels of alternative electron acceptors (i.e., nitrate, iron (III), or sulfate), the degradation of catechol and phenol may occur via anaerobic respiration using the benzoyl-CoA pathway as mentioned in Section 6.3.4, above. The redox environment of the bioanode may also be altered, depending on the abundance of such electron acceptors and the extent of anaerobic respiration. However,

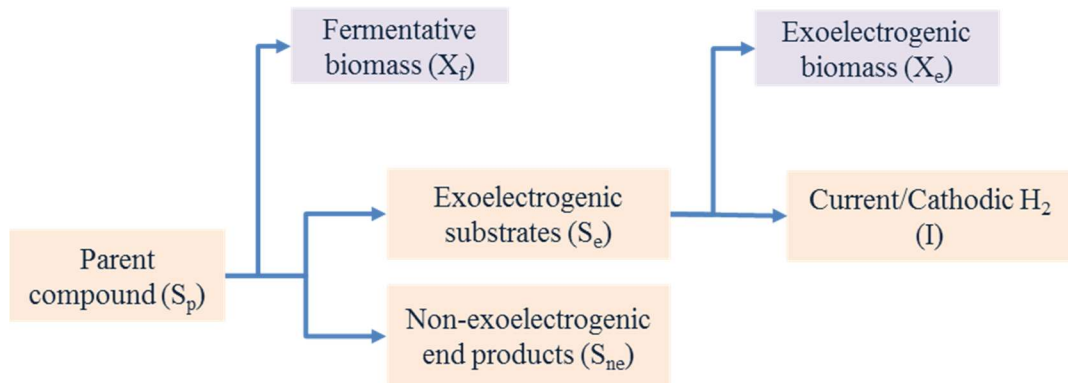
the presence of such alternative electron acceptors will divert electrons from exoelectrogenesis, thus lowering the MEC Coulombic efficiency.



**Figure 6.8.** Removal of catechol and phenol (A) and current production (B) in a MEC bioanode under microaerophilic conditions.

### 6.3.7 Substrate Utilization and Partitioning of Electron Equivalents

Based on the experimental evidence presented in this chapter, a framework of substrate utilization and partitioning into biomass and other products in the MEC bioanode was developed as presented in Figure 6.9. The parent compound ( $S_p$ ) was first fermented to exoelectrogenic substrates ( $S_e$ ; e.g., acetate,  $H_2$ ) and non-exoelectrogenic end products ( $S_{ne}$ ; e.g., catechol, phenol). Fermentative biomass ( $X_f$ ) was produced with an observed biomass yield coefficient of  $Y_{obs,1}$ . In the second step, only exoelectrogenic substrates were utilized to produce electric current ( $I$ ), which in turn resulted in cathodic  $H_2$  production. Exoelectrogenic biomass ( $X_e$ ) was produced with an observed biomass yield coefficient of  $Y_{obs,2}$ . All coefficients and variables are expressed in COD units to illustrate the partitioning of electron equivalents.



**Figure 6.9.** Substrate utilization and partitioning in a MEC bioanode in two sequential sub-processes: fermentation, followed by exoelectrogenesis.

To develop the substrate fractionation factors in the two sub-processes (i.e., fermentation and exoelectrogenesis), a mass balance was performed. Biomass production was expressed using  $Y_{obs}$  and the respective substrate utilized, as follows:

$$X_f = Y_{obs,1}S_p \quad 6.5$$

$$X_e = Y_{obs,2}S_e \quad 6.6$$

The mass balance equation during the exoelectrogenic step was as follows:

$$S_e = X_e + I = Y_{obs,2}S_e + I \quad 6.7$$

Based on the definition of anode efficiency,  $\alpha = I/S_p$  (See Section 3.3.3, above),  $I$  was expressed as

$$I = \alpha S_p \quad 6.8$$

By substituting Equation 6.8 to Equation 6.7,  $S_e$  was expressed in terms of  $S_p$ ,  $Y_{obs,2}$ , and  $\alpha$ , as follows:

$$S_e = \frac{\alpha S_p}{1 - Y_{obs,2}} \quad 6.9$$

Then, a mass balance was developed for the fermentative step, as follows:

$$S_p = X_f + S_e + S_{ne} \quad 6.10$$

Substituting the expression of  $X_f$  (Equation 6.5) and  $S_e$  (Equation 6.9) to Equation 6.10,  $S_{ne}$  was expressed as follows:

$$S_{ne} = S_p \left( 1 - Y_{obs,1} - \frac{\alpha}{1 - Y_{obs,2}} \right) \quad 6.11$$

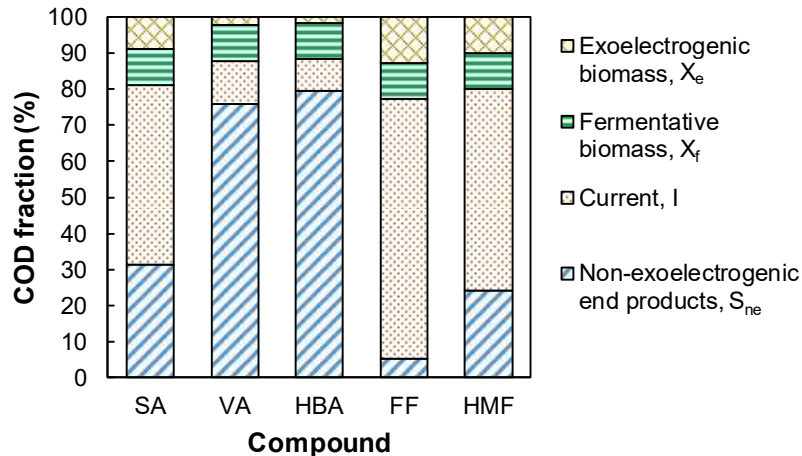
As an illustration, and assuming an initial  $S_p$  mass of 100 g COD, completely transformed in the MEC bioanode, the resulting biomass and products were calculated and results are shown in Table 6.5. The  $\alpha$  value for each compound was based on the experimentally measured anode efficiency reported in Section 6.3.1, above (Table 6.2).

The values of the biomass yield coefficients for the fermenters and exoelectrogens were assumed based on the following reasoning. An overall  $Y_{obs}$ , accounting for both  $X_f$  and  $X_e$ , was experimentally estimated as 0.23 g biomass-COD/g substrate-COD reported in Chapter 8. Typical values of true yield coefficient ( $Y$ , not accounting for decay) for fermentative and anaerobic processes are 0.18 and 0.11- 0.71 g-biomass-COD/g-degradable-COD, respectively (Rittmann and McCarty, 2001). Considering the measured overall  $Y_{obs}$  and literature reported  $Y$  values for fermenters and anaerobic respiring bacteria, values of  $Y_{obs,1}$  and  $Y_{obs,2}$  were assumed to be 0.1 and 0.15 g biomass-COD/g substrate-COD, respectively.

**Table 6.5.** Substrate utilization and partitioning to biomass and other products with numerical illustration for the two furanic and three phenolic compounds used in the present study.

Variable (g COD)	Fractionation factor	Parent compound				
		SA	VA	HBA	FF	HMF
$S_p$	1	100	100	100	100	100
$S_e$	$\frac{\alpha}{1 - Y_{obs,2}}$	59	14	11	85	66
$S_{ne}$	$1 - Y_{obs,1} - \frac{\alpha}{1 - Y_{obs,2}}$	31	76	79	5	24
I	$\alpha$	50	12	9	72	56
$X_f$	$Y_{obs,1}$	10	10	10	10	10
$X_e$	$Y_{obs,2}$	9	2	2	13	10

Based on the above-presented equations, the electron equivalents distribution between biomass ( $X_f$  and  $X_e$ ), current ( $I$ ), and left-over, non-exoelectrogenic products ( $S_{ne}$ ) are reported in Table X and further illustrated in Figure 6.10. Consistent with the observation that VA and HBA were mostly transformed to catechol and phenol as dead-end fermentation products (see Sections 6.3.2 and 6.3.3, above), a very high fraction of VA and HBA electron equivalents ended up as non-exoelectrogenic products ( $S_{ne}$ ). In contrast, most of the SA, FF and HMF electron equivalents were converted to current, which in turn resulted in cathodic  $H_2$  production. In addition, because acetate production from VA was very low and no acetate was produced from HBA (see Section 6.3.3), the production of exoelectrogenic biomass from VA and HBA was much lower than that from SA, FF and HMF (Figure 6.10). The small amount of  $X_e$  produced from HBA could be due to growth using minor, non-acetate exoelectrogenic substrates, which is consistent with the extremely low current ( $< 0.2$  mA) observed in the HBA bioanode batch run (see Section 6.3.1, above).



**Figure 6.10.** Electron equivalents partitioning to biomass, current and non-exoelectrogenic end products per unit of each compound utilized.



An important application of the above-presented, mass-based framework is to simulate bioprocesses in MEC bioanodes, by introducing kinetic rate expressions for the utilization of  $S_p$  and  $S_e$ , as well as for biomass production.  $S_p$  utilization in the fermentation sub-process can be described by Monod kinetics, while  $S_e$  utilization in the exoelectrogenic sub-process can be described by Nernst-Monod or Butler-Volmer kinetics (Hamelers et al., 2011; Kato Marcus et al., 2007; Korth et al., 2015). Using rate expressions and the above-described fractionation factors of electron equivalents in each sub-process, mass rate balance equations for either batch or CSTR reactors can then be developed for dynamic simulation of the overall process. The values of three parameters are needed to calculate fractionation factors,  $\alpha$ ,  $Y_{obs,1}$ , and  $Y_{obs,2}$ . Although the value of  $\alpha$  can be easily measured experimentally, obtaining values of  $Y_{obs,1}$  and  $Y_{obs,2}$  is more complex as the total biomass ( $X_e + X_f$ ) is usually measured. For well-understood, specific stoichiometric reactions,  $Y_{obs,1}$  and  $Y_{obs,2}$  may be estimated based on bioenergetic principles (Rittmann and McCarty, 2001). Adopting  $Y_{obs,1}$  and  $Y_{obs,2}$  values from studies based on fermentation and exoelectrogenesis requires cautious examination of the definition and applicability of the observed yield coefficient, because of partial oxidation. To distinguish biomass associated with the biofilm or in suspension, appropriate fractionation factors can further be developed and applied. Although the above-described mass balance-based framework was developed based on individual parent compounds, simulation of a mixture of known compounds used as bioanode feed can be implemented by accounting for the metabolic fate of each individual compound. In the case where a complex, un-defined organic mixture is used as a bioanode feed, the values of  $\alpha$ ,  $Y_{obs,1}$  and  $Y_{obs,2}$  will need to be obtained experimentally or from the literature.

## 6.4 Summary

MEC bioanode batch runs conducted with individual furanic and phenolic compounds resulted in different exoelectrogenic activity. A higher fraction of electron equivalents of the furanic compounds (FF and HMF) was converted to electric current through exoelectrogenesis, than that of the phenolic compounds (SA, VA and HBA), making the furanic compounds more favorable substrates for used in the MEC bioanode than the phenolic compounds. Among the three phenolic compounds, SA supported exoelectrogenesis to a much higher degree than VA and HBA, as a result of a much higher extent of biotransformation. Further investigation on the biotransformation pathways revealed that the aromatic ring cleavage was the limiting step during the fermentative transformation of VA and HBA.

The great difference in the extent of fermentative biotransformation of SA, VA and HBA is rooted in the number and position of their –OH and –O–CH<sub>3</sub> substituents. The syringyl arrangement of the –OH and –O–CH<sub>3</sub> groups enables the transformation of SA to pyrogallol, whose aromatic ring can be easily cleaved using the well-established phloroglucinol pathway even under strict fermentative conditions. In contrast, the guaiacyl and *p*-hydroxyphenyl position of –OH and –O–CH<sub>3</sub> in VA and HBA does not support the formation of a trihydroxylated benzene as a central intermediate that can then enter the phloroglucinol pathway. Instead, VA and HBA are decarboxylated to dead-end products such as catechol and phenol, respectively. Further biotransformation of catechol and phenol under fermentative conditions was not observed in alternative microbial communities tested, except in a microbial community from an environmental sample of a contaminated sediment.

The findings reported in this chapter provide further understanding on the metabolic fate of individual furanic and phenolic compounds in the MEC bioanode. The finding that the extent of fermentative biotransformation of the phenolic compounds is related to the number and position of –OH and –O-CH<sub>3</sub> substituents, resulting from different classes of lignin derivatives, is significant information for the use and treatment of biomass-derived waste streams using bioelectrochemical systems. To overcome metabolic limitations in MEC bioanodes, selective enrichment of fermentative bacteria, capable of metabolizing complex compounds to a high extent, should be considered. On the other hand, it is also important for future studies to discover and/or engineer exoelectrogenic species capable of directly utilizing a wider range of complex substrates.

# CHAPTER 7

## INHIBITORY EFFECT OF FURANIC AND PHENOLIC COMPOUNDS IN MEC BIOANODE

### 7.1 Introduction

In lignocellulosic hydrolysates and pyrolysates, furfural and 5-hydroxymethylfurfural are the primary furan derivatives present at a total concentration up to 5 g/L, while phenolic compounds, including alcohols, aldehydes and acids, are present at a total concentration up to 3 g/L (Mills et al., 2009). While furanic and phenolic compounds are well-known inhibitors of dark fermentation for H<sub>2</sub> and ethanol production, their potential inhibitory effect on the bioanode microbial activity has been scarcely reported. A study showed that syringaldehyde, *trans*-4-hydroxy-3-methoxy and 4-hydroxy cinnamic acids at a concentration above 20 mM, as well as benzyl alcohol and acetophenone at 0.2 mM, severely inhibited electricity generation from glucose using a microbial fuel cell (MFC) (Catal et al., 2008). Work reported in Chapter 5 showed that a mixture of furfural (FF), 5-hydroxymethylfurfural (HMF), syringic acid (SA), vanillic acid (VA), and 4-hydroxybenzoic acid (HBA) at a total concentration of 1.2 g/L in a batch MEC bioanode produced significantly lower current and H<sub>2</sub> than at lower concentrations of 0.2 – 0.8 g/L, suggesting inhibition by a high concentration of the mixture of furanic and phenolic compounds. However, an in-depth analysis of the observed inhibition is still lacking.

In a bioanode, where soluble external terminal electron acceptors (e.g., nitrate and sulfate) are absent, the conversion of high molecular weight, complex compounds occurs via fermentation followed by exoelectrogenesis (Kiely et al., 2011b). Fermentative

bacteria first convert the complex compounds to simpler molecules, among which acetate is a key electron donor used in subsequent exoelectrogenesis (Kiely et al., 2011b). There are two sub-steps in exoelectrogenesis: intracellular metabolism of electron donor and extracellular electron transfer to the anode electrode (TerAvest and Ajo-Franklin, 2016; Torres et al., 2010). Inhibition of either sub-step can lead to failure of current production. In parallel with exoelectrogenesis, methanogenesis can also occur using acetate and/or H<sub>2</sub>/CO<sub>2</sub> resulting from the fermentation of complex compounds, which, however, results in a decrease of cathodic H<sub>2</sub> production. The results reported in Chapter 5 showed that although the current decreased by 64%, as a result of inhibition by the furanic and phenolic mixture at 1.2 g/L, the transformation rate of the individual furanic and phenolic compounds increased by more than two-fold with an increase of the total mixture concentration from 0.8 to 1.2 g/L. Acetate accumulated at high levels with the decreased current, while was not detected with normal current production when the anode was fed with the compounds mixture at a total concentration of less than 1.2 g/L. These results demonstrate that inhibition by the furanic and phenolic compounds in the MEC bioanode primarily impacted the acetate-consuming process (i.e., exoelectrogenesis) as opposed to the acetate-producing process (i.e., fermentation). Thus, the work reported in this chapter focused on the inhibitory effect of furanic and phenolic compounds on exoelectrogenesis.

The following questions were to be answered: (1) Are the parent compounds or their transformation products responsible for the observed inhibition of exoelectrogenesis? (2) Which compound(s) in the mixture is/are the inhibitor(s)? (3) Do these compounds interact synergistically leading to more severe inhibition? To address these questions, the objective of the work reported in this chapter was to assess the

potential inhibitory effect of the two furanic (FF and HMF) and three phenolic compounds (SA, VA and HBA), as well as their biotransformation products, on exoelectrogenesis in a MEC bioanode.

## **7.2 Materials and Methods**

### **7.2.1 MEC Bioanode**

The work reported in this chapter was conducted with the MEC bioanode developed as described in Chapter 5. The total anode biomass concentration measured as protein was  $352 \pm 10$  and  $471 \pm 101$  mg/L, before and after the experiments reported here, respectively; approximately 90% of the biomass was biofilm-associated, whereas 10% was in suspension. The established biofilm microbial community mainly consisted of *Geobacter*, *Anaerovorax*, *Acetobacterium*, *Eubacterium* and unclassified *Clostridia* spp., including exoelectrogens, putative furanic and phenolic degraders, and other acetogenic fermentative bacteria, as described in Chapter 5.

### **7.2.2 Batch Runs with Parent Compounds Mixture**

In order to determine whether the parent compounds or their transformation products are inhibitory to exoelectrogenesis, two experiments were conducted. First, six consecutive 24-h batch runs were performed with an increasing initial total concentration of the parent compounds mixture (0.8, 1.2, 2.4, 3.6, 6.0 and 8.0 g/L). Exogenous acetate was not added. The selection of the initial concentration range was based on the results reported in Chapter 5, which showed that the mixture at 0.8 g/L was non-inhibitory, whereas at 1.2 g/L was inhibitory to exoelectrogenesis. The 0.8 g/L run was a non-

inhibitory control. In between each batch run, the anode chamber was drained and fresh anolyte added. In these batch runs, the anode microbial community experienced an increasing initial concentration of the parent compounds mixture, and the response of exoelectrogenesis in terms of current and cathodic H<sub>2</sub> production was monitored. The second experiment was conducted in a single batch run with the parent compounds mixture added repetitively every 24 h at a non-inhibitory concentration (0.8 g/L). Unlike the first experiment, the second experiment created a condition where the dose of the parent compounds was kept low, but the concentration of transformation products gradually increased. Based on the observation that complete transformation of the parent compounds mixture at 0.8 g/L occurred within 24 h (see Chapter 5), the concentration of the mixture was not expected to increase with daily feedings of 0.8 g/L. In addition, the anolyte was not replaced throughout this experiment, thus resulting in the accumulation of transformation products. A control experiment was conducted with repetitive additions of sodium acetate (NaAc) at increasing concentrations (0.1 – 10 g/L) in the bioanode without any furanic or phenolic compounds.

### 7.2.3 Batch Runs with Individual Parent Compounds

In order to determine which compounds contributed to the observed inhibition of exoelectrogenesis, individual parent compounds (FF, HMF, SA, VA and HBA) were tested in separate batch runs. For each compound, a batch run was initiated with fresh anolyte and 1 g/L NaAc as the exogenous exoelectrogenic substrate. Exogenous NaAc was added in excess to avoid differences in current production due to the difference in the extent of biotransformation of each of the furanic and phenolic compounds tested (see

Chapter 6). After 1 h of incubation with NaAc, but without any furanic or phenolic compound added (non-inhibited, control condition), one of the five compounds was added to the anode chamber at increasing levels of 0.8, 1.2, 2.4 and 3.6 g/L at 1, 3, 5 and 7 h, respectively (unless otherwise stated). The goal of sequential additions of each compound at increasing levels was to result in more than 50% inhibition based on current production. Based on the results of the compounds mixture, higher than 50% inhibition was observed with the mixture at 3.6 g/L. Thus, same concentrations as the mixture in the range of 0.8 - 3.6 g/L were selected for the individual compounds. The exoelectrogenic response was monitored by the current, recorded every 5 min, and cathodic H<sub>2</sub> production measured before each subsequent compound addition. A control run with 1 g/L NaAc, in the absence of any inhibitor, was conducted prior to each batch run for all the compounds tested.

#### 7.2.4 Batch Runs with Catechol and Phenol

Catechol and phenol, which were persistent transformation products of the five compounds mixture, were further determined to be transformation products of VA and HBA, respectively (see Chapter 6). The potential inhibitory effect of catechol and phenol was evaluated in batch runs following the same procedure as described above for the individual parent compounds. The levels of catechol or phenol added to the bioanode were pre-selected as 0.8, 1.2 and 2.4 g/L, based on the fact that VA or HBA at 3.6 g/L (the highest total level added) can produce 2.4 g/L of catechol or 2.5 g/L of phenol at the most (1:1 molar ratio). In the batch run conducted with catechol, where a low extent of



inhibition was observed after a total addition of 2.4 g/L, another 1.2 g/L was added to result in a significant inhibition.

#### 7.2.5 Extent of Inhibition and IC<sub>50</sub> Calculations

The extent of inhibition was calculated based on the ratio of the decreased current under inhibition ( $I_{inh}$ ) to that under non-inhibited, control conditions ( $I_{non-inh}$ ) as follows:

$$Inhibition (\%) = \left(1 - \frac{I_{inh}}{I_{non-inh}}\right) \times 100 \quad 7.1$$

The inhibitory concentration at 50% inhibition (IC<sub>50</sub>) is defined as the inhibitor concentration at which the current decreases by 50% compared to the current under non-inhibited conditions (i.e., control).

#### 7.2.6 Synergy Assessment

Potential synergistic inhibition was evaluated by comparing the observed effect of the compounds mixture to the additive effect of its components. The additive effect was calculated from the experimental data of individual compounds using three methods: effect summation, concentration addition, and independent action.

The effect summation method considers the inhibitory effect of a mixture to be equal to the sum of the inhibitory effect of each component on its own at the component concentration in the mixture (Silva et al., 2002). The inhibitory effect of a mixture ( $E_{mix}$ ) can be calculated as follows:

$$E_{mix} = \sum_{i=1}^n E_{i,c_i} \quad 7.2$$

where  $E_{i,C_i}$  is the inhibitory effect of component  $i$  on its own at the component concentration in the mixture ( $C_i$ ), and  $n$  is the total number of components in the mixture. For a range of mixture concentration with known composition,  $E_{mix}$  was calculated and a dose-response curve was established.

The concentration addition method assumes that all components in a mixture act in a similar way; one component of a mixture can be replaced by an equal fraction of an equieffective concentration of another without diminishing the overall effect of the mixture (Silva et al., 2002). Based on this concept, the components with additive effect in a mixture satisfy the following equation (Cedergreen, 2014; Liu et al., 2015a):

$$\sum_{i=1}^n \frac{C_i}{EC_{i,x}} = 1 \quad 7.3$$

where  $EC_{i,x}$  is the effect concentration of component  $i$  exhibiting  $x\%$  inhibition on its own,  $C_i$  is the concentration of component  $i$  in the mixture exhibiting the same  $x\%$  inhibition, and  $n$  is the total number of components in the mixture.

To calculate the mixture concentration exhibiting  $x\%$  inhibition ( $C_{mix,x}$ ), both sides of Equation 7.3 were divided by  $C_{mix,x}$  to obtain the following expression (Liu et al., 2015a):

$$C_{mix,x} = \frac{1}{\sum_{i=1}^n \frac{f_i}{EC_{i,x}}} \quad 7.4$$

where  $f_i$  is the fraction of component  $i$  in the mixture (i.e.,  $f_i = C_i/C_{mix,x}$ ), and  $n$  is the total number of components in the mixture? For a range of  $x\%$ ,  $C_{mix,x}$  was calculated and

a dose-response curve was established. Based on the dose-response curve, the mixture effect at a certain mixture concentration can be obtained.

The independent action method is based on probability analysis of stochastic events. Assuming that each component acts independently at different target sites, the probability of not being inhibited by a mixture equals the probability of not being inhibited by any of the components (Backhaus et al., 2004). Thus, the probability of being inhibited by the mixture ( $P_{mix}$ ) can be calculated as follows:

$$P_{mix} = 1 - (1 - P_1)(1 - P_2) \cdots (1 - P_i) \cdots (1 - P_n) \quad 7.5$$

where  $P_i$  is the probability of being inhibited by component  $i$ , and  $n$  is the total number of components in the mixture.

The inhibitory effect of a mixture at a specified concentration ( $E_{mix,C}$ ) can then be calculated as follows (Backhaus et al., 2004):

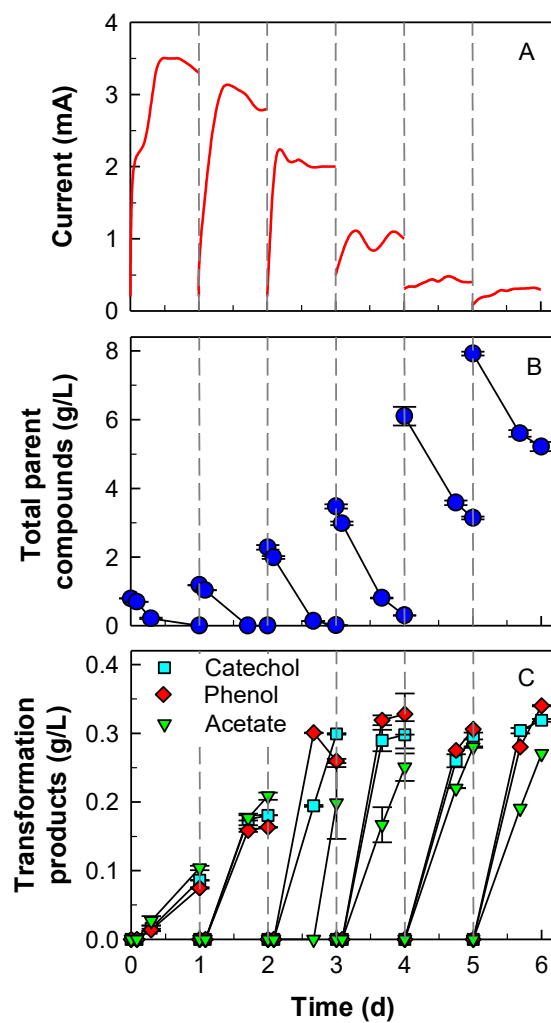
$$E_{mix,C_{mix}} = 1 - (1 - E_{1,C_1})(1 - E_{2,C_2}) \cdots (1 - E_{i,C_i}) \cdots (1 - E_{n,C_n}) \quad 7.6$$

where  $E_{i,C_i}$  is the inhibitory effect of component  $i$  on its own at the concentration in the mixture, and  $n$  is the total number of components in the mixture. For a range of  $C_{mix}$ , where  $C_{mix} = \sum_{i=1}^n C_i$ ,  $E_{mix,C_{mix}}$  was calculated and a dose-response curve was established.

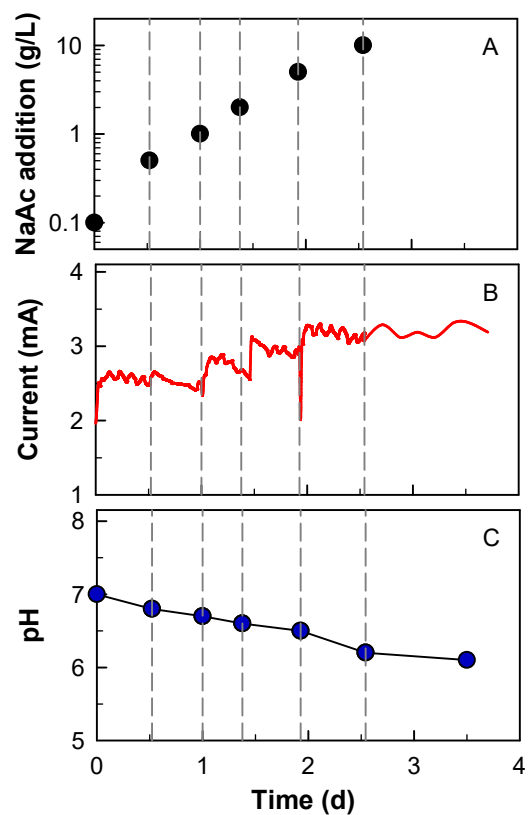
## 7.3 Results and Discussion

### 7.3.1 Inhibitory Effect of the Furanic and Phenolic Mixture

In the six batch runs conducted with 0.8, 1.2, 2.4, 3.6, 6.0 and 8.0 g/L of the furanic and phenolic mixture (FF, HMF, SA, VA and HBA), the maximum current in each batch run decreased with increasing initial total concentration of the mixture (Figure 7.1A). The first batch run at 0.8 g/L served as a non-inhibited control based on the findings reported in Chapter 5, in which the furanic and phenolic mixture at 0.8 g/L did not have any negative impact on exoelectrogenesis. Higher initial concentrations of 1.2 - 8.0 g/L resulted in a current decrease, with a more than 50% decrease at 3.6 g/L (4<sup>th</sup> batch run) and 91% decrease at 8.0 g/L (last batch run; Figure 7.1A). Similar to the current, the H<sub>2</sub> production rate decreased from 0.18 L/L-d to non-detected in the last batch run conducted with 8.0 g/L. For the batch runs with high initial mixture concentrations (3.6 – 8.0 g/L), 1.0 N NaOH was added upon each substrate addition to adjust the pH to 7.0, thus compensating for the acidity of the phenolic compounds added. The anolyte pH slightly decreased from 7.0 and remained at 6.7 or above during all batch runs. Such pH values are above the generally accepted inhibiting pH value (6.0) for *Geobacter* spp. (Torres et al., 2008). In addition, the control experiment conducted with 0.1 – 10 g/L NaAc showed that the current increased with increasing NaAc concentration, even with a decreasing pH from 7.0 to 6.0 (Figure 7.2). Thus, the decreased current in the batch runs conducted with the furanic and phenolic mixture is attributed to the inhibitory effect of these compounds and not to potential transfer limitations of electrons and protons.



**Figure 7.1.** Current (A), total concentration of the parent compounds (B), and transformation products (C) in consecutive batch runs conducted with increasing initial total concentrations of the parent compounds mixture from 0.8 to 8 g/L. Error bars represent stand deviations ( $n = 2$ ).



**Figure 7.2.** Current (B) and pH (C) during a control batch run conducted with sequential additions of sodium acetate (NaAc) at concentrations of 0.1 - 10 g/L (A) in the absence of any furanic or phenolic compounds.

The results of the study reported in Chapter 5, which was conducted one year before the inhibition study with the same MEC, showed that exoelectrogenesis was inhibited by more than 66% by the same furanic and phenolic mixture at 1.2 g/L. Thus, the work reported in this chapter showed a higher tolerance of the bioanode to these compounds (11 and 69% inhibition at 1.2 and 3.6 g/L, respectively). The increased tolerance is partially attributed to a 3-fold increase of biofilm-associated biomass during the 1-year MEC operation. Dominant microbial species in the biofilm were almost identical to those reported in Chapter 5, but a higher relative abundance of the fermentative species over exoelectrogens was observed after the 1-year MEC operation. Thus, a more robust and tolerant biofilm can be developed through prolonged exposure of the microbial community to the five furanic and phenolic compounds.

Consistent with the results reported in Chapter 5, the transformation rate of the parent compounds did not decrease when exoelectrogenesis was inhibited (Figure 7.1B). In fact, the transformation rate of the parent compounds in the 3.6 - 8.0 g/L runs was more than 1.5-fold higher than in the 0.8 g/L run (3.4-3.9 vs. 2.0 g/L-d), although the current decreased by more than 69%. The detected transformation products were catechol, phenol and acetate, whose concentration increased as the parent compounds were transformed during each batch run (Figure 7.1C). Catechol and phenol were transformation products of VA and HBA, respectively. The highest observed concentration of catechol (0.32 g/L) and phenol (0.34 g/L) represents 82% of VA and 86% of HBA transformed, respectively, based on 1:1 molar ratio between the parent compounds and their transformation products. The acetate accumulation rate was higher in the 3.6 - 8.0 g/L runs than in the 0.8 g/L run (0.25 - 0.29 vs. 0.1 g/L-d), which indicates

that the acetate consumption by the exoelectrogens was slower than its production by the fermenters in the 3.6 – 8.0 g/L runs. The increased transformation rate of the parent compounds and acetate accumulation in contrast to the decreased current, confirm that non-exoelectrogenic activities (e.g., fermentation) were not impacted in the bioanode, but instead, exoelectrogenesis was mainly inhibited. Although not observed in the relatively short duration experiments conducted in the present study, severe inhibition of exoelectrogenesis in MEC systems operated over long periods may result in the accumulation of high levels of fermentation products and lead to feedback inhibition of fermentation.

The fermentative process in the MEC bioanode used in this study involves different reactions and microbial species from those found in H<sub>2</sub> and ethanol dark fermentation studies, which are usually based on sugar degradation. In the present study, fermentation in the MEC anode refers to the transformation of furanic and phenolic compounds to mainly acetate, carried out by furanic and phenolic degraders (such as *Acetobacterium* and *Eubacterium* spp.), as mentioned in Chapter 5. H<sub>2</sub> and ethanol dark fermentation refers to the conversion of sugars to H<sub>2</sub> and ethanol by certain *Clostridium* spp. and yeasts. The furanic and phenolic fermenting bacteria, which can grow on these compounds, are presumably less susceptible to inhibition than microbial species involved in H<sub>2</sub> and ethanol fermentations, as well as exoelectrogenesis.

Gas in the bioanode headspace consisted of CO<sub>2</sub> and CH<sub>4</sub>; H<sub>2</sub> was not detected in the anode. CO<sub>2</sub> produced by both fermentation and exoelectrogenesis varied from 10 to 20 mL per run, without a clear correlation to the exoelectrogenic response in these batch runs. However, a lower CH<sub>4</sub> production was observed while exoelectrogenesis was

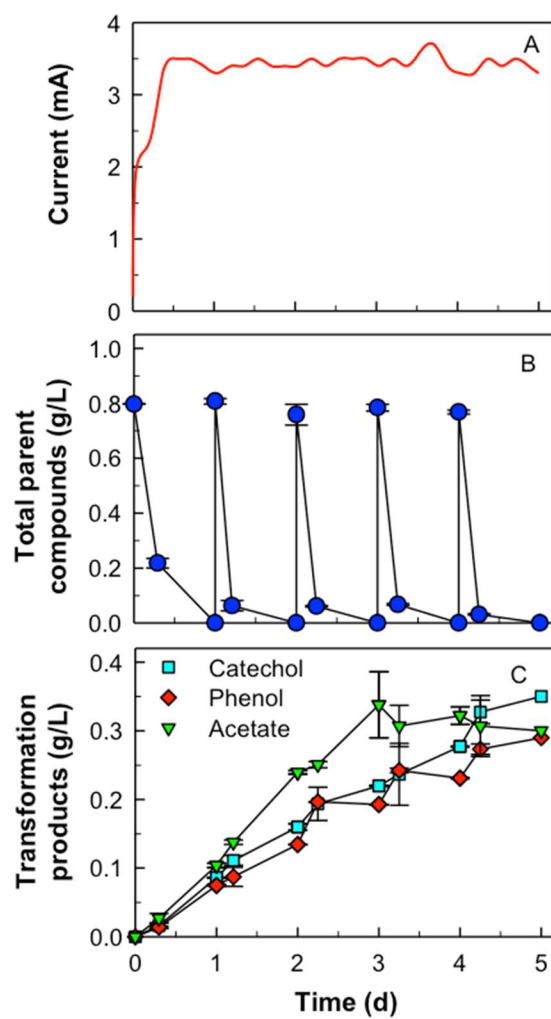


inhibited in the 3.6 - 8.0 g/L runs, compared to the other batch runs conducted with lower initial mixture concentrations (2 - 3 mL vs. 9 - 12 mL). Thus, the observed decrease in current production was not caused by competition for electron equivalents with methanogens. It has been reported that methanogenesis in mixed cultures was inhibited significantly by FF and HMF at 5-10 g/L, as well as phenolic compounds at 1.2 g/L, and that more severe inhibition was observed with mixtures (Monlau et al., 2014; Palmqvist and Hahn-Hägerdal, 2000). In addition, methanogenesis could also be impacted by low pH. A desired pH range for methanogenesis is 6.5 – 7.6 (Rittmann and McCarty, 2001). In the above-discussed batch runs, the lowest anolyte pH value observed in each run was 6.7 - 6.9. However, a small proton concentration gradient may exist at the anolyte-biofilm interface and within the depth of the biofilm, resulting in a slightly lower pH value inside the biofilm.

### 7.3.2 Inhibition by Parent Compounds vs. Transformation Products

In the second experiment, when the furanic and phenolic mixture was added daily to the anode at an initial, non-inhibitory concentration of 0.8 g/L, the current remained at 3.5 mA throughout five mixture additions (Figure 7.3A), while the cathodic H<sub>2</sub> production rate was stable at 0.18 ± 0.02 L/L-d. The pH decreased from 7.0 to 6.5 over the course of the experiment, although it was adjusted to 7.0 by 1.0 N NaOH upon each addition of the 0.8 g/L mixture. The resulting steady current and H<sub>2</sub> production rate are in contrast to those observed in the first experiment conducted with increasing initial total concentration of the five compounds mixture. The parent compounds were totally transformed within 1 d before the addition of the next mixture (Figure 7.3B). Thus, the

total concentration of the parent compounds mixture remained below 0.8 g/L at all times in the second experiment. The five additions of the parent compounds mixture led to an accumulation of transformation products reaching a concentration comparable to that resulting from the addition of 3.6 - 8.0 g/L parent compounds mixture (Figure 7.1C and Figure 7.3C). Five daily additions of 0.8 g/L are equivalent to a cumulative addition of 4.0 g/L. Thus, the results of the second experiment can be compared to those of the 3.6 g/L batch run in the first experiment. The fact that the transformation products were at comparable concentrations in both experiments, and that the current decreased only in the first experiment (but not in the second), indicates that the transformation products were not the cause of the observed inhibition. Instead, the initial concentration of the parent compounds, which was the main difference between the two experiments, had a clear impact on the current. As discussed above, in the first experiment the current decreased with an increasing dose of the parent compounds mixture from 0.8 to 3.6 g/L and higher; the second experiment avoided one-time, high doses of the parent compounds by distributing a total 4.0 g/L dose in five days (0.8 g/L per day), and the current was not impacted. Therefore, it is concluded that the observed inhibition of exoelectrogenesis was due to the parent compounds, rather than to their transformation products.

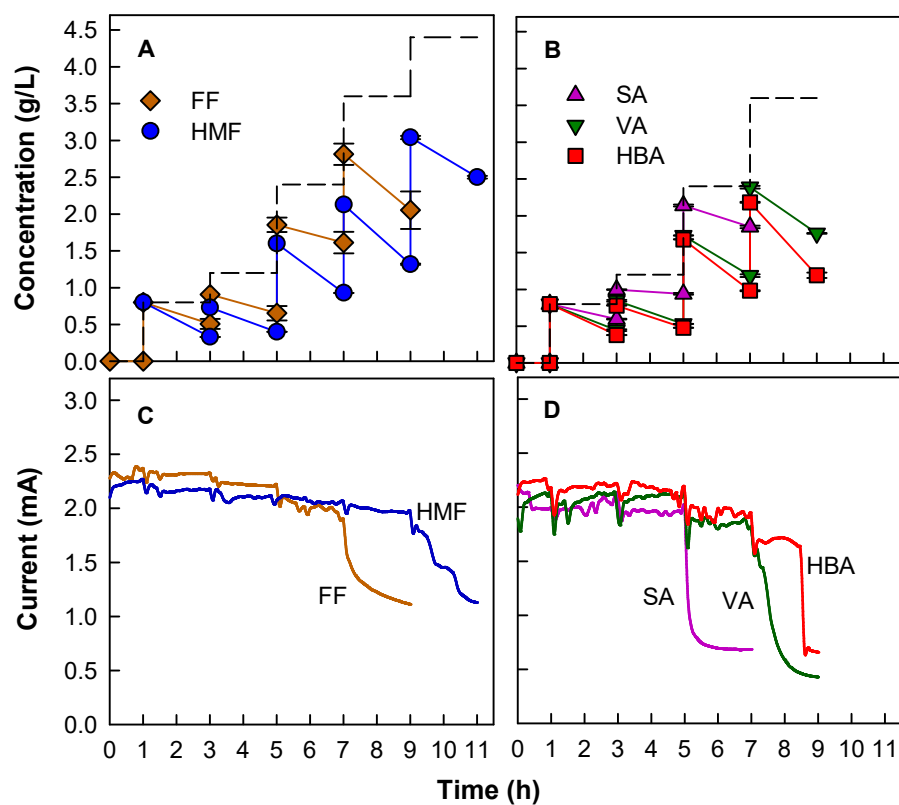


**Figure 7.3.** Current (A), total concentration of the parent compounds (B), and transformation products (C) in a single batch run conducted with repetitive additions of 0.8 g/L parent compounds mixture. Error bars represent standard deviations ( $n = 2$ ).

### 7.3.3 Inhibitory Effect of Individual Parent Compounds

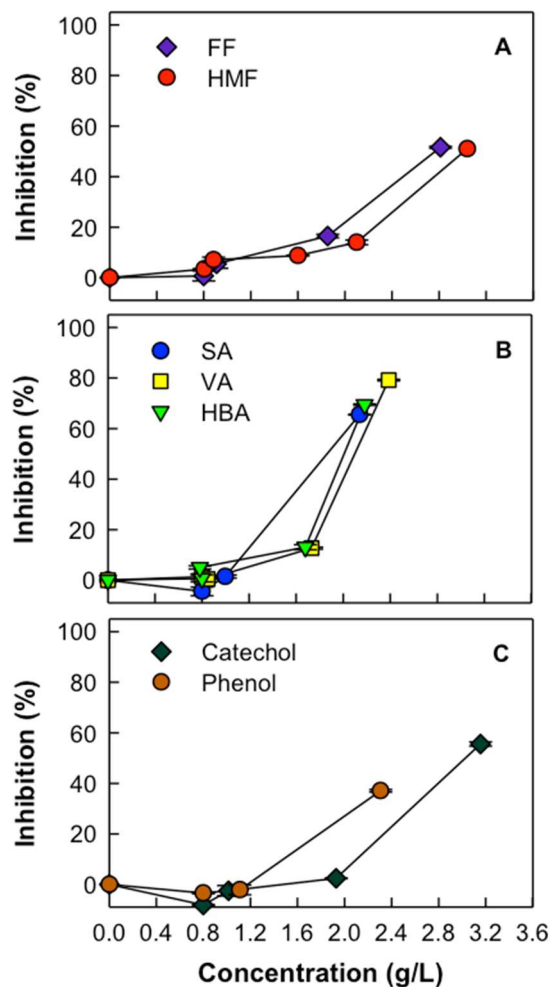
To further investigate which of the parent compounds was responsible for the observed inhibition, each compound (FF, HMF, SA, VA and HBA) was added at increasing levels to the bioanode which was also amended with 1 g/L NaAc. During the control runs with 1 g/L NaAc, which were performed before testing every compound, the current was steady for 9 h in each run, ranging from 2.0 to 2.5 mA. The concentration of NaAc, which was the exogenous exoelectrogenic substrate, did not show a significant decrease in 9 h ( $P = 0.57$ ), because a relatively high concentration of NaAc was used to avoid current drop due to exoelectrogenic substrate limitation. This observation also demonstrates that the acetate consumption rate would not have been a sufficiently sensitive parameter to describe the inhibitory effect on exoelectrogenesis. Instead, current was used as the primary parameter to evaluate the rate of exoelectrogenesis.

While increasing levels of the individual furanic and phenolic compounds were added to the bioanode, active biotransformation of the compounds resulted in concentrations lower than the pre-specified amounts (Figure 7.4). Meanwhile, higher than 50% current decrease was observed for all compounds with a total addition up to 3.6 g/L (in 9 h), except for HMF (Figure 7.4). It is noteworthy that the attained highest concentration of HMF at 7 h upon a total addition of 3.6 g/L was significantly lower than that of FF as a result of fast transformation (Figure 7.4), which resulted in lower inhibition. In order to achieve a comparable concentration of HMF to that of FF, an extra 1.8 g/L HMF was added at 9 h to make the highest attained concentration of HMF equal to 3.0 g/L. The current decreased upon this last HMF addition (Figure 7.4).

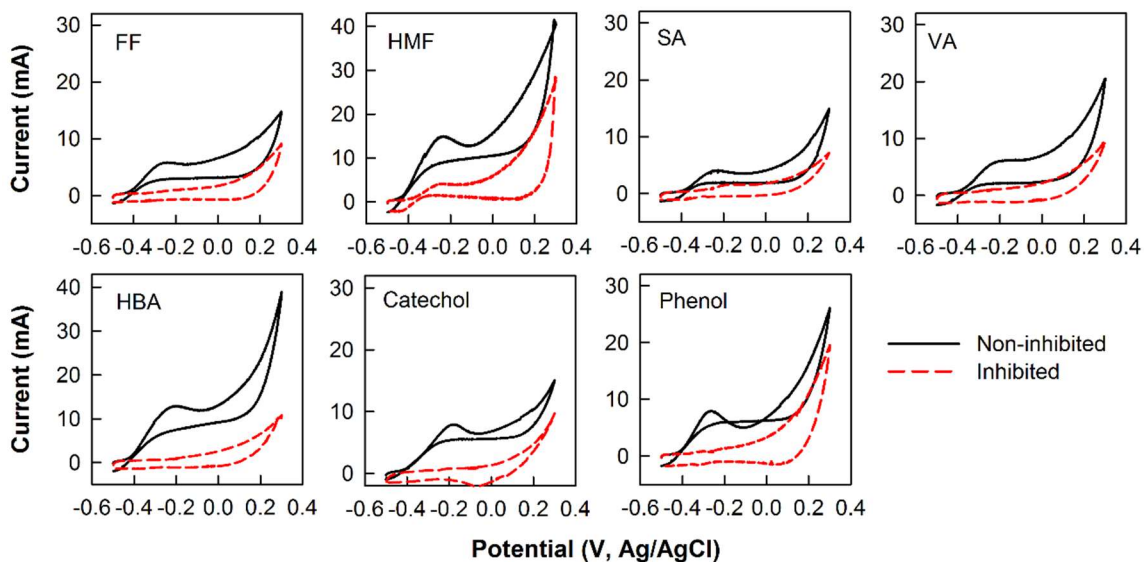


**Figure 7.4.** Time course of the concentration of individual compounds (A and B) and current (C and D) in batch runs conducted with sequential additions of individual compounds at increasing levels. Broken lines indicate pre-specified, cumulative concentration in the absence of transformation. Error bars represent standard deviations ( $n = 2$ ). Abbreviations: furfural (FF), 5-hydroxymethylfurfural (HMF), syringic acid (SA), vanillic acid (VA), and 4-hydroxybenzoic acid (HBA).

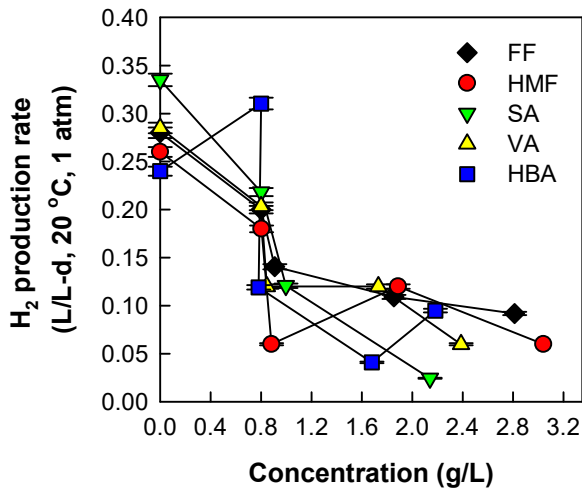
The extent of inhibition at increasing concentrations of the five parent compounds is shown in Figure 7.5A, B. The reported concentration of each compound is that measured immediately after each addition. At concentrations of 0.8 g/L and below, no inhibition was observed with any of the tested compounds. Thus, 0.8 g/L was a non-inhibitory concentration for all five compounds. At concentrations from 0.8 to 1.8 g/L, low inhibition (< 20%) was observed for these five parent compounds. However, when the individual compounds were present at 2.1 - 3.0 g/L, the current decreased by more than 50%. The suppressed exoelectrogenic activity was further confirmed by cyclic voltammetry (Figure 7.6). The current under inhibited conditions was lower than under non-inhibited conditions at all applied potential values (-0.5 to +0.3 V vs. Ag/AgCl). The fact that the current under inhibited conditions did not increase with increasing anode potential to a level comparable to that under non-inhibited conditions rules out the possibility that the observed decrease in current production at inhibition was caused by a limited anode potential. In addition, oxidation peaks observed under non-inhibited conditions disappeared under inhibited conditions. Similar to the current, the H<sub>2</sub> production rate showed a generally decreasing trend in response to the increasing furanic and phenolic compounds concentrations attained immediately after addition (Figure 7.7). However, the H<sub>2</sub> production rate was not as reliable and sensitive as the current. The reported H<sub>2</sub> production rates are mean values at each time interval (1 or 2 h). In addition, H<sub>2</sub> back diffusion to the anode may have occurred as previously reported and discussed in Chapter 5.



**Figure 7.5.** Inhibitory effect of individual furanic (A) and phenolic compounds (B), as well as transformation products (C) on exoelectrogenesis based on current decrease in batch runs conducted with sequential additions of individual compounds at increasing levels. Error bars represent standard deviations ( $n = 6$ ). Abbreviations: furfural (FF), 5-hydroxymethyl furfural (HMF), syringic acid (SA), vanillic acid (VA), and 4-hydroxybenzoic acid (HBA).



**Figure 7.6.** Bioanode cyclic voltammetry plots under non-inhibited and maximum inhibition conditions in batch runs conducted with individual compounds. Abbreviations: furfural (FF), 5-hydroxymethylfurfural (HMF), syringic acid (SA), vanillic acid (VA), and 4-hydroxybenzoic acid (HBA).



**Figure 7.7.** Effect of individual compounds concentrations on the cathodic  $H_2$  production rate in batch runs conducted with sequential additions of individual compounds at increasing concentrations. Error bars represent standard deviations ( $n = 2$ ). Abbreviations: furfural (FF), 5-hydroxymethylfurfural (HMF), syringic acid (SA), vanillic acid (VA), and 4-hydroxybenzoic acid (HBA).



The  $IC_{50}$  values of FF, HMF, SA, VA and HBA and the extent of inhibition observed at the highest concentration of each parent compound attained in the batch runs are shown in Table 7.1. The reported  $IC_{50}$  values are system-specific, particularly dependent on bioanode biomass concentration, and thus may not be generally applicable to all MEC systems. Nevertheless, it is noteworthy that FF and HMF had higher  $IC_{50}$  values (2.7 and 3.0 g/L) than SA, VA and HBA (1.9, 2.1 and 2.0 g/L), indicating a higher tolerance of the exoelectrogens to the furanic compounds. In addition, a higher extent of inhibition was observed with the phenolic compounds (65 – 80%) than with the furanic compounds (51 – 53%). Thus, overall, the phenolic compounds were more inhibitory to the exoelectrogenesis than the furanic compounds. A plot of  $IC_{50}$  versus  $\log K_{ow}$  values of the five compounds (Figure 7.8) shows that the furanic compounds, which have considerably lower  $\log K_{ow}$  values, have significantly higher  $IC_{50}$  values than the phenolic compounds, which have higher  $\log K_{ow}$  values. Such a distinct difference between the furanic and phenolic compounds suggests that hydrophobicity differences may correspond to different modes of inhibition, as further discussed below.

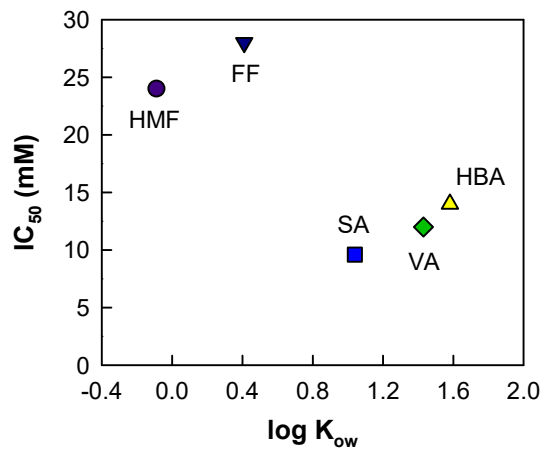
**Table 7.1.** Inhibitory concentration (IC<sub>50</sub>) and extent of inhibition observed at the highest concentration of each parent compound attained in batch runs<sup>a,b</sup>.

Compound	IC <sub>50</sub>		Highest concentration		Inhibition <sup>c</sup> (%)
	g/L	mM	g/L	mM	
Furfural (FF)	2.7	28	2.8	29	53
5-Hydroxymethylfurfural (HMF)	3.0	24	3.0	24	51
Syringic acid (SA)	1.9	9.6	2.1	11	65
Vanillic acid (VA)	2.1	12	2.4	14	80
4-Hydroxybenzoic acid (HBA)	2.0	14	2.2	16	70

<sup>a</sup> Runs conducted with sequential additions of individual compounds at increasing concentrations.

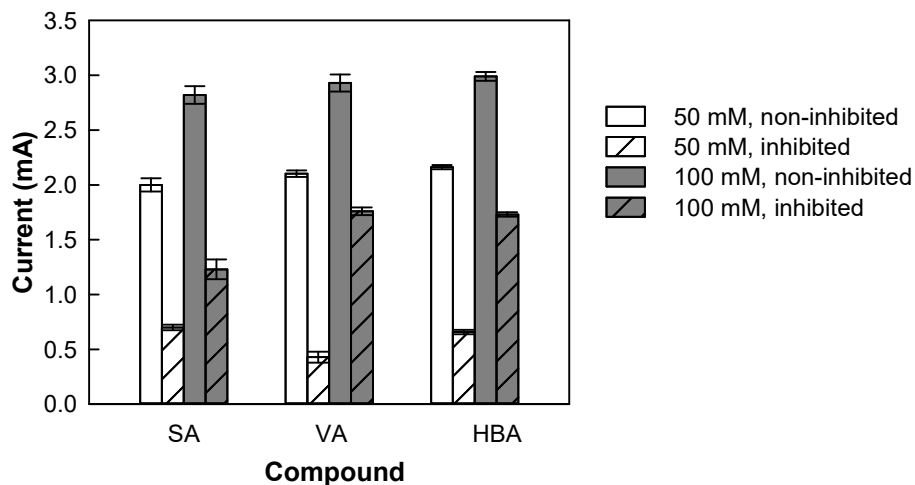
<sup>b</sup> All data are mean values with a coefficient of variation lower than 5% ( $n = 2$ ).

<sup>c</sup> Inhibition at the highest concentration attained (column 4 and 5).



**Figure 7.8.** IC<sub>50</sub> and log K<sub>ow</sub> values of the five parent compounds. Abbreviations: furfural (FF), 5-hydroxymethyl furfural (HMF), syringic acid (SA), vanillic acid (VA), and 4-hydroxybenzoic acid (HBA).

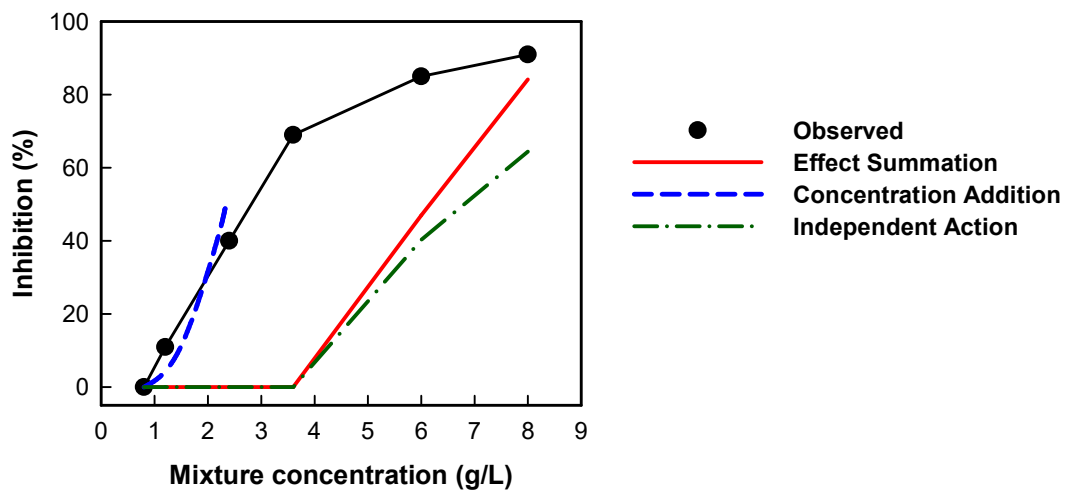
The pH at the end of the batch runs conducted with individual phenolic compounds (6.3 -6.5) was lower than that with the furanic compounds (6.7), which is attributed to the sequential additions of the acidic phenolic compounds. To assess potential contribution of the low pH to the observed inhibition, SA, VA and HBA were tested again with analyte at an increased phosphate buffer strength from 50 mM to 100 mM. The pH remained above 6.7 in the runs conducted with a 100 mM buffer. The current under non-inhibited conditions ( $I_{\text{non-inh}}$ ) in the 100 mM buffer runs was approximately 1.5-fold higher than that in the 50 mM runs, which is attributed to the higher ionic and buffer strength (Figure 7.9) (Harrington et al., 2015; Torres et al., 2008). However, the current decrease ( $I_{\text{non-inh}} - I_{\text{inh}}$ ) was comparable under these two conditions at the same SA, VA and HBA concentrations. Thus, the phenolic compounds can result in significant inhibition even at a nearly neutral pH.



**Figure 7.9.** Effect of buffer strength on the extent of inhibition by three phenolic acids. Error bars represent standard deviations ( $n = 3$ ). Abbreviations: syringic acid (SA), vanillic acid (VA), and 4-hydroxybenzoic acid (HBA).

The results obtained with the individual compounds indicate that all five parent compounds (FF, HMF, SA, VA and HBA) contributed to the inhibition observed with the compounds mixture. Whether these compounds interact synergistically or not was further assessed by comparing the observed extent of inhibition of the mixture to the additive effect calculated from the extent of inhibition of the five components. As shown in Figure 7.10, the observed mixture inhibition was higher than the additive effect predicted by the effect summation method. Such an increased combined inhibition has been widely reported for furfural, aromatic compounds, and acetic acid in dark fermentation (Mussatto and Roberto, 2004; Zaldivar and Ingram, 1999; Zaldivar et al., 1999). It is noteworthy that at a mixture concentration below 3.6 g/L, the five compounds were below their non-inhibitory concentration (i.e., 0.8 g/L as discussed above), but jointly resulted in significant inhibition up to 69% (Figure 7.10). This result indicates that these compounds, even at low, non-inhibitory concentrations, are of concern for a mixture containing a large number of individual compounds. While the effect summation method can provide important information, it is unreliable for synergy quantification with non-linear dose-response curves (Kortenkamp and Altenburger, 1999). Instead, the concentration addition and independent action methods were used for synergy assessment. These two methods assume similar and dissimilar modes of action, respectively (Cedergreen, 2014). The calculated additive inhibition based on the concentration addition method matched the observed inhibition of the mixture at a concentration range of 0.8 - 2.4 g/L (Figure 7.10), indicating additivity in this concentration range, beyond which calculations were not possible due to the lack of experimental data of individual compounds at higher concentrations. The independent

action method, on the other hand, predicted an additive inhibitory effect lower than the observed inhibition of the mixture (Figure 7.10). Considering that concentration addition usually predicts a larger effect than independent action and is more commonly used for risk assessment (Cedergreen, 2014), it is concluded that there was no synergistic interaction between the five compounds based on the concentration addition method.



**Figure 7.10.** Comparison of observed inhibition by the five parent compounds mixture to the additive inhibition calculated from the individual components based on effect summation, concentration addition and independent action methods.

At a concentration of up to 1.8 g/L, none of the compounds resulted in higher than 20% inhibition of exoelectrogenesis (Figure 7.5), whereas 1 g/L is typically reported to be highly inhibitory to dark fermentation for H<sub>2</sub> and ethanol production (Quéméneur et al., 2012). Thus, compared to H<sub>2</sub> and ethanol fermenters, the exoelectrogens in the present study were more tolerant to furanic and phenolic compounds. However, the following two factors should be taken into account. First, in contrast to dark fermentative cultures, which are mostly suspended, the exoelectrogens in the present study resided mostly in the biofilm of the anode electrode, as discussed above. Biofilm formation can create concentration gradients of toxic substances due to mass transfer limitations. Also, sensitive species in the biofilm can be protected from toxic substances by more resistant species which can even detoxify such compounds (Akinosho et al., 2015; Moons et al., 2009). Second, the bioanode used in this study had been exposed to the five parent compounds for over 2 years before the inhibition experiments were conducted. As mentioned above, prolonged exposure to the furanic and phenolic compounds led to increased tolerance to these compounds of the bioanode microbial community, including the exoelectrogens.

#### 7.3.4 Inhibitory Effect of Catechol and Phenol

Catechol and phenol were persistent transformation products in MEC runs conducted with the five compounds mixture. However, as discussed above, the transformation products were not responsible for the observed inhibition by the parent compounds mixture, in which case catechol and phenol were present at a concentration 50% lower than that of each parent compound. It is possible that catechol and phenol are intrinsically

inhibitory, but their inhibition was not detected at the low concentrations attained in these tests (below 0.35 g/L). When catechol and phenol were added individually to the bioanode, they caused a current decrease of 56 and 36% at 3.2 and 2.3 g/L, respectively (Figure 7.5). Cyclic voltammetry under inhibition also showed decreased current and disappearance of oxidation peaks as compared to that conducted under non-inhibited (i.e., control) conditions (Figure 7.6). Therefore, catechol and phenol, tested as representatives of the transformation products, can be inhibitory if present at a high concentration. In addition, electrosorption of catechol and phenol on carbon electrodes was previously reported (Ayranci and Conway, 2001; Suresh et al., 2012). Although addition of catechol (3.6 g/L) and phenol (2.4 g/L) to an un-inoculated, abiotic anode did not impact the MEC current, whether or not and to what extent electrosorption could have impacted current production by the MEC bioanode MEC, and thus could have affected exoelectrogenesis, is not clear.

The extent of inhibition by catechol and phenol was lower than that of the three phenolic parent compounds at comparable concentrations (Figure 7.5B, C). While VA and HBA at 2.4 and 2.2 g/L resulted in 80 and 70% inhibition, respectively (Figure 7.5B), the maximum concentrations of catechol and phenol that could be produced from the above-mentioned VA and HBA concentrations (1.6 and 1.5 g/L, respectively) resulted in less than 20% inhibition (Figure 7.5C). This observation is another evidence supporting the conclusion that the parent compounds were responsible for the observed inhibition by the mixture. Nevertheless, given the possibility of an increased, combined inhibitory effect of compounds at their respective non-inhibitory concentrations, as discussed above, a combination of transformation products (known and unknown) even at relatively low



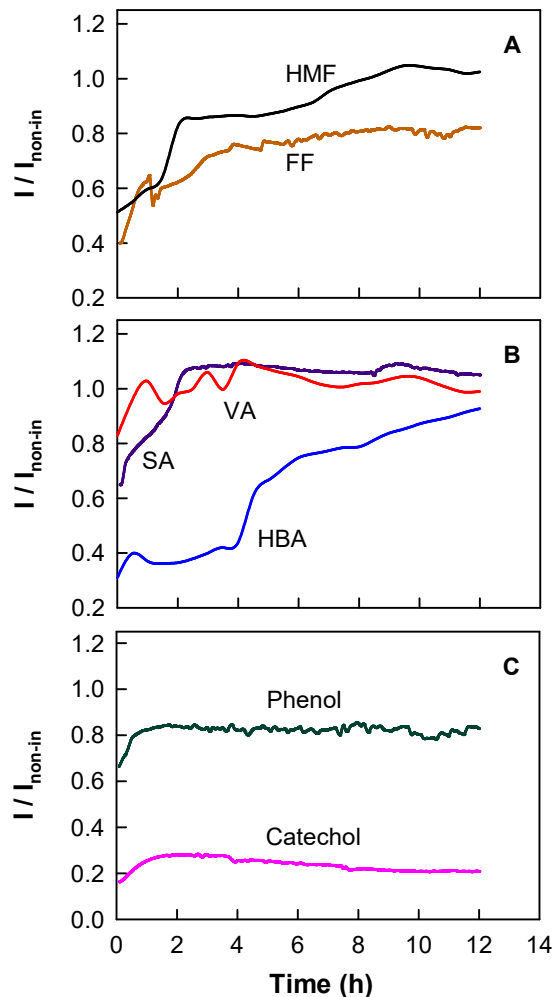
concentrations could exacerbate the inhibitory effect of the parent compounds. Catechol and phenol are widely found in lignocellulose-derived waste streams (Monlau et al., 2014; Palmqvist and Hahn-Hägerdal, 2000). Thus, their potential inhibitory effect on exoelectrogenesis should be considered when lignocellulosic residuals are used in bioelectrochemical systems.

### 7.3.5 Reversibility of Inhibition

The current, which was decreased significantly in the batch runs conducted with the parent compounds mixture at 3.6 g/L, fully recovered in 6 h after the anode was drained and fresh anolyte added along with the parent compounds mixture at 0.8 g/L. However, after the extended and more severe inhibition during the subsequent batch runs at 6 and 8 g/L, the current did not recover in 6 d. As reported in Chapter 5, inhibition of exoelectrogenesis by the parent compounds mixture at 1.2 g/L was reversed. Thus, the reversibility of the inhibition may be related to the compound's concentration and the duration of inhibition.

With the only exception of inhibition by catechol, higher than 80% current recovery was observed for all compounds with a recovery period varying from 2 to 12 h, after the anode was washed three times and replenished with fresh anolyte and 1 g/L NaAc (Figure 7.11). No residual inhibitors were detected after the anode was washed. Exoelectrogenesis inhibited by SA, VA and phenol recovered quickly in about 2 h, but it took about 12 h to recover from inhibition by FF, HMF and HBA (Figure 7.11). Exoelectrogenesis after inhibition by catechol, however, did not recover in 12 h or an extended duration of 7 d (data not shown). The anode was then amended with an

electroactive inoculum, and the current increased gradually in the following days. Thus, unlike the other compounds, catechol caused an irreversible inhibition of exoelectrogenesis, which did not recover in 7 d. The difference in reversibility of inhibition and rate of recovery may be related to different modes of inhibition of these compounds.



**Figure 7.11.** Recovery of exoelectrogenesis from inhibition by individual furanic (A) and phenolic (B) compounds, as well as transformation products (C) in batch runs conducted with fresh anolyte and 1 g/L NaAc. Current ( $I$ ) was normalized to that achieved under non- inhibited, control conditions ( $I_{\text{non-in}}$ ). Abbreviations: furfural (FF), 5-hydroxymethyl

furfural (HMF), syringic acid (SA), vanillic acid (VA), and 4-hydroxybenzoic acid (HBA).

Little is known about the modes of inhibition of furanic and phenolic inhibitors to exoelectrogenesis, but the inhibitory effects of these compounds on dark fermentation have been reported and may shed light on the observed exoelectrogenesis inhibition. FF and HMF are known to inhibit glycolytic enzymes essential to central metabolism of  $H_2$  and ethanol fermenters (Almeida et al., 2009). They also lead to significant NADH consumption used in reductive transformations, thus decreasing intracellular levels of NADH (Ask et al., 2013). FF has been reported to damage yeast DNA (Almeida et al., 2009). In contrast to FF and HMF, which primarily target intracellular sites, phenolic compounds compromise cell membrane integrity and functionality by partitioning into cell membranes, changing membrane permeability and fluidity (Heipieper et al., 1994; Monlau et al., 2014; Palmqvist and Hahn-Hägerdal, 2000).

Based on exoelectrogenesis principles, several of the above-mentioned modes of inhibition may have affected different aspects of exoelectrogenesis, which warrants further investigation at the cellular/molecular level. As mentioned above, the first step in exoelectrogenesis is intracellular metabolism of the electron donor (i.e., acetate in the present study), during which electrons are transferred to NADH. The second step is extracellular electron transfer. The NADH formed in the first step passes through cytochromes in the cell membrane and eventually transfers the electrons to outer membrane proteins, which are able to deliver the electrons to the anode electrode via direct contact, conductive pili or soluble mediators in the anolyte (TerAvest and Ajo-Franklin, 2016; Torres et al., 2010). Because FF and HMF can cause increased intracellular NADH consumption (Ask et al., 2013), they could negatively impact the

NADH yield in the first step of exoelectrogenesis, resulting in less NADH available for current production. As the second step of exoelectrogenesis relies greatly on membrane-bound proteins to perform electron transfer to the anode electrode (TerAvest and Ajo-Franklin, 2016; Torres et al., 2010), exoelectrogenesis can be highly susceptible to phenolic inhibition, which targets cell membranes.

It was suggested that aromatic compounds with a  $\log K_{ow}$  value in the range 1-5 can partition into the inner layer of biological membranes and cause membrane swelling, leading to loss of physiological functions (Heipieper et al., 1994). Compounds with a  $\log K_{ow} < 1$  or  $> 5$  can typically cause different types of inhibition other than cell membrane disruption (Heipieper et al., 1994). Thus, SA, VA, HBA and phenol, with  $\log K_{ow}$  values of 1.04, 1.43, 1.58 and 1.46 (Hansch et al., 1995), falling within  $\log K_{ow}$  range of 1 - 5, have great potential to accumulate in cell membranes and risk disrupting membrane functions. In contrast, catechol has a  $\log K_{ow}$  of 0.88 (Hansch et al., 1995), (i.e., lower than 1), indicating that cell membrane may not be the primary target of catechol. In fact, catechol has been reported to damage cell DNA and inactivate protein (Schweigert et al., 2001). The possibility that catechol has a different mode of inhibition than the other phenolic compounds is consistent with the above-discussed difference in the reversibility of inhibition. Thus, with  $\log K_{ow}$  values lower than 1, catechol, FF and HMF might act similarly, inhibiting intracellular sites, whereas other phenolic compounds with higher  $\log K_{ow}$  values (1.04 - 1.58) may disrupt cell membranes. Although the mechanism(s) of exoelectrogenesis inhibition warrant(s) further exploration at the cellular/molecular level, such activity was beyond the scope of the present study.

## 7.4 Summary

The present study shows that exoelectrogens have a relatively high tolerance to individual furanic and phenolic compounds. However, a combination of these five compounds at non-inhibitory concentrations in a mixture resulted in significant inhibition, which was primarily caused by the parent compounds, as opposed to their transformation products. Furanic and phenolic compounds caused a different extent of inhibition, and different modes of inhibition may be at play, which can be related to the physico-chemical properties of these compounds. The findings of this chapter provide further insight into observed inhibition reported in Chapter 5. Although inhibition mechanisms of exoelectrogens warrant further exploration at the cellular/molecular level, the present study has addressed several important issues of bioanode inhibition, such as the inhibited process (i.e., fermentation vs. exoelectrogenesis), responsible inhibitors (i.e., parent compounds vs. transformation products), and the inhibitor mixture effect on exoelectrogenesis inhibition (i.e., synergistic or not). These aspects are necessary in support of future efforts to elucidate the inhibition mechanism(s).

In complex lignocellulose-derived streams, presence of suitable exoelectrogenic substrate (e.g., acetate) and other readily biodegradable components (e.g., sugars), at high levels relative to inhibitory substances, may help ease inhibition. However, waste streams with complex chemical composition may exacerbate inhibitory effects. To overcome such problems, enhanced tolerance of the bioanode microbial community can be achieved by bioanode microbial pre-enrichment in the presence of potential inhibitors. A continuous-flow bioanode operation can also be considered to reduce the inhibitory effect of the parent compounds on exoelectrogenesis.

# CHAPTER 8

## PERFORMANCE EVALUATION OF A CONTINUOUS-FLOW BIOANODE MEC FED WITH FURANIC AND PHENOLIC COMPOUNDS

### 8.1 Introduction

MEC offers dual benefits of waste treatment and renewable H<sub>2</sub> production, which makes it an attractive technology to be integrated into biofuel production for sustainable H<sub>2</sub> supply and biomass-derived waste management. The work reported in Chapter 5 showed that the mixture of two furanic (FF, HMF) and three phenolic compounds (SA, VA, and HBA) was completely transformed in a batch-fed MEC bioanode at a Coulombic efficiency of 44 – 69%. In addition, Lewis et al. (2015) used a complex, biomass-pyrolysis derived stream, which contained furanic and phenolic compounds along with sugars and volatile fatty acids, in a continuously fed and recirculated batch MEC anode, and achieved a H<sub>2</sub> production rate as high as 4.3 L/L<sub>anode-d</sub> (22 °C, 1 atm). These studies based on batch systems demonstrate great potential of MEC to transform problematic furanic and phenolic compounds and to produce renewable H<sub>2</sub>. However, in order to promote the implementation of MEC technology in the overall biofuel production process, assessment of continuous-flow MEC operating conditions is needed.

Several studies have investigated continuous-flow MECs with domestic and synthetic wastewater, as well as digestate (Escapa et al., 2012; Gao et al., 2014; Gil-Carrera et al., 2013). However, our fundamental understanding of the effect of continuous-flow operating conditions on MEC performance is still limited, in part due to

the complexity of the waste streams used. Considering that furanic and phenolic compounds are challenging components of lignocellulose-derived waste streams, in-depth evaluation of the effect of continuous-flow bioanode MEC operating conditions on the conversion of these compounds will enhance our understanding of the performance of MEC fed with complex waste streams resulting from the pretreatment of lignocellulosic biomass. In addition, because furanic and phenolic compounds are inhibitory to exoelectrogenesis at high concentrations (see Chapter 7), the extent of inhibition under different continuous-flow operating conditions should also be assessed.

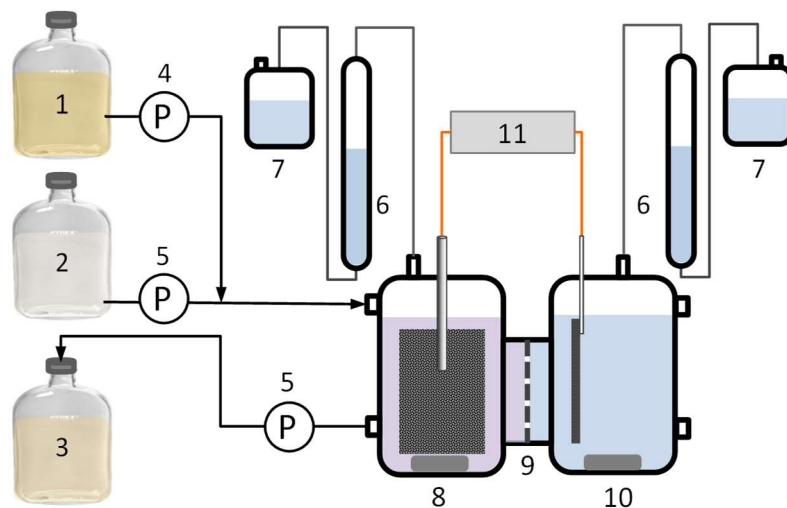
The objective of the work reported in this chapter was to evaluate the response of a continuous-flow MEC bioanode, fed with a mixture of the selected furanic and phenolic compounds, to various hydraulic retention times (HRT), organic loading rates (OLR), and applied voltage.

## **8.2 Materials and Methods**

### **8.2.1 Continuous-flow Anode MEC**

The batch-fed MEC described in Section 5.2.1 was converted to a continuous-flow anode MEC shown in Figure 8.1. Two influent pumps and one effluent pump were connected to the anode inlet and outlet ports, respectively. Two positive displacement pumps (Fluid Metering Inc., Syosset, NY) were used for anolyte influent and effluent. A syringe pump (Cole Parmer, Hills, IL) was used for substrate addition. All three pumps ran for 10 min every 3 h controlled by an electronic timer (ChronTrol Corporation; San Diego, CA); the influent anolyte and substrate pumps were turned ON after the effluent pump was turned OFF. A potentiostat (Interface 1000, Gamry Instruments, Warminster, PA) was used to

set a voltage of 0.6 V at the anode against the cathode using the two-electrode setup. The working electrode lead of the potentiostat was connected to the MEC anode, and both the counter and reference electrode leads were connected to the MEC cathode. The anolyte was microbial growth medium and the catholyte was phosphate buffer, both at pH 7.0, with composition described in Section 4.2.1 and Section 5.2.1, respectively. The substrate stock solution was a mixture of the five compounds at equal electron equivalents (each at 3.12 g COD/L) and a total concentration of 10 g/L (15.6 g COD/L) dissolved in the anolyte solution.



**Figure 8.1.** Continuous-flow bioanode MEC. 1, mixture of furanic and phenolic compounds; 2, anolyte; 3, effluent waste; 4, syringe pump; 5, positive displacement pump; 6, glass burette; 7, acid brine displacement reservoir; 8, anode chamber; 9, cation exchange membrane; 10, cathode chamber; 11, potentiostat.



### 8.2.2 Evaluation of the Effect of HRT, OLR and Applied Voltage

The effect of HRT, OLR and applied voltage on MEC performance was evaluated in three consecutive operational phases. During each phase, one of the parameters was varied while the values of the other two parameters were fixed. First, the HRT was reduced step-wise from 24 to 12 and then to 6 h at a constant OLR of 0.2 g/L-d (Phase I), followed by the increase of OLR from 0.2 to 0.8 and then to 3.2 g/L-d at a constant HRT of 6 h (Phase II), by changing the influent substrate concentration accordingly. The applied voltage was then increased from 0.6 to 1.0 V (anode relative to cathode) at an HRT of 6 h and OLR of 3.2 g/L-d (Phase III). Each change of MEC condition was made after stable operation was reached and maintained for at least 4 days. While the cathode was not operated as a continuous-flow, the catholyte was replaced every 2-4 days when the pH increased from 7.0 to 7.5. In this study the OLR values are expressed based on the total mass of the five compounds mixture used as the bioanode substrate; a factor of 1.56 can be used to convert g/L-d to g COD/L-d based on the theoretical oxygen demand of the compounds (Table 2.1). Thus, the applied OLR values are equivalent to 0.3, 1.2 and 5.0 g COD/L-d. Lewis et al. (2015) tested a switchgrass pyrolysate in a MEC anode at an OLR up to 10 g COD/L-d, in which approximately 27% was accounted by furanic and phenolic compounds. Thus, the maximum OLR used in this study (5 g COD/L-d) is well above the equivalent OLR of furanic and phenolic compounds in the pyrolysate used by Lewis et al. (2015). In order to assess potential H<sub>2</sub> production and compound transformation through abiotic reactions, an abiotic batch assay was conducted with an uninoculated anode at 0.6 and then 1.0 V. Assessment at each condition lasted for 7 days with close monitoring of the current, H<sub>2</sub> production and the concentration of the five

compounds. Additionally, an open circuit control batch assay was conducted with an active MEC bioanode for 7 days, in order to assess the fermentative transformation of the five compounds mixture in the bioanode. The initial concentration of the five compounds mixture used in the control assays was 0.8 g/L, which was the highest influent concentration of the five compounds mixture used in the continuous-flow bioanode MEC.

### 8.2.3 Inhibition Test of Continuous-flow Bioanode

The inhibitory effect of the mixture of five parent compounds on exoelectrogenesis was evaluated in the continuous-flow bioanode MEC, and the extent of inhibition was compared to that observed in the batch MEC runs discussed in Chapter 7. At a HRT of 6 h, three influent concentrations of the furanic and phenolic mixture were used, 0.8, 1.2 and 3.6 g/L, equivalent to OLR of 3.2, 4.8 and 14.4 g/L-d, respectively. The operation with 0.8 g/L influent concentration was a non-inhibitory control, same as the initial concentrations used in the batch MEC (see Section 7.2.2). The current was monitored and the extent of inhibition was calculated based on the current decrease, as described in Section 7.2.5.

### 8.2.4 Anode Microbial Community Analysis

Analysis of the MEC anode microbial community was performed after stable operation was achieved with OLR of 0.2 (day 35) and 3.2 g/L-d (day 58), both at an HRT of 6 h, representing the microbial communities at low and high OLR conditions. The genomic DNA extraction from the biofilm, followed by DNA purity check and quantification, was conducted as described in Section 3.2.8. Each extracted DNA sample was sequenced in

duplicate for 16S rRNA gene using Illumina MiSeq (Research and Testing Laboratory; Lubbock, TX). Primer sets 28F/388R (5'- GAGTTTGATCNTGGCTCAG -3'/5' - TGCTGCCTCCCGTAGGAGT-3') and 519wF/909R (5'-CAGCMGCCGCGGTAA - 3'/5'-TTTCAGYCTTGCGRCCGTAC-3') were used for partial 16S rRNA gene of Bacteria and Archaea, respectively. The obtained sequences were clustered into Operational Taxonomic Units (OTUs) at 4% divergence using the UPARSE algorithm. The centroid sequence of each OTU was used for taxonomic classification using the USEARCH global alignment program. The sequences of the abundant species (>1 %) were deposited to GenBank, National Center for Biotechnology Information (NCBI; www.ncbi.nlm.nih.gov/) with sequence accession numbers from KT799852 to KT799875.

#### 8.2.5 Biomass Yield Coefficient Calculations

The observed yield coefficient ( $Y_{obs}$ ) is defined as follows:

$$Y_{obs} = \frac{\Delta X_{total}}{\Delta sCOD} \quad 8.1$$

where  $\Delta X_{total}$  is the total biomass COD change (mg/L), and  $\Delta sCOD$  is the soluble COD removed (mg/L).

$\Delta X_{total}$  is calculated from the protein concentration as follows:

$$\Delta X_{total} = 1.42 \frac{\Delta P_{biofilm} + \Delta P_{planktonic}}{0.55} \quad 8.2$$

where 0.55 is the mass fraction of protein in *E.coli* cell, and 1.42 is the COD equivalent of biomass based on the empirical formula of  $C_5H_7O_2N$  (Rittmann and McCarty, 2001).

$\Delta P_{biofilm}$  and  $\Delta P_{planktonic}$  are biofilm protein accumulation and planktonic protein collected in the effluent, respectively, over a period of stable operation (d), calculated as follows:

$$\Delta P_{biofilm} = P_{biofilm,t} - P_{biofilm,t_0} \quad 8.3$$

$$\Delta P_{planktonic} = \frac{P_{planktonic,t}}{HRT} (t - t_0) \quad 8.4$$

where  $P_{biofilm,t}$  is the biofilm protein concentration (mg/L) measured at time t, and  $P_{biofilm,t_0}$  is the biofilm protein concentration measured at a previous time  $t_0$ .  $P_{planktonic,t}$  is planktonic protein concentration measured at time t, and (t -  $t_0$ ) is the operational duration (d). All protein concentrations are normalized to the anode liquid volume.

$\Delta sCOD$  is cumulative COD removed during the operational period (d), calculated as follows:

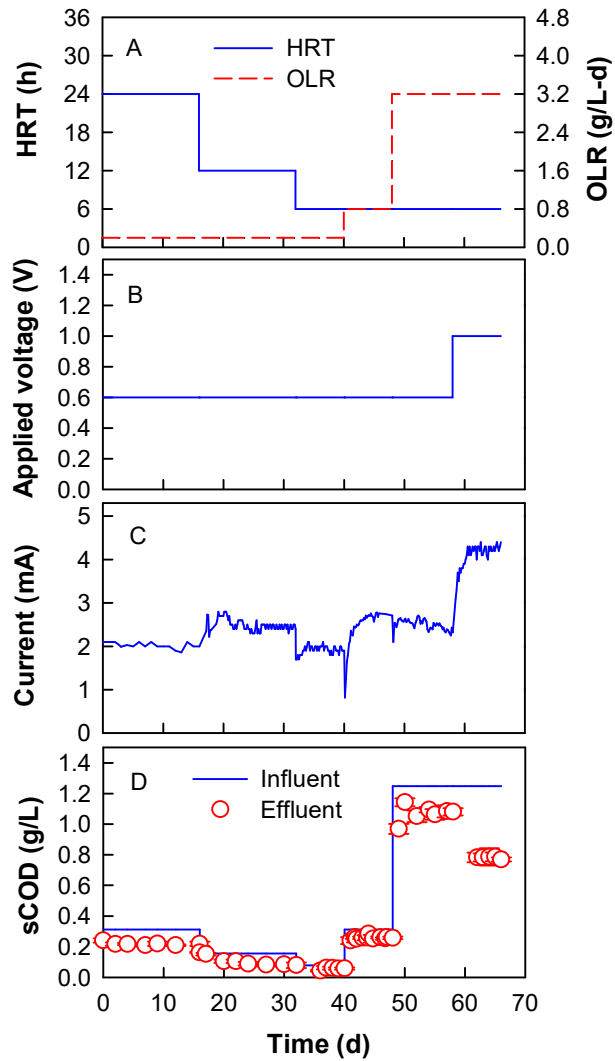
$$\Delta sCOD = \frac{sCOD_{inf} - sCOD_{eff}}{HRT} (t - t_0) \quad 8.5$$

where  $sCOD_{inf}$  and  $sCOD_{eff}$  are the influent and effluent soluble COD concentrations (mg/L).

### 8.3 Results and Discussion

MEC operation consisted of three consecutive phases (total duration 66 days) for the evaluation of the effect of HRT, OLR and applied voltage: Phase I (40 days), varying HRT values from 24 to 6 h at constant OLR of 0.2 g/L-d and voltage of 0.6 V; Phase II (18 days), varying OLR values from 0.2 to 3.2 g/L-d at constant HRT of 6 h and voltage of 0.6 V; Phase III (8 days), varying applied voltage at constant HRT of 6 h and OLR of

3.2 g/L-d (Figure 8.2A, B). The MEC performance in response to each operating condition is discussed below.



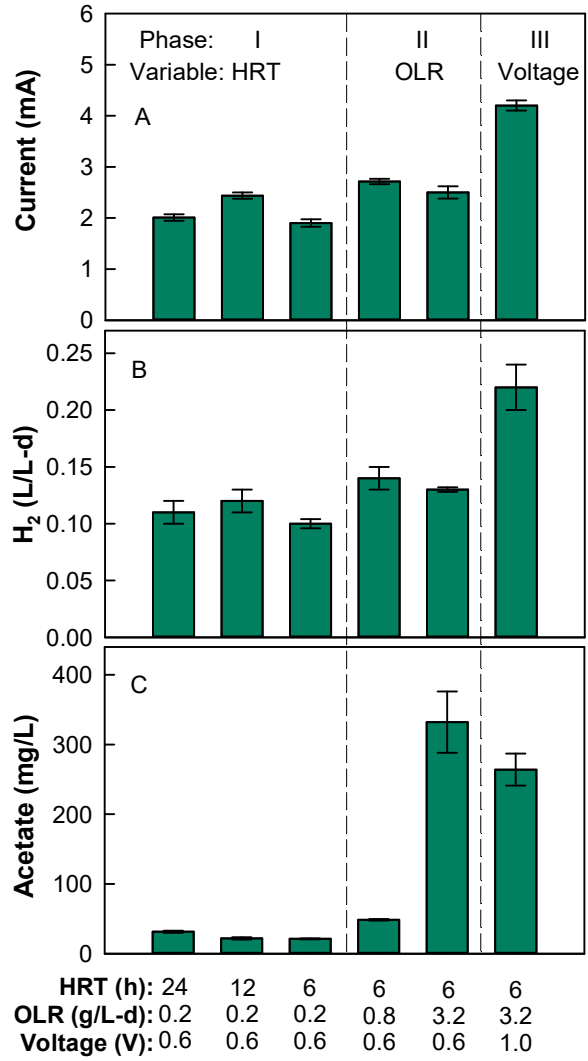
**Figure 8.2.** MEC response to various operating conditions. (A) HRT and OLR; (B) applied voltage; (C) current; (D) influent and effluent sCOD. Error bars represent mean values  $\pm$  one standard deviation,  $n = 3$ .

### 8.3.1 Phase I – Effect of HRT on MEC performance

HRT is an important design parameter for a continuous-flow process. For a MEC, a short HRT allows a high substrate throughput and H<sub>2</sub> production rate for a given influent substrate concentration, but may result in a low extent of substrate biotransformation and COD removal. In the present study, the effect of HRT was assessed at a constant OLR of 0.2 g/L-d and an applied voltage of 0.6 V.

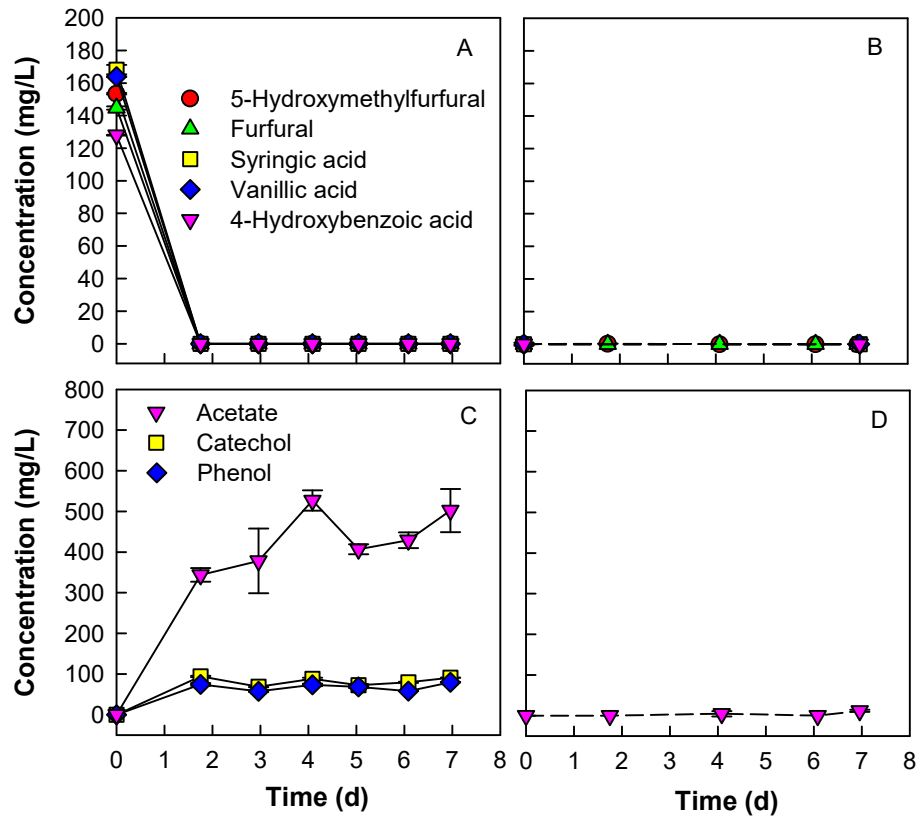
Upon each change of HRT from 24 to 12, and then to 6 h, current reached a relatively stable value within 2 days, followed by a stable effluent sCOD in 7 days (Figure 8.2C, D). The operation continued for another 4-8 days after a stable effluent sCOD was reached, during which the MEC performance was evaluated (Figure 8.3). At a constant OLR of 0.2 g/L-d, the current increased from 2.0 to 2.4 mA when the HRT was reduced from 24 to 12 h, and then decreased to 1.9 mA when the HRT was further reduced to 6 h (Figure 8.3A; Phase I). Consistent with the measured current, the H<sub>2</sub> production rate at an HRT of 12 h was slightly higher than at an HRT of 24 h or 6 h (Figure 8.3B; Phase I), but the difference was not statistically significant ( $P = 0.208$ ). The bioanode and effluent acetate concentration remained below 35 mg/L at all HRT values (Figure 8.3C; Phase I). In the open circuit control assay, where only fermentation took place, acetate was produced reaching 502 mg/L at an initial substrate concentration of 800 mg/L of the mixture of the five compounds (Figure 8.4). Therefore, acetate was a major fermentation product, consistent with the results reported in Chapter 5 using the same mixture and in Chapter 6 using individual compounds. Catechol and phenol were also detected as fermentation products. Based on the results reported in Chapter 6, catechol and phenol were metabolites of VA and HBA, respectively. Because acetate is a

known substrate for exoelectrogenesis (Kiely et al., 2011b; Logan and Rabaey, 2012), the observed low acetate concentration during the continuous-flow MEC operation in the present study indicates comparable rates of acetate production (i.e., fermentation) and consumption (i.e., exoelectrogenesis) at an HRT of 6 - 24 h and an OLR of 0.2 g/L-d. The five furanic and phenolic compounds were completely transformed at all HRT values tested during Phase I (Table 8.1). The sCOD removal ranged from 28 to 41%, and was the highest at an HRT of 12 h (Table 8.1), which is consistent with the higher current measured at an HRT of 12 h than at HRTs of 24 and 6 h. The Coulombic efficiency, which ranged from 60 to 76%, was not statistically significantly different at the three HRT values tested at an OLR of 0.2 g/L-d ( $P = 0.088$ ) (Table 8.1).



**Figure 8.3.** Current (A), H<sub>2</sub> production rate (B) and acetate concentration (C) during stable MEC operation at various HRT, OLR and applied voltage values. Error bars represent mean values  $\pm$  one standard deviation,  $n \geq 4$ .





**Figure 8.4.** Concentration of the five parent compounds (A, anode; B, cathode) and detected metabolites (C, anode; D, cathode) during an open circuit batch assay. Error bars represent mean values  $\pm$  one standard deviation,  $n = 2$ .

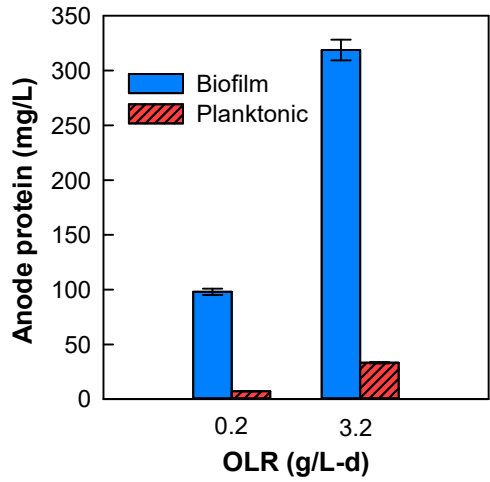
**Table 8.1.** MEC Performance under Various HRT, OLR and Applied Voltage Conditions.

Parameter	Operational Phase					
	I		II		III	
Duration (d)	16	16	8	8	10	8
Applied voltage (V)	0.6	0.6	0.6	0.6	0.6	1.0
HRT (h)	24	12	6	6	6	6
OLR (g/L-d)	0.2	0.2	0.2	0.8	3.2	3.2
Influent parent compounds (mg/L)	200	100	50	200	800	800
Effluent parent compounds (mg/L)	ND <sup>a</sup>	ND	ND	4 ± 1 <sup>b</sup>	16 ± 2	5 ± 2
Parent compounds conversion (%)	> 99	> 99	> 99	98 ± 0.6	99 ± 0.2	99 ± 0.3
sCOD removal (%)	31 ± 1	47 ± 3	30 ± 10	18 ± 2	14 ± 1	37 ± 1
Coulombic efficiency (%)	74 ± 5	60 ± 4	76 ± 18	44 ± 3	13 ± 1	8.0 ± 0.3

<sup>a</sup> None detected.

<sup>b</sup> Mean ± standard deviation ( $n \geq 4$ ).

Overall, complete transformation of the five parent compounds at an OLR of 0.2 g/L-d was observed at all HRT values tested. The MEC performance at the three HRTs and an OLR of 0.2 g/L-d varied by no more than 25% in terms of H<sub>2</sub> production rate, sCOD removal, and Coulombic efficiency ( $0.11 \pm 0.01$  L/L-d,  $34 \pm 7\%$ , and  $73 \pm 6\%$ , respectively; mean  $\pm$  standard deviation); a HRT of 12 h resulted in a slightly higher current and sCOD removal. Due to the fact that the influent concentration ( $C_{in}$ ), HRT, and OLR are inter-related (i.e.,  $OLR = C_{in}/HRT$ ), a decrease of HRT at a constant OLR was achieved by decreasing the influent concentration. Thus, the influent concentration, in addition to the HRT, can have an effect on the overall MEC performance. On the other hand, the relatively small variation of the MEC performance in response to the change of HRT is attributed to the fact that more than 90% of the anode biomass was in the biofilm (Figure 8.5). Thus, the impact of HRT on the overall anode biomass retention time was expected to be less significant than that in a fully suspended-growth biomass bioreactor. The shortest HRT tested (6 h) is considered as an appropriate operating condition because of the following: (1) a short HRT allows a relatively high substrate throughput and a small anode volume; (2) a nearly complete transformation of the furanic and phenolic compounds was achieved (even at higher OLR values; Table 8.1, Phase II); and (3) the overall efficiency of H<sub>2</sub> production was not considerably lower than that at longer HRT values. Compared to previously reported HRT values used for bioelectrochemical systems, which ranged from hours to days (Escapa et al., 2012; Gao et al., 2014; Gil-Carrera et al., 2013), even the relatively short HRT of 6 h used in the present study was sufficient for the transformation of the furanic and phenolic compounds.



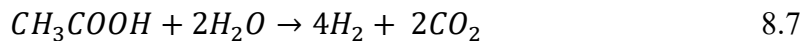
**Figure 8.5.** MEC anode protein concentration normalized to anode empty bed volume at various OLR values and an HRT of 6 h. Error bars represent mean values  $\pm$  one standard deviation,  $n = 2$ .

### 8.3.2 Phase II – Effect of OLR on MEC performance

When the OLR was increased from 0.2 to 0.8 g/L-d, both the current and H<sub>2</sub> production rate increased significantly from 1.9 to 2.7 mA and from 0.10 to 0.14 L/L-d ( $P < 0.05$ ), respectively. However, the current and H<sub>2</sub> production rate did not increase any further when the OLR was increased from 0.8 to 3.2 g/L-d (Figure 8.3; Phase II). To understand which sub-process (i.e., fermentation or exoelectrogenesis) limited the H<sub>2</sub> production rate at an OLR of 3.2 g/L-d, the acetate concentration was examined. As discussed in Section 8.3.1, the measured acetate concentration was the result of the relative rate of production by fermentation and consumption by exoelectrogenesis. At an OLR of 3.2 g/L-d, the effluent acetate level was 332 mg/L, more than 6-fold higher than that at lower OLR values ( $P < 0.05$ ) (Figure 8.3C; Phase II). The high acetate concentration in the effluent shows that the rate of acetate consumption by exoelectrogenesis could not keep up with the rate of acetate production by fermentation. Considering the liquid phase of the MEC anode compartment as a continuous-flow, stirred tank reactor (CSTR) at steady-state, the following equation applies relative to acetate:

$$0 = r_f - r_e - \frac{C}{HRT} \quad 8.6$$

where  $r_f$  is the acetate production rate by fermentation,  $r_e$  is the acetate consumption rate by exoelectrogenesis, and  $C$  is the measured acetate concentration in the bioanode and the effluent during stable operation. The acetate consumption rate ( $r_e$ ) at an OLR of 3.2 g/L-d was back calculated as equal to 1.4 mM/d based on the measured H<sub>2</sub> production rate and the following stoichiometric equation:



Based on eq 1, the acetate production rate ( $r_f$ ) at an OLR of 3.2 g/L-d was back calculated as 23.5 mM/d. The fact that  $r_f$  (23.5 mM/d) is 17-fold greater than  $r_e$  (1.4 mM/d) demonstrates that the rate of exoelectrogenesis was considerably slower than that of fermentation. Moreover, compared with the  $r_f$  at OLR of 0.8 g/L-d (4.7 mM/d), the acetate production rate was 5-fold higher at an OLR increased by 4-fold, while the acetate consumption rate ( $r_e$ ) remained the same. Thus, increasing the OLR improved the rate of acetate production by fermentation, but not the rate of acetate consumption by exoelectrogenesis. Therefore, it is concluded that the  $H_2$  production at an OLR of 3.2 g/L-d was limited by the rate of acetate-supported exoelectrogenesis, as opposed to the rate of fermentation resulting in acetate production.

Possible reasons for the limited rate of exoelectrogenesis at an OLR of 3.2 g/L-d are discussed below. The measured acetate concentration at an OLR of 3.2 g/L-d (332 mg/L) was substantially higher than the previously reported value (111 mg/L) of the half saturation constant ( $K_s$ ) for acetate utilization in mixed bioanode communities (Lee et al., 2009b). Thus, substrate concentration could not be considered as a rate-limiting factor of exoelectrogenesis at the highest OLR of 3.2 g/L-d used in the present study. Although furanic and phenolic compounds can be inhibitory to microbial activity, the influent concentration of 0.8 g/L (at an OLR of 3.2 g/L-d and HRT of 6 h) was not inhibitory, as shown in Chapter 7. Thus, inhibition of exoelectrogenesis was not the cause of the lack of increased  $H_2$  production at an OLR of 3.2 g/L-d. In fact, the lack of current increase observed here is consistent with the results reported in Section 5.3.4, in which acetate was used as the MEC substrate at increasing concentrations from 200 to 800 mg/L, but the maximum current was not increased. It is plausible that the extracellular electron

transfer reached its maximum rate under the existing electrochemical and microbial conditions, and it could not be further increased by increasing the OLR. Furthermore, the limited rate of electron transfer prevented faster growth of exoelectrogens, which could in turn have limited the overall rate of electron transfer, i.e., current. This explanation is supported by the evidence that increasing the applied voltage resulted in significantly higher current and H<sub>2</sub> production rate at the same OLR of 3.2 g/L-d (Section 8.3.5, below).

The H-type reactor used in the present study is a proof-of-concept design, has a relatively large internal resistance due to the distance between the anode and cathode electrodes, as well as the use and/or the type of the ion exchange membrane (Logan et al., 2008). In addition, Harrington et al. (2015) reported that a carbon-felt anode, which is the type of electrode used in the present study, can suffer from ion transport limitation, although its porous structure provides a large surface area for biofilm attachment and development. For electrons to be transferred from the exoelectrogens to the anode and then to the cathode, an equal number of charges (i.e., ions) must be transported out of the anode biofilm to the anolyte and then to the catholyte to achieve electroneutrality. Thus, ineffective ion transport can limit the current and thus cathodic H<sub>2</sub> production. Another electrochemical constraint can be the relatively small specific surface area of the cathode used in the present study (12 m<sup>2</sup>/m<sup>3</sup>) compared with the typical range of 10-100 m<sup>2</sup>/m<sup>3</sup> for a 250 mL-reactor according to a recent review (Logan et al., 2015). Other reasons for the lack of increased H<sub>2</sub> production, from the perspective of microbial interactions, are discussed in Section 8.3.4, below.

Similar to the limited increase of H<sub>2</sub> production observed in the present study at an OLR of 5.0 g COD/L-d, Escapa et al. (2012) reported a Monod-type saturation of H<sub>2</sub> production above an OLR of 2.0 g COD/L-d in a membrane-less MEC fed with domestic wastewater. However, the cause of the observed plateaued H<sub>2</sub> production may be different from that in the present study. Escapa et al. (2012) observed a significant loss of cathodic H<sub>2</sub> to methanogenesis and anodic re-oxidation. In contrast, in the present study, the cathode efficiency was as high as 99%, and thus cathodic H<sub>2</sub> loss was minimal. Besides, as discussed above, the H<sub>2</sub> production at high OLR used in the present study was limited by exoelectrogenesis as opposed to fermentation; the limiting sub-process in the study conducted by Escapa et al. (2012) was not clear.

The sCOD removal and Coulombic efficiency decreased with the increase of OLR (Table 8.1). At an OLR of 3.2 g/L-d, aromatic metabolites were detected in the effluent, such as catechol (0.12 g/L) and phenol (0.11 g/L), which indicates a relatively low extent of biodegradation of the phenolic compounds. Nevertheless, more than 98% of the parent compounds were transformed at the two OLR values tested in Phase II (Table 8.1). Therefore, increasing the OLR enhanced the H<sub>2</sub> production rate to a certain extent, but with the trade-off of lower effluent quality, i.e., higher effluent sCOD concentration.

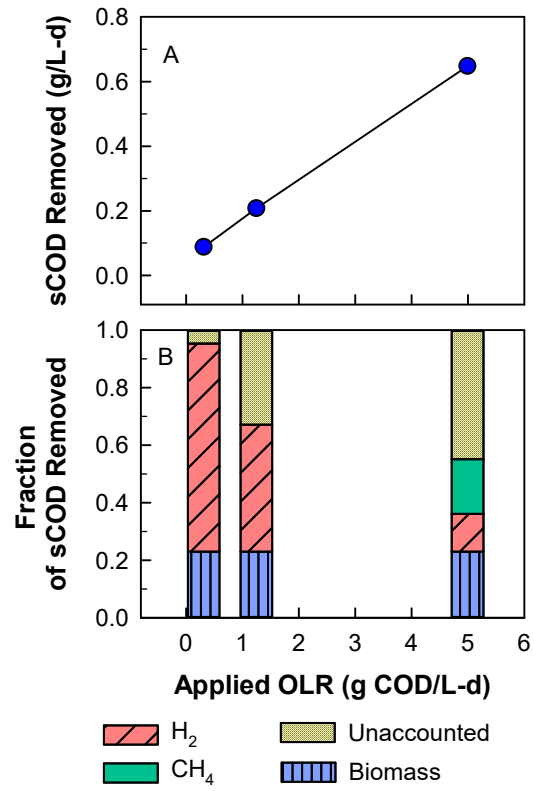
Compared to the batch-fed MEC bioanode study (reported in Chapter 5), which used the same substrate (i.e., mixture of the five compounds) at an initial/influent substrate concentration range (0.2 – 0.8 g/L), the H<sub>2</sub> production rate during the continuous-flow MEC bioanode operation was 1.4 to 2-fold higher than the maximum rate obtained during batch operation reported in Section 5.3. The H<sub>2</sub> loss in the batch MEC, possibly caused by H<sub>2</sub> diffusion from the cathode to the anode, as discussed in



Section 5.3, was not observed during the continuous-flow operation in the present study (i.e., cathode efficiency > 99%). However, the extent of sCOD removal was lower in the continuous-flow MEC (13 - 28% vs. 49 - 61%) due to the shorter residence time (6 h) compared to the batch incubation duration (7 d).

### 8.3.3 Phase II – Effect of OLR on COD Balance

A COD balance was performed based on the rate of sCOD removal, H<sub>2</sub>, biomass and methane production at the various OLRs. The sCOD removal rate (g/L-d) increased linearly with increasing applied OLR (Figure 8.6A). However, the fraction of the COD removed as H<sub>2</sub> decreased (Figure 8.6B). Thus, the lack of increased H<sub>2</sub> production at high OLR was not due to the MEC's capacity to utilize COD, but rather to a limited contribution of the COD removed towards exoelectrogenesis.



**Figure 8.6.** Soluble COD removed (A) and its components (B) at various OLR values and an HRT of 6 h.

The anode biomass, quantified by protein measurement, increased by 3-fold as the OLR increased from 0.2 to 3.2 g/L-d (Figure 8.5). The biomass observed yield coefficient ( $Y_{obs}$ ) was estimated as 0.23 g biomass-COD/g COD removed (or 0.16 g VSS/g COD removed) at both OLR of 0.2 and 3.2 g/L-d. Thus, the 3-fold increase of COD removal rate at the OLR of 3.2 g/L-d (Figure 8.6A) was expected to result in 3-fold increase of biomass growth. In addition, despite the higher COD removal rate at the increasing OLR, the fraction of electron equivalents used for biomass synthesis (23%) remained constant. The  $Y_{obs}$  value estimated in the present study is consistent with the theoretical yield coefficient of exoelectrogens calculated based on thermodynamics (0.1 – 0.3 g VSS/g COD) by Wilson and Kim (2016) as well as the biomass yield estimated in a glucose-fed bioanode (up to 0.54 g biomass-C/g substrate-C, equivalent to 0.38 g VSS/g COD) by Freguia et al. (2007). It is noteworthy that the biofilm-associated biomass fraction of the total anode biomass did not change with the OLR (93 and 91 % at OLR of 0.2 and 3.2 g/L-d, respectively; Figure 8.5). Biofilm formation offers a number of benefits for microbial growth (Hall-Stoodley et al., 2004), among which long residence time, syntrophic interactions, and resistance to toxic substances are significant advantages. In the present study, biofilm formation on the wall of the anode chamber was not observed. Two possible explanations for the lack of wall growth are a) the very short hydraulic retention time of 6 h; and b) the high specific surface area of the carbon felt used as the anode electrode.

It is noteworthy that methane was detected in the bioanode only at an OLR of 3.2 g/L-d with a production rate of 0.09 L/L-d, accounting for 19% of the measured sCOD removed (Figure 8.6B). The electron flow diverted to methane is equivalent to 0.36 L/L-d

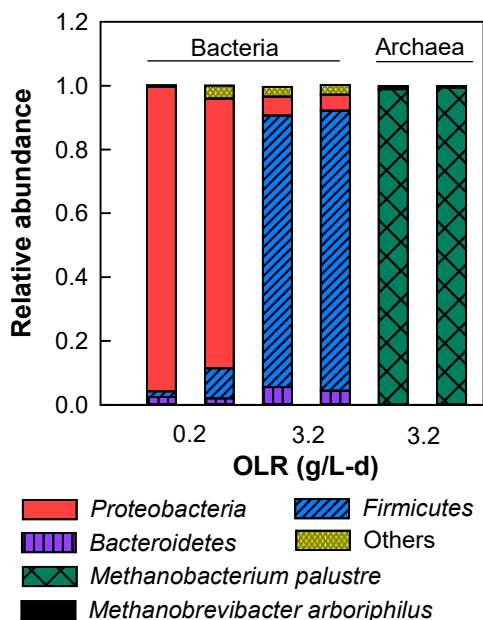
of H<sub>2</sub> production, which is a significant loss compared to the observed H<sub>2</sub> production rate of 0.13 L/L-d. If methane production had not occurred, the H<sub>2</sub> production rate at OLR of 3.2 g/L-d would have been 0.49 L/L-d, representing a 3.5-fold increase from that observed at an OLR of 0.8 g/L-d. The forgoing discussion assumes that the observed methane production was due to hydrogenotrophic methanogenesis. As discussed in Section 8.3.4, below, acetoclastic methanogens were not detected.

After accounting for H<sub>2</sub>, CH<sub>4</sub>, and biomass production, 5 – 45% of the COD removed remained unaccounted for (Figure 8.6B). Bacterial carbon storage as polymers represented 34-65% of the total bioanode biomass has previously been reported (Freguia et al., 2007). Because in the present study the biomass was quantified by protein measurement, carbon storage in polymeric substances was not accounted for. Therefore, increasing the OLR to 3.2 g/L-d affected the distribution of electron equivalents, resulting in a higher fraction used for methanogenesis and a lower fraction used for exoelectrogenesis, but the fraction used for biomass production remained constant.

#### 8.3.4 Phase II – Effect of OLR on Anode Microbial Community

The anode microbial community consisted of three major bacterial phyla: *Proteobacteria*, *Firmicutes* and *Bacteroidetes*. However, the relative abundance of these phyla was considerably different at OLR of 0.2 and 3.2 g/L-d (Figure 8.7). At the low OLR (0.2 g/L-d), the microbial community was dominated by *Proteobacteria*, in which more than 80% were *Geobacter* spp., closely related to *G. sulfurreducens*, a well-known exoelectrogen, and other *Geobacter* spp. reported in bioelectrochemical systems (> 97% identity) (Butler et al., 2012; Kobayashi et al., 2013). In contrast, at the high OLR (3.2

g/L-d), *Firmicutes* was the major phylum, distributed in the genera of *Anaerovorax* (16-19%; duplicate analysis), *Acetobacterium* (12-14%), *Eubacterium* (7-9%), *Phascolarctobacterium* (3-4%), *Clostridium* (3%), and unclassified *Clostridia spp.* (42-50%). The characteristics of the detected *Firmicutes* phylotypes are discussed below. The only described species in the *Anaerovorax* genus is *A. ordorimutans*, which ferments putrescine to acetate, butyrate and hydrogen (Matthies et al., 2000). A number of strains of *Acetobacterium* and *Eubacterium* are acetogenic and able to metabolize methoxylated aromatic compounds, such as syringic and vanillic acid (Bache and Pfennig, 1981; Genthner et al., 1981; Sharak Genthner and Bryant, 1987). In particular, the *Eubacterium sp.* detected in the present study is phylogenetically close to *Eubacterium limosum* (99% identity), which is known to perform homoacetogenesis and can also grow on methoxylated aromatic compounds (Genthner et al., 1981; Sharak Genthner and Bryant, 1987). *Phascolarctobacterium sp.* detected in the present study was closely related to *P. faecium* (99% identity), which can convert succinate to propionate (Del Dot et al., 1993). *Clostridium spp.* are mostly obligate anaerobes and usually produce mixtures of organic acids and alcohols from carbohydrates (Vos et al., 2009). To date, only a few exoelectrogens belonging to *Firmicutes* have been isolated, such as *Clostridium butyricum* EG3 (Park et al., 2001), *Desulfitobacterium hafniense* strain DCB2 (Milliken and May, 2007), and two *Thermincola* strains (Marshall and May, 2009; Wrighton et al., 2008). However, none of these species was detected or was closely related to the phylotypes identified in the present study. Therefore, the *Firmicutes* species in the present study are considered to be fermenters and acetogens, which metabolically differ from the *Proteobacteria* dominated by exoelectrogenic *Geobacter spp.*



**Figure 8.7.** Anode microbial community composition in duplicate at various OLR values and an HRT of 6 h.

Although the relative abundance of exoelectrogens decreased at the high OLR used in the present study, it does not necessarily mean that the size of the exoelectrogenic population decreased, because the total biomass concentration increased at the high OLR by a factor of 3 (Figure 8.5). However, it is clear that the relative size of the non-exoelectrogenic population increased considerably and disproportionately to that of the exoelectrogens with the increase of OLR from 0.2 to 3.2 g/L-d (Figure 8.7). Excessive growth of fermenters and acetogens was expected to result in a higher acetate production rate and acetate accumulation at higher levels, which is consistent with the calculated production rate and measured acetate concentration as discussed in Section 8.3.2, above. Therefore, the higher OLR favored the growth of the non-exoelectrogens to a higher extent than that of the exoelectrogens. The furanic and phenolic compounds used in the

present study are fermentable compounds, which are not directly used by exoelectrogens (Section 5.3). Thus, increasing the loading rate of these substrates enriched fermenters more directly than exoelectrogens. Moreover, in contrast to fermenters, which do not require an external electron acceptor, exoelectrogens rely on the anode electrode as the electron acceptor and thus their growth can be impacted by electrochemical conditions. In fact, as discussed in Section 8.3.2, above, the existing electrochemical conditions are considered as a bottleneck for further increasing the extracellular electron transfer rate. Therefore, limiting electrochemical conditions at the OLR of 3.2 g/L-d could be another reason for the observed decreased relative abundance of exoelectrogens.

The change of biofilm composition was observed in 24 days (6 days at an OLR of 0.2 g/L, 8 days at 0.8 g/L-d, and then 10 days at 3.2 g/L-d). For the observed dramatic change in the bioanode microbial community composition in a relatively short time, the biofilm coverage was more likely low, which was confirmed based on visual observation and the measured, anode surface area-normalized biomass (0.02 and 0.07 g VSS/m<sup>2</sup> at OLR of 0.2 and 3.2 g/L-d, respectively). Such low biofilm coverage is not uncommon. Harrington et al. (2015) observed sporadic monolayer biofilm on a MEC graphite felt electrode using scanning electron microscopy, and suggested that low biofilm coverage may be characteristic of high surface area electrodes, in contrast to high biofilm coverage on small and flat electrodes. The biofilm structure is generally non-uniform (Van Loosdrecht et al., 1997; Wimpenny and Colasanti, 1997). Uneven and heterogeneous distribution of biomass on the anode electrode surface has been demonstrated by several experimental and modeling studies (Franks et al., 2009; Picioreanu et al., 2007; Viridis et al., 2012).

Archaeal species were detected at an OLR of 3.2 g/L-d, but not at 0.2 g/L-d. The detected *Archaea* were two methanogens: *Methanobacterium palustre* (99%) and *Methanobrevibacter arboriphilus* (1%) (Figure 8.7). The detection of methanogens is consistent with the methane production at an OLR of 3.2 g/L-d discussed in Section 8.3.3, above. In addition, both *Methanobacterium palustre* and *Methanobrevibacter arboriphilus* are hydrogenotrophic methanogens using H<sub>2</sub> and CO<sub>2</sub>, but not acetate (Garcia, 1990), which is consistent with the observed acetate accumulation at an OLR of 3.2 g/L-d (Figure 8.3C, Phase II). Absence of acetoclastic methanogens in bioanode has previously been reported and explained by outcompetition by exoelectrogens, given that the half-saturation concentration ( $K_s = 177\text{--}427$  mg COD/L) of acetoclastic methanogens is orders of magnitude higher than that of exoelectrogens ( $K_s = 0.64$  mg COD/L) (Parameswaran et al., 2010). The development of methanogens is considered a consequence of the excessive growth of fermenters at high OLR, which could have produced higher levels of H<sub>2</sub> and CO<sub>2</sub>. In contrast, at low OLR, the H<sub>2</sub> produced by fermentation could have been rapidly utilized by the exoelectrogens which dominated the microbial community over the fermenters (Figure 8.7). The negative impact of methanogenesis is primarily the diversion of electrons away from exoelectrogenesis and current production, resulting in lower Coulombic efficiency. A secondary impact is competition of hydrogenotrophic methanogens with exoelectrogens for substrate (i.e., H<sub>2</sub>) and nutrients in the biofilm.

The microbial community analysis confirmed that a high OLR caused an imbalanced growth of fermentative and exoelectrogenic bacteria. This is another explanation of the limited rate of exoelectrogenesis relative to fermentation, besides the

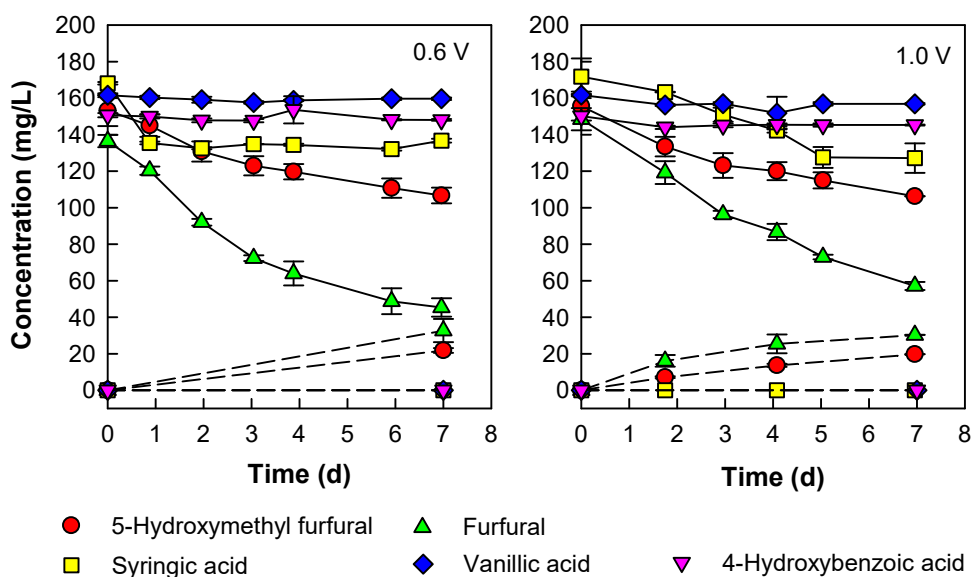


electrochemical constraints discussed in Section 8.3.2, above. Pinto et al. (2011) developed a multi-population MEC mathematical model which included microbial physiological groups such as fermenters, exoelectrogens, and methanogens, and predicted that the increase of H<sub>2</sub> production rate was less significant at higher organic loadings. However, it is not clear how the effect of organic loading on microbial interactions was accounted for and related to the H<sub>2</sub> production. Consistent with the model prediction (Pinto et al., 2011), the present study showed a similar H<sub>2</sub> production plateau, but has also provided microbial community evidence on the shift relative to the abundance of fermenters and exoelectrogens and the development of methanogens as a result of increased OLR. These findings have important implications on MEC applications with complex, fermentable waste streams derived from the pretreatment of lignocellulosic biomass.

#### 8.3.5 Phase III – Effect of Applied Voltage on MEC Performance

The effect of increased applied voltage was investigated at an OLR of 3.2 g/L-d and HRT of 6 h, a condition where exoelectrogenesis was limited as discussed in Section 8.3.2, above. Upon the increase of voltage from 0.6 to 1.0 V, the current gradually increased from 2.5 to 4.2 mA in 2 days, and then reached a plateau at  $4.2 \pm 0.1$  mA (Figure 8.2C; 60-68 d). The abiotic controls conducted at 0.6 V and 1.0 V showed negligible current production ( $< 0.05$  mA). The fate of the furanic and phenolic compounds in the abiotic controls at 0.6 and 1.0 V was very similar (Figure 8.8). It is noteworthy that electrochemical reactions and diffusion of the compounds through the ion exchange membrane to the cathode took place during the abiotic control assays. In the abiotic

assays at both 0.6 and 1.0 V, on average, 13% and 22% of 5-hydroxymethyl furfural and furfural, respectively, diffused to the catholyte through the ion exchange membrane in 7 days. Another 20% and 40% of HMF and FF, respectively, was transformed presumably through electrochemical reactions. The detected products were 2,5-bis(hydroxymethyl)furan and furoic acid, consistent with the results reported in Chapter 5. The phenolic compounds were more stable than the furanic compounds, with more than 74% of syringic acid and 95% of vanillic and 4-hydroxybenzoic acid remaining in the anolyte at both 0.6 and 1.0 V. None of the five compounds was detected in the catholyte with an active bioanode even at open circuit (Figure 8.4). Overall, the extent of diffusion and electrochemical reactions was the same at both 0.6 and 1.0 V. Therefore, the observed improvement in current production at 1.0 V was not associated with any abiotic electrochemical reactions triggered by the voltage increase.



**Figure 8.8.** Concentration of the furanic and phenolic compounds in anode (solid lines) and cathode (dashed lines) during the abiotic batch assays conducted at 0.6 V and 1.0 V. Error bars represent mean values  $\pm$  one standard deviation,  $n = 2$ .

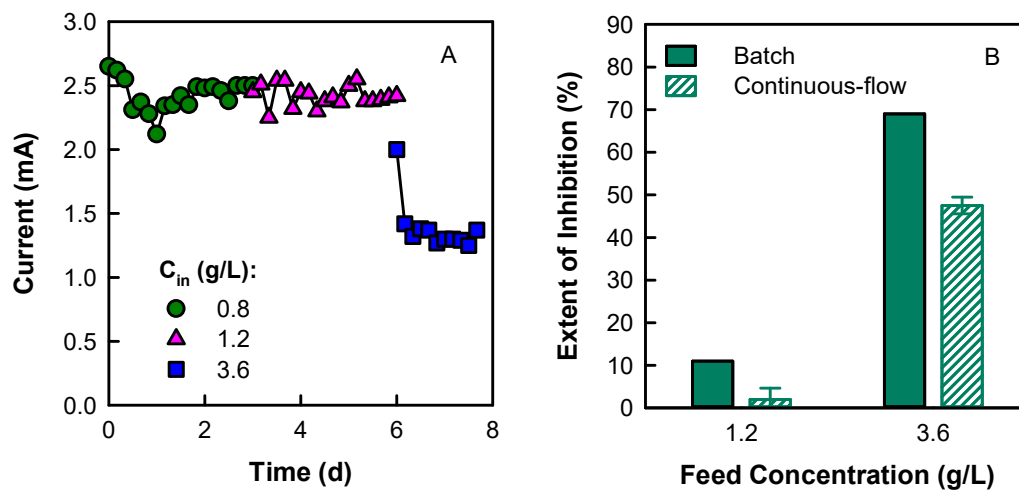
The H<sub>2</sub> production rate at 1.0 V was 1.7-fold higher than at 0.6 V (Figure 8.3B, Phase III). The acetate level at 1.0 V (264 mg/L) was lower than that at 0.6 V (332 mg/L), indicating that the rate of acetate consumption by exoelectrogenesis was enhanced at the higher voltage (Figure 8.3C; Phase III). A higher applied voltage potentially increased the free energy gain of the exoelectrogens, and facilitated electron and charge transport, thus compensating for the electrochemical constraints discussed in Section 8.3.2, above. The sCOD removal efficiency increased by 2.6-fold, but the Coulombic efficiency decreased (Table 8.1), as the extent of current increase was less than that of sCOD removal. The differences in current, H<sub>2</sub> production, sCOD removal, Coulombic efficiency, and acetate concentration at 0.6 and 1.0 V were all statistically significant ( $P < 0.05$ ). The concentrations of catechol and phenol, two detected metabolites (both at  $0.12 \pm 0.01$  g/L), were not significantly different from those at the lower voltage ( $0.12 \pm 0.02$  g/L,  $P = 0.705$  and  $0.11 \pm 0.004$  g/L,  $P = 0.169$ , respectively). The open circuit control assay confirmed that catechol and phenol were fermentation products (Figure 8.4). Results reported in Chapter 5 showed that catechol and phenol were not used by exoelectrogens. Thus, the change in applied voltage was not expected to affect the effluent concentration of catechol and phenol. The electrical and overall energy efficiencies at 1.0 V decreased from 242 to 150 %, and from 14 to 9%, respectively, compared with those at 0.6 V. A recent review by Lu and Ren (2016) summarized MEC performance at various applied voltage values in studies using a large variety of substrates from acetate to lignocellulosic biorefinery byproducts. They showed a general trend of increased MEC performance but decreased energy efficiency with an increased

voltage in the range of 0.2 - 1.2 V, attributed to a higher energy input which in turn facilitates electron transfer in exoelectrogenesis.

### 8.3.6 Inhibition of Continuous-flow Bioanode

Based on the results reported in Chapter 7, the parent furanic and phenolic compounds are more inhibitory than their biotransformation products. Work reported in this chapter shows that the parent compounds were rapidly transformed at an HRT of 6 h during the continuous-flow bioanode operation, resulting in extremely low effluent concentration (Table 8.1). Whether the inhibitory effect of the furanic and phenolic compound mixture can be overcome in the continuous-flow bioanode operation, by virtue of the CSTR effect (i.e., the reactor substrate concentration is well below the influent substrate concentration under steady-state conditions), was further examined.

When the influent concentration increased from 0.8 g/L (i.e., non-inhibitory, control; see Chapter 7) to 1.2 g/L, the current of the continuous-flow MEC remained almost unchanged (Figure 8.9A). However, when the influent concentration was further increased to 3.6 g/L, the current decreased from  $2.4 \pm 0.1$  to  $1.3 \pm 0.04$  mA. The extent of inhibition at 1.2 g/L influent concentration was  $2 \pm 2.6\%$ , which is considered negligible, especially with the large standard deviation. However, an influent concentration of 3.6 g/L resulted in a  $47 \pm 2\%$  inhibition. Compared to the observed extent of inhibition in the batch operation at the same mixture concentrations (11% at 1.2 g/L and 69% at 3.6 g/L), the continuous-flow anode experienced a considerably lower inhibitory effect of the furanic and phenolic compounds (Figure 8.9B).



**Figure 8.9.** Current production in the continuous-flow bioanode MEC at 0.8, 1.2 and 3.6 g/L influent concentration of the furanic and phenolic compounds (A) and comparison of extent of inhibition between the batch and continuous-flow operation (B). Error bars represent mean values  $\pm$  one standard deviation ( $n = 6$ ).

The anode pH during the stable operation at 0.8, 1.2 and 3.6 g/L influent concentrations was 7.0, 6.5, and 6.4, respectively. The small difference in pH between the 1.2 and 3.6 g/L operation was not considered as the cause of the observed decreased current in the 3.6 g/L operation. During the 3.6 g/L operation where 47% inhibition was observed, the respective effluent concentrations of the parent compounds mixture, catechol, and phenol, were 0.18, 0.17, and 0.24 g/L, which are all below the non-inhibitory concentration of each individual compound (0.8 g/L; see Chapter 7). As discussed in Section 7.3.3, mixture components below their respective non-inhibitory concentrations jointly can result in significant inhibition, known as “something from nothing” effect (i.e., additive but not synergistic effect). In addition, the influent and effluent pumps ran intermittently (every 3 hours); thus, the bioanode was not operated as an ideal continuous-flow reactor. The effluent was collected and measured at the end of 3-h intervals. Thus, the inhibitor concentration experienced by the bioanode microbial community at the beginning of the 3-hour cycle could be higher than what was measured at the end of the cycle.

## 8.4 Summary

Work reported in this chapter evaluated the performance of a continuous-flow bioanode MEC fed with furanic and phenolic compounds at different operating conditions. All HRTs tested (6 - 24 h) resulted in complete transformation of the parent compounds at an OLR of 0.2 g/L-d and applied voltage of 0.6 V. Increasing OLR led to increased H<sub>2</sub> production to a certain degree, but a high OLR favored the growth of fermenters over exoelectrogens and promoted methanogenesis. The consequence of the imbalanced growth was limited exoelectrogenesis and lack of increased H<sub>2</sub> production. Increasing the MEC voltage significantly improved the H<sub>2</sub> production rate when exoelectrogenesis was limited.

Compared to batch operation, the continuous-flow anode is advantageous for its higher tolerance to inhibition by furanic and phenolic compounds and higher H<sub>2</sub> production rate. However, disadvantages of the continuous-flow anode operation are low extent of biotransformation and thus low COD removal.

The effect of MEC operating conditions on microbial activity and interactions reported in this chapter provides new insights into the performance of continuous-flow bioelectrochemical systems fed with complex waste streams resulting from the pretreatment of lignocellulosic biomass.

## CHAPTER 9

### CONCLUSIONS AND RECOMMENDATIONS

#### 9.1 Conclusions

This study investigated the biotransformation of two furanic and three phenolic compounds in MECs for H<sub>2</sub> production. The conversion efficiency and H<sub>2</sub> production were assessed in MECs operated with both batch-fed and continuous-flow bioanodes. The metabolic fate of individual compounds was elucidated. The inhibitory effect of a mixture of the five compounds and each individual compound was evaluated. The specific role of exoelectrogenic and non-exoelectrogenic microorganisms in the bioanode microbial community was delineated. The following conclusions can be drawn based on the results of this study:

1. Furanic and phenolic compounds, which are inhibitory and problematic components in biomass-derived streams, were productively utilized in a MEC to produce H<sub>2</sub>. The five compounds as a mixture (0.2 – 1.2 g/L) were transformed in the MEC bioanode within 7 days in batch runs. The resulting Coulombic efficiency (44 – 69%) was comparable to that of wastewater-fed MECs, and the H<sub>2</sub> yield (26 - 42%) was significantly higher than that achieved by dark fermentation of glucose using mixed cultures.
2. The furanic compounds (FF and HMF) were more productive bioanode substrates than the phenolic compounds (SA, VA, and HBA), resulting in higher anode efficiency and H<sub>2</sub> production. Among the three phenolic compounds, VA and HBA produced very low cathodic H<sub>2</sub>, as a result of low extent of biotransformation.



3. The furanic and phenolic compounds were not directly utilized by bioanode exoelectrogens. Instead, fermentation of the parent compounds first took place, resulting in mainly acetate, which was used subsequently in exoelectrogenesis. The fermentation proceeded independently from the rate and extent of exoelectrogenesis, but the extent of fermentative transformation controlled the bioanode exoelectrogenic activity.
4. The number and position of hydroxyl ( $-OH$ ) and methoxy ( $-O-CH_3$ ) substituents of SA, VA and HBA made a significant difference in the pathways and extent of fermentative biotransformation of these phenolic compounds. SA with the syringyl arrangement of substituents entered the phloroglucinol pathway after demethylation and decarboxylation, resulting in aromatic ring cleavage with the production of acetate. However, the phloroglucinol pathway does not apply to di- or mono-hydroxylated benzenes produced from VA and HBA biotransformation. Thus, catechol and phenol, observed as persistent metabolites, accounted for 80% of the initially added VA and HBA, respectively. Previously reported, alternative ring-cleaving pathways for catechol and phenol transformation were either absent in the bioanode microbial community or unfavorable due to high energy-demand reactions.
5. The MEC anode biofilm microbial community consisted of three major phyla: *Proteobacteria*, *Bacteroidetes*, and *Firmicutes*. Phylogenetic analysis identified species closely related to putative exoelectrogens, furanic and phenolic degraders, and other fermentative bacteria, supporting the observed, sequential fermentative/exoelectrogenic biotransformation in the MEC bioanode.

6. The growth of hydrogenotrophic methanogens was stimulated at a high organic loading rate of the furanic and phenolic compounds, diverting electron equivalents away from exoelectrogens, thus negatively impacting the bioanode Coulombic efficiency and overall MEC performance.
7. The  $IC_{50}$  of individual compounds determined in inhibition batch assays was 2.7 - 3.0 g/L for the furanic and 1.9 - 2.1 g/L for the phenolic compounds, suggesting that the phenolic compounds were more inhibitory than the furanic compounds, which is related to the hydrophobicity (i.e.,  $K_{ow}$  values) of these compounds.
8. A combination of the five compounds at non-inhibitory concentrations in a mixture resulted in significant inhibition; the mixture inhibitory effect was determined to be additive, but not synergistic. Only exoelectrogenesis in the bioanode was inhibited, but not fermentation, primarily caused by the parent compounds, as opposed to their transformation products.
9. In a continuous-flow bioanode MEC, complete transformation of the parent furanic and phenolic compounds was achieved at all hydraulic retention times tested (6 – 24 h) and a low organic loading rate (OLR, 0.31 g COD/L-d). The  $H_2$  production rate was improved by increasing the OLR or the applied voltage. However, the trade-offs of using high OLR and applied voltage were lower biotransformation extent of the parent compounds, lower MEC effluent quality (i.e., lower COD removal), and lower overall energy efficiency.
10. Further increase of  $H_2$  production rate in the continuous-flow bioanode MEC was limited by the rate of exoelectrogenesis. Maintaining a balanced growth of

exoelectrogenic and non-exoelectrogenic species in the bioanode was a challenge at a high OLR.

## 9.2 Recommendations

This research is the first comprehensive study of the biotransformation of furanic and phenolic compounds in MECs for H<sub>2</sub> production. Results of this study have provided information on the extent of biotransformation, metabolic fate, and inhibitory effect of furanic and phenolic compounds, which can be used to guide the research and application of MECs for integration in biofuel production.

The transformation of furanic compounds in bioanodes may be further investigated to fully understand the metabolic pathways. Quantifying abiotic electrochemical transformation of furanic compounds and identifying more furanic metabolites may be necessary. This study found that SA with a syringyl structure was more prone to biodegradation and more favorable for H<sub>2</sub> production in MEC than VA and HBA with guaiacyl and *p*-hydroxyphenyl structures, respectively. This is an important structure implication on biodegradation and exoelectrogenic potential, but further confirmation based on an expanded range and number of biomass-derived phenolic compounds should be considered.

Inhibition mechanisms of furanic and phenolic compounds on exoelectrogenesis warrant further exploration. According to established toxicological nomenclature there is a great difference between mode and mechanism of inhibition, the former referring to the terminal target (site and/or physiological process) of an inhibitor, as opposed to the step-by-step description of the inhibitory effect at the cellular/molecular level as is the case of

the inhibition mechanism. Although this study provides significant information on the inhibited process, responsible inhibitors, and the inhibitor mixture effect, as well as indications of modes of inhibition, the overall emphasis was on the process (i.e., exoelectrogenesis), as opposed to inhibition mechanisms at the cellular/molecular level. Thus, a mechanistic understanding of furanic and phenolic compounds on exoelectrogens may be further investigated, by using model exoelectrogenic species and advanced molecular biology and proteomics techniques.

Potential limitations related to the electroactive biofilm in the MEC anode were suggested in this study, but more comprehensive investigation is recommended to provide conclusive evidence. Mass transfer limitations can be studied through mathematical modeling to depict gradients of substrates, proton, and redox potential at the microscale in the biofilm. Electrochemical impedance spectroscopy can be a useful tool to measure mass transfer related resistance. Advanced microscopic techniques (e.g., confocal microscopy) can be applied to assess the coverage and distribution of biomass (active or inactive) on the anode electrode. Advanced molecular biology techniques, such as quantitative PCR and transcriptomic analysis, can provide better insight into microbial functions and dynamics, than the microbial community analysis based on 16S rRNA gene used in this study.

This study used a conventional H-type MEC reactor without optimizing the reactor configuration. Limitations of exoelectrogenesis were observed under continuous-flow operation and a high organic loading rate. Thus, for MEC scale-up, reactor configuration should be investigated and optimized. The feedstocks in scaled-up MECs for practical applications are expected to be more complex than the furanic and phenolic

compounds used in this study. The effect of other inhibitory compounds, the presence of easily degradable substrates, and the availability of soluble electron acceptors (e.g.,  $\text{NO}_3^-$ ,  $\text{Fe}^{2+}$ , and  $\text{SO}_4^{2-}$ ) should be investigated.

## REFERENCES

- Abe, T., Masai, E., Miyauchi, K., Katayama, Y., Fukuda, M. 2005. A tetrahydrofolate-dependent *O*-demethylase, LigM, is crucial for catabolism of vanillate and syringate in *Sphingomonas paucimobilis* syk-6. *J. Bacteriol.*, **187**(6), 2030-2037.
- Akinosho, H., Rydzak, T., Borole, A., Ragauskas, A., Close, D. 2015. Toxicological challenges to microbial bioethanol production and strategies for improved tolerance. *Ecotoxicology*, **24**(10), 2156-2174.
- Almeida, J.R.M., Bertilsson, M., Gorwa-Grauslund, M.F., Gorsich, S., Liden, G. 2009. Metabolic effects of furaldehydes and impacts on biotechnological processes. *Appl. Microbiol. Biotechnol.*, **82**, 625-638.
- Ask, M., Bettiga, M., Mapelli, V., Olsson, L. 2013. The influence of hmf and furfural on redox-balance and energy-state of xylose-utilizing *Saccharomyces cerevisiae*. *Biotechnol. Biofuels*, **6**(1), 1-13.
- Ayranci, E., Conway, B.E. 2001. Removal of phenol, phenoxide and chlorophenols from waste-waters by adsorption and electrosorption at high-area carbon felt electrodes. *J. Electroanal. Chem.*, **513**(2), 100-110.
- Bache, R., Pfennig, N. 1981. Selective isolation of *Acetobacterium woodii* on methoxylated aromatic acids and determination of growth yields. *Arch. Microbiol.*, **130**(3), 255-261.
- Backhaus, T., Arrhenius, Å., Blanck, H. 2004. Toxicity of a mixture of dissimilarly acting substances to natural algal communities: Predictive power and limitations of independent action and concentration addition. *Environ. Sci. Technol.*, **38**(23), 6363-6370.
- Baron, D., LaBelle, E., Coursolle, D., Gralnick, J.A., Bond, D.R. 2009. Electrochemical measurement of electron transfer kinetics by *Shewanella oneidensis* MR-1. *J. Biol. Chem.*, **284**(42), 28865-28873.
- Berman, M.H., Frazer, A.C. 1992. Importance of tetrahydrofolate and ATP in the anaerobic *O*-demethylation reaction for phenylmethylethers. *Appl. Environ. Microbiol.*, **58**(3), 925-931.
- Bond, D.R., Strycharz-Glaven, S.M., Tender, L.M., Torres, C.I. 2012. On electron transport through geobacter biofilms. *ChemSusChem*, **5**(6), 1099-1105.
- Boopathy, R., Bokang, H., Daniels, L. 1993. Biotransformation of furfural and 5-hydroxymethyl furfural by enteric bacteria. *Journal of Industrial Microbiology*, **11**(3), 147-150.
- Boopathy, R., Daniels, L. 1991. Isolation and characterization of a furfural degrading sulfate-reducing bacterium from an anaerobic digester. *Current Microbiology*, **23**(6), 327-332.

- Borole, A., Mielenz, J., Vishnivetskaya, T., Hamilton, C. 2009. Controlling accumulation of fermentation inhibitors in biorefinery recycle water using microbial fuel cells. *Biotechnol. Biofuels*, **2**(1), 7.
- Borole, A.P., Hamilton, C.Y., Schell, D.J. 2013. Conversion of residual organics in corn stover-derived biorefinery stream to bioenergy via a microbial fuel cell. *Environ. Sci. Technol.*, **47**(1), 642-648.
- Borole, A.P., Mielenz, J.R. 2011. Estimating hydrogen production potential in biorefineries using microbial electrolysis cell technology. *Int. J. Hydrogen Energy*, **36**(22), 14787-14795.
- Borole, A.P., Reguera, G., Ringeisen, B., Wang, Z.-W., Feng, Y., Kim, B.H. 2011. Electroactive biofilms: Current status and future research needs. *Energy Environ. Sci.*, **4**(12), 4813-4834.
- Brune, A., Schink, B. 1992. Phloroglucinol pathway in the strictly anaerobic *Pelobacter acidigallici*: Fermentation of trihydroxybenzenes to acetate via triacetic acid. *Arch. Microbiol.*, **157**(5), 417-424.
- Brune, A., Schink, B. 1990. Pyrogallol-to-phloroglucinol conversion and other hydroxyl-transfer reactions catalyzed by cell extracts of *Pelobacter acidigallici*. *J. Bacteriol.*, **172**(2), 1070-1076.
- Brune, G., Schoberth, S.M., Sahn, H. 1983. Growth of a strictly anaerobic bacterium on furfural (2-furaldehyde). *Appl. Environ. Microbiol.*, **46**(5), 1187-1192.
- Butler, J., Young, N., Aklujkar, M., Lovley, D. 2012. Comparative genomic analysis of *Geobacter sulfurreducens* KN400, a strain with enhanced capacity for extracellular electron transfer and electricity production. *BMC Genomics*, **13**, 471.
- Caccavo, F., Lonergan, D.J., Lovley, D.R., Davis, M., Stolz, J.F., McNerney, M.J. 1994. *Geobacter sulfurreducens* sp. nov., a hydrogen- and acetate-oxidizing dissimilatory metal-reducing microorganism. *Appl. Environ. Microbiol.*, **60**(10), 3752-3759.
- Call, D., Logan, B.E. 2008. Hydrogen production in a single chamber microbial electrolysis cell lacking a membrane. *Environ. Sci. Technol.*, **42**(9), 3401-3406.
- Cao, G., Ren, N., Wang, A., Guo, W., Xu, J., Liu, B. 2010. Effect of lignocellulose-derived inhibitors on growth and hydrogen production by thermoanaerobacterium *Thermosaccharolyticum* W16. *Int. J. Hydrogen Energy*, **35**(24), 13475-13480.
- Catal, T. 2016. Comparison of various carbohydrates for hydrogen production in microbial electrolysis cells. *Biotechnology & Biotechnological Equipment*, **30**(1), 75-80.
- Catal, T., Fan, Y., Li, K., Bermek, H., Liu, H. 2008. Effects of furan derivatives and phenolic compounds on electricity generation in microbial fuel cells. *J. Power Sources*, **180**(1), 162-166.
- Cedergreen, N. 2014. Quantifying synergy: A systematic review of mixture toxicity studies within environmental toxicology. *PLoS One*, **9**(5), e96580.

- ChemAxon. Chemaxon calculator plugins, ChemAxon
- Chen, S., Dong, X. 2005. *Proteiniphilum acetatigenes* gen. nov., sp. nov., from a USAB reactor treating brewery wastewater. *Int. J. Syst. Evol. Microbiol.*, **55**(6), 2257-2261.
- Cheng, H.-Y., Liang, B., Mu, Y., Cui, M.-H., Li, K., Wu, W.-M., Wang, A.-J. 2015. Stimulation of oxygen to bioanode for energy recovery from recalcitrant organic matter aniline in microbial fuel cells (MFCs). *Water Res.*, **81**, 72-83.
- Cheng, S., Logan, B.E. 2007. Sustainable and efficient biohydrogen production via electrohydrogenesis. *Proc. Natl. Acad. Sci. U. S. A.*, **104**(47), 18871-18873.
- Cusick, R.D., Kiely, P.D., Logan, B.E. 2010. A monetary comparison of energy recovered from microbial fuel cells and microbial electrolysis cells fed winery or domestic wastewaters. *Int. J. Hydrogen Energy*, **35**(17), 8855-8861.
- Del Dot, T., Osawa, R., Stackebrandt, E. 1993. *Phascolarctobacterium faecium* gen. nov, spec. nov., a novel taxon of the sporomusa group of bacteria. *Syst. Appl. Microbiol.*, **16**(3), 380-384.
- Dhar, B.R., Elbeshbishy, E., Hafez, H., Lee, H.-S. 2015. Hydrogen production from sugar beet juice using an integrated biohydrogen process of dark fermentation and microbial electrolysis cell. *Bioresour. Technol.*, **198**, 223-230.
- Ditzig, J., Liu, H., Logan, B.E. 2007. Production of hydrogen from domestic wastewater using a bioelectrochemically assisted microbial reactor (BEAMR). *Int. J. Hydrogen Energy*, **32**(13), 2296-2304.
- Dominguez-Benetton, X., Sevda, S., Vanbroekhoven, K., Pant, D. 2012. The accurate use of impedance analysis for the study of microbial electrochemical systems. *Chem. Soc. Rev.*, **41**(21), 7228-7246.
- Dykstra, C.M., Giles, H.D., Banerjee, S., Pavlostathis, S.G. 2015. Fate and biotransformation of phytosterols during treatment of pulp and paper wastewater in a simulated aerated stabilization basin. *Water Res.*, **68**, 589-600.
- EPA, U. 2012. Estimation programs interface suite™ for microsoft® windows, v 4.11, United States Environmental Protection Agency,. Washington, DC, USA.
- Escapa, A., Gil-Carrera, L., García, V., Morán, A. 2012. Performance of a continuous flow microbial electrolysis cell (MEC) fed with domestic wastewater. *Bioresour. Technol.*, **117**, 55-62.
- Esteve-Núñez, A., Sosnik, J., Visconti, P., Lovley, D.R. 2008. Fluorescent properties of c-type cytochromes reveal their potential role as an extracytoplasmic electron sink in *Geobacter sulfurreducens*. *Environ. Microbiol.*, **10**(2), 497-505.
- Evans, W.C., Fuchs, G. 1988. Anaerobic degradation of aromatic compounds. *Annual Review of Microbiology*, **42**(1), 289-317.
- Fernando, E., Keshavarz, T., Kyazze, G. 2013. Simultaneous co-metabolic decolourisation of azo dye mixtures and bio-electricity generation under



- thermophilic (50 °C) and saline conditions by an adapted anaerobic mixed culture in microbial fuel cells. *Bioresour. Technol.*, **127**, 1-8.
- Folkerts, M., Ney, U., Kneifel, H., Stackebrandt, E., Witte, E.G., Förstel, H., Schoberth, S.M., Sahm, H. 1989. *Desulfovibrio furfuralis* sp. nov., a furfural degrading strictly anaerobic bacterium. *Syst. Appl. Microbiol.*, **11**(2), 161-169.
- Franks, A.E., Nevin, K.P., Jia, H., Izallalen, M., Woodard, T.L., Lovley, D.R. 2009. Novel strategy for three-dimensional real-time imaging of microbial fuel cell communities: Monitoring the inhibitory effects of proton accumulation within the anode biofilm. *Energy Environ. Sci.*, **2**(1), 113-119.
- Freguia, S., Rabaey, K., Yuan, Z., Keller, J. 2007. Electron and carbon balances in microbial fuel cells reveal temporary bacterial storage behavior during electricity generation. *Environ. Sci. Technol.*, **41**(8), 2915-2921.
- Freguia, S., Rabaey, K., Yuan, Z., Keller, J. 2008. Syntrophic processes drive the conversion of glucose in microbial fuel cell anodes. *Environ. Sci. Technol.*, **42**(21), 7937-7943.
- Friman, H., Schechter, A., Ioffe, Y., Nitzan, Y., Cahan, R. 2013. Current production in a microbial fuel cell using a pure culture of *Cupriavidus basilensis* growing in acetate or phenol as a carbon source. *Microb. Biotechnol.*, **6**(4), 425-434.
- Fuchs, G., Boll, M., Heider, J. 2011. Microbial degradation of aromatic compounds — from one strategy to four. *Nat. Rev. Microbiol.*, **9**(11), 803-816.
- Ganesan, A., Chaussonnerie, S., Tarrade, A., Dauga, C., Bouchez, T., Pelletier, E., Le Paslier, D., Sghir, A. 2008. *Cloacibacillus evryensis* gen. nov., sp. nov., a novel asaccharolytic, mesophilic, amino-acid-degrading bacterium within the phylum 'Synergistetes', isolated from an anaerobic sludge digester. *Int. J. Syst. Evol. Microbiol.*, **58**(9), 2003-2012.
- Gao, Y., Ryu, H., Santo Domingo, J.W., Lee, H.-S. 2014. Syntrophic interactions between H<sub>2</sub>-scavenging and anode-respiring bacteria can improve current density in microbial electrochemical cells. *Bioresour. Technol.*, **153**, 245-253.
- Garcia, J.-L. 1990. Taxonomy and ecology of methanogens. *FEMS Microbiol. Rev.*, **87**(3-4), 297-308.
- Genthner, B.R., Davis, C.L., Bryant, M.P. 1981. Features of rumen and sewage sludge strains of *Eubacterium limosum*, a methanol- and H<sub>2</sub>-CO<sub>2</sub>-utilizing species. *Appl. Environ. Microbiol.*, **42**(1), 12-19.
- Gess, P., Pavlostathis, S.G. 1997. Desorption of chlorinated organic compounds from a contaminated estuarine sediment. *Environ. Toxicol. Chem.*, **16**(8), 1598-1605.
- Gil-Carrera, L., Escapa, A., Mehta, P., Santoyo, G., Guiot, S.R., Morán, A., Tartakovsky, B. 2013. Microbial electrolysis cell scale-up for combined wastewater treatment and hydrogen production. *Bioresour. Technol.*, **130**, 584-591.
- Gorby, Y.A., Yanina, S., McLean, J.S., Rosso, K.M., Moyles, D., Dohnalkova, A., Beveridge, T.J., Chang, I.S., Kim, B.H., Kim, K.S., Culley, D.E., Reed, S.B., Romine, M.F., Saffarini, D.A., Hill, E.A., Shi, L., Elias, D.A., Kennedy, D.W.,

- Pinchuk, G., Watanabe, K., Ishii, S.i., Logan, B., Nealson, K.H., Fredrickson, J.K. 2006. Electrically conductive bacterial nanowires produced by *Shewanella oneidensis* strain MR-1 and other microorganisms. *Proc. Natl. Acad. Sci. U. S. A.*, **103**(30), 11358-11363.
- Gorny, N., Schink, B. 1994. Anaerobic degradation of catechol by *Desulfobacterium* sp. Strain CAT2 proceeds via carboxylation to protocatechuate. *Appl. Environ. Microbiol.*, **60**(9), 3396-3400.
- Haddock, J.D., Ferry, J.G. 1989. Purification and properties of phloroglucinol reductase from *Eubacterium oxidoreducens* G-41. *J. Biol. Chem.*, **264**(8), 4423-4427.
- Hall-Stoodley, L., Costerton, J.W., Stoodley, P. 2004. Bacterial biofilms: From the natural environment to infectious diseases. *Nat Rev Micro*, **2**(2), 95-108.
- Hamelers, H.V.M., ter Heijne, A., Stein, N., Rozendal, R.A., Buisman, C.J.N. 2011. Butler–volmer–monod model for describing bio-anode polarization curves. *Bioresour. Technol.*, **102**(1), 381-387.
- Hansch, C., Leo, A., Hoekman, D.H. 1995. *Exploring qsar.: Hydrophobic, electronic, and steric constants*. American Chemical Society, Washington DC.
- Harrington, T.D., Babauta, J.T., Davenport, E.K., Renslow, R.S., Beyenal, H. 2015. Excess surface area in bioelectrochemical systems causes ion transport limitations. *Biotechnol. Bioeng.*, **112**(5), 858-866.
- He, Z., Wagner, N., Minteer, S.D., Angenent, L.T. 2006. An upflow microbial fuel cell with an interior cathode: Assessment of the internal resistance by impedance spectroscopy. *Environ. Sci. Technol.*, **40**(17), 5212-5217.
- He, Z., Wiegel, J. 1995. Purification and characterization of an oxygen-sensitive reversible 4-hydroxybenzoate decarboxylase from *Clostridium hydroxybenzoicum*. *Eur. J. Biochem.*, **229**(1), 77-82.
- He, Z., Mansfeld, F. 2009. Exploring the use of electrochemical impedance spectroscopy (EIS) in microbial fuel cell studies. *Energy Environ. Sci.*, **2**(2), 215-219.
- Healy, J.B., Young, L.Y. 1979. Anaerobic biodegradation of eleven aromatic compounds to methane. *Appl. Environ. Microbiol.*, **38**(1), 84-89.
- Hedbavna, P., Rolfe, S.A., Huang, W.E., Thornton, S.F. 2016. Biodegradation of phenolic compounds and their metabolites in contaminated groundwater using microbial fuel cells. *Bioresour. Technol.*, **200**, 426-434.
- Heipieper, H.J., Weber, F.J., Sikkema, J., Keweloh, H., de Bont, J.A.M. 1994. Mechanisms of resistance of whole cells to toxic organic solvents. *Trends Biotechnol.*, **12**(10), 409-415.
- Huang, D.-Y., Zhou, S.-G., Chen, Q., Zhao, B., Yuan, Y., Zhuang, L. 2011. Enhanced anaerobic degradation of organic pollutants in a soil microbial fuel cell. *Chem. Eng. J.*, **172**(2–3), 647-653.

- Imam, T., Capareda, S. 2012. Characterization of bio-oil, syn-gas and bio-char from switchgrass pyrolysis at various temperatures. *J. Anal. Appl. Pyrolysis*, **93**, 170-177.
- Ishii, S.i., Suzuki, S., Norden-Krichmar, T.M., Tenney, A., Chain, P.S.G., Scholz, M.B., Nealson, K.H., Bretschger, O. 2013. A novel metatranscriptomic approach to identify gene expression dynamics during extracellular electron transfer. *Nat Commun*, **4**, 1601.
- Jones, S., Holladay, J., Valkenburg, C., Stevens, D. 2009. Production of gasoline and diesel from biomass via fast pyrolysis, hydrotreating and hydrocracking: A design case. Pacific Northeast National Laboratory. PNNL-18284.
- Jönsson, L.J., Alriksson, B., Nilvebrant, N.-O. 2013. Bioconversion of lignocellulose: Inhibitors and detoxification. *Biotechnol. Biofuels*, **6**(1), 16.
- Kadier, A., Simayi, Y., Kalil, M.S., Abdeshahian, P., Hamid, A.A. 2014. A review of the substrates used in microbial electrolysis cells (MECs) for producing sustainable and clean hydrogen gas. *Renewable Energy*, **71**, 466-472.
- Kaiser, J.-P., Hanselmann, K. 1982. Fermentative metabolism of substituted monoaromatic compounds by a bacterial community from anaerobic sediments. *Arch. Microbiol.*, **133**(3), 185-194.
- Kang, C.S., Eaktasang, N., Kwon, D.Y., Kim, H.S. 2014. Enhanced current production by *Desulfovibrio desulfuricans* biofilm in a mediator-less microbial fuel cell. *Bioresour. Technol.*, **165**, 27-30.
- Kasai, D., Masai, E., Miyauchi, K., Katayama, Y., Fukuda, M. 2004. Characterization of the 3-o-methylgallate dioxygenase gene and evidence of multiple 3-O-methylgallate catabolic pathways in *Sphingomonas paucimobilis* SYK-6. *J. Bacteriol.*, **186**(15), 4951-4959.
- Kaufmann, F., Wohlfarth, G., Diekert, G. 1998. O-demethylase from *Acetobacterium dehalogenans*. *Eur. J. Biochem.*, **253**(3), 706-711.
- Kiely, P.D., Rader, G., Regan, J.M., Logan, B.E. 2011a. Long-term cathode performance and the microbial communities that develop in microbial fuel cells fed different fermentation endproducts. *Bioresour. Technol.*, **102**(1), 361-366.
- Kiely, P.D., Regan, J.M., Logan, B.E. 2011b. The electric picnic: Synergistic requirements for exoelectrogenic microbial communities. *Curr. Opin. Biotechnol.*, **22**(3), 378-385.
- Klinke, H., Thomsen, A., Ahring, B. 2004a. Inhibition of ethanol-producing yeast and bacteria by degradation products produced during pre-treatment of biomass. *Appl. Microbiol. Biotechnol.*, **66**.
- Klinke, H.B., Thomsen, A.B., Ahring, B.K. 2004b. Inhibition of ethanol-producing yeast and bacteria by degradation products produced during pre-treatment of biomass. *Appl. Microbiol. Biotechnol.*, **66**(1), 10-26.
- Kobayashi, H., Saito, N., Fu, Q., Kawaguchi, H., Vilcaez, J., Wakayama, T., Maeda, H., Sato, K. 2013. Bio-electrochemical property and phylogenetic diversity of

- microbial communities associated with bioelectrodes of an electromethanogenic reactor. *J. Biosci. Bioeng.*, **116**(1), 114-117.
- Koopman, F., Wierckx, N., de Winde, J.H., Ruijsenaars, H.J. 2010. Identification and characterization of the furfural and 5-(hydroxymethyl)furfural degradation pathways of *Cupriavidus basilensis* HMF14. *Proc. Natl. Acad. Sci. U. S. A.*, **17**(11), 4919-4924.
- Kortenkamp, A., Altenburger, R. 1999. Approaches to assessing combination effects of oestrogenic environmental pollutants. *Sci. Total Environ.*, **233**(1-3), 131-140.
- Korth, B., Rosa, L.F.M., Harnisch, F., Picioreanu, C. 2015. A framework for modeling electroactive microbial biofilms performing direct electron transfer. *Bioelectrochemistry*, **106**, 194-206.
- Kreikenbohm, R., Pfennig, N. 1985. Anaerobic degradation of 3,4,5-trimethoxybenzoate by a defined mixed culture of *Acetobacterium woodii*, *Pelobacter acidigallici*, and *Desulfobacter postgatei*. *FEMS Microbiol. Lett.*, **31**(1), 29-38.
- Kuhn, E.P., Suflita, J.M., Rivera, M.D., Young, L.Y. 1989. Influence of alternate electron acceptors on the metabolic fate of hydroxybenzoate isomers in anoxic aquifer slurries. *Appl. Environ. Microbiol.*, **55**(3), 590-598.
- Lalaurette, E., Thammannagowda, S., Mohagheghi, A., Maness, P.-C., Logan, B.E. 2009. Hydrogen production from cellulose in a two-stage process combining fermentation and electrohydrogenesis. *Int. J. Hydrogen Energy*, **34**(15), 6201-6210.
- Lee, H.-S., Torres, C.I., Parameswaran, P., Rittmann, B.E. 2009a. Fate of H<sub>2</sub> in an upflow single-chamber microbial electrolysis cell using a metal-catalyst-free cathode. *Environ. Sci. Technol.*, **43**(20), 7971-7976.
- Lee, H.-S., Torres, C.s.I., Rittmann, B.E. 2009b. Effects of substrate diffusion and anode potential on kinetic parameters for anode-respiring bacteria. *Environ. Sci. Technol.*, **43**(19), 7571-7577.
- Lee, H.-S., Vermaas, W.F.J., Rittmann, B.E. 2010. Biological hydrogen production: Prospects and challenges. *Trends Biotechnol.*, **28**(5), 262-271.
- Lewis, A.J., Ren, S., Ye, X., Kim, P., Labbe, N., Borole, A.P. 2015. Hydrogen production from switchgrass via an integrated pyrolysis-microbial electrolysis process. *Bioresour. Technol.*, **195**, 231-241.
- Li, X.-H., Liang, D.-W., Bai, Y.-X., Fan, Y.-T., Hou, H.-W. 2014. Enhanced H<sub>2</sub> production from corn stalk by integrating dark fermentation and single chamber microbial electrolysis cells with double anode arrangement. *Int. J. Hydrogen Energy*, **39**(17), 8977-8982.
- Lide, D.R. 1995. *Handbook of chemistry and physics 76th ed.* CRC Press, Inc., Boca Raton, FL.
- Liu, H., Grot, S., Logan, B.E. 2005. Electrochemically assisted microbial production of hydrogen from acetate. *Environ. Sci. Technol.*, **39**(11), 4317-4320.

- Liu, L., Liu, S.-S., Yu, M., Zhang, J., Chen, F. 2015a. Concentration addition prediction for a multiple-component mixture containing no effect chemicals. *Anal. Methods*, **7**(23), 9912-9917.
- Liu, Z., Zhang, C., Wang, L., He, J., Li, B., Zhang, Y., Xing, X.-H. 2015b. Effects of furan derivatives on biohydrogen fermentation from wet steam-exploded cornstalk and its microbial community. *Bioresour. Technol.*, **175**, 152-159.
- Logan, B. 2009. Exoelectrogenic bacteria that power microbial fuel cells. *Nat. Rev. Microbiol.*, **7**, 375-381.
- Logan, B.E., Call, D., Cheng, S., Hamelers, H.V.M., Sleutels, T.H.J.A., Jeremiasse, A.W., Rozendal, R.A. 2008. Microbial electrolysis cells for high yield hydrogen gas production from organic matter. *Environ. Sci. Technol.*, **42**(23), 8630-8640.
- Logan, B.E., Rabaey, K. 2012. Conversion of wastes into bioelectricity and chemicals by using microbial electrochemical technologies. *Science*, **337**(6095), 686-690.
- Logan, B.E., Wallack, M.J., Kim, K.-Y., He, W., Feng, Y., Saikaly, P.E. 2015. Assessment of microbial fuel cell configurations and power densities. *Environ. Sci. Technol. Lett.*, **8**(2), 206-214.
- Lovley, D.R., Giovannoni, S.J., White, D.C., Champine, J.E., Phillips, E.J.P., Gorby, Y.A., Goodwin, S. 1993. *Geobacter metallireducens* gen. nov. sp. nov., a microorganism capable of coupling the complete oxidation of organic compounds to the reduction of iron and other metals. *Arch. Microbiol.*, **159**(4), 336-344.
- Lu, L., Hou, D., Wang, X., Jassby, D., Ren, Z.J. 2016a. Active H<sub>2</sub> harvesting prevents methanogenesis in microbial electrolysis cells. *Environ. Sci. Technol. Lett.*, **3**(8), 286-290.
- Lu, L., Ren, Z.J. 2016. Microbial electrolysis cells for waste biorefinery: A state of the art review. *Bioresour. Technol.*, **215**, 254-264.
- Lu, L., Xing, D., Ren, N. 2012. Pyrosequencing reveals highly diverse microbial communities in microbial electrolysis cells involved in enhanced H<sub>2</sub> production from waste activated sludge. *Water Res.*, **46**(7), 2425-2434.
- Lu, L., Xing, D., Xie, T., Ren, N., Logan, B.E. 2010. Hydrogen production from proteins via electrohydrogenesis in microbial electrolysis cells. *Biosens. Bioelectron.*, **25**(12), 2690-2695.
- Lu, M., Chan, S., Babanova, S., Bretschger, O. 2016b. Effect of oxygen on the per-cell extracellular electron transfer rate of *Shewanella oneidensis* MR-1 explored in bioelectrochemical systems. *Biotechnol. Bioeng.*, n/a-n/a.
- Luo, H., Liu, G., Zhang, R., Jin, S. 2009. Phenol degradation in microbial fuel cells. *Chem. Eng. J.*, **147**(2-3), 259-264.
- Madigan, M.T., Martinko, J.M., Dunlap, P.V., Clark, D.P. 2009. *Brock biology of microorganisms*. Pearson Benjamin Cummings, San Francisco, CA.
- Magnuson, T.S., Isoyama, N., Hodges-Myerson, A.L., Davidson, G., Maroney, M.J., Geesey, G.G., Lovley, D.R. 2001. Isolation, characterization and gene sequence

- analysis of a membrane-associated 89 kDa Fe(III) reducing cytochrome c from *Geobacter sulfurreducens*. *Biochem. J.*, **359**(Pt 1), 147-152.
- Malvankar, N.S., Vargas, M., Nevin, K.P., Franks, A.E., Leang, C., Kim, B.-C., Inoue, K., Mester, T., Covalla, S.F., Johnson, J.P., Rotello, V.M., Tuominen, M.T., Lovley, D.R. 2011. Tunable metallic-like conductivity in microbial nanowire networks. *Nat Nano*, **6**(9), 573-579.
- Manohar, A.K., Bretschger, O., Nealson, K.H., Mansfeld, F. 2008. The use of electrochemical impedance spectroscopy (EIS) in the evaluation of the electrochemical properties of a microbial fuel cell. *Bioelectrochemistry*, **72**(2), 149-54.
- Marcus, A., Torres, C.I., Rittmann, B.E. 2007. Conduction-based modeling of the biofilm anode of a microbial fuel cell. *Biotechnol. Bioeng.*, **98**(6), 1171-1182.
- Marone, A., Carmona-Martínez, A.A., Sire, Y., Meudec, E., Steyer, J.P., Bernet, N., Trably, E. 2016. Bioelectrochemical treatment of table olive brine processing wastewater for biogas production and phenolic compounds removal. *Water Res.*, **100**, 316-325.
- Marshall, C.W., May, H.D. 2009. Electrochemical evidence of direct electrode reduction by a thermophilic gram-positive bacterium, *Thermincola ferriacetica*. *Energy Environ. Sci.*, **2**(6), 699-705.
- Marsili, E., Baron, D.B., Shikhare, I.D., Coursolle, D., Gralnick, J.A., Bond, D.R. 2008. *Shewanella* secretes flavins that mediate extracellular electron transfer. *Proc. Natl. Acad. Sci. U. S. A.*, **105**(10), 3968-3973.
- Marsili, E., Sun, J., Bond, D.R. 2010. Voltammetry and growth physiology of *Geobacter sulfurreducens* biofilms as a function of growth stage and imposed electrode potential. *Electroanalysis*, **22**(7-8), 865-874.
- Matthies, C., Evers, S., Ludwig, W., Schink, B. 2000. *Anaerovorax odorimutans* gen. nov., sp. nov., a putrescine-fermenting, strictly anaerobic bacterium. *Int. J. Syst. Evol. Microbiol.*, **50**(4), 1591-1594.
- Mavrovouniotis, M.L. 1990. Group contributions for estimating standard Gibbs energies of formation of biochemical compounds in aqueous solution. *Biotechnol. Bioeng.*, **36**(10), 1070-1082.
- Milliken, C.E., May, H.D. 2007. Sustained generation of electricity by the spore-forming, Gram-positive, *Desulfitobacterium hafniense* strain DCB2. *Appl. Microbiol. Biotechnol.*, **73**(5), 1180-1189.
- Mills, T.Y., Sandoval, N.R., Gill, R.T. 2009. Cellulosic hydrolysate toxicity and tolerance mechanisms in *Escherichia coli*. *Biotechnol. Biofuels*, **2**(1), 1-11.
- Monlau, F., Sambusiti, C., Barakat, A., Quéméneur, M., Trably, E., Steyer, J.P., Carrère, H. 2014. Do furanic and phenolic compounds of lignocellulosic and algae biomass hydrolyzate inhibit anaerobic mixed cultures? A comprehensive review. *Biotechnol. Adv.*, **32**(5), 934-951.

- Montpart, N., Rago, L., Baeza, J.A., Guisasola, A. 2015. Hydrogen production in single chamber microbial electrolysis cells with different complex substrates. *Water Res.*, **68**, 601-615.
- Moons, P., Michiels, C.W., Aertsen, A. 2009. Bacterial interactions in biofilms. *Crit. Rev. Microbiol.*, **35**(3), 157-168.
- Mussatto, S.I., Roberto, I.C. 2004. Alternatives for detoxification of diluted-acid lignocellulosic hydrolyzates for use in fermentative processes: A review. *Bioresour. Technol.*, **93**(1), 1-10.
- Nealson, K.H., Rowe, A.R. 2016. Electromicrobiology: Realities, grand challenges, goals and predictions. *Microb. Biotechnol.*, **9**(5), 595-600.
- Newman, D.K., Kolter, R. 2000. A role for excreted quinones in extracellular electron transfer. *Nature*, **405**(6782), 94-97.
- Okamoto, A., Saito, K., Inoue, K., Nealson, K.H., Hashimoto, K., Nakamura, R. 2014. Uptake of self-secreted flavins as bound cofactors for extracellular electron transfer in *Geobacter* species. *Energy Environ. Sci.*, **7**(4), 1357-1361.
- Palmqvist, E., Hahn-Hägerdal, B. 2000. Fermentation of lignocellulosic hydrolysates. II: Inhibitors and mechanisms of inhibition. *Bioresour. Technol.*, **74**(1), 25-33.
- Parameswaran, P., Zhang, H., Torres, C.I., Rittmann, B.E., Krajmalnik-Brown, R. 2010. Microbial community structure in a biofilm anode fed with a fermentable substrate: The significance of hydrogen scavengers. *Biotechnol. Bioeng.*, **105**(1), 69-78.
- Park, H.S., Kim, B.H., Kim, H.S., Kim, H.J., Kim, G.T., Kim, M., Chang, I.S., Park, Y.K., Chang, H.I. 2001. A novel electrochemically active and Fe(III)-reducing bacterium phylogenetically related to *Clostridium butyricum* isolated from a microbial fuel cell. *Anaerobe*, **7**(6), 297-306.
- Park, L.K.-E., Ren, S., Yiacoumi, S., Ye, X.P., Borole, A.P., Tsouris, C. 2016. Separation of switchgrass bio-oil by water/organic solvent addition and pH adjustment. *Energy Fuels*, **30**(3), 2164-2173.
- Parpot, P., Bettencourt, A.P., Chamoulaud, G., Kokoh, K.B., Belgsir, E.M. 2004. Electrochemical investigations of the oxidation–reduction of furfural in aqueous medium: Application to electrosynthesis. *Electrochim. Acta*, **49**(3), 397-403.
- Pham, H., Boon, N., Marzorati, M., Verstraete, W. 2009. Enhanced removal of 1,2-dichloroethane by anodophilic microbial consortia. *Water Res.*, **43**(11), 2936-2946.
- Phelps, C.D., Young, L.Y. 1997. Microbial metabolism of the plant phenolic compounds ferulic and syringic acids under three anaerobic conditions. *Microb Ecol.*, **33**(3), 206-215.
- Piciooreanu, C., Head, I.M., Katuri, K.P., van Loosdrecht, M.C.M., Scott, K. 2007. A computational model for biofilm-based microbial fuel cells. *Water Res.*, **41**(13), 2921-2940.

- Pinto, R.P., Srinivasan, B., Escapa, A., Tartakovsky, B. 2011. Multi-population model of a microbial electrolysis cell. *Environ. Sci. Technol.*, **45**(11), 5039-5046.
- Piotrowski, J.S., Zhang, Y., Sato, T., Ong, I., Keating, D., Bates, D., Landick, R. 2014. Death by a thousand cuts: The challenges and diverse landscape of lignocellulosic hydrolysate inhibitors. *Front. Microbiol.*, **5**, 1-8.
- Pirbadian, S., Barchinger, S.E., Leung, K.M., Byun, H.S., Jangir, Y., Bouhenni, R.A., Reed, S.B., Romine, M.F., Saffarini, D.A., Shi, L., Gorby, Y.A., Golbeck, J.H., El-Naggar, M.Y. 2014. *Shewanella oneidensis* MR-1 nanowires are outer membrane and periplasmic extensions of the extracellular electron transport components. *Proc. Natl. Acad. Sci. U. S. A.*
- Quéménéur, M., Hamelin, J., Barakat, A., Steyer, J.-P., Carrère, H., Trably, E. 2012. Inhibition of fermentative hydrogen production by lignocellulose-derived compounds in mixed cultures. *Int. J. Hydrogen Energy*, **37**(4), 3150-3159.
- Rabaey, K., Boon, N., Höfte, M., Verstraete, W. 2005. Microbial phenazine production enhances electron transfer in biofuel cells. *Environ. Sci. Technol.*, **39**(9), 3401-3408.
- Rasmussen, H., Sørensen, H.R., Meyer, A.S. 2014. Formation of degradation compounds from lignocellulosic biomass in the biorefinery: Sugar reaction mechanisms. *Carbohydr. Res.*, **385**, 45-57.
- Reguera, G., McCarthy, K.D., Mehta, T., Nicoll, J.S., Tuominen, M.T., Lovley, D.R. 2005. Extracellular electron transfer via microbial nanowires. *Nature*, **435**(7045), 1098-1101.
- Ren, L., Siegert, M., Ivanov, I., Pisciotta, J.M., Logan, B.E. 2013a. Treatability studies on different refinery wastewater samples using high-throughput microbial electrolysis cells (MECs). *Bioresour. Technol.*, **136**(0), 322-328.
- Ren, L., Siegert, M., Ivanov, I., Pisciotta, J.M., Logan, B.E. 2013b. Treatability studies on different refinery wastewater samples using high-throughput microbial electrolysis cells (MECs). *Bioresour. Technol.*, **136**, 322-328.
- Ren, N., Wang, A., Cao, G., Xu, J., Gao, L. 2009. Bioconversion of lignocellulosic biomass to hydrogen: Potential and challenges. *Biotechnol. Adv.*, **27**(6), 1051-1060.
- Ren, S., Ye, X.P., Borole, A.P., Kim, P., Labbé, N. 2016. Analysis of switchgrass-derived bio-oil and associated aqueous phase generated in a semi-pilot scale auger pyrolyzer. *J. Anal. Appl. Pyrolysis*, **119**, 97-103.
- Ren, Z., Ward, T.E., Regan, J.M. 2007. Electricity production from cellulose in a microbial fuel cell using a defined binary culture. *Environ. Sci. Technol.*, **41**(13), 4781-4786.
- Rice, E.W., Eaton, A.D., Baird, R.B. 2012. *Standard methods for the examination of water and wastewater 22nd ed.* APHA, AWWA, WEF, Washington, DC.



- Rimboud, M., Pocaznoi, D., Erable, B., Bergel, A. 2014. Electroanalysis of microbial anodes for bioelectrochemical systems: Basics, progress and perspectives. *PCCP*, **16**(31), 16349-16366.
- Rittmann, B.E., McCarty, P.L. 2001. *Environmental biotechnology: Principles and applications*. McGraw-Hill, New York, NY.
- Ross, D.E., Flynn, J.M., Baron, D.B., Gralnick, J.A., Bond, D.R. 2011. Towards electrosynthesis in *Shewanella*: Energetics of reversing the mtr pathway for reductive metabolism. *PLoS One*, **6**(2), e16649.
- Rozendal, R.A., Hamelers, H.V.M., Euverink, G.J.W., Metz, S.J., Buisman, C.J.N. 2006. Principle and perspectives of hydrogen production through biocatalyzed electrolysis. *Int. J. Hydrogen Energy*, **31**(12), 1632-1640.
- Rozendal, R.A., Jeremiase, A.W., Hamelers, H.V.M., Buisman, C.J.N. 2008. Hydrogen production with a microbial biocathode. *Environ. Sci. Technol.*, **42**(2), 629-634.
- Sander, R. 2014. Compilation of henry's law constants, version 3.99. *Atmos. Chem. Phys. Discuss.*, **14**(21), 29615-30521.
- Schie, P.M.v., Young, L.Y. 2000. Biodegradation of phenol: Mechanisms and applications. *Biorem. J.*, **4**(1), 1-18.
- Schink, B., Philipp, B., Müller, J. 2000. Anaerobic degradation of phenolic compounds. *Naturwissenschaften*, **87**(1), 12-23.
- Schweigert, N., Zehnder, A.J.B., Eggen, R.I.L. 2001. Chemical properties of catechols and their molecular modes of toxic action in cells, from microorganisms to mammals. *Environ. Microbiol.*, **3**(2), 81-91.
- Sembing, T., Winter, J. 1990. Demethylation of aromatic compounds by strain B10 and complete degradation of 3-methoxybenzoate in co-culture with *Desulfosarcina* strains. *Appl. Microbiol. Biotechnol.*, **33**(2), 233-238.
- Sharak Genthner, B.R., Bryant, M.P. 1987. Additional characteristics of one-carbon-compound utilization by *Eubacterium limosum* and *Acetobacterium woodii*. *Appl. Environ. Microbiol.*, **53**(3), 471-476.
- Silva, E., Rajapakse, N., Kortenkamp, A. 2002. Something from “nothing” – eight weak estrogenic chemicals combined at concentrations below NOECs produce significant mixture effects. *Environ. Sci. Technol.*, **36**(8), 1751-1756.
- Sleat, R., Mah, R.A. 1985. *Clostridium populeti* sp. nov., a cellulolytic species from a woody-biomass digester. *Int. J. Syst. Bacteriol.*, **35**(2), 160-163.
- Sleutels, T.H.J.A., Hamelers, H.V.M., Rozendal, R.A., Buisman, C.J.N. 2009. Ion transport resistance in microbial electrolysis cells with anion and cation exchange membranes. *Int. J. Hydrogen Energy*, **34**(9), 3612-3620.
- Snider, R.M., Strycharz-Glaven, S.M., Tsoi, S.D., Erickson, J.S., Tender, L.M. 2012. Long-range electron transport in *Geobacter sulfurreducens* biofilms is redox gradient-driven. *Proc. Natl. Acad. Sci. U. S. A.*, **109**(38), 15467-15472.

- Song, T.-s., Wu, X.-y., Zhou, C.C. 2014. Effect of different acclimation methods on the performance of microbial fuel cells using phenol as substrate. *Bioprocess and Biosystems Engineering*, **37**(2), 133-138.
- Speers, A.M., Reguera, G. 2012. Electron donors supporting growth and electroactivity of *Geobacter sulfurreducens* anode biofilms. *Appl. Environ. Microbiol.*, **78**(2), 437-444.
- Sun, D., Wang, A., Cheng, S., Yates, M., Logan, B.E. 2014. *Geobacter anodireducens* sp. nov., an exoelectrogenic microbe in bioelectrochemical systems. *Int. J. Syst. Evol. Microbiol.*, **64**(Pt 10), 3485-3491.
- Suresh, S., Srivastava, V.C., Mishra, I.M. 2012. Adsorption of catechol, resorcinol, hydroquinone, and their derivatives: A review. *International Journal of Energy and Environmental Engineering*, **3**(1), 32.
- Tartakovsky, B., Manuel, M.F., Wang, H., Guiot, S.R. 2009. High rate membrane-less microbial electrolysis cell for continuous hydrogen production. *Int. J. Hydrogen Energy*, **34**(2), 672-677.
- Taylor, B.F. 1983. Aerobic and anaerobic catabolism of vanillic acid and some other methoxy-aromatic compounds by *Pseudomonas* sp. Strain PN-1. *Appl. Environ. Microbiol.*, **46**(6), 1286-1292.
- TerAvest, M.A., Ajo-Franklin, C.M. 2016. Transforming exoelectrogens for biotechnology using synthetic biology. *Biotechnol. Bioeng.*, **113**(4), 687-697.
- Torres, C.I., Kato Marcus, A., Rittmann, B.E. 2008. Proton transport inside the biofilm limits electrical current generation by anode-respiring bacteria. *Biotechnol. Bioeng.*, **100**(5), 872-881.
- Torres, C.I., Marcus, A.K., Lee, H.-S., Parameswaran, P., Krajmalnik-Brown, R., Rittmann, B.E. 2010. A kinetic perspective on extracellular electron transfer by anode-respiring bacteria. *FEMS Microbiol. Rev.*, **34**(1), 3-17.
- Tschech, A., Fuchs, G. 1989. Anaerobic degradation of phenol via carboxylation to 4-hydroxybenzoate: In vitro study of isotope exchange between  $^{14}\text{CO}_2$  and 4-hydroxybenzoate. *Arch. Microbiol.*, **152**(6), 594-599.
- Tschech, A., Schink, B. 1986. Fermentative degradation of monohydroxybenzoates by defined syntrophic cocultures. *Arch. Microbiol.*, **145**(4), 396-402.
- Van Loosdrecht, M.C.M., Picioreanu, C., Heijnen, J.J. 1997. A more unifying hypothesis for biofilm structures. *FEMS Microbiol. Ecol.*, **24**(2), 181-183.
- van Schie, P.M., Young, L.Y. 1998. Isolation and characterization of phenol-degrading denitrifying bacteria. *Appl. Environ. Microbiol.*, **64**(7), 2432-2438.
- Virdis, B., Harnisch, F., Batstone, D.J., Rabaey, K., Donose, B.C. 2012. Non-invasive characterization of electrochemically active microbial biofilms using confocal raman microscopy. *Energy Environ. Sci.*, **5**(5), 7017-7024.

- Vos, P.D., Garrity, G.M., Jones, D., Krieg, N.R., Ludwig, W., Rainey, F.A., Schleifer, K.-H., Whitman, W.B. 2009. *Bergey's manual of systematic bacteriology. Volume 3. The firmicutes. 2 ed.* Springer, Dordrecht, NY.
- Vuyyuru, K.R., Strasser, P. 2012. Oxidation of biomass derived 5-hydroxymethylfurfural using heterogeneous and electrochemical catalysis. *Catal. Today*, **195**(1), 144-154.
- Wagner, R.C., Regan, J.M., Oh, S.-E., Zuo, Y., Logan, B.E. 2009. Hydrogen and methane production from swine wastewater using microbial electrolysis cells. *Water Res.*, **43**(5), 1480-1488.
- Wang, A., Liu, W., Ren, N., Cheng, H., Lee, D.-J. 2010. Reduced internal resistance of microbial electrolysis cell (MEC) as factors of configuration and stuffing with granular activated carbon. *Int. J. Hydrogen Energy*, **35**(24), 13488-13492.
- Wang, A., Sun, D., Cao, G., Wang, H., Ren, N., Wu, W.-M., Logan, B.E. 2011. Integrated hydrogen production process from cellulose by combining dark fermentation, microbial fuel cells, and a microbial electrolysis cell. *Bioresour. Technol.*, **102**(5), 4137-4143.
- Wang, H., Ren, Z.J. 2013. A comprehensive review of microbial electrochemical systems as a platform technology. *Biotechnol. Adv.*, **31**(8), 1796-1807.
- Wierckx, N., Koopman, F., Ruijssenaars, H., Winde, J. 2011a. Microbial degradation of furanic compounds: Biochemistry, genetics, and impact. *Appl. Microbiol. Biotechnol.*, **92**(6), 1095-1105.
- Wierckx, N., Koopman, F., Ruijssenaars, H.J., de Winde, J.H. 2011b. Microbial degradation of furanic compounds: Biochemistry, genetics, and impact. *Appl. Microbiol. Biotechnol.*, **92**(6), 1095-1105.
- Wilson, E.L., Kim, Y. 2016. The yield and decay coefficients of exoelectrogenic bacteria in bioelectrochemical systems. *Water Res.*, **94**, 233-239.
- Wimpenny, J.W.T., Colasanti, R. 1997. A unifying hypothesis for the structure of microbial biofilms based on cellular automaton models. *FEMS Microbiol. Ecol.*, **22**(1), 1-16.
- Wrighton, K.C., Agbo, P., Warnecke, F., Weber, K.A., Brodie, E.L., DeSantis, T.Z., Hugenholtz, P., Andersen, G.L., Coates, J.D. 2008. A novel ecological role of the firmicutes identified in thermophilic microbial fuel cells. *ISME J.*, **2**(11), 1146-1156.
- Xing, D., Cheng, S., Regan, J.M., Logan, B.E. 2009. Change in microbial communities in acetate- and glucose-fed microbial fuel cells in the presence of light. *Biosens. Bioelectron.*, **25**(1), 105-111.
- Yalkowsky, S.H., Dannenfelser, R.M. 1992. Aquasol database of aqueous solubility. *College of Pharmacy, University of Arizona, Tucson, AZ.*
- Yalkowsky, S.H., He, Y. 2003. *Handbook of aqueous solubility data.* CRC Press, Boca Raton, FL.

- Yamamuro, A., Kouzuma, A., Abe, T., Watanabe, K. 2014. Metagenomic analyses reveal the involvement of syntrophic consortia in methanol/electricity conversion in microbial fuel cells. *PLoS One*, **9**(5), e98425.
- Yaws, C.L. 2003. Yaws' handbook of thermodynamic and physical properties of chemical compounds, Knovel.
- Zaldivar, J., Ingram, L.O. 1999. Effect of organic acids on the growth and fermentation of ethanogenic *Escherichia coli* LY01. *Biotechnol. Bioeng.*, **66**(4), 203-210.
- Zaldivar, J., Martinez, A., Ingram, L.O. 1999. Effect of selected aldehydes on the growth and fermentation of ethanogenic *Escherichia coli*. *Biotechnol. Bioeng.*, **65**(1), 24-33.
- Zhang, F., Liu, J., Ivanov, I., Hatzell, M.C., Yang, W., Ahn, Y., Logan, B.E. 2014. Reference and counter electrode positions affect electrochemical characterization of bioanodes in different bioelectrochemical systems. *Biotechnol. Bioeng.*, n/a-n/a.
- Zhang, X., He, W., Ren, L., Stager, J., Evans, P.J., Logan, B.E. 2015. COD removal characteristics in air-cathode microbial fuel cells. *Bioresour. Technol.*, **176**, 23-31.
- Zhang, X., Wiegel, J. 1990. Isolation and partial characterization of a clostridium species transforming para-hydroxybenzoate and 3,4-dihydroxybenzoate and producing phenols as the final transformation products. *Microb Ecol*, **20**(1), 103-121.
- Zhang, Y., Han, B., Ezeji, T.C. 2012. Biotransformation of furfural and 5-hydroxymethyl furfural (hmf) by clostridium acetobutylicum atcc 824 during butanol fermentation. *New Biotechnology*, **29**(3), 345-351.
- Zhi, W., Ge, Z., He, Z., Zhang, H. 2014. Methods for understanding microbial community structures and functions in microbial fuel cells: A review. *Bioresour. Technol.*, **171**(0), 461-468.
- Ziemer, C.J. 2014. Newly cultured bacteria with broad diversity isolated from eight-week continuous culture enrichments of cow feces on complex polysaccharides. *Appl. Environ. Microbiol.*, **80**(2), 574-585.